STUDY TOWARD WIDER APPLICATION OF ADAPTIVE ARRAYS(Dissertation_全文)

AUTHOR(S):

Kikuma, Nobuyoshi

STUDY TOWARD WIDER APPLICATION OF ADAPTIVE ARRAYS

by

Nobuyoshi KIKUMA

February 1987

Department of Electrical Engineering
Kyoto University,
Kyoto 606, Japan

STUDY TOWARD
WIDER APPLICATION OF ADAPTIVE ARRAYS

by
Nobuyoshi KIKUMA

February 1987

Department of Electrical Engineering
Kyoto University,
Kyoto 606, Japan

DOCTORAL THESIS

SUBMITTED TO

THE FACULTY OF ENGINEERING

KYOTO UNIVERSITY

ACKNOWLEDGMENTS

The author wishes to express his hearty and sincere gratitude to Professor Iwane Kimura for his constant guidance and critical supervision throughout the work.

The author is deeply indebted to Assoc. Prof. Kazuaki Takao for his continual guidance and encouragement. It would have been impossible to accomplish this thesis without his suggestions and criticisms.

The author also wishes to express his hearty appreciation to Professors Susumu Kato, Toru Ogawa and Fumio Ikegami for their valuable discussions.

The author is grateful to Drs. Syoichiro Fukao, Kozo Hashimoto, Toru Sato and Yoshiharu Omura for their many discussions.

The author very much appreciates the contributions Mr. Tatsuro Yano and Mr. Minoru Ueda made when they were a graduate student and a bachelor candidate student, respectively, at Kyoto University.

The author also wishes to acknowledge many members in Kimura's Laboratory of the Department of Electrical Engineering and Radio Atmospheric Science Center of Kyoto University for their discussions. Especially, the author wishes to express his thanks to Messrs. Kiyoshi Kono and Koichi Takahara for their help in making drawings concerning the present study.

It should be added that all numerical computations were carried out at the Data Processing Center, Kyoto University.

PREFACE

This thesis deals with theoretical studies on the adaptive arrays toward their wider applications. The efficient utilization of frequency spectrum is one of the recent important topics in the field of communication. From this viewpoint, the receiving systems are required to reject the unwanted waves in a complicated radio environment. Passive countermeasure such as shielding or uniformly low sidelobes has been conventionally used against the interference. While the strength, angle of arrival and other parameters of the interference are not known a priori, such an approach must prepare for all possibilities, which may lead to unnecessary redundant, expensive system. On the other hand, an adaptive array is an "active" system that suppresses the unwanted signal while maintaining the desired signal. We strongly propose applications of the adaptive array. In future, it is expected that the adaptive array is also applied to ease the problem of site selection of the earth station for satellite communication in the area of crowded terrestrial communication network.

So far the characteristics of the adaptive arrays have been investigated in detail, but the further investigations remain which will make the adaptive arrays applicable to the conditions under which the conventional algorithms have not functioned well. The subjects of our study toward wider applications of adaptive arrays are as follows:

(1) realization of an adaptive array with phase-only control for the convenience of hardware implementation.

(2) enhancement of adaptability under the effect of coherent

interference.

(3) remedy for degradation of performance in the presence of setting error in the constraint conditions.

(4) improvement toward broadband adaptation (where the desired signal and interferences are broadband signals).

(5) pursuit of the optimum initial values in the optimization algorithms based on the steepest gradient method.

After survey of the previous works on the adaptive arrays, the concept of the adaptive array with the directional constraints is described at first. Afterward, the above subjects are examined individually in detail. Theoretical and numerical analyses give the good understanding on the devised and improved adaptive array system in each subject, which will enable the future prospect of the adaptive arrays to be much brighter.

CONTENTS

CHAPTER 1

GENERAL INTRODUCTION

Recently, an increase of amounts of communication has complicated the radio environments, so interference among communications is becoming a serious problem. Accordingly, it is expected that improvement of characteristics of antennas which play important roles in transmitting and receiving informative electromagnetic waves will contribute to effective and efficient utilization of frequencies. For the transmitters, the antennas are desired which intensively radiate waves toward the receivers while not emitting them to the unnecessary directions. For the receivers, on the other hand, the antennas are expected to extract only the desired wave from noisy radio environments, and hence applications of a nature of the antenna as a spatial filter (selection of incident waves based on directivity of antennas) is given much attention as significant means.

As far as the receiving antennas are concerned, they have been designed to increase the gain of mainbeam while preserving the whole sidelobe levels to be uniformly low for the case of no knowledge on the interfering waves. For this purpose, signal reception using an antenna array has long been an attractive solution. It is because an antenna array has many advantages over a single antenna in terms of the mainbeam direction, beamwidth, sidelobe level and pattern null directions, which can be easily controlled by choosing the phase and amplitude of electrical excitation of each element antenna. As the representative pattern-synthesized arrays, the Dolph-Chebyshev array[1], Taylor array[2] (which is more applicable for continuous distributions) and so on, are well

known.

If the incident directions of interferences are fixed, deterministic design procedures as mentioned above can be applicable to reject interferences by steering nulls toward them. In general, however, the incident directions and the time of occurrence of interferences may be undeterministic. Therefore, the conventional procedure for array design fails to reject interferences selectively and must prepare for all possibilities. For the purpose, it requires a large number of antenna elements on the large aperture and hence is inefficient for the more realistic case where the interferences impinge from specific directions.

It is the adaptive antenna arrays that have appeared as the systems more flexibly coping with this problem. The term, "adaptive", is used to describe the ability of a system to change its characteristics in accordance with the condition, especially radio environments under which it is operating. Adaptive arrays are composed of antennas that detect the signals of interest and a real-time adaptive signal processor which automatically adjusts the array pattern so that a measure of quality of the array performance is improved. In addition, the advent of highly compact, inexpensive and speedy digital computers has now made it possible to exploit well-known results from statistical detection and estimation theory and from control theory to develop adaptive array systems. Adaptive arrays require the a priori knowledge on the characteristics of the desired signal. Using this knowledge, the adaptive arrays distinguish the desired signal from the unwanted interferences and noise, and extract only the desired signal from the noisy radio environments.

So far the detailed characteristics of the adaptive arrays have been clarified, but the further investigations remain with us so that the adaptive arrays may become applicable to the conditions under which they

have not functioned well as yet. In this thesis, we proceed to studies on the adaptive arrays toward their wider applications.

In Chapter 2, we first make survey of the previous works on the adaptive arrays and grasp the transition of them systematically.

In Chapter 3, we introduce the adaptive array under the directional constraints that will be adopted throughout this thesis and present derivation of the optimum weights and the algorithms for controlling the weights. Our method of analysis makes use of the well-known Lagrange multipliers. As for the optimization algorithms, the asymptotic and iterative algorithm based on the steepest gradient method and the direct calculation algorithm by sampled matrix inversion are presented. Numerical examples are also shown.

In Chapter 4, an adaptive antenna array system with phase-only control and under the principle of directionally constrained minimization of power (DCMP) is discussed. A new penalty function is introduced for the system in order to take into consideration the protection of the desired signal while minimizing the unwanted interference and/or noise. Because of the analytical limitation, computer simulation experiments are extensively carried out. The constraint coefficient that is the most important factor of the penalty function is especially investigated, and the optimum choice is given. It is also shown that the theoretical consideration leads to the same value. Finally, the quantization of phase-shifters is attempted.

In Chapter 5, the adaptive array under the directionally constrained minimization of power (DCMP) algorithm is improved by injecting a "pseudo noise." It is effective to protect the desired signal from cancellation or distortion in such cases as; (1) where a coherent interference is incident, or (2) where the desired signal direction for the constraint

contains some pointing error, or (3) when the desired signal is broadbanded. The optimum amount of pseudo noise to be injected is also discussed and its formula is given. We name this system "tamed adaptive antenna array" since its killing capability is somewhat moderated so as not to hurt the desired signal. Next, extending the problem of pointing error, we study the effects of general setting errors in the constraint conditions. In practice, if this setting contains some error, the desired signal will be taken for the unwanted one and hence become a target of suppression. To prevent this malfunction, we employ the tamed adaptive array again and demonstrate its effectiveness against such imperfect constraint. We consider two examples that cause such effects, i.e., the mutual coupling and random input errors.

Chapter 6 deals with a technique which enables the adaptive array to suppress the coherent interferences. The conventional adaptive arrays which work under the guiding principles of output minimization have difficulties: If the interference is coherent with the desired signal such as in a multipath environment, the system tends to cancel the desired signal by using the coherent interference, which is also discussed on the directionally constrained minimization of power (DCMP) adaptive array in Chapter 5. In the new technique, the array is divided into sub-arrays, whose input correlation matrices are adaptively averaged so as to produce a Toeplitz matrix which would be obtained when the interference did not correlate with the desired signal. The averaged matrix is now free from correlation terms between the desired signal and interference, and therefore may be used to derive the optimum weight for the array element just as in the ordinary radio environment of incoherent interference. Although this technique can be applied to any adaptive arrays, the demonstration is made in the DCMP system. Theoretical analysis and

numerical examples show how highly the adaptive array with this new technique is capable to suppress the coherent and incoherent interferences. Next, this technique is coupled with the sampled matrix inversion (SMI) algorithm and the transient performance is observed by the computer simulation.

Chapter 7 is devoted to introducing an alternative principle of power minimization under a correlation constraint. Unlike the conventional directional constraints, this new principle sets the constraint condition on the cross correlation value between the input desired signal and its array output. This principle is applied to reception of the broadband desired signal and to countermeasure against the pointing error that is a problem peculiar to the conventional directional constraints. Numerical results show the performance of the adaptive array with this new principle.

In Chapter 8, the effect of initial weight values on the transient characteristics is investigated on three kinds of adaptive arrays under different principles, i.e., the directionally constrained minimization of power (DCMP), the least mean square (LMS) and the maximum signal-to-noise ratio (MSN). Analysis and computer simulation demonstrate how the convergence rate is affected by the initial setting. Afterward, the best choice of the initial value is discussed.

In Chapter 9, summary and conclusions are described to declare the various performances of the adaptive array systems of our interest.

CHAPTER 2

A SURVEY OF THE PREVIOUS WORKS ON THE ADAPTIVE ARRAYS

According to "IEEE standard definitions of terms for antennas" in Ref.[3], adaptive arrays are defined as "a system having circuit elements associated with its radiating elements such that some of the antenna properties are controlled by the received signal." Adaptive arrays derive from the fields where wave motions are treated, such as retrodirective or self-phasing arrays[4],[5], sidelobe cancellers[6], adaptive filters [7],[8], acoustic or sonar arrays[10],[11], and seismometers[12],[13]. The functions of the adaptive arrays are classified into adaptive beamforming and adaptive null steering according to their purposes[14]. Adaptive beamforming is to automatically steer the mainbeam of the array to the direction of the object, which is also called auto-focusing. Adaptive null steering, on the other hand, is to produce the pattern nulls in the directions of unwanted waves. Recently, most researches on the adaptive arrays concentrate on the latter subject.

The first system of adaptive null steering is a sidelobe canceller proposed by Howells[6]. This system consists of a main, high gain antenna and several auxiliary antennas as shown in Fig.2.1. The auxiliary antenna gains are normally designed to be comparable with the sidelobe level of the main antenna gain pattern, and the amount of desired target signal received by the auxiliaries is negligible compared with the desired signal in the main antenna. The purpose of the auxiliary antennas is to provide independent replicas of interferences in the sidelobes of the main pattern for their cancellation. Thus, this system can create the nulls to the

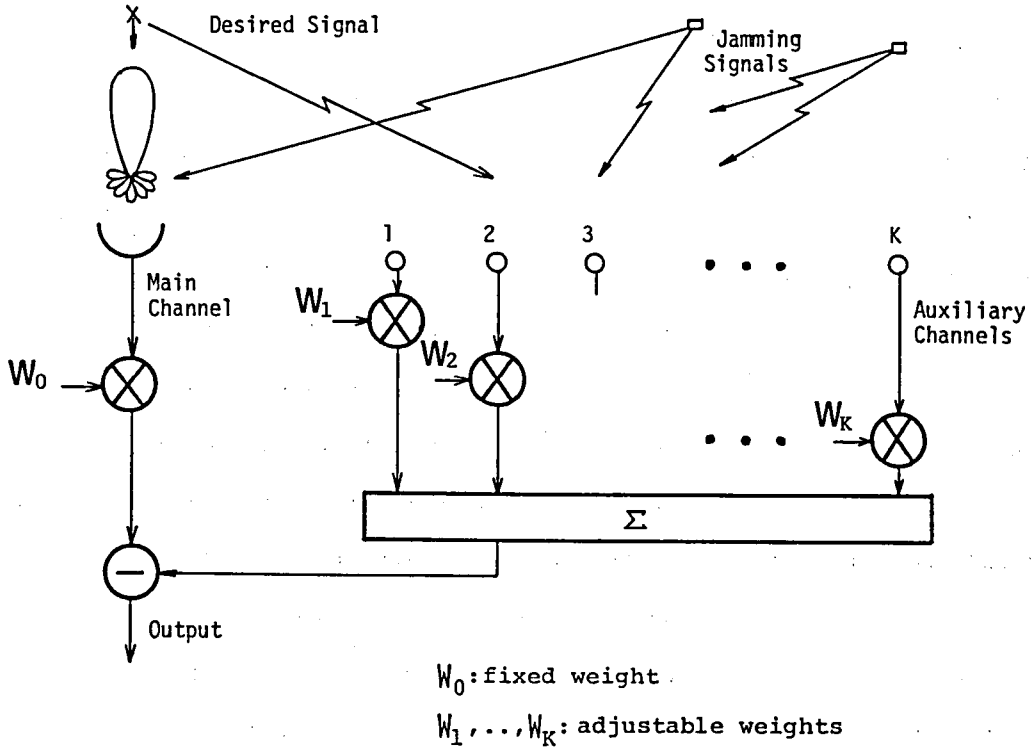

Fig.2.1 Structure of sidelobe canceller.

directions of the interferences in the synthetic pattern.

As understood from performance of the sidelobe canceller, the most significant function of adaptive null steering is to flexibly control the amplitudes and phases of the interferences in the individual array elements and synthesize those channel outputs so that the interferences may be cancelled at the array output. Therefore, tapped-delay-line (transversal) filters with variable gain amplifiers associated with each element are generally used to achieve cancellation of the interferences, which is shown in Fig.2.2. This system composes the combined filter in spatial and time domain by connecting the filters with the array. In narrowband applications, a phase shifter and an amplifier with variable gain can be employed in place of a tapped-delay-line filter.

In the adaptive array systems, the apriori knowledge on the desired signal, i.e., the center frequency, incident direction, modulation method and so on, are effectively utilized for extracting the actual desired signal from noisy radio environments. Learning the information on the radio environments, the adaptive array systems change their spatial and frequency characteristics to match the environments. Therefore, they do not require in advance the knowledge about the conditions of unwanted noises (interferences and isotropic noise). For adaptation, various criteria have been proposed. Among them are

(1) maximum signal-to-noise ratio (MSN),

(2) least mean square error (LMS),

(3) maximum likelihood ratio (MLR),

(4) constrained minimization of power (CMP),

and so on.

Adaptive nulling based on the MSN criterion was developed for an intermediate frequency (IF) radar sidelobe canceller as represented by the

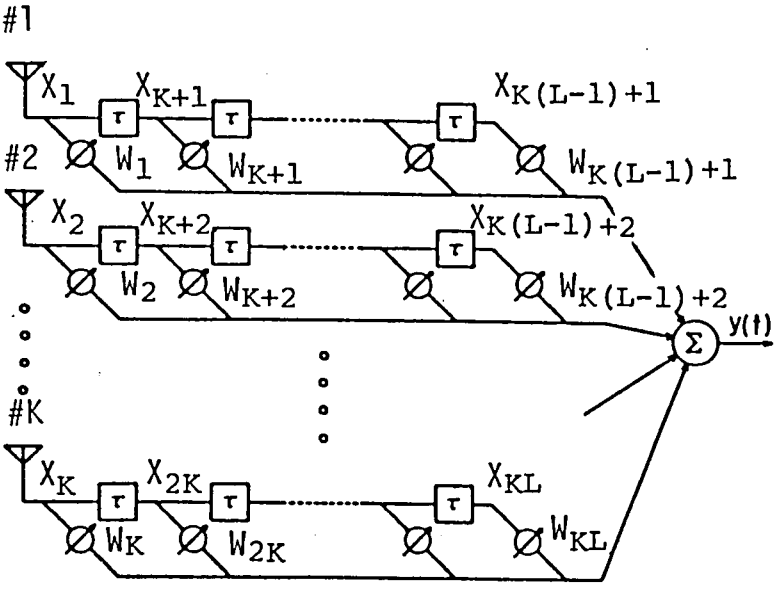

X:input, y:output, W:weight, τ:time delay

Fig.2.2 Configuration of an adaptive array with tapped-delay-line (transversal) filters.

patent of Howells[6]. Applebaum analyzed this approach and established the control-law theory governing the operation of an adaptive control loop for each array element[15]. The Applebaum algorithm maximizes the output signal-to-noise ratio (SNR) with the assumptions that the desired signal is absent most of the time and the direction of arrival of the desired signal is known. Therefore, this algorithm is frequently applied to the fields of pulsed radar or sonar systems where the desired signal is negligible compared with the jamming signals, and in practice the noise correlation matrix required for processing is approximated by the received signals at each element. His scheme is shown in Fig.2.3. The control law can be approximated by the actual implementations only if the feedback loop gain is sufficiently high. As he pointed out, however, instabilities in feedback loops may occur if the loop gains are allowed to become excessive. Furthermore, Brennan and Reed developed this MSN algorithm as an adaptive radar[16], and they presented the effects of control loops noise on the performance of the MSN adaptive array, i.e., the degradation of the output signal-to-noise ratio[17]. They derived the expressions for the first and the second order loops. For reducing the effects of control loop noise, they introduced the concept of hard limiting in the control loops and demonstrated the effectiveness of this technique[18].

Array signal processing scheme based on the least mean square error (LMS) criterion was developed for the adaptive filter presented by Widrow et al.[8]. They applied this concept to the adaptive arrays and established the LMS algorithm for the adaptive array[9]. Fig.2.4 shows the LMS adaptive array system. This adaptive algorithm adjusts the weights to minimize the error between the reference signal and the array output. It is performed either by the digital feedback control based on a steepest gradient method or by the analogue feedback control. With those

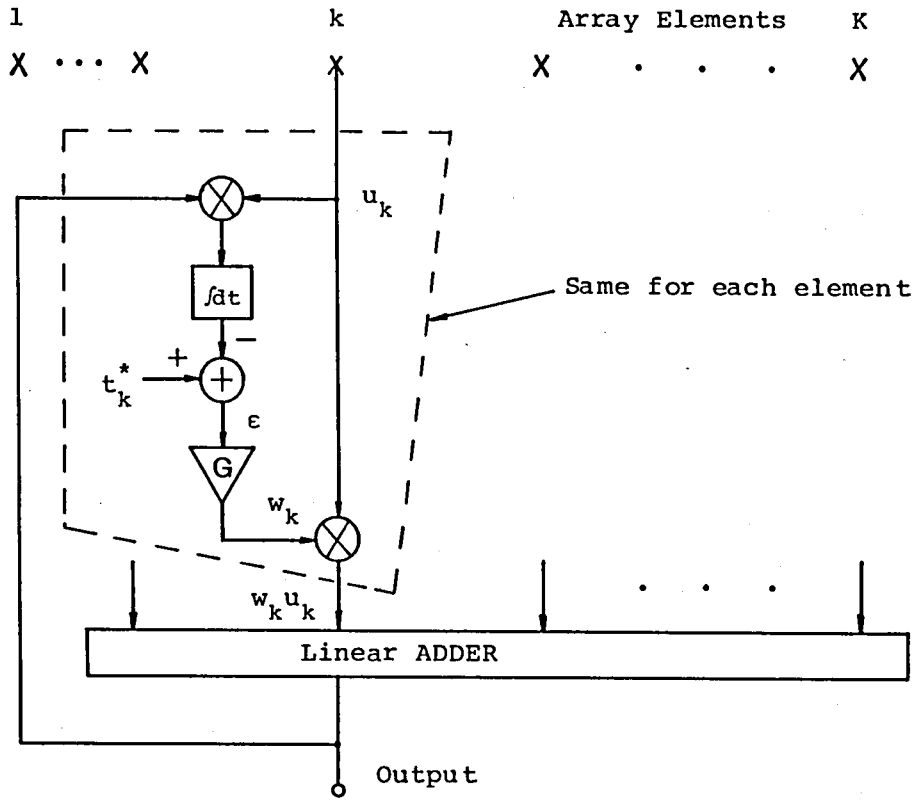

t_k^*:steering signal, u_k:input signal,

W_k:weight

Fig.2.3 Weight control scheme of Howells-Applebaum (MSN) adaptive array.

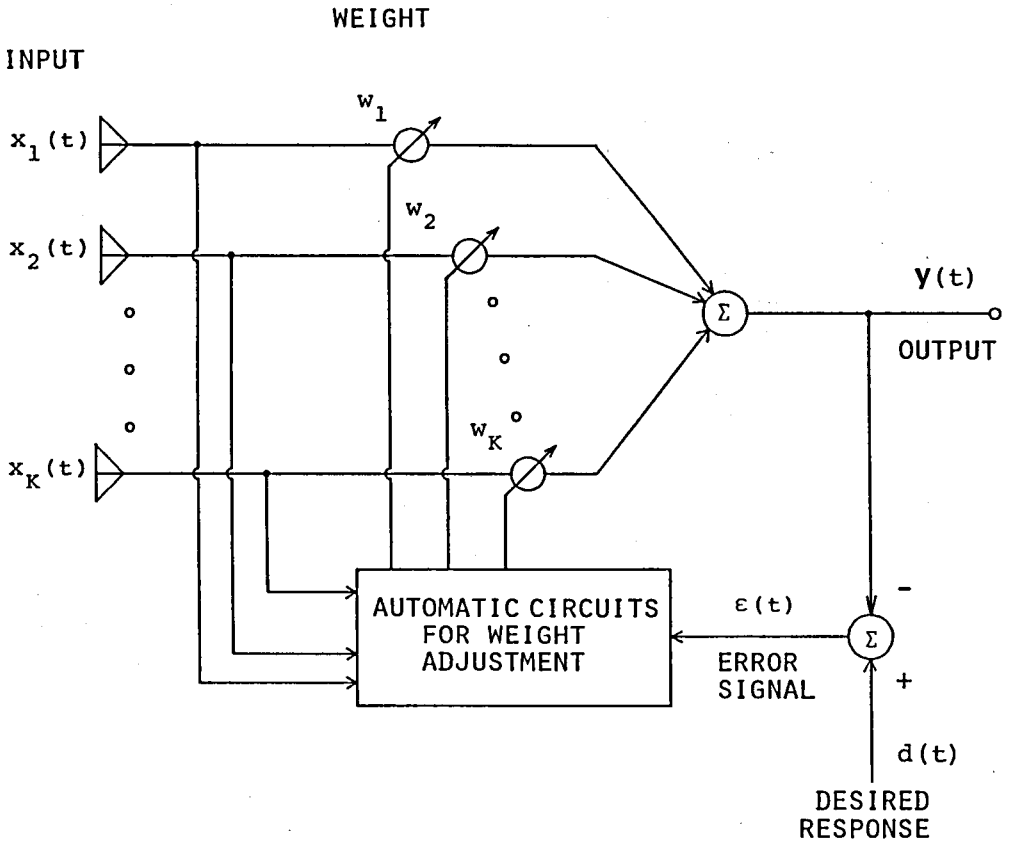

Fig.2.4 Weight control scheme of least mean square (LMS) adaptive array.

controls, the weights converge asymptotically to their optimum condition. The LMS algorithm has a merit of carrying out the adaptive null steering and adaptive beamforming at the same time, namely, it can automatically track the desired signal while also nulling interferences. On the other hand, there is a contradiction that the desired signal itself is required for the best reference signal. In practice, artificially generated (pilot) signal which is also known to the receiver is transmitted with the desired signal and used as a reference signal in the LMS array system, thus the minimization of the error between the array output and the reference signal causes pattern nulls in the directions of interferences. For the case of the amplitude modulated (AM) signal, its carrier is frequently used as a reference signal, but it was reported in Ref.[19] that the gain of the beamforming is degraded according to the degree of modulation. To make matters worse, it was shown in Ref.[19] that the LMS algorithm is unable to be applied to the other modulation methods such as frequency modulation (FM). Griffiths pointed out the limitation of the above methods with the reference signal, i.e., the fact that the presence of the actual desired signal in adaptation processing may cause a bias of weights from their optimum solution[20]. He proposed the alternative adaptive algorithm for LMS processing using the estimated correlation vector between the received signals at each channel and the reference signal. Estimation of the correlation vector requires the apriori knowledge on the spectral density and the incident direction of the desired signal. Thus, although his method cannot carry out the adaptive beamforming, it may be effective for real-time processing if the estimations could be performed easily. Chang and Tuteur also proposed the adaptive algorithm based on the LMS method which resembles Griffiths' concept[21]. It is evident that these alternative algorithms are similar

to the MSN algorithm with the steering vector. Zahm, however, pointed out that it results in the large amount of deteriorations in output signal-to-noise ratio if the estimation of the incident direction of the desired signal includes some errors[22].

In the field of seismology, Capon et al. proposed the procedures for designing the maximum-likelihood estimator in time domain and frequency domain[23]. Their method is, however, so used for the seismometers' records that off-line processing may be significant. Lacoss presented the adaptive algorithm based on the minimum-variance estimate which converges to the maximum-likelihood estimator[13]. This algorithm is designed for minimizing the system output power subject to a constraint by a steepest gradient method. He also proposed the clipped gradient method for reducing the influences of significantly anomalous data on the weights of processor. His method required the occurrence of the same waveform of the desired signal at the same time at each element, thus spatial correction filter which compensates the misalignment between the wavefront and the array geometry was indispensable. This method resembles the hard limiting in the MSN system. The above described methods made the real-time processing of the MLR possible. The MLR algorithm is very similar to the algorithm based on the constrained minimization of power (CMP) which is mentioned later.

Griffiths also proposed the adaptive algorithm based on the maximum likelihood ratio (MLR) criterion and the maximum signal-to-noise ratio (MSN) criterion[24]. The algorithm for achieving the MLR processor is derived based on the fact that under the high signal-to-noise ratio environment, the LMS processor may tend to the MLR processor. Thus, the high power pilot signal was used for adaptation. The algorithm for achieving the MSN processor also uses the steepest gradient method in the

following manner. At first, negative gradient direction of the performance measure (the output power in this case) with respect to the weights may be chosen. Then, the gradient components which minimize the desired signal may be estimated and be subtracted from the gradient to which the output power may be reduced. Detailed analysis for MSN processor was not performed because of the complexity due to the nonlinearity of the problem. Computer simulations were carried out to compare the performances of the systems obtained by the LMS, MLR and MSN algorithms. These results showed that the MSN algorithm gives the higher output signal-to-noise ratio than the LMS and MLR algorithm, however, the frequency characteristics is poorer than the others.

Applebaum introduced the MSN adaptive array with the constraint of mainbeam to prevent the above degradation of frequency characteristics to the desired signal[25]. Booker and Ong discussed the adaptive method for processing the seismometer array data subject to constraints[26]. The examples of some constraint conditions were expressed and analyzed. They suggested the possibility of the constraint condition which utilizes the information on the expected incident direction of the desired signal. Thus, some constraint conditions of the desired signal had been given much attention.

Frost summarized and analyzed in detail the LMS method subject to constraints and considered some applications of this method[27]. He presented the new constraint condition which designates the frequency characteristics of the system in digital filter form in the broadside direction to which the mainbeam is steered by a spatial correction filter. It is often called "fidelity constraint"[28]. He also presented the method to prevent the accumulation of errors in the iterative application of algorithm due to the truncation or quantization in digital computer.

Furthermore, Frost proposed a method of minimizing the output power under the linear constraint condition and established the CMP (constrained minimization of power) criterion[29]. Takao et al. paid attention to the redundancy of the spatial correction filter, and proposed the principle of directionally constrained minimization of power (DCMP) which incorporates the directional information into the constraint condition without the spatial correction filter[30]. Since the characteristics of the system with the DCMP are determined only by the weights, it is more flexible and feasible toward wider applications.

As shown above, various types of adaptive arrays have been developed by many researchers. As the algorithms for real-time processing, the digital or analogue feedback control based on the steepest gradient method is mainly adopted. Zahm presented the analytical method for evaluating the dynamic behavior of the LMS adaptive array based on the feedback control when exposed to the actual environment[31]. He showed that the time constant of decrease of the output interference power depends on its input power. Later, Reed proposed the direct calculation of the optimum weights with the estimated input correlation by the sampled input data[32]. It is a so-called sampled matrix inversion (SMI) algorithm. Although the SMI algorithm depends on accuracy of estimation of the input correlation matrix, the convergence to the optimum condition is not affected by the radio environments and hence rapid optimization can be attained compared with the gradient method.

In 1964, the first "special issue on active and adaptive antennas" was published by IEEE Transactions on Antennas and Propagation. At that time, it was a fledgling field and characterized by retrodirective and self-steering or self-focusing array systems. These were largely based on phase-lock loop and phase-conjugate network schemes. In 1970's, further

investigation was performed, leading to the second publication of "special issue on adaptive antennas" by the same IEEE Transactions in 1976. It included the adaptive interference nulling as the key capability. The passage of another decade brought us to the third special issue in the series on adaptive antennas in 1986. Just as the second special issue differed markedly from the first, so the third issue differs markedly from the second due to inclusion of the key capability for high-resolution spatial spectrum estimation. Another marked difference between the third issue and the second is the scope and level of research and development activity. In the third issue, four major groupings were chosen: (a) spatial spectrum estimation; (b) adaptive look-direction constraints; (c) adaptive algorithms/techniques; (d) applications oriented contributions. Also, recently, some authors have paid attention to the adaptive array for multipath environments where coherent interferences exist. In the following, the outlines of recent studies on the adaptive arrays and their applications are given.

The high resolution algorithms for direction finding of incident signals have been developed by Pisarenko[33], Ligget[34], Owsley[35], Schmidt[36],[37], Reddi[38], Bienvenu and Kopp[39], Johnson and Degraff[40], and Wax et al.[41]. These algorithms adopt the eigenstructure technique and yield asymptotically unbiased estimates. Among them, Schmidt presented much-referenced MUSIC (multiple signal classification) algorithm, which provides estimates of number of signals, directions of arrival, and so on[36],[37]. He showed the examples and comparisons with methods based on maximum likelihood (ML) and maximum entropy (ME), as well as conventional beamforming. Gabriel also presented the method of direction finding using spectral estimation techniques in adaptive processing antenna systems[42]. Haber and Zoltowski addressed

the investigation of spatial spectrum estimation in a coherent multiple signal environment, utilizing an array in motion[43].

For constraining the broadband desired signal, Er and Cantoni introduced the directional derivatives constraints[44]. They demonstrated the effects of introducing derivative constraints to the optimum processor by computer studies. Further, they concluded that the beamwidth in the look direction can be made as broad as desired at the price of reducing array gain. Buckley and Griffiths extended the works of Er and Cantoni, and they presented an adaptive broadband structure which employed a gradient-based weight adjustment algorithm to minimize output variance subject to a set of linear constraints on broadband directional derivatives in the desired look direction[45]. They employed a generalized sidelobe cancelling structure in which a nonadaptive (conventional) beamformer operates in parallel with an adaptive beamformer[25],[46]. By computer studies using unconstrained power minimization algorithm, they demonstrated effectiveness of their system and pointed out dependence of the system on the location of the phase reference point for the array. In addition, they developed an efficient orthogonal representation for impinging broadband sources and used it to specify a minimal set of constraint equations for the beamformer[47]. Takao and Ishizaki carried out comparison of three broadband techniques, namely, derivative constraints, multiple constraints, and a correlation constraint[48],[49], and clarified their respective characteristics. Er and Cantoni also presented a new set of linear constraints for designing broadband time domain element-space array processors. The set of linear constraints were used to ensure that the desired response of the processor over a frequency band of interest in a specified look direction could be approximated. This approach enabled the adaptive array system to achieve

the much-desired robustness against presteering vector error, and also other types of errors and mismatches[50].

The earliest prior work on the problem of signal cancellation due to coherence is that of Gabriel[51] and Widrow[52], who discussed some "spatial dither" techniques for destroying coherence by moving the antenna elements in some way. However, this techniques are not very specific and do not provide a clear general procedure. Therefore, additional research was necessary.

Shan and Kailath developed an adaptive array beamformer able to work well even when the desired signal and the interference are coherent, which is based on the uniform spatial smoothing technique[53],[54]. The spatial smoothing was originally suggested by Evans et al.[55] to resolve coherent sources. However, as we point out later, this technique has an essential limitation of suppressing coherent interferences. Similar to Evans et al., Shan and Kailath also applied their scheme to direction finding of coherent sources in conjunction with eigenstructure techniques[56],[57] and showed high resolution of the technique by simulation studies. Su, Shan and Widrow addressed this difficult coherent sources problem and presented a parallel spatial processing structure which results in a spatially smoothed maximum-likelihood estimate[58].

Duvall proposed the beamformer structures that separate the desired signal and the coherent interference through subtractive preprocessor in the adaptive beamformer[52], which makes use of two beamformers, i.e., master (Frost) beamformer and slaved beamformer as shown in Fig.2.5. This beamformer was named "Duvall beamformer". Komiyama and Takao also independently presented the same beamformer structure[59]. Citron and Kailath presented a new eigenvector technique with Duvall beamformer and demonstrated its robustness against the background noise[60]. However, as

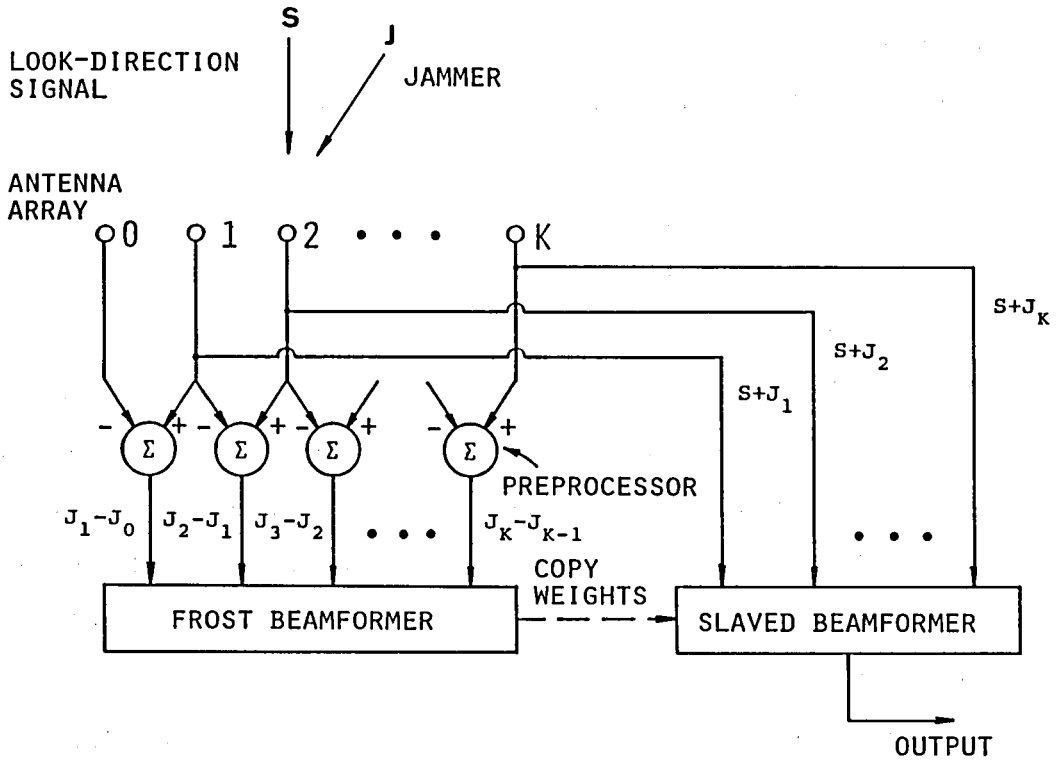

Fig.2.5 Block diagram of Duvall beamformer.

pointed out by Luthra, this Duvall beamformer is unable to null more than one coherent interference[61]. In Ref.[61], Luthra presented an alternative technique that does not require the spatial smoothing and is capable of nulling coherent or incoherent interferences while maintaining a fixed gain in the look direction. The architecture of this approach is similar to the Duvall beamformer, except instead of using the Frost beamformer in the master array, his original beamformer is introduced that calculates the array weights such that nulls are guaranteed in the directions of the interferences.

Surveying the studies summarized briefly in this chapter, we will employ mainly the adaptive array under the DCMP (directionally constrained minimization of power) principle. In the following chapters, we will present the detailed analysis and improvement on this DCMP system and some numerical results with digital computer for demonstrating the performance of this system.

CHAPTER 3

ADAPTIVE ARRAY UNDER DIRECTIONAL CONSTRAINTS

3.1 Introduction

In this chapter, we pay attention to the adaptive array which operates under the principle of the directionally constrained minimization of power (DCMP). First, we describe the general configuration of the adaptive array system and present the definition and notation of controllable system parameters and signals in Section 3.2. In Section 3.3, we explain the constraint condition for the DCMP principle and give the optimum solution which can be derived by solving the constrained minimization problem with the method of the Lagrange multipliers. Section 3.4 is devoted to the description of two representative algorithms for sampling control system by which we can obtain the optimum solution in actual radio environments. In Section 3.5, we analyze the optimum performance of the adaptive array and show it numerically for the simple case where the narrowband signals are incident on the array.

3.2 Description of the Concept

3.2.1 Receiving System of an Array and Processor

Prior to the main discussion on the adaptive array, descriptions of the receiving system are in order here. Fig.3.1 shows a general configuration of a K-element, L-tap adaptive array with transversal filters. In this figure, the adaptive processor is not depicted for

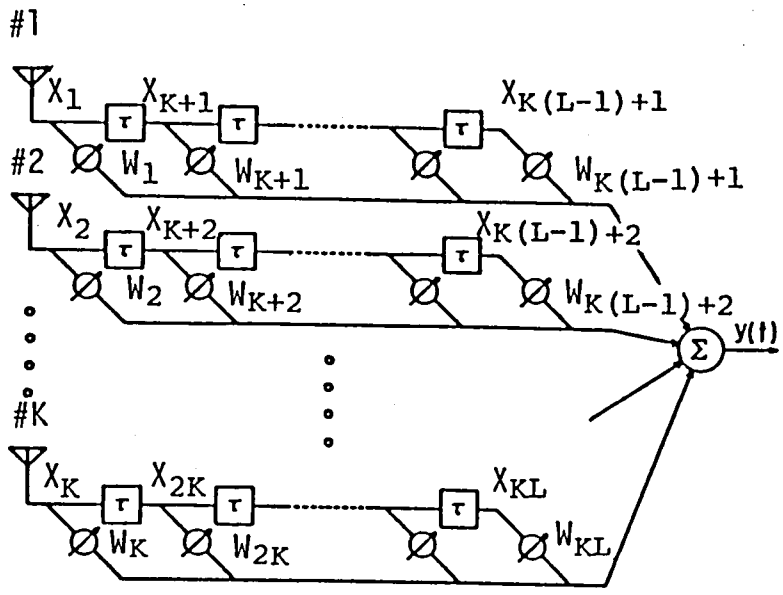

Fig.3.1 A general configuration of a K-element, L-tap adaptive array with transversal filters.

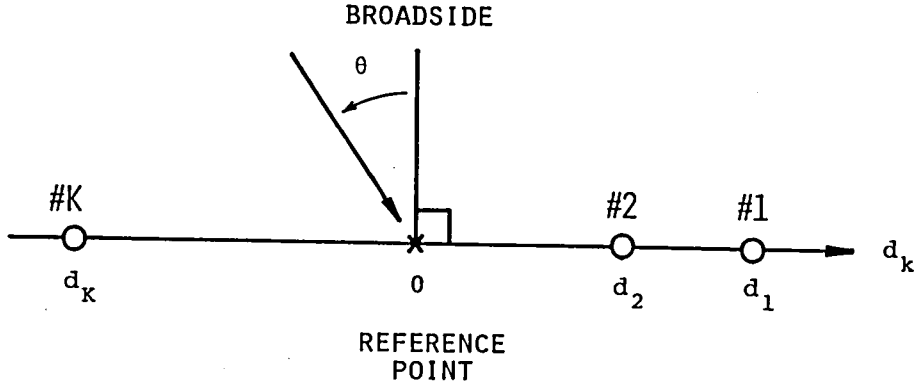

Fig.3.2 The coordinates on the baseline of the linear array.

simplicity. The time delay between the adjacent taps, τ, is equal to one quarter of the period of the center frequency of the desired signal, f_o, i.e., $\tau=1/(4f_o)$. Thus, the phase of the signal at this frequency is made to lag through the time delay by the amount of $\pi/2$, so that delayed and undelayed signal are orthogonal to each other. The w_p's(p=1, 2,.., KL) represent the variable weights which are usually positive or negative gains of the amplifiers attached to each tap point. All the weights are real. For convenience of the following formulations, we adopt vectorial expression, and denote the weights in the form of column vector as

$$\mathbf{W} = [w_1, w_2, \ldots, w_{KL}]^T \tag{3.1}$$

where the superscript T means the transpose. Hereafter, we will call **W** the weight vector. On the other hand, the x_p's(p=1, 2,.., KL) in Fig.3.1 represent the input signals at the tap point and they are connected to the corresponding weights. According to the same manner as the weights, we express the input signals in a vectorial form as follows:

$$\mathbf{X} = [x_1, x_2, \ldots, x_{KL}]^T \tag{3.2}$$

which will be called the input vector hereafter. Thus, the output of the array, y, can be given in the form of a scalar product of **X** and **W** as

$$y = \mathbf{X}^T\mathbf{W} = \mathbf{W}^T\mathbf{X} \tag{3.3}$$

The above descriptions are independent of the arrangement of the antenna elements so that we do not refer to the antenna array itself.

3.2.2 Models of Signals

In general, the input vector **X** consists of the desired signal and undesired noise. Besides, the undesired noise includes three kinds of components; (a) the coherent interference, (b) the incoherent interference, (c) the internal (thermal) noise. For simplicity, we will call the waves of (a) and (b), c-interference and i-interference,

respectively, in this thesis. The c-interference has the same source as the desired signal, but arrives through a different path, which is usually seen in multipath propagation. The i-interference, e.g., jammer, is uncorrelated with the desired signal. The internal (thermal) noise which appears at each tap with the equal average power. It is independent not only of the external waves but also of each other at different taps. We denote the input components of the desired signal, the c-interference, the i-interference and the internal noise at the p-th tap point as s_p, c_p, i_p and n_p, respectively, and vector forms are again adopted for them as follows:

$$\mathbf{S} = [s_1, s_2, \ldots, s_{KL}]^T \tag{3.4}$$

$$\mathbf{C} = [c_1, c_2, \ldots, c_{KL}]^T \tag{3.5}$$

$$\mathbf{I} = [i_1, i_2, \ldots, i_{KL}]^T \tag{3.6}$$

$$\mathbf{N} = [n_1, n_2, \ldots, n_{KL}]^T \tag{3.7}$$

Thus, eq.(3.2) can also be expressed as

$$\mathbf{X} = \mathbf{S} + \mathbf{C} + \mathbf{I} + \mathbf{N} \tag{3.8}$$

Here, we introduce various input parameters such as SNR(signal-to-noise ratio), SIR(signal-to-interference ratio) and CSR(coherent-to-signal power ratio) which are defined by the following:

(1) Input SNR is the power ratio of the input desired signal to the internal noise both of which are defined at each tap.

(2) Input SIR is the power ratio of the input desired signal to the i-interference both of which are defined in terms of the wave field.

(3) Input CSR (denoted by r) is the power ratio of the c-interference to the desired signal both of which are defined in terms of the wave field.

Next, we treat the input signals statistically. The correlation matrix of the input signals at tap points is defined as follows:

$$R_{xx} = E[\mathbf{X}\mathbf{X}^T] \tag{3.9}$$

where E[ ] denotes the expectation. Under the assumption of ergodicity, the correlation matrix is normally estimated by temporal averaging. It is to be noted that R_{xx} is a KL-dimensional symmetric matrix, which can be easily proved by the direct application of transpose operation on eq.(3.9). Under consideration of the correlation between the input signals, we obtain the following equation using eq's.(3.8) and (3.9):

$$R_{xx} = R_{dd} + R_{ii} + P_n U \tag{3.10}$$

where

$$R_{dd} = E[(\mathbf{S}+\mathbf{C})(\mathbf{S}+\mathbf{C})^T] \tag{3.11}$$

$$R_{ii} = E[\mathbf{I}\mathbf{I}^T] \tag{3.12}$$

$$P_n = E[n_p^2] \quad (p=1, 2, \ldots, KL) \tag{3.13}$$

where R_{dd} is a correlation matrix of both the desired signal and the c-interference, R_{ii} is a correlation matrix of the i-interference, P_n is the input power of the internal noise at each tap, and U is the identity matrix. R_{dd} and R_{ii} are positive semidefinite and P_n is positive (i.e., $P_n U$ is positive definite). Therefore, R_{xx} is positive definite as well as symmetric.

3.3 Constraint Condition and Optimum Solution

We introduce DCMP (Directionally Constrained Minimization of Power) approach[30]. The system tries to minimize the output power under the constraint that it must maintain a constant response to the incoming signal from a specified direction at a certain frequency. The general form of linear constraint with regard to the weights may be expressed as follows:

$$\mathbf{C}_d^T\mathbf{W} = \mathbf{H} \tag{3.14}$$

where C_d is a [KL×N] matrix called the constraint matrix provided N is the number of constraints, and H is a N-th order column vector called the constrained response vector.

Now, we will derive the simplest constraint. Suppose a K-element, L-tap array receives a CW signal with the unit amplitude, the arrival angle θ_d and frequency f_d. Then, its array output, y_d, is expressed as follows:

$$y_d = \sum_{k=1}^{K} \sum_{q=1}^{L} w_{k+(q-1)K} \cdot (1/\sqrt{L}) \cos\{2\pi f_d t + \Psi_{kq}(\theta_d)\} \tag{3.15}$$

where $\Psi_{kq}(\theta_d)$ represents the phase of the signal at the k-th element, q-th tap with respect to the reference point, and multiplication of $1/\sqrt{L}$ means that the input signal at each channel is divided by the passive and lossless power-divider and supplied to each tap. In this system, $\Psi_{kq}(\theta_d)$ has the following relationship:

$$\Psi_{kq}(\theta_d) = \Psi_{k1}(\theta_d) - (2\pi\tau)(q-1) \quad (k=1,..,K;q=1,..,L) \tag{3.16}$$

Particularly, with the linear array, $\Psi_{kq}(\theta_d)$ is expressed as

$$\Psi_{kq}(\theta_d) = -(2\pi d_k/\lambda) \sin\theta_d - (2\pi\tau)(q-1) \quad (k=1,..,K;q=1,..,L) \tag{3.17}$$

where λ is the wavelength, and d_k is the distance(either positive or negative) measured from the reference point which is defined in the coordinates shown by Fig.3.2. Here, we will constrain this signal so that its array output may have the following waveform:

$$y_d = A \cos(2\pi f_d t + \xi) \tag{3.18}$$

where A and ξ are the amplitude and phase of the specified response, respectively. Therefore, θ_d and f_d will be called the constrained direction and constrained frequency, respectively. Identifying eq.(3.15) with eq.(3.18), we obtain the following two equations:

$$\sum_{k=1}^{K} \sum_{q=1}^{L} w_{k+(q-1)K} \cdot (1/\sqrt{L}) \cos\{\Psi_{kq}(\theta_d)\} = A \cos\xi \tag{3.19}$$

$$\sum_{k=1}^{K}\sum_{q=1}^{L} w_{k+(q-1)K}\cdot(1/\sqrt{L})\sin\{\Psi_{kq}(\theta_d)\} = A\sin\xi \tag{3.20}$$

Thus, we can express eq's.(3.19) and (3.20) in the form given by eq.(3.14) and C_d and **H** in this case are given as follows:

$$C_d = (1/\sqrt{L})\begin{bmatrix} \cos\{\Psi_{11}(\theta_d)\} & \sin\{\Psi_{11}(\theta_d)\} \\ \cos\{\Psi_{21}(\theta_d)\} & \sin\{\Psi_{21}(\theta_d)\} \\ \vdots & \vdots \\ \cos\{\Psi_{K1}(\theta_d)\} & \sin\{\Psi_{K1}(\theta_d)\} \\ \cos\{\Psi_{12}(\theta_d)\} & \sin\{\Psi_{12}(\theta_d)\} \\ \vdots & \vdots \\ \cos\{\Psi_{KL}(\theta_d)\} & \sin\{\Psi_{KL}(\theta_d)\} \end{bmatrix} \tag{3.21}$$

$$\mathbf{H} = [A\cos\xi,\ A\sin\xi]^T \tag{3.22}$$

As seen from the above two equations, the number of the constraints is 2 (N=2) for the simplest constraint condition. We will call the constraint condition given by eq's.(3.21) and (3.22) "the single constraint." For simplicity, we set A=1, and ξ=0 throughout this paper. In addition, we can set the constraints for multiple θ_d's and f_d's by using the same straightforward manner and extending the column of C_d and correspondingly the row of **H**.

The total output power of the array system, P_{out}, is given by

$$P_{out} = E[y^2] = \mathbf{W}^T R_{xx}\mathbf{W} \tag{3.23}$$

P_{out} is a quadratic form with respect to **W**. Since R_{xx} is positive definite as stated previously, P_{out} grows up when every term of W increases.

Now, the problem is to find **W** which minimizes the output power subject to the given constraint condition and the formulation is given below:

$$\min_{\mathbf{W}} (P_{out} = \mathbf{W}^T R_{xx}\mathbf{W}) \tag{3.24}$$

$$\text{subject to } C_d{}^T\mathbf{W} = \mathbf{H} \tag{3.25}$$

Constrained minimization problem can be solved by the well-known method of

Lagrange multipliers. The following analysis is after Frost[27],[29].

The cost function Q(W) is defined as follows by introducing N-th order column vector consisting of undetermined Lagrange multipliers, Λ:

$$Q(W) = \frac{1}{2} W^T R_{xx} W + \Lambda^T (C_d^T W - H) \tag{3.26}$$

where coefficient 1/2 is introduced for mathematical simplicity. Eq.(3.26) is a quadratic function of W with positive definite matrix coefficient so that it has a unique minimum. Therefore, taking the gradient of Q(W) with respect to W and equating the result to zero, we can obtain the optimum solution. That is,

$$\nabla_W Q(W) = R_{xx} W + C_d \Lambda = 0 \tag{3.27}$$

and thus the optimum weight vector, W_{opt}, can be written as follows:

$$W_{opt} = - R_{xx}^{-1} C_d \Lambda \tag{3.28}$$

where R_{xx}^{-1} evidently exists since R_{xx} is positive definite. Next, we must determine the expression of Λ in terms of the previously defined vectors and matrices. Considering that the optimum weight vector must also satisfy the constraint condition given by eq.(3.14), we obtain the following equation by substituting eq.(3.28) into eq.(3.14):

$$C_d^T W_{opt} = - C_d^T R_{xx}^{-1} C_d \Lambda = H \tag{3.29}$$

Solving eq.(3.29) with respect to Λ, we can determine the Lagrange multipliers vector which is written as follows:

$$\Lambda = - (C_d^T R_{xx}^{-1} C_d)^{-1} H \tag{3.30}$$

The existence of $(C_d^T R_{xx}^{-1} C_d)^{-1}$ can be proved easily because R_{xx} is positive definite and C_d has full rank. Thus, substituting eq.(3.30) into eq.(3.28) gives the expression of W_{opt} as follows:

$$W_{opt} = R_{xx}^{-1} C_d (C_d^T R_{xx}^{-1} C_d)^{-1} H \tag{3.31}$$

Here, we will investigate the DCMP principle further. The output power P_{out} consists of the desired signal component (including c-interference),

i-interference component and internal noise component. Denoting these components by P^{d}_{out}, P^{i}_{out} and P^{n}_{out}, we have

$$P^{d}_{out} = W^{T}R_{dd}W \tag{3.32}$$

$$P^{i}_{out} = W^{T}R_{ii}W \tag{3.33}$$

$$P^{n}_{out} = P_{n}W^{T}W \tag{3.34}$$

We can interpret geometrically that the optimum point minimizing $Q(W)$ exists on the N-dimensional hyperplane given by

$$\Sigma = \{ W \mid C_{d}^{T}W = H \} \tag{3.35}$$

which will be called constraint plane. If we denote the gradients of the P^{d}_{out}, P^{i}_{out} and P^{n}_{out} on the constraint plane Σ by G_d, G_i and G_n, respectively, then the optimum weight W_{opt} is such that makes

$$G_d + G_i + G_n = 0 \quad \text{at } W = W_{opt} \tag{3.36}$$

Namely, it is the three gradients that cancel each other at the optimum point. Consider the special case that the c-interference is absent and also that the constraint condition is accurately settled. Then, since P^{d}_{out} is kept constant on the constraint plane, we have $G_d = 0$ on this plane and eq.(3.36) turns to be

$$G_i + G_n = 0 \quad \text{at } W = W_{opt} \tag{3.37}$$

Thus, G_i and G_n are shown to be equal in magnitude. It should be emphasized that the powers P^{i}_{out} and P^{n}_{out} are not necessarily balanced at the optimum point. Fig.3.3 shows conceptually the relation given by eq.(3.37).

As the measure of the system performance, we define the output SINR(signal-to-interference-plus-noise ratio) by

$$SINR = \frac{P^{d}_{out}}{P^{i}_{out} + P^{n}_{out}} \tag{3.38}$$

In general, the higher value of SINR brings about the better performance of the adaptive array.

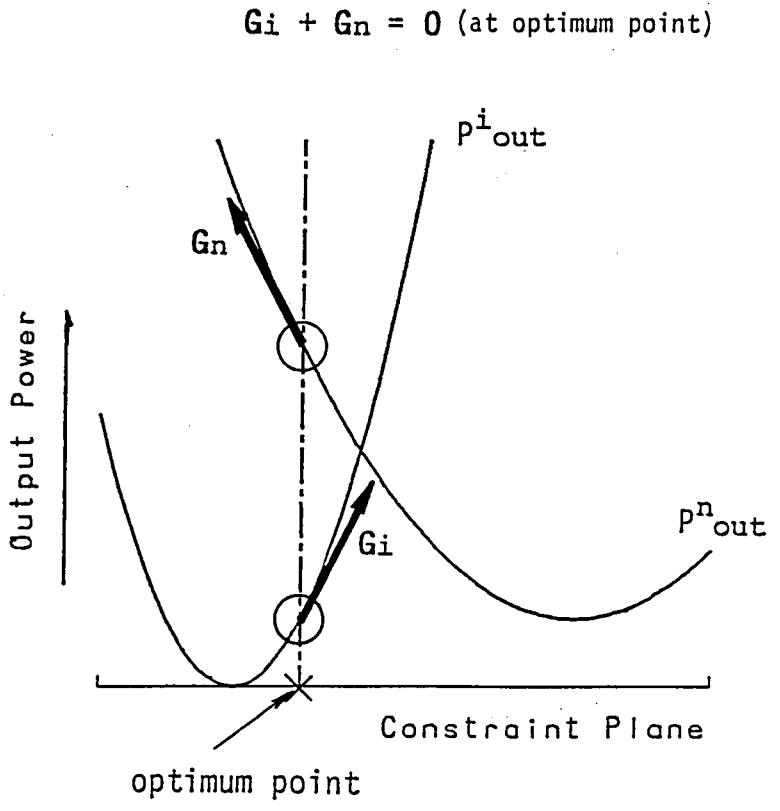

P^i_{out} = output power of interference

P^n_{out} = output power of thermal noise

Gi = power gradient of interference

Gn = power gradient of thermal noise

Fig.3.3 The relation between the interference and internal noise output powers at the optimum point on the constraint plane.

3.4 Algorithms for Sampling Control System

In this section, we introduce two algorithms for the sampling control system to get the optimum weight vector given by eq.(3.31). Since the speed of operation of digital computers has increased over the last few years and their costs have also fallen, digital implementation of adaptive arrays has attracted much interest. This makes the DCMP principle more useful. Accordingly, flexible processing algorithms must be incorporated for the accurate control of each weight.

3.4.1 The Steepest Gradient Method

The steepest gradient method is often adopted to iteratively and asymptotically converge the weight vector to its optimum. In this method, the weight vector is changed toward the direction to which the gradient of the cost function with respect to the weight vector is the steepest. Thus, the basic algorithm can be expressed as follows:

$$\mathbf{W}(m+1) = \mathbf{W}(m) - \mu \nabla_{\mathbf{W}} Q[\mathbf{W}(m)] \tag{3.39}$$

where m is an iteration number and μ is a parameter called a step size which determines the amount of change of weight vector and controls the stability and rate of convergence. In the following analysis, the method of Lagrange multipliers is also employed for the formulation and R_{xx} is temporarily assumed to be known. The cost function is a function of $\mathbf{W}$ and $\mathbf{W}$ varies with iteration, so that Lagrange multipliers are function of iteration number m. The cost function is expressed in place of eq.(3.26) as follows:

$$Q[\mathbf{W}(m)] = \frac{1}{2}\, \mathbf{W}^T(m) R_{xx} \mathbf{W}(m) + \Lambda^T(m)[C_d{}^T \mathbf{W}(m) - H] \tag{3.40}$$

where $\Lambda(m)$ is a vector of undetermined Lagrange multipliers at the m-th

iteration. Thus, the gradient of eq.(3.40) with respect to $\mathbf{W}(m)$ is given by

$$\nabla_{\mathbf{W}} Q[\mathbf{W}(m)] = R_{xx}\mathbf{W}(m) + C_d\Lambda(m) \tag{3.41}$$

Substituting eq.(3.41) into eq.(3.39), we obtain the following algorithm:

$$\mathbf{W}(m+1) = \mathbf{W}(m) - \mu[R_{xx}\mathbf{W}(m) + C_d\Lambda(m)] \tag{3.42}$$

In the above algorithm, however, the undetermined Lagrange multipliers vector is still included. Since the constraint condition must be satisfied for $\mathbf{W}(m+1)$, we have the following equation:

$$C_d^T\mathbf{W}(m+1) = C_d^T\mathbf{W}(m) - \mu[C_d^T R_{xx}\mathbf{W}(m) + C_d^T C_d\Lambda(m)] = \mathbf{H} \tag{3.43}$$

Solving eq.(3.43) with respect to $\Lambda(m)$, we can obtain the Lagrange multipliers vector which is written as follows:

$$\Lambda(m) = \frac{1}{\mu}(C_d^T C_d)^{-1}[C_d^T\mathbf{W}(m) - \mathbf{H}] - (C_d^T C_d)^{-1}C_d^T R_{xx}\mathbf{W}(m) \tag{3.44}$$

where it is noteworthy that $[C_d^T\mathbf{W}(m) - \mathbf{H}]$ in eq.(3.44) is not assumed to be zero. This intention will be explained later. Then, substituting eq.(3.44) into eq.(3.42) and operating some arithmetical manipulations gives the DCMP algorithm expressed as follows:

$$\mathbf{W}(m+1) = P[\mathbf{W}(m) - \mu R_{xx}\mathbf{W}(m)] + \mathbf{F} \tag{3.45}$$

with

$$P = U - C_d(C_d^T C_d)^{-1}C_d^T \tag{3.46}$$

$$\mathbf{F} = C_d(C_d^T C_d)^{-1}\mathbf{H} \tag{3.47}$$

where P is the projection matrix onto the constraint plane Σ and $\mathbf{F}$ is the orthogonal vector to that plane, the latter fact of which is easily proved by operating P to $\mathbf{F}$ and getting zero vector as the result. In addition, since the relation $C_d^T\mathbf{F} = \mathbf{H}$ holds, $\mathbf{F}$ is found to be the shortest vector that satisfy the constraint condition. In fact, $\mathbf{F}$ is the uniform weight vector with the mainbeam of the array pointed to the constrained direction, which is cleared in Section 3.5. Therefore, using P and $\mathbf{F}$, we

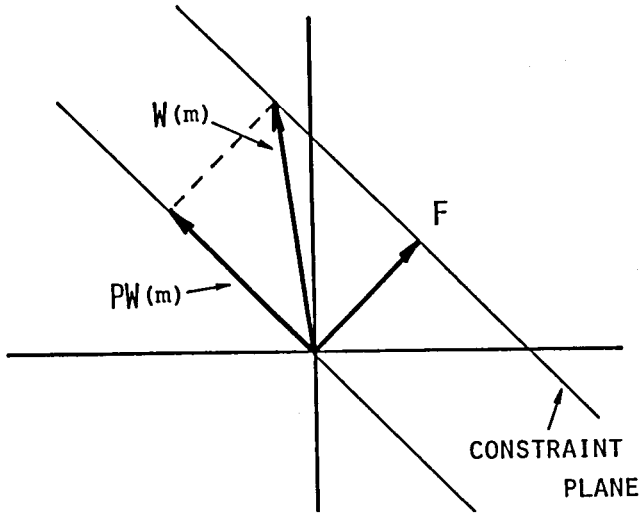

Fig.3.4 Division of a weight vector into the components parallel to and perpendicular to the constraint plane.

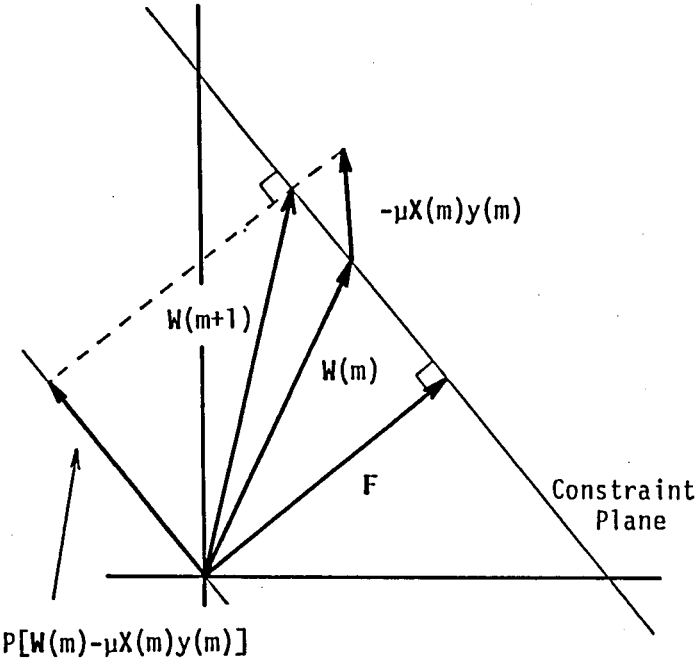

Fig.3.5 Geometrical interpretation of DCMP steepest gradient algorithm.

can express $\mathbf{W}(m)$ as follows:

$$\mathbf{W}(m) = P\mathbf{W}(m) + \mathbf{F} \tag{3.48}$$

where $P\mathbf{W}(m)$ and $\mathbf{F}$ are orthogonal to each other. The relation of eq.(3.48) is illustrated in Fig.3.4 for simple two-dimensional weight vector.

Next, in the actual system, the correlation matrix R_{xx} is not known, and it is necessary to adopt some estimate of this matrix. We approximate R_{xx} in eq.(3.45) by $\mathbf{X}(m)\mathbf{X}^T(m)$ where $\mathbf{X}(m)$ represents the sampled value of the input vector at the m-th iteration. Thus, the practical form of the algorithm is written as follows:

$$\mathbf{W}(m+1) = P[\mathbf{W}(m) - \mu\mathbf{X}(m)y(m)] + \mathbf{F} \tag{3.49}$$

where

$$y(m) = \mathbf{X}^T(m)\mathbf{W}(m) = \mathbf{W}^T(m)\mathbf{X}(m) \tag{3.50}$$

and $y(m)$ represents the sampled value of array output at the m-th iteration. Here, the following should be noticed: The relation $C_d{}^T\mathbf{W}(m)=\mathbf{H}$ is not assumed to hold and the relation $C_d{}^T\mathbf{W}(m+1)=\mathbf{H}$ is always guaranteed throughout the derivation of the algorithm shown by eq.(3.49). This means that even if once the weight vector at the m-th iteration does not satisfy the constraint condition because of some errors, the weight vector at the next (m+1)-th iteration does not run away from the constraint plane. Therefore, even a large number of the iterative application of this algorithm does not accumulate the errors in each weight value. Fig.3.5 shows the geometrical interpretation of this adaptive algorithm, which demonstrates the function of error correction.

In a digital loop, the problem of stability must be argued. The loop stability in a digital loop depends on the loop gain which corresponds to a step size μ in our problem. After Frost[27],[29], for the proof of convergence of the algorithm, the behavior of the Euclidian norm of the difference vector between the actual weight vector and the optimum weight

vector is examined which must converge to zero as the iteration number increases. Taking the expectation of both sides of eq.(3.49) gives the following equation:

$$E[\mathbf{W}(m+1)] = P\{E[\mathbf{W}(m)] - \mu R_{xx}E[\mathbf{W}(m)]\} + \mathbf{F} \tag{3.51}$$

We define the difference vector $\mathbf{V}(m)$ by

$$\mathbf{V}(m) = E[\mathbf{W}(m)] - \mathbf{W}_{opt} \tag{3.52}$$

Subtracting the optimum weight vector from both sides of eq.(3.51) and using eq's.(3.48) and (3.52) and the relation $PR_{xx}\mathbf{W}_{opt}=\mathbf{0}$, we get the following equation in terms of $\mathbf{V}(m)$:

$$\begin{aligned}\mathbf{V}(m+1) &= [U - \mu PR_{xx}P]\mathbf{V}(m) \\ &= [U - \mu PR_{xx}P]^{m+1}\mathbf{V}(0)\end{aligned} \tag{3.53}$$

From eq.(3.53), it follows that the matrix $PR_{xx}P$ determines both the convergence and steady-state performance of this algorithm. $PR_{xx}P$ is a KL-dimensional symmetric matrix because both P and R_{xx} are symmetric. Therefore, KL eigenvectors of this matrix are all orthogonal to each other. Since direct calculation shows that $PR_{xx}PC_d=0$ and N column vectors of the constraint matrix C_d are linearly independent of each other, the matrix $PR_{xx}P$ has N zero eigenvalues, corresponding to the column vectors of C_d[27]. It is also shown in Ref.[27] that the matrix $PR_{xx}P$ has KL-N nonzero eigenvalues. Therefore, the N eigenvectors whose eigenvalues are zero are normal to the constraint plane and the remaining KL-N eigenvectors whose eigenvalues are nonzero lie entirely within the constraint plane. On the other hand, if $\mathbf{W}(0)$ is such that satisfies $C_d^T\mathbf{W}(0)=\mathbf{H}$, for example, $\mathbf{W}(0)=\mathbf{F}$, then we can confirm $P\mathbf{V}(0)=\mathbf{V}(0)$ easily. It means that $\mathbf{V}(0)$ also lies within the constraint plane. Consequently, the initial difference vector $\mathbf{V}(0)$ can be expressed by a linear combination of the KL-N eigenvectors of $PR_{xx}P$ whose associated eigenvalues are nonzero. Then, $\mathbf{V}(0)$ is expressed as follows:

$$\mathbf{V}(0) = \sum_{p=1}^{KL-N} a_p \mathbf{G}_p \tag{3.54}$$

where $\mathbf{G}_p$'s(p=1, 2,.., KL-N) are eigenvectors of $PR_{xx}P$ with nonzero eigenvalues. a_p's(p=1, 2,.., KL-N) are undetermined coefficients. Substituting eq.(3.54) into eq.(3.53) and operating some arithmetical manipulations, we obtain the following expression:

$$\mathbf{V}(m+1) = \sum_{p=1}^{KL-N} a_p(1 - \mu\lambda_p)^{m+1}\mathbf{G}_p \tag{3.55}$$

where λ_p's are eigenvalues associated with the eigenvectors $\mathbf{G}_p$'s. If we choose μ to satisfy the relation $0 < (1 - \mu\lambda_p) < 1$ for all p(=1, 2,.., KL-N), convergence of eq.(3.55) to zero vector, namely, that of eq.(3.49) to the optimum weight vector may be guaranteed in an expectation sense. Thus, μ must be chosen as follows for the convergence of the algorithm:

$$0 < \mu < \frac{1}{\lambda_{max}} \tag{3.56}$$

where λ_{max} is the maximum eigenvalue of $PR_{xx}P$ and proved in Ref.[27] to be related to the maximum eigenvalue of R_{xx}, i.e., σ_{max} by

$$0 < \lambda_{max} \leq \sigma_{max} \tag{3.57}$$

In practice, since the calculation of λ_{max} needs much labor and we must keep the ultimate weight vector obtained by the algorithm from being misadjusted by some additional noise, the sufficient condition of eq.(3.56) is adopted for safety in consideration of eq.(3.57), which is expressed as follows[27],[29]:

$$0 < \mu < \frac{2}{3\ \mathrm{trace}(R_{xx})} \tag{3.58}$$

where "trace" denotes the sum of the diagonal elements of the matrix. Therefore, trace(R_{xx}) in eq.(3.58) means the sum of the powers of the tap voltages and evidently satisfies

$$\sigma_{max} \leq \mathrm{trace}(R_{xx}) \tag{3.59}$$

In addition, to attain the more stable performance in the steady state, we can smooth the feedback amount of $\mathbf{X}(m)y(m)$ in the algorithm of eq.(3.49)[62]. It is called a smoothing algorithm and expressed as follows:

$$\mathbf{W}(m+1) = P[\mathbf{W}(m) - \mu\Delta(m)] + \mathbf{F} \tag{3.60}$$

with

$$\Delta(m) = \frac{1}{J}\sum_{i=1}^{J}\mathbf{X}(m_i)y(m_i) \tag{3.61}$$

where J is the number of smoothing and m_i denotes the i-th side-iteration number between the m-th iteration and the following (m+1)-th iteration.

3.4.2 Direct Method by Sampled Matrix Inversion

An alternative to the steepest gradient method in the previous section is a direct method by sampled matrix inversion (SMI)[32],[63],[64]. The gradient method has the difficulty that the convergence is slow for the smaller eigenvalues of the matrix $PR_{xx}P$, as is easily seen from eq.(3.55). Thus, the requirement for algorithms which make convergence more rapid even for the smaller eigenvalues has stimulated researches aiming at efficient methods of performing more direct matrix inversion. In the SMI method, an estimate of the correlation matrix is made by averaging successive data samples, and this estimated correlation matrix is used directly in eq.(3.31) to get the optimum weight vector.

The general algorithm for the estimate can be expressed as follows:

$$\begin{cases} R_{xx}(1) = \mathbf{X}(1)\mathbf{X}^T(1) \\ R_{xx}(m) = (1-\beta)R_{xx}(m-1) + \beta\mathbf{X}(m)\mathbf{X}^T(m) \quad (m=2,\ 3,\ldots) \end{cases} \tag{3.62}$$

where β is a parameter which satisfies $0 < \beta < 1$ and controls the time constant for the estimate. When $\beta = 1/m$, eq.(3.62) is rewritten by

$$R_{xx}(m) = \frac{1}{m}\sum_{i=1}^{m} \mathbf{X}(i)\mathbf{X}^T(i) \tag{3.63}$$

Eq.(3.63) means that the correlation matrix is estimated by the uniform averaging of $\mathbf{X}(i)\mathbf{X}^T(i)$'s(i=1, 2,..,m). We will call this approach "the simple SMI" hereafter. If, on the other hand, β is constant at every iteration, eq.(3.62) can be rewritten by

$$R_{xx}(m) = (1-\beta)^{m-1}R_{xx}(1) + \beta\sum_{i=2}^{m}(1-\beta)^{m-i}\mathbf{X}(i)\mathbf{X}^T(i) \quad (m=2, 3,..) \tag{3.64}$$

From the above algorithm, it follows that the older data samples have the less contribution to $R_{xx}(m)$ in an exponential manner. This approach is called the deweighting matrix estimate and is useful for nonstationary radio environments.

Using the estimated matrix of eq.(3.62) in eq.(3.31), we obtain the weight vector at the m-th iteration which is expressed as follows:

$$\mathbf{W}(m) = R_{xx}^{-1}(m)C_d[C_d^T R_{xx}^{-1}(m)C_d]^{-1}\mathbf{H} \tag{3.65}$$

If the $R_{xx}(m)$ is ill-conditioned or singular, we may render it invertible by augmenting its diagonals by a small amount.

Alternatively, inverting the both sides of eq.(3.62) by the matrix inversion formula[63], we can obtain the inverse matrix $R_{xx}^{-1}(m)$ recursively as

$$R_{xx}^{-1}(m) = \frac{1}{1-\beta}R_{xx}^{-1}(m-1) + \frac{\beta R_{xx}^{-1}(m-1)\mathbf{X}(m)\mathbf{X}^T(m)R_{xx}^{-1}(m-1)}{(1-\beta)^2 + \beta(1-\beta)\mathbf{X}^T(m)R_{xx}^{-1}(m-1)\mathbf{X}(m)} \tag{3.66}$$

In this way, we need not calculate R_{xx}^{-1} straightforward, so the total time of calculation for the weight vector is reduced.

In addition, we may smooth the second term of eq.(3.62) or eq.(3.66) by using some data samples before adding it to each first one. After this

smoothing, the optimum weight vector is obtained by using the resultant matrix in eq.(3.65). This aim is to efficiently attain the more accurate estimate and the more stable performance, which is in common with the gradient method.

3.5 Analysis of Optimum Performance

3.5.1 Complex Expression for Analysis

When the input signals are CW or narrowband, we can treat them in complex expressions and evaluate the performance of the antenna system in terms of the response to CW. In this case, each channel of the array system has only to have two taps and thus each two-tap filter can be expressed by one complex weight as shown by Fig.3.6. In the following analysis, this complex notation is introduced. Then, from eq's.(3.1), (3.21) and (3.22), matrices $\mathbf{W}$, C_d and $\mathbf{H}$ must be modified as follows:

$$\mathbf{W} = [w_1+jw_{1+K},\ w_2+jw_{2+K},\ldots,\ w_K+jw_{2K}]^T \tag{3.67}$$

$$\mathbf{C}_d = (1/\sqrt{2})[\exp\{j\Psi_1(\theta_d)\},\ldots,\ \exp\{j\Psi_K(\theta_d)\}]^T \tag{3.68}$$

$$H = 1 \text{ (scalar)} \tag{3.69}$$

where

$$\Psi_k(\theta_d) = \Psi_{k1}(\theta_d) \quad (k=1,\ 2,..,\ K) \tag{3.70}$$

which represent the phase of the signal from the constrained direction θ_d at each array element with respect to the reference point. Thus, the constraint condition of eq.(3.14) is modified as

$$\mathbf{C}_d^T\mathbf{W}^* = H \tag{3.71}$$

where superscript * denotes the complex conjugate. With the complex notation of input vector $\mathbf{X}$ defined by

$$\mathbf{X} = [x_1+jx_{1+K},\ x_2+jx_{2+K},\ldots,\ x_K+jx_{2K}]^T, \tag{3.72}$$

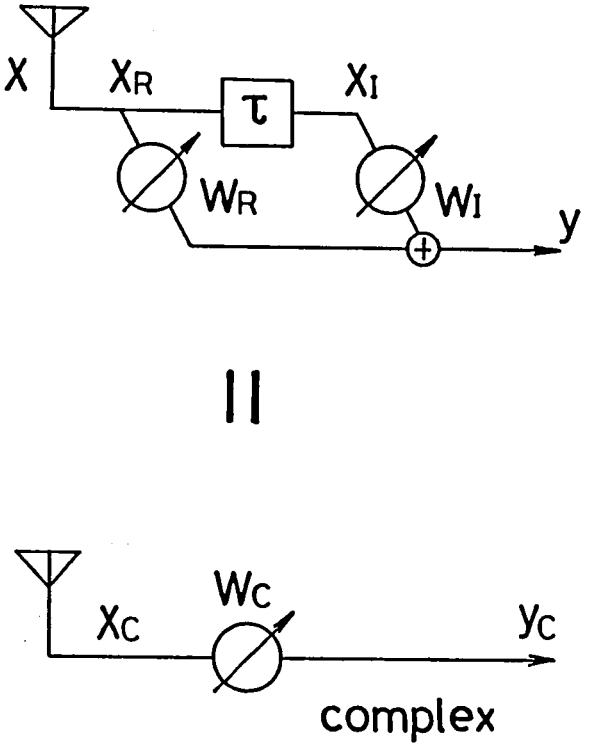

Fig.3.6 The relation between two-tap transversal filter and one complex weight.

the complex array output is expressed as follows:

$$y = \mathbf{X}^T\mathbf{W}^* = \mathbf{W}^\dagger\mathbf{X} \tag{3.73}$$

where superscript † denotes the complex conjugate transpose. The real array output can be obtained by taking the real part of the complex one. It is to be noted here that the inner product of two complex vectors is in compliance with Euclidian inner-product notation. The output power is thus expressed as

$$P_{out} = E[yy^*] = \mathbf{W}^\dagger R_{xx}\mathbf{W} \tag{3.74}$$

where

$$R_{xx} = E[\mathbf{X}\mathbf{X}^\dagger] \tag{3.75}$$

R_{xx} is a complex correlation matrix which is Hermitian and positive definite.

Now, we will derive the complex optimum weight vector. The cost function $Q(\mathbf{W})$ is defined as follows:

$$Q(\mathbf{W}) = \mathbf{W}^\dagger R_{xx}\mathbf{W} + \Lambda(\mathbf{C}_d^T\mathbf{W}^* - H) \tag{3.76}$$

where Λ is the complex undetermined Lagrange multiplier. The gradient of eq.(3.76) with respect to $\mathbf{W}^*$ is given by

$$\nabla_{\mathbf{W}^*}Q(\mathbf{W}) = R_{xx}\mathbf{W} + \mathbf{C}_d\Lambda \tag{3.77}$$

where concerning the operation of complex differentiation, we follow Ref.[65]. A necessary condition for eq.(3.76) to be minimized is that the gradient be equal to zero so that

$$R_{xx}\mathbf{W} + \mathbf{C}_d\Lambda = \mathbf{0} \tag{3.78}$$

Therefore, the optimum weight vector is given by

$$\mathbf{W}_{opt} = - R_{xx}^{-1}\mathbf{C}_d\Lambda \tag{3.79}$$

where Λ remains to be determined. This value may now be evaluated from the conjugate constraint condition of eq.(3.71):

$$\mathbf{C}_d^\dagger\mathbf{W}_{opt} = - \mathbf{C}_d^\dagger R_{xx}^{-1}\mathbf{C}_d\Lambda = H^* \tag{3.80}$$

It then follows that the scalar Λ is given by

$$\Lambda = -(\mathbf{C}_d^{\dagger}\mathbf{R}_{xx}^{-1}\mathbf{C}_d)^{-1}\mathbf{H}^* \tag{3.81}$$

Combining eq.(3.79) and eq.(3.81), we can obtain the complex optimum weight vector which is written as follows:

$$\mathbf{W}_{opt} = \mathbf{R}_{xx}^{-1}\mathbf{C}_d(\mathbf{C}_d^{\dagger}\mathbf{R}_{xx}^{-1}\mathbf{C}_d)^{-1}\mathbf{H}^* \tag{3.82}$$

Likewise, the complex expressions of two algorithms for sampling control system given by eq's.(3.49), (3.62), (3.65) and (3.66) are derived as follows:

(a) Steepest gradient method

$$\mathbf{W}(m+1) = \mathbf{P}[\mathbf{W}(m) - \mu\mathbf{X}(m)y^*(m)] + \mathbf{F} \tag{3.83}$$

with

$$\mathbf{P} = \mathbf{U} - \mathbf{C}_d(\mathbf{C}_d^{\dagger}\mathbf{C}_d)^{-1}\mathbf{C}_d^{\dagger} = \mathbf{U} - (2/K)\mathbf{C}_d\mathbf{C}_d^{\dagger} \tag{3.84}$$

$$\mathbf{F} = \mathbf{C}_d(\mathbf{C}_d^{\dagger}\mathbf{C}_d)^{-1}\mathbf{H}^* = (2\mathbf{H}^*/K)\mathbf{C}_d \tag{3.85}$$

(b) Sampled matrix inversion (SMI)

$$\mathbf{W}(m) = \mathbf{R}_{xx}^{-1}(m)\mathbf{C}_d[\mathbf{C}_d^{\dagger}\mathbf{R}_{xx}^{-1}(m)\mathbf{C}_d]^{-1}\mathbf{H}^* \tag{3.86}$$

with

$$\begin{cases} \mathbf{R}_{xx}(1) = \mathbf{X}(1)\mathbf{X}^{\dagger}(1) \\ \mathbf{R}_{xx}(m) = (1-\beta)\mathbf{R}_{xx}(m-1) + \beta\mathbf{X}(m)\mathbf{X}^{\dagger}(m) \quad (m=2,\ 3,..) \end{cases} \tag{3.87}$$

or

$$\begin{cases} \mathbf{R}_{xx}^{-1}(1) = \{\mathbf{X}(1)\mathbf{X}^{\dagger}(1)\}^{-1} \\ \mathbf{R}_{xx}^{-1}(m) = \dfrac{1}{1-\beta}\,\mathbf{R}_{xx}^{-1}(m-1) \\ \qquad + \dfrac{\beta\,\mathbf{R}_{xx}^{-1}(m-1)\mathbf{X}(m)\mathbf{X}^{\dagger}(m)\mathbf{R}_{xx}^{-1}(m-1)}{(1-\beta)^2 + \beta(1-\beta)\mathbf{X}^{\dagger}(m)\mathbf{R}_{xx}^{-1}(m-1)\mathbf{X}(m)} \quad (m=2,\ 3,..) \end{cases} \tag{3.88}$$

Here, it should be noticed that the vector $\mathbf{F}$ of eq.(3.85) offers the uniform complex weight with the mainbeam of the array steered to the constrained direction, which is easily seen from the elements of $\mathbf{C}_d$ given by eq.(3.68) and the relation $\mathbf{C}_d^{T}\mathbf{F}^*=\mathbf{H}$.

3.5.2 Performance Analysis and Numerical Examples

Next, we consider the optimum performance for the simple case where two narrowband signals, the desired signal and one i-interference, are incident on the array and the thermal noise exists at each weight. The complex input vectors of the desired signal and the i-interference are given by

$$\mathbf{S}(t) = s(t)\mathbf{Z}_s = (1/\sqrt{2})s(t)[\exp\{j\Psi_1(\theta_s)\},\ldots,\exp\{j\Psi_K(\theta_s)\}]^T \quad (3.89)$$

$$\mathbf{I}(t) = i(t)\mathbf{Z}_i = (1/\sqrt{2})i(t)[\exp\{j\Psi_1(\theta_i)\},\ldots,\exp\{j\Psi_K(\theta_i)\}]^T \quad (3.90)$$

where $s(t)$ and $i(t)$ represent the complex instantaneous signals at the reference point of the desired signal and the i-interference, respectively, and $\mathbf{Z}_s$ and $\mathbf{Z}_i$ their phasor vectors. θ_s and θ_i are the angles of arrival of the desired signal and the i-interference, respectively, and $\Psi_k(\theta_s)$ and $\Psi_k(\theta_i)$ are their phases at the k-th element. Since the desired signal arrives from the constrained direction θ_d, it holds that $\mathbf{Z}_s=\mathbf{C}_d$. Thus, the complex correlation matrix R_{xx} can be expressed as follows by using eq's.(3.10)-(3.13), (3.89) and (3.90):

$$R_{xx} = P_n U + P_s \mathbf{C}_d \mathbf{C}_d^{\dagger} + P_i \mathbf{Z}_i \mathbf{Z}_i^{\dagger} \quad (3.91)$$

where P_s and P_i are the input powers of the desired signal and the i-interference and given by the following equations:

$$P_s = \lim_{T\to\infty} \frac{1}{T} \int_0^T |s(t)|^2 dt \quad (3.92)$$

$$P_i = \lim_{T\to\infty} \frac{1}{T} \int_0^T |i(t)|^2 dt \quad (3.93)$$

Now, we define the following matrix:

$$R_n = P_n U + P_i \mathbf{Z}_i \mathbf{Z}_i^{\dagger} \quad (3.94)$$

which is a correlation matrix of the unwanted noise components. Then, eq.(3.91) is expressed as follows:

$$R_{xx} = R_n + P_s \mathbf{C}_d \mathbf{C}_d^{\dagger} \quad (3.95)$$

Therefore, using the matrix inversion formula[63], the inversion of R_{xx} of eq.(3.95) is written as follows:

$$R_{xx}^{-1} = R_n^{-1} - \frac{P_s R_n^{-1} C_d C_d^{\dagger} R_n^{-1}}{1 + P_s C_d^{\dagger} R_n^{-1} C_d} \tag{3.96}$$

Similarly, the inversion of R_n of eq.(3.94) is given by

$$R_n^{-1} = \frac{1}{P_n} U - \frac{2P_i Z_i Z_i^{\dagger}}{P_n(2P_n + KP_i)} \tag{3.97}$$

After postmultiplying R_{xx}^{-1} of eq.(3.96) by C_d and operating some arithmetic manipulations, $R_{xx}^{-1}C_d$ is expressed as follows:

$$R_{xx}^{-1} C_d = \zeta R_n^{-1} C_d \tag{3.98}$$

where

$$\zeta = \frac{1}{1 + P_s C_d^{\dagger} R_n^{-1} C_d} \tag{3.99}$$

Substituting eq.(3.97) into eq.(3.98) yields the following equation:

$$R_{xx}^{-1} C_d = \frac{\zeta}{P_n} C_d - \frac{2\zeta P_i Z_i^{\dagger} C_d}{P_n(2P_n + KP_i)} Z_i \tag{3.100}$$

Thus, the optimum weight vector is expressed as follows by using eq's.(3.82), (3.100) and the uniform weight vector $\mathbf{F}$ given by eq.(3.85):

$$W_{opt} = \frac{(2P_n + KP_i)\mathbf{F} - (2P_i Z_i^{\dagger}\mathbf{F})Z_i}{2P_n + KP_i(1 - |Z_i^T \mathbf{F}^*|^2/|H|^2)} \tag{3.101}$$

In the optimum state with the weight vector of eq.(3.101), the output power P_{out} is given by

$$P_{out} = W_{opt}^{\dagger} R_{xx} W_{opt} \tag{3.102}$$

This output power can be divided into the three components which are contributed by the desired signal, i-interference and thermal noise, respectively, and they are expressed as follows by using eq's.(3.91) and (3.101):

$$\begin{aligned} P^S{}_{out} &= P_s W_{opt}^{\dagger} C_d C_d^{\dagger} W_{opt} \\ &= P_s |H^*|^2 \end{aligned} \tag{3.103}$$

$$P^{i}_{out} = P_i \mathbf{W}_{opt}{}^{\dagger} \mathbf{Z}_i \mathbf{Z}_i{}^{\dagger} \mathbf{W}_{opt}$$

$$= P_i |\mathbf{Z}_i{}^{T} \mathbf{F}^{*}|^2 \frac{(2P_n)^2}{\{2P_n + KP_i(1 - |\mathbf{Z}_i{}^{T} \mathbf{F}^{*}|^2/|H|^2)\}^2} \tag{3.104}$$

$$P^{n}_{out} = P_n \mathbf{W}_{opt}{}^{\dagger} \mathbf{W}_{opt}$$

$$= \frac{2}{K} P_n |H|^2 + \frac{2KP_n P_i{}^2 |\mathbf{Z}_i{}^{T} \mathbf{F}^{*}|^2 (1 - |\mathbf{Z}_i{}^{T} \mathbf{F}^{*}|^2/|H|^2)}{\{2P_n + KP_i(1 - |\mathbf{Z}_i{}^{T} \mathbf{F}^{*}|^2/|H|^2)\}^2} \tag{3.105}$$

where $\mathbf{Z}_i{}^{T} \mathbf{F}^{*}$ represents the response in the direction of the i-interference of the directional pattern by the uniform weight $\mathbf{F}$. Especially when the linear equispaced array with the element spacing of "d" is used, the $\mathbf{Z}_i{}^{T} \mathbf{F}^{*}$ is expressed as follows:

$$\mathbf{Z}_i{}^{T} \mathbf{F}^{*} = A_{di} H \tag{3.106}$$

$$A_{di} = \frac{\sin\{(K\pi d/\lambda)(\sin \theta_d - \sin \theta_i)\}}{K \sin\{(\pi d/\lambda)(\sin \theta_d - \sin \theta_i)\}} \tag{3.107}$$

Assuming that the strong i-interference arrives within the sidelobe region of the array so that we can set $(|\mathbf{Z}_i{}^{T} \mathbf{F}^{*}|^2/|H|^2) \ll 1$ and $2P_n \ll KP_i$, we can approximate eq's.(3.104) and (3.105) as follows:

$$P^{i}_{out} \simeq P_i |\mathbf{Z}_i{}^{T} \mathbf{F}^{*}|^2 \{2P_n/(KP_i)\}^2 \propto (1/P_i) \tag{3.108}$$

$$P^{n}_{out} \simeq (2/K) P_n (|H|^2 + |\mathbf{Z}_i{}^{T} \mathbf{F}^{*}|^2) \propto P_n \tag{3.109}$$

Eq.(3.108) designates that the output power of the i-interference, P^{i}_{out}, is nearly in inverse proportion to its input power, P_i. This effect is called "power inversion". Furthermore, in eq.(3.108), $P_i |\mathbf{Z}_i{}^{T} \mathbf{F}^{*}|^2$ represents the output power of the i-interference in the case of receiving it with the uniform weight $\mathbf{F}$. By reforming eq.(3.108), we obtain the following equation:

$$\frac{P_i |\mathbf{Z}_i{}^{T} \mathbf{F}^{*}|^2}{P^{i}_{out}} \simeq (K/2)^2 (P_i/P_n)^2 \tag{3.110}$$

This parameter is called "processing gain" which represents the degree of suppression of the i-interference by the adaptive optimum weight with

reference to that by the uniform weight. The higher value of it means the better performance of the system. From eq.(3.110), it turns out that the stronger i-interference over the thermal noise level yields the higher processing gain and that the more number of array elements also leads to the higher one. On the other hand, $(2/K)P_n|H|^2$ in eq.(3.109) is equal to the output power of the thermal noise by the uniform weight system and the additional term $(2/K)P_n|Z_i^T F^*|^2$ is its increment for the suppression of the strong i-interference in the optimum state. The ratio of both terms is expressed as follows:

$$\frac{(2/K)P_n|Z_i^T F^*|^2}{(2/K)P_n|H|^2} = |Z_i^T F^*|^2/|H|^2 \ll 1 \qquad (3.111)$$

which is found to be very small under the present assumption.

Thus, it is proved that with the DCMP adaptive array, the desired signal can be preserved and the strong i-interference can be suppressed at the expense of slight increment of the thermal noise at the array output, resulting in the high output SINR.

Next, we will show the numerical examples. They are carried out on a 4-element (K=4), 2-tap (L=2) equispaced linear array with isotropic array elements and the element spacing of a half wavelength. The desired signal and i-interference are narrowband plane waves. The parameters of input used in the following examples are shown in Table 3.1. Fig.3.7 shows the directional patterns and frequency characteristics in the direction of the i-interference. (a) and (b) in Fig.3.7 correspond to the results of the uniform weight system and the adaptive optimum weight system, respectively. In the uniform weight system of (a), the system has the finite response in the direction of the i-interference, which results in the low output SINR of -5.61dB. In the optimum weight system of (b), on the contrary, we can see that while the desired signal is preserved at the

prescribed level, the null point is created in the direction and frequency of the i-interference. Therefore, a higher output SINR is obtained which is 22.85dB. As the reference, the values of output power of each component are shown in Table 3.2. We can find that the output power of the i-interference is very small compared with that of the thermal noise in the adaptive optimum system. The reason for this is that the DCMP principle tries to balance both output-power gradients of the i-interference and the thermal noise on the constraint plane, not both output powers themselves.

Table 3.1 Input data used in the numerical examples of Fig.3.7.

desired signal (S)	angle of arrival : $\theta_s = 0°$
	power : $P_s = 1$
incoherent (I)	angle of arrival : $\theta_i = 60°$
interference	power : $P_i = 100$
thermal noise	power : $P_n = 0.01$

Table 3.2 Output components and SINR corresponding to the results in Fig.3.7.

	(a) uniform weight	(b) optimum weight
desired signal	1.0	1.0
i-interference	3.64	9.79×10^{-9}
thermal noise	5.0×10^{-3}	5.19×10^{-3}
SINR (dB)	-5.61	22.85

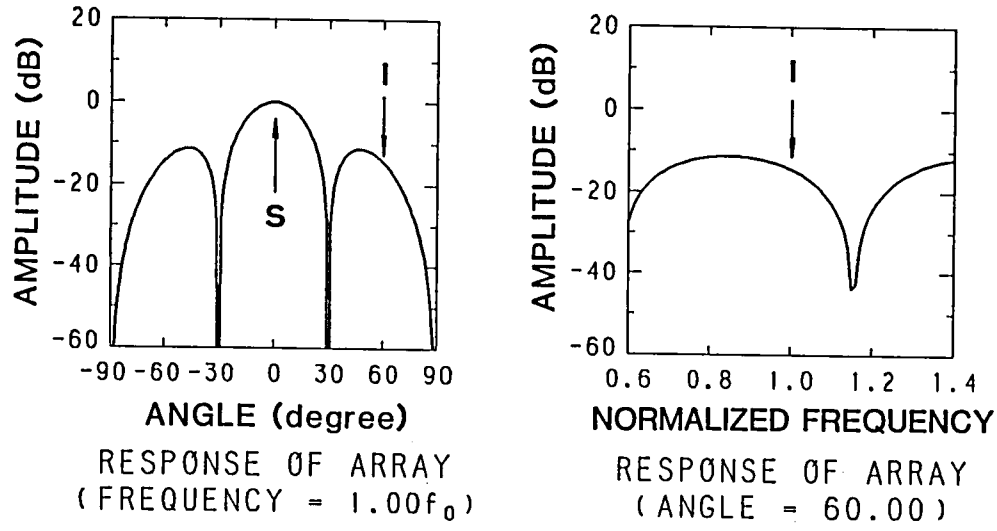

(a) uniform weight

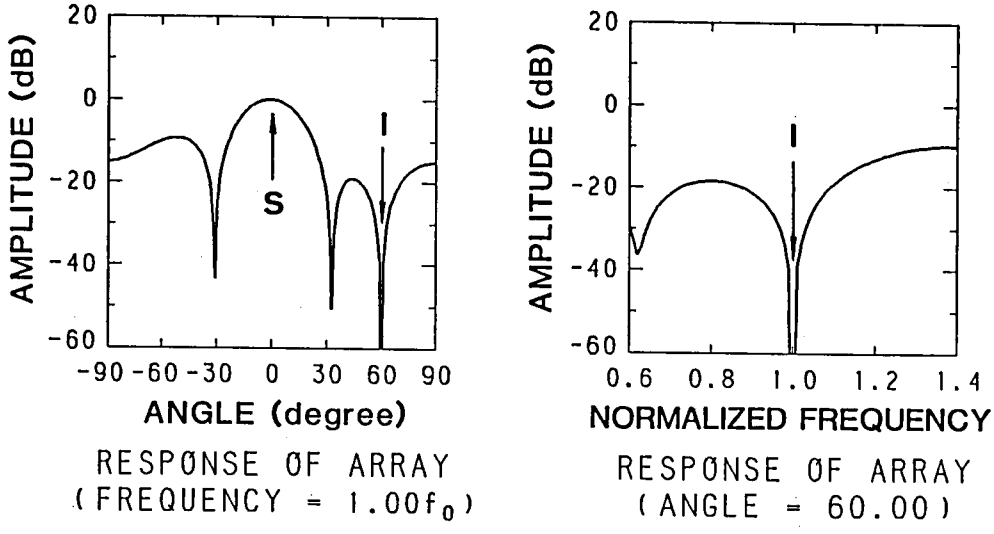

(b) optimum weight

Fig.3.7 Directional patterns and frequency characteristics in the incoherent interference direction: (a) uniform weight system, (b) optimum weight system.

CHAPTER 4

ADAPTIVE ARRAY WITH PHASE-ONLY CONTROL

4.1 Introduction

Phase-only adjustment approach is frequently made in the pattern synthesis of antenna arrays because of the convenience of hardware implementation. Besides, if we can introduce the quantized phase-shifters, this approach becomes more attractive in terms of easy reproduction of phase adjustment. On the other hand, adaptive array systems usually require the control of both amplitude and phase to achieve the optimum weighting to suppress the interferences. A suboptimum adaptive system, however, may be constructed with phase-only control after the analogy of deterministic array synthesis. In fact, several papers have reported the efforts along this line[66]-[69]. All of them, however, either adopted the guiding principle of the least mean square error (LMS) or followed the power minimization algorithm in the absence of the desired signal. As to how to preserve the desired signal, an algorithm is proposed which works to minimize the weight perturbation[70], but this assumes the known positions where to place the pattern nulls. Thus, we have yet to seek for the answer to compose the adaptive array with phase-only control under the mainbeam constraint. In the present chapter, we will show the results of the adaptive array under the principle of directionally constrained minimization of power (DCMP) with the weights solely consisting of phase-shifters[30],[71].

In Section 4.2, we discuss the basic principle and define a new

penalty function for phase-only control with the mainbeam constraint. Because of the analytical limitation, computer simulation experiments on this type of adaptive array are extensively carried out in Section 4.3. Afterward, the results obtained in Section 4.3 are reviewed theoretically in Section 4.4. In Section 4.5, the quantization of phase-shifters is attempted. Finally, Section 4.6 states concluding remarks.

4.2 The Basic Principle

We treat input signals in the complex expression. Fig.4.1 shows the structure of the linear adaptive array solely consisting of phase-shifters. The system is assumed to be composed of K-element isotropic antennas, each of which is accompanied with a phase-shifter denoted by ϕ_1, ϕ_2, ..., or ϕ_K in the figure. Also, ϕ_k shall represent the status of each phase-shifter. Let the complex signals at the input and output terminals of each channel be X_1, X_2, ..., X_K; and X_{p1}, X_{p2}, ..., X_{pK}; respectively as shown in the figure. Thus, the array output y is given by the sum of X_{p1}, X_{p2}, ..., and X_{pK} which is written as follows:

$$y = \sum_{k=1}^{K} X_{pk} = \sum_{k=1}^{K} X_k \exp(-j\phi_k) \tag{4.1}$$

Now, we will let $Y(\theta)$ represent the complex response of the array to the signal with the unit amplitude arriving from the direction θ. Then, the $Y(\theta)$ can be expressed as follows:

$$Y(\theta) = \sum_{k=1}^{K} \exp\{-j\psi_k(\theta)\} \tag{4.2}$$

where

$$\psi_k(\theta) = (2\pi d_k/\lambda)\sin\theta + \phi_k \quad (k=1, 2,.., K) \tag{4.3}$$

i.e., they are the total phase delays of the signal at the outputs of

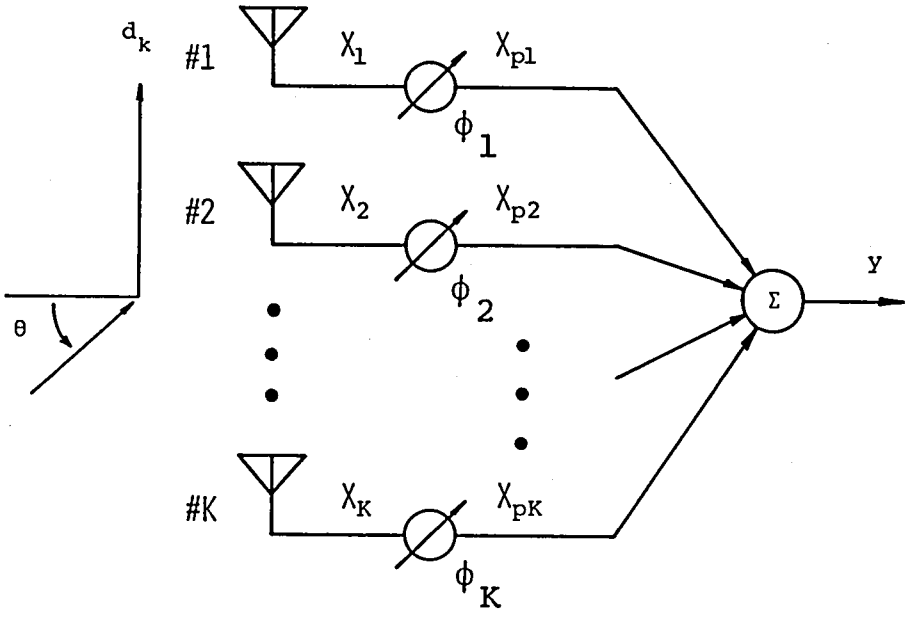

X : INPUT, Y : OUTPUT, φ : PHASE SHIFTER

Fig.4.1 Adaptive array with phase-only control.

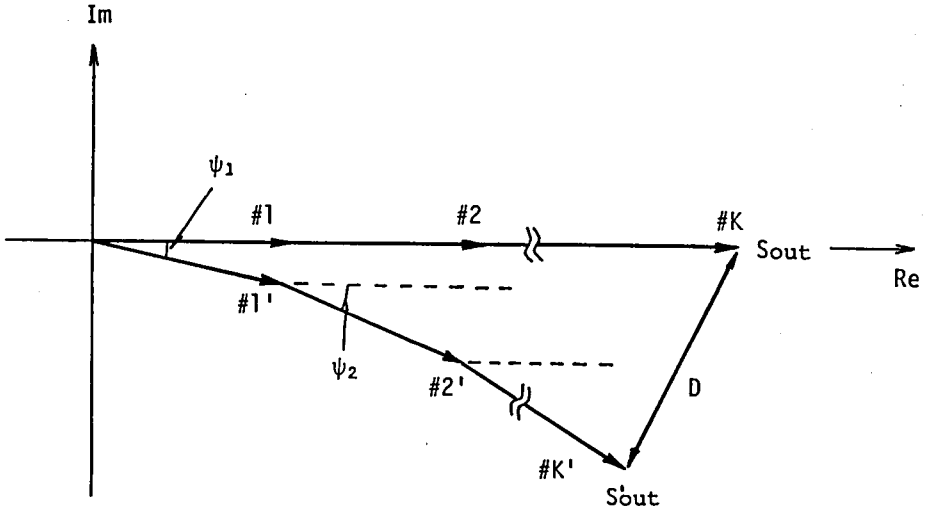

Fig.4.2 Vector diagram of element contribution to the output where $\psi_k=\psi_k(\theta_d)$ (k=1,..,K).

phase-shifters with respect to the array center. $d_k(k=1, \ldots, K)$ is the position of the k-th element antenna with the reference at the center, and λ is the wavelength.

First, we consider the case where the external interferences do not exist. It is a matter of course that the optimum (i.e., maximum signal-to-noise ratio) condition requires all channels to produce the outputs of the equal amplitudes and the same phases in this case. This situation corresponds to the S_{out} in Fig.4.2 and it can be expressed as follows:

$$S_{out} = Y(\theta_d) = 1 + \cdots + 1 = K \tag{4.4}$$

by setting

$$\psi_k(\theta_d) = 0, \text{ namely } \phi_k = -(2\pi d_k/\lambda)\sin\theta_d \quad (k=1, 2, .., K) \tag{4.5}$$

When the interferences are present, the condition given by eq.(4.5) must be abandoned because the phase-shifter should be readjusted to form nulls in the pattern in order to suppress the interferences to attain the maximum signal-to-interference-plus-noise ratio (SINR). The complex response to the desired signal in this case is designated as S'_{out} in Fig.4.2, which can be expressed as follows in general:

$$S'_{out} = Y(\theta_d) = \sum_{k=1}^{K} \exp\{-j\psi_k(\theta_d)\} \tag{4.6}$$

In Fig.4.2, for simplicity, those $\psi_k(\theta_d)$'s are denoted as ψ_k's(k=1,2,.., K). Here, it should be kept in mind that the principle of minimizing the output works to suppress the desired signal as well, and this S'_{out} tends to be nullified. Unfortunately, the rigid constraint condition for protection of the desired signal adopted in the ordinary DCMP adaptive array, i.e., specifying the response of the system to the input coming from a prescribed direction, cannot be used in this case. That is because such a rigid condition may determine the status of the phase-shifters by

itself. This problem is not encountered in the LMS system which has only to imitate the reference signal.

Now, we will impose penalty on the increase of the deviation of S'_{out} from S_{out}, i.e., $D=|S'_{out}-S_{out}|$ in Fig.4.2, in order to protect the desired signal. As the penalty function to be minimized, the sum of the output power and the squared D occurs to us readily. However, since the algorithm based on this penalty function is a little complicated, we adopt an alternative penalty function denoted by Q. It is defined as the sum of the output power and the squares of the distances of the useless components in the contribution to the output by all channels in the figure, and it is given by

$$Q(\Phi) = P_{out} + \beta P_s \sum_{k=1}^{K} [\exp\{-j\psi_k(\theta_d)\} - \exp(-j\psi_{ko})]^2$$

$$= P_{out} + \beta P_s \sum_{k=1}^{K} [\{\cos \psi_k(\theta_d) - \cos \psi_{ko}\}^2 + \{\sin \psi_k(\theta_d) - \sin \psi_{ko}\}^2], \quad (4.7)$$

or

$$Q(\Phi) = P_{out} + 2 \beta P_s \sum_{k=1}^{K} [1 - \cos\{\psi_k(\theta_d) - \psi_{ko}\}] \quad (4.8)$$

where

$$\psi_{ko} = 0 \quad (4.9)$$

$$\Phi = [\phi_1, \ldots, \phi_K]^T \quad (4.10)$$

where superscript T denotes transpose and P_s and P_{out} are the desired signal input and total output, respectively. β is named "constraint coefficient" which is non-negative. The value of this β is decisive on the performance of the system and the target of our discussion. We will define

$$\phi_{ko} = - (2\pi d_k/\lambda)\sin \theta_d \quad (k=1, 2,.., K) \quad (4.11)$$

which are the phase-shifts giving equi-phase condition for the desired signal as discussed in eq's.(4.4) and (4.5). Then, eq.(4.8) becomes

$$Q(\Phi) = P_{out} + 2\,\beta\,P_s \sum_{k=1}^{K}\{1 - \cos(\phi_k - \phi_{ko})\} \tag{4.12}$$

which reflects directly the effect of the phase-shift of each channel on the deviation from equi-phase condition.

Next, we introduce the steepest gradient approach as the algorithm to control the phase-shifters. The iterative gradient-type algorithm are given by

$$\phi_k(m+1) = \phi_k(m) - \mu\{\partial Q(\Phi)/\partial\phi_k\}_m \qquad (k=1,\ 2,..,\ K) \tag{4.13}$$

where m is the number of iteration and μ is the step size. In eq.(4.13), the partial derivative of the penalty function, Q in eq.(4.12), in terms of the phase-shift of each channel is necessary, and it is given by the following equation:

$$\frac{\partial Q(\Phi)}{\partial\phi_k} = \frac{\partial P_{out}}{\partial\phi_k} + 2\beta P_s \sin(\phi_k - \phi_{ko}) \qquad (k=1,\ 2,..,\ K) \tag{4.14}$$

We must investigate $\partial P_{out}/\partial\phi_k$ in eq.(4.14) further.

Here, several definitions are in order:

$$\mathbf{X} = [X_1,\ X_2,\ \ldots,\ X_K]^T \tag{4.15}$$

$$\mathbf{X}_p = [X_{p1},\ X_{p2},\ \ldots,\ X_{pK}]^T \tag{4.16}$$

$$\Phi_e = [\exp(j\phi_1),\ \exp(j\phi_2),\ \ldots,\ \exp(j\phi_K)]^T \tag{4.17}$$

$$\Phi = \begin{bmatrix} \exp(j\phi_1) & & & \\ & \exp(j\phi_2) & & 0 \\ & & \cdot & \\ & 0 & & \cdot \\ & & & \exp(j\phi_K) \end{bmatrix} \tag{4.18}$$

In addition, the operators of partial differentiation in terms of

$\exp(j\phi_k)$, $\exp(-j\phi_k)$ and ϕ_k will be denoted by

$$\nabla_e{}^T = \left[\frac{\partial}{\partial\{\exp(j\phi_1)\}} , \frac{\partial}{\partial\{\exp(j\phi_2)\}} , \ldots , \frac{\partial}{\partial\{\exp(j\phi_K)\}} \right] \tag{4.19}$$

$$\nabla_{e^*}{}^T = \left[\frac{\partial}{\partial\{\exp(-j\phi_1)\}} , \frac{\partial}{\partial\{\exp(-j\phi_2)\}} , \ldots , \frac{\partial}{\partial\{\exp(-j\phi_K)\}} \right] \tag{4.20}$$

$$\nabla_p{}^T = \left[\frac{\partial}{\partial\phi_1} , \frac{\partial}{\partial\phi_2} , \ldots , \frac{\partial}{\partial\phi_K} \right] \tag{4.21}$$

Using the vectors given by eq's.(4.15) and (4.17), the array output y of eq.(4.1) can also be expressed as

$$y = \mathbf{X}^T\Phi_e{}^* = \Phi_e{}^\dagger\mathbf{X} \tag{4.22}$$

where superscripts * and † stand for conjugate and conjugate transpose, respectively. Thus, the output power is given by

$$P_{out} = E[y^*y] = \Phi_e{}^\dagger E[\mathbf{X}\mathbf{X}^\dagger]\Phi_e = \Phi_e{}^\dagger R_{xx}\Phi_e \tag{4.23}$$

where E[ ] denotes the expectation and R_{xx} is the correlation matrix of the inputs defined by

$$R_{xx} = E[\mathbf{X}\mathbf{X}^\dagger] \tag{4.24}$$

which is obviously a Hermitian matrix. According to Ref.[65], we can derive

$$\begin{aligned} \frac{\partial P_{out}}{\partial\phi_k} &= \frac{\partial\exp(j\phi_k)}{\partial\phi_k}\cdot\frac{\partial P_{out}}{\partial\exp(j\phi_k)} + \frac{\partial\exp(-j\phi_k)}{\partial\phi_k}\cdot\frac{\partial P_{out}}{\partial\exp(-j\phi_k)} \\ &= j\exp(j\phi_k)\cdot\frac{\partial P_{out}}{\partial\exp(j\phi_k)} - j\exp(-j\phi_k)\cdot\frac{\partial P_{out}}{\partial\exp(-j\phi_k)} \end{aligned} \tag{4.25}$$

$$(k=1, 2, .., K)$$

Applying the vectorial notation to eq.(4.25), we obtain

$$\begin{aligned} \nabla_p P_{out} &= j\Phi\nabla_e P_{out} - j\Phi^*\nabla_{e^*}P_{out} \\ &= j\Phi R_{xx}{}^*\Phi_e{}^* - j\Phi^* R_{xx}\Phi_e \end{aligned} \tag{4.26}$$

As in Ref.[68], y is delayed by $\pi/2$ and the delayed one is denoted as y',

i.e.,

$$y' = -jy \tag{4.27}$$

Using this y', we have

$$\begin{aligned} E[\mathbf{X}_p^* \cdot y'] &= -jE[(\Phi^*\mathbf{X})^* \cdot \mathbf{X}^T\Phi_e^*] \\ &= -j\Phi E[\mathbf{X}^*\mathbf{X}^T]\Phi_e^* \\ &= -j\Phi R_{xx}^*\Phi_e^* \end{aligned} \tag{4.28}$$

and

$$\begin{aligned} E[\mathbf{X}_p \cdot y'^*] &= jE[(\Phi^*\mathbf{X}) \cdot (\mathbf{X}^T\Phi_e^*)^*] \\ &= j\Phi^* E[\mathbf{X}\mathbf{X}^\dagger]\Phi_e \\ &= j\Phi^* R_{xx}\Phi_e \end{aligned} \tag{4.29}$$

Therefore, eq.(4.26) can be expressed as follows by using eq's.(4.28) and (4.29):

$$\nabla_p P_{out} = - E[\mathbf{X}_p^* \cdot y'] - E[\mathbf{X}_p \cdot y'^*] \tag{4.30}$$

or, in terms of each element,

$$\frac{\partial P_{out}}{\partial \phi_k} = - E[X_{pk}^* \cdot y'] - E[X_{pk} \cdot y'^*] \qquad (k=1, 2,.., K) \tag{4.31}$$

Finally, we obtain from eq.(4.14)

$$\frac{\partial Q(\Phi)}{\partial \phi_k} = 2\beta P_s \sin(\phi_k - \phi_{ko}) - E[X_{pk}^* \cdot y'] - E[X_{pk} \cdot y'^*] \tag{4.32}$$

$$(k=1, 2,.., K)$$

In eq.(4.32), the expected values of $X_{pk}^* \cdot y'$ and $X_{pk} \cdot y'^*$ are included, but in practice they may be approximated by their instantaneous values, as is usually the case with the gradient algorithm of the ordinary DCMP system. Thus, with the initial phase-shifts satisfying the equi-phase condition for the desired signal, the algorithm which is given by eq.(4.13) can be expressed as

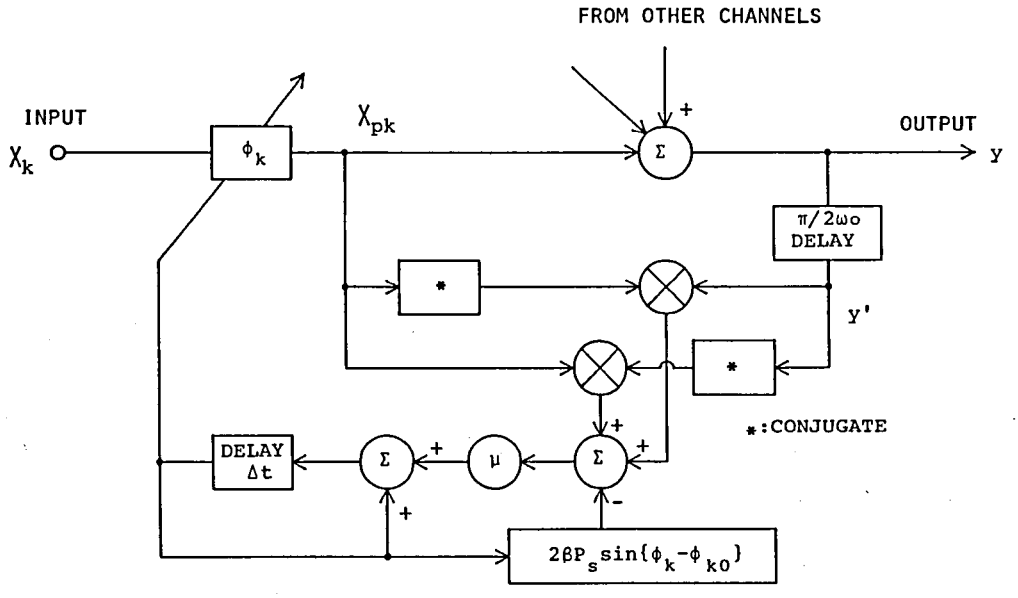

Fig.4.3 Block diagram representation of the adaptive algorithm with phase-only control under the mainbeam constraint.

$$\phi_k(0) = \phi_{ko}$$

$$\phi_k(m+1) = \phi_k(m) - \mu[2\beta P_s \sin\{\phi_k(m) - \phi_{ko}\} - X_{pk}^*(m)\cdot y'(m) - X_{pk}(m)\cdot y'^*(m)] \quad (4.33)$$

$$(k=1, 2,.., K)$$

where $X_{pk}(m)$'s(k=1,2,..,K) and y'(m) represent the sampled values at the m-th iteration of X_{pk}'s(k=1,2,..,K) and y', respectively. Block diagram representation of the above algorithm is shown in Fig.4.3. Furthermore, for the sake of preventing the system behavior from the instantaneous fluctuation, we can average several sampled data and update the phase-shifters with this averaged one instead of updating them sample by sample. It is called a smoothing algorithm, which is given by

$$\phi_k(m+1) = \phi_k(m) - \mu[2\beta P_s \sin\{\phi_k(m) - \phi_{ko}\} - \Delta_k(m)] \quad (4.34)$$

with

$$\Delta_k(m) = \sum_{i=1}^{J} [X_{pk}^*(m_i)\cdot y'(m_i) + X_{pk}(m_i)\cdot y'^*(m_i)] \quad (4.35)$$

$$(k=1, 2,.., K)$$

where J is the number of data for smoothing and m_i denotes the i-th side-iteration number between the m-th iteration and the next (m+1)-th iteration.

4.3 Computer Simulation

The problem of the algorithm proposed in the previous section are (i) that the relation between the variables, ϕ_k's(k=1,..., K), and the penalty function Q is nonlinear as discussed in Ref.[70], and (ii) that the constraint is not rigid. The absence of a closed-form solution is the greatest difficulty to analyze the general characteristics of the system. Therefore, computer simulation experiments on the basis of eq's.(4.34) and

(4.35) are carried out in place of the theoretical analysis. Especially, the optimum choice of the value β is extensively pursued since it decides the point of compromise between the suppression of the interferences and protection of the desired signal.

In the following computer simulation, we adopt a 4-element, equally spaced linear array with the element spacing of a half wavelength as the standard array system. As to the inputs, we consider two external waves, the desired signal and one i-interference, are incident on the array, and the thermal noise with equal power exists at each channel. For convenience, we will call the i-interference merely the interference here. Table 4.1 shows the radio environment we used as the standard throughout the computer simulation. In this table, P_o represents the sum of the input powers at each channel. In the later examples, only those parameters that are different from this table will be clarified, while other parameters not mentioned are the same as shown in the table. For adaptation by sampling feedback, the step-size, μ and the number of the

Table 4.1 Input data used in the computation.

desired signal (S)	angle of arrival	: $\theta_s = 0°$
	power	: $P_s = 1$
interference (I)	angle of arrival	: $\theta_i = -50°$
	power	: $P_i = 100$
thermal noise	power	: $P_n = 0.01$
step-size		: $\mu = 10^{-3}/P_o$
number of samples for smoothing		: $J = 10$
constraint coefficient		: $\beta = 4$

Note: $P_o = P_s + P_i + P_n$ (sum of the inputs)

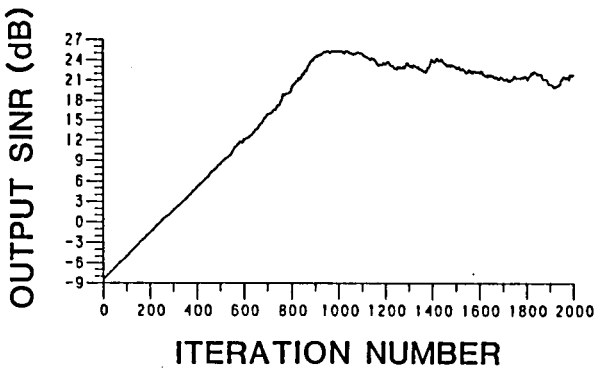

(a)

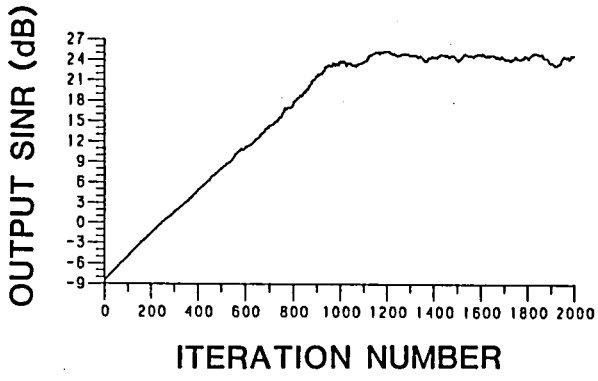

(b)

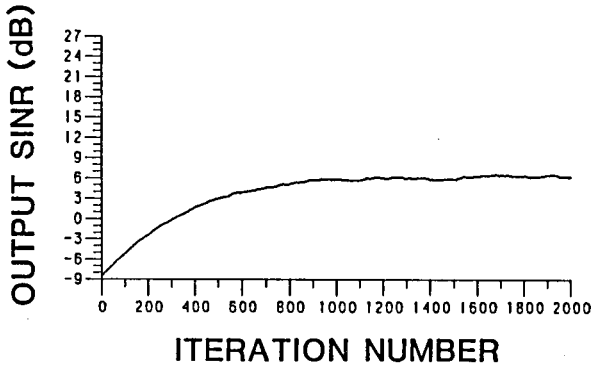

(c)

Fig.4.4 β-value (constraint weight) and attained SINR (K=4, P_i=100): (a) β=1, (b) β=4, (c) β=50.

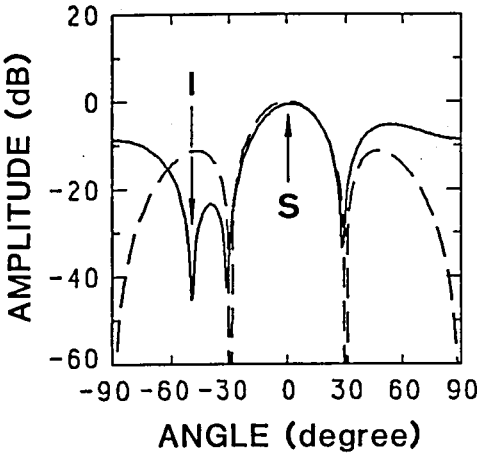

(a)

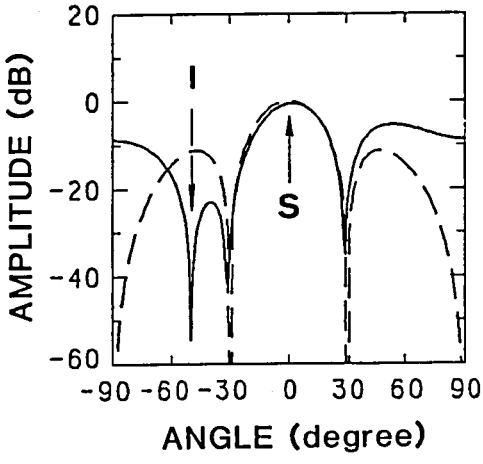

(b)

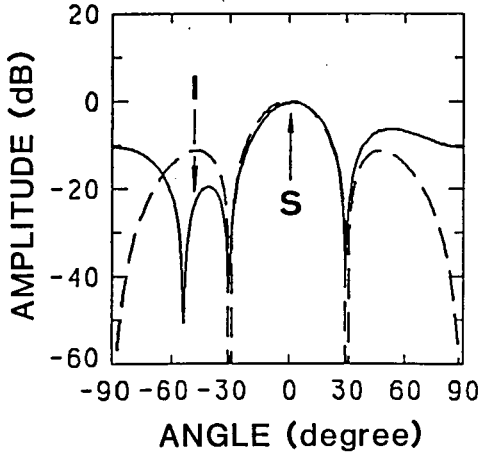

(c)

Fig.4.5
The directional patterns corresponding to Fig.4.4:
(a) β=1, SINR=21.89dB,
(b) β=4, SINR=24.82dB,
(c) β=50, SINR= 6.27dB.
The dashed and solid lines represent the initial and final (at 2,000-th iteration) patterns, respectively. I and S in the figures show the angles of arrival of the interference and the desired signal, respectively.

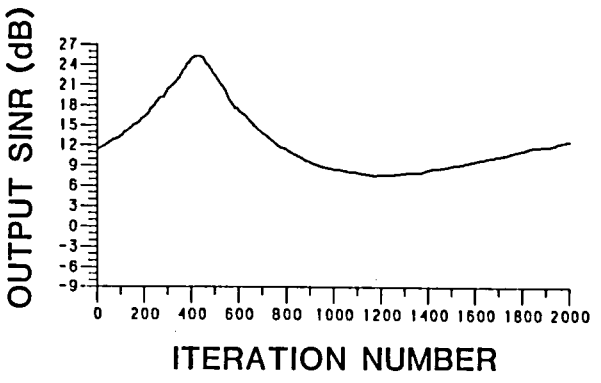

(a)

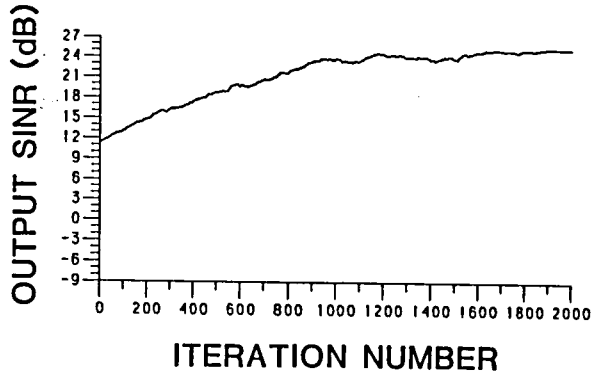

(b)

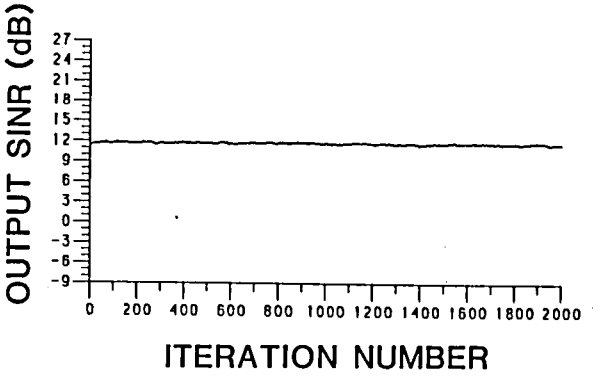

(c)

Fig.4.6 β-value (constraint weight) and attained SINR (K=4, P_i=1): (a) β=1, (b) β=4, (c) β=50.

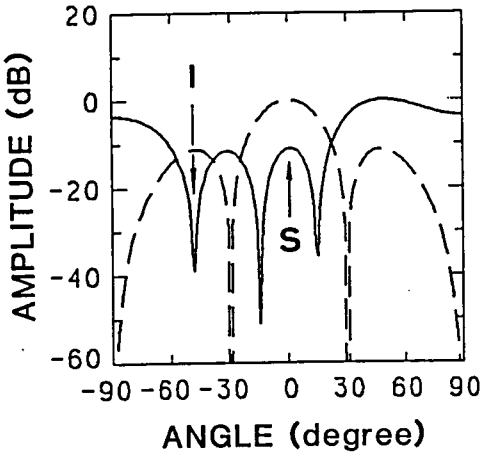

(a)

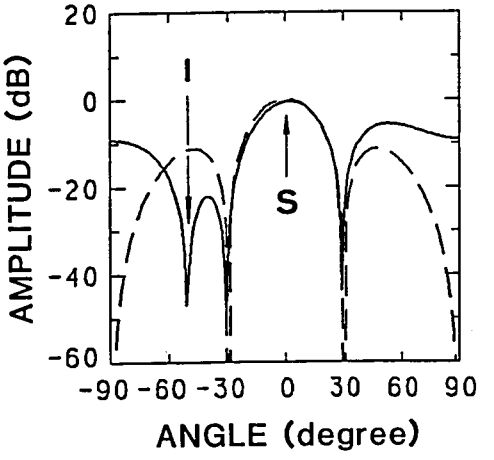

(b)

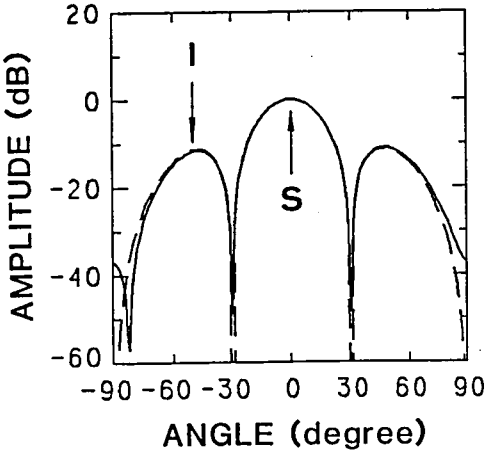

(c)

Fig.4.7
The directional patterns corresponding to Fig.4.6:
(a) β=1, SINR=12.79dB,
(b) β=4, SINR=25.31dB,
(c) β=50, SINR=11.68dB.
The dashed and solid lines represent the initial and final (at 2,000-th iteration) patterns, respectively. I and S in the figures show the angles of arrival of the interference and the desired signal, respectively.

samples for smoothing, J have first been selected after our past experience in the ordinary types of adaptive arrays, and also confirmed by various experiments on this type. The figures shown in Table 4.1 are the results selected after these trials.

Fig.4.4 shows the process of adaptation in terms of the temporal variation of the signal-to-interference-plus-noise ratio (SINR) of the output for various values of β. (a), (b) and (c) represent the results where β=1, β=4 and β=50, respectively. The directional patterns corresponding to Fig.4.4 are shown in Fig.4.5. The dashed and solid curves in Fig.4.5 describe the initial and final patterns, respectively. It is clearly observed in (c) that too large β cannot give a good SINR due to insufficient suppression of the interference. On the other hand, (a), the case of small β may seem excellent, but a close look will reveal that the desired signal is slowly diminishing. Fig.4.6 shows the process of adaptation in the case of the smaller value of the interference power, i.e., P_i=1. (a), (b) and (c) correspond to the same case of β as shown in Fig.4.4. The directional patterns for Fig.4.6 are shown in Fig.4.7 where the curves are described in the same manner as Fig.4.5. The trend of diminishing of the desired signal is more remarkably observed in Fig's.4.5(a) and 4.6(a), demonstrating low SINR by small β. In (c)'s of Fig's.4.5 and 4.6 where β is too large, on the other hand, the adaptation is hardly performed. After all, we have found too large or too small β brings about unsatisfactory performance.

Next, Fig.4.8 demonstrates the relationship between β and output SINR for four different values of P_i's, namely, (a) P_i=0.1, (b) P_i=1, (c) P_i=10 and (d) P_i=100. The SINR's are read after 2,000 times of iteration. In Fig.4.8, we learn that the value of β is a decisive factor on the output SINR, and that β=4 is the best choice. The achieved output SINR does not

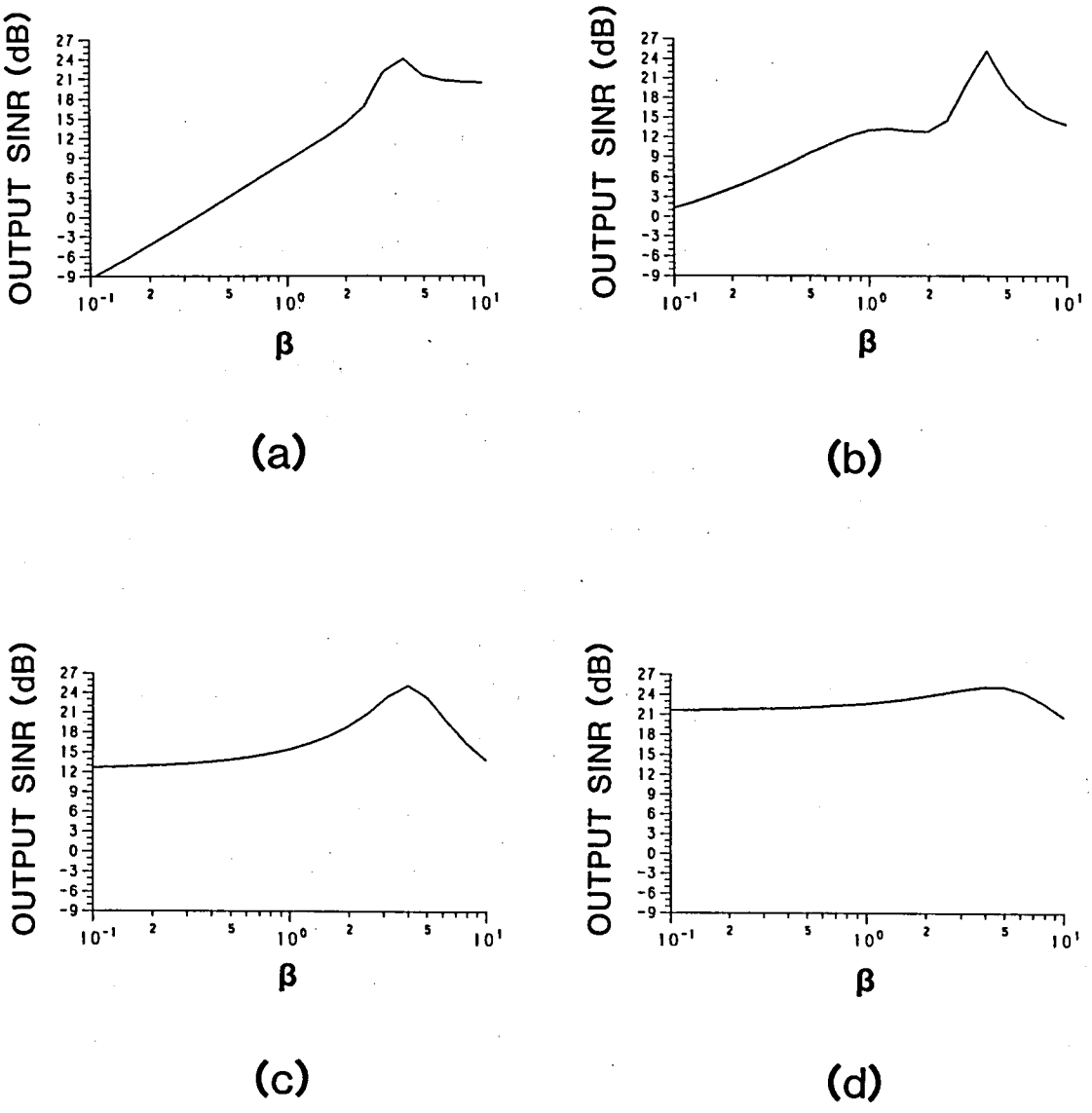

Fig.4.8 Search for optimum β (K=4):
(a) P_i=0.1, (b) P_i=1, (c) P_i=10, (d) P_i=100.

seem to depend on the magnitude of P_i.

A number of computer simulations were carried out for other values of θ_i's, the angles of arrival of the interference, and we obtained similar results so long as θ_i lies outside of the mainbeam.

4.4 Theoretical Discussion

In this section, we will consider the meaning of the results obtained just above. First, the output will be divided into three components as the following.

$$P_{out} = P^s{}_{out} + P^i{}_{out} + P^n{}_{out} \tag{4.36}$$

where the superscripts s, i and n stand for the desired signal, interference and noise components, respectively. The partial derivatives of the penalty function in terms of the phase-shifts are obtained by using eq.(4.8) as

$$\frac{\partial Q}{\partial \phi_k} = \frac{\partial P^s{}_{out}}{\partial \phi_k} + \frac{\partial P^i{}_{out}}{\partial \phi_k} + \frac{\partial P^n{}_{out}}{\partial \phi_k} + 2\beta P_s \sin \psi_k(\theta_d) \tag{4.37}$$

$$(k=1, 2,.., K)$$

Now, the output voltage of the desired signal shall be given by

$$y^s = \sqrt{P_s}\, Y(\theta_d) = \sqrt{P_s} \sum_{k=1}^{K} \exp\{-j\psi_k(\theta_d)\} \tag{4.38}$$

Then, letting ψ_k substitute for $\psi_k(\theta_d)$ temporarily for convenience, we have

$$P^s{}_{out} = E[y^{s*} y^s] = P_s[K + \sum_{k\neq n}^{K} \sum \cos(\psi_k - \psi_n)] \tag{4.39}$$

$$\frac{\partial P^s{}_{out}}{\partial \phi_k} = -2P_s \cdot \sum_{n=1}^{K} \sin(\psi_k - \psi_n)$$

$$= -2P_s\{\sin \psi_k \cdot \sum_{n=1}^{K} \cos \psi_n - \cos \psi_k \cdot \sum_{n=1}^{K} \sin \psi_n\} \tag{4.40}$$

Combining eq's.(4.37) and (4.40), we obtain

$$\frac{\partial Q}{\partial \phi_k} = \frac{\partial P^i{}_{out}}{\partial \phi_k} + \frac{\partial P^n{}_{out}}{\partial \phi_k} + 2P_s\{\sin \psi_k \ (\beta - \sum_{n=1}^{K} \cos \psi_n) + \cos \psi_k \cdot \sum_{n=1}^{K} \sin \psi_n\} \tag{4.41}$$

In eq.(4.41), only the third term contains the desired signal component. Now, let

$$\beta = \varepsilon K \ (\varepsilon \geq 0) \tag{4.42}$$

and name the third term in eq.(4.41) D_3 which can be expressed as

$$\begin{aligned} D_3 &= 2P_s\{\sin \psi_k \ (\varepsilon K - \sum_{n=1}^{K} \cos \psi_n) + \cos \psi_k \cdot \sum_{n=1}^{K} \sin \psi_n\} \\ &= \frac{\partial}{\partial \phi_k} [P_s\{(\varepsilon K - \sum_{n=1}^{K} \cos \psi_n)^2 + (\sum_{n=1}^{K} \sin \psi_n)^2\}] \\ &= \frac{\partial}{\partial \phi_k} \{P_s|\varepsilon S_{out} - S'_{out}|^2\} \end{aligned} \tag{4.43}$$

If

$$\varepsilon = 1, \text{ namely, } \beta = K, \tag{4.44}$$

then eq.(4.43) becomes the derivative of the deviation from the ideal situation for the desired signal in the absence of the interference. With this meaning of the third term, we have finally come to understand the significance of eq.(4.41). The first and second terms respond to reduce the interference and noise, respectively, while the third term works to protect the desired signal. This is the interpretation of the previous results by computer simulation.

In order to verify this consideration, further computation is done for various numbers of elements K other than K=4. The results of β versus SINR are shown in Fig.4.9. (a), (b) and (c) correspond to the results where K=3, K=6 and K=8, respectively. The SINR's are the values read after 2,000 times of iteration, similar to Fig.4.8. From Fig.4.9, it is

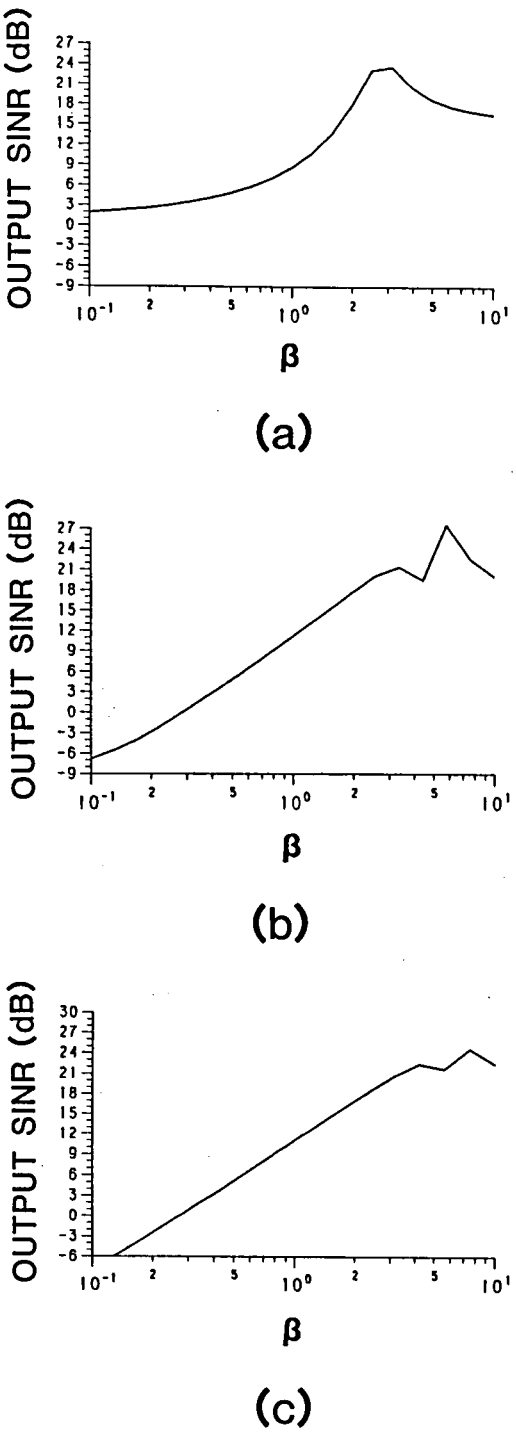

Fig.4.9 Optimum β for various element numbers (P_i=1): (a) K=3, (b) K=6, (c) K=8.

evident that the β satisfying eq.(4.44) gives the best performance.

In practice, the apriori knowledge on the desired signal input P_S is necessary when we adopt the penalty function of eq.(4.7). P_S may be estimated by the power of the transmitter of the desired signal and the distance between the transmitter and receiver. Since the estimation may not be accurate enough, we should not expect the optimum choice of β. According to the previous discussion, the value of β which is smaller than the optimum is fatal for it is destined to cancel the desired component. Therefore, a somewhat larger value of β than the optimum value K is advisable for safety. Fortunately, the dependence of SINR on β is not very sensitive as shown in the Fig's.4.8 and 4.9, and thus the above treatment does not sacrifice the performance seriously.

4.5 Quantization of Phase-Shifters

In conventional phased arrays, quantized phase-shifters are frequently used because of various reasons such as cost or controllability. It would be advantageous if this sort of implementation could be adopted in our adaptive array without serious sacrifice of its capability. In order to get a rough idea of how many bits of quantization of phase are necessary, we kept the same algorithm in the computer simulation as before, and replaced the analogue phase-shifters with quantized ones only after the system reached convergence. Fig.4.10 demonstrates the dependence of the output SINR on the bit numbers for various angles of arrival of the interference. The dashed lines in the figure correspond to the results obtained by the analogue phase-shifters. Many other experiments with different power of interference, though whose figures are not shown here for simplicity, have convinced us that the stronger interference results

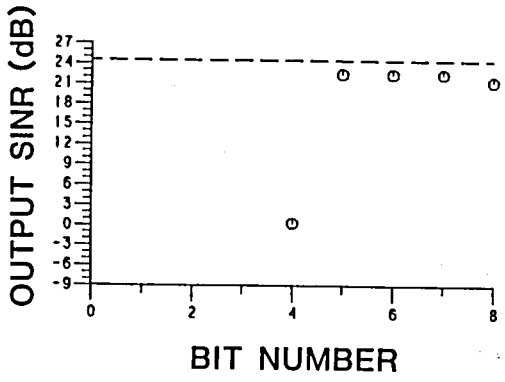

(a)

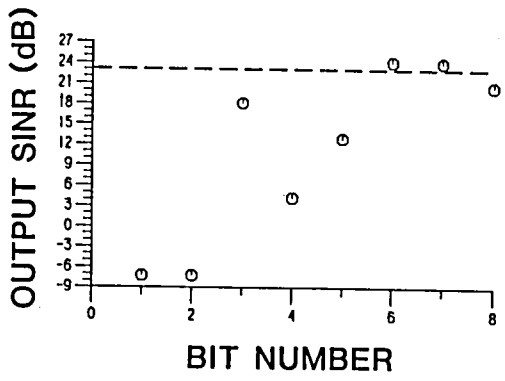

(b)

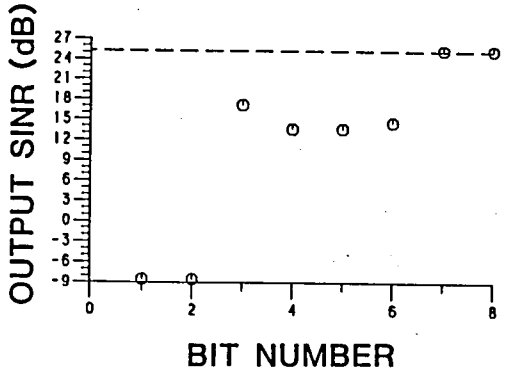

(c)

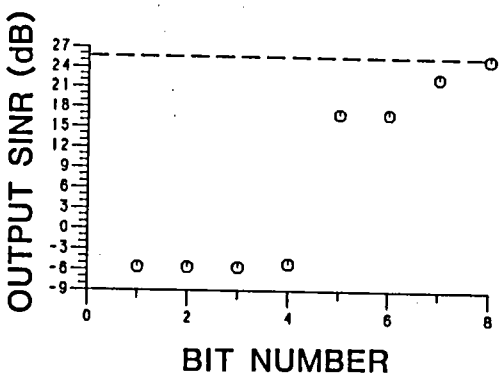

(d)

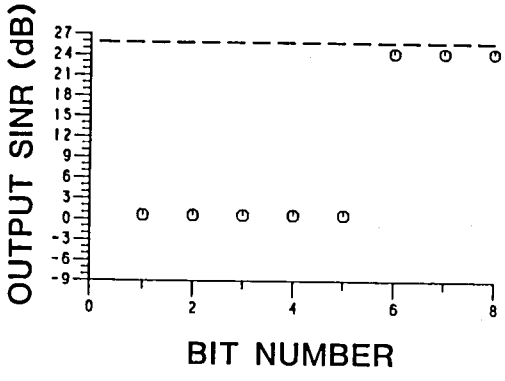

(e)

Fig.4.10
Bit numbers and attained SINR (K=4):
(a) θ_i=-20°, (b) θ_i=-40°,
(c) θ_i=-50°, (d) θ_i=-60°,
(e) θ_i=-70°.
The dashed lines correspond to the results obtained by the analogue phase-shifters.

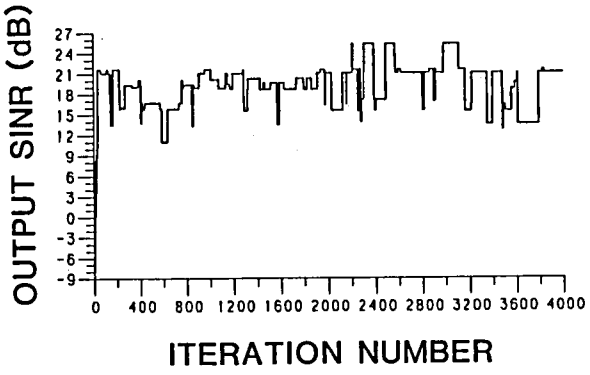

(a)

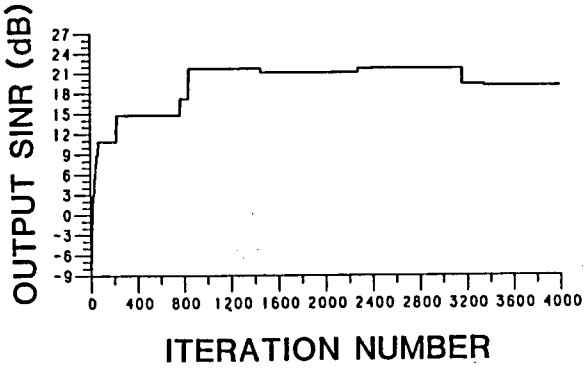

(b)

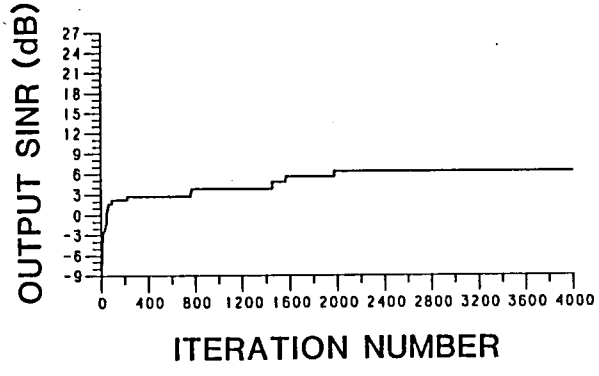

(c)

Fig.4.11 Performance of the quantized phase-shifter system: (a) $\mu=2\times10^{-2}/P_o$, (b) $\mu=1.5\times10^{-2}/P_o$, (c) $\mu=1\times10^{-2}/P_o$.

in the worse SINR. This is against the general fact of adaptive arrays, and should be interpreted that the delicate discrepancy of the phase values fails to cancel the interference.

The inspection of Fig.4.10 leads us to conclude that at least seven or eight bits of quantization are necessary for the adaptive arrays. Next, the behavior during the process of adaptation is examined with 8-bit phase-shifters, while the same algorithm for the analogue system is used. Fig.4.11 shows the results for three different choices of the step-size. (a), (b) and (c) correspond to the cases where $\mu=2\times10^{-2}/P_o$, $\mu=1.5\times10^{-2}/P_o$ and $\mu=1\times10^{-2}/P_o$, respectively. It is remarkable that the step-size about ten times that for the analogue system whose results are already shown in Fig.4.4(b) is necessary for the quantized system. Also, the performance of the system is very sensitive on this choice of the step-size. This means that the compromise between the transient and static characteristics of the system control must be made with very narrow margin.

4.6 Concluding Remarks

In this chapter, an adaptive antenna array system with phase-only control and under the principle of DCMP (directionally constrained minimization of power) was discussed. In this case, the rigid constraint condition for protection of the desired signal such as adopted in the ordinary DCMP adaptive array could not be employed successfully. Therefore, a new penalty function had to be devised for the system, which must take into consideration the more flexible protection of the desired signal while minimizing the unwanted interference and/or noise. Because of the analytical limitation, computer simulation experiments were extensively carried out for narrowband signals. The constraint

coefficient that is the most important factor of the penalty function was especially investigated. As the results, it turned out that too large or too small constraint coefficient yields low SINR and that its optimum value exists which offers compromise between the protection of the desired signal and suppression of the interference. Thus, the optimum choice of the constraint coefficient was given numerically. It was also shown that the theoretical consideration leads to the same value. Finally, the attempt to quantize the phase-shifters was reported, and it is shown to be unsatisfactory for practical use.

At the end of this chapter, we will add the following remarks. It is clear that we can also apply our new algorithm to the directional pattern synthesis with phase-only control, similar to techniques discussed in Ref.[70]. Unlike the adaptive null steering, the radio environment is specified for design in this case and we can use this algorithm to obtain the optimum phase-shifts for the given specification. One of the greatest advantages of this algorithm is to be able to attain the low sidelobes at a partial angular sector by assuming that the interferences impinge from the intended directions. Besides, since we have only to quantize the phase-shifts after the optimum ones are obtained in the analogue means, we do not have such difficulties about quantization as in the adaptive null steering. Thus, the quantized phase-shifters can be introduced successfully in this case.

CHAPTER 5

TAMED ADAPTIVE ANTENNA ARRAY

5.1 Introduction

An adaptive array requires some instruction on how to discriminate the desired signal from the unwanted interferences. In the case of the adaptive antenna under the algorithm of directionally constrained minimization of power(DCMP)[30], the system is taught the direction of arrival of the desired signal, and forced to make a constant voltage response of its transfer function to this signal. Several problems such as the following arise from this guideline:

(a) If an interference which is coherent with the desired signal arrives, as is usually the case in multipath propagation, the system tends to utilize this interference to cancel the desired signal in order to minimize the output power[55],[72]-[75].

(b) When the prescribed angle of arrival of the desired signal is not accurate enough, the system takes the desired signal for unwanted interference and tries to suppress it[30].

(c) When the desired signal is broadbanded, its sideband component which does not satisfy the above constraint becomes a target for the system to suppress[48],[76],[77].

All (a), (b) and (c) result from the excessive fidelity of the system to the given mission to minimize the output power. In those cases where nulls must be formed in the vicinity of the constrained direction or frequency, the control algorithm usually guides the variable weights to

extremely large values in magnitude. This may be compared to super-directive arrays. By analogy, it is expected that the cancelling can be moderated if we add some amount of internal noise to prevent the system from being too super-directive, i.e., not so fierce as to harm the desired signal. The idea of taming the adaptive array by injecting additional noise(internal or thermal) is not new, but simply turned down for the following reasons:

(1) the contamination of the desired signal by the added noise.

(2) the reduction of the capability to suppress the interference.

Fortunately, the nature of the DCMP system allows us to add "pseudo" noise, instead of real noise, during its feedback processing so that we may avoid deteriorating the SNR of the output, solving the problem (1). The second concern comes from the misbelief that the adaptive array balances the internal and external noises. In fact, it is their gradients in terms of the weights that are balanced as discussed in Chapter 3. When we look at the components of the output of the adaptive antenna, we notice that the external interference is very much smaller than the internal (thermal) noise component. Therefore, we can moderate the cancellation capability of this system and still have good suppression against the external interference. This is how we reached the concept of the "Tamed Adaptive Antenna Array"[78],[79].

As another cancellation problem, we will study the effects of mutual coupling and random input errors on the steady-state performance of the DCMP adaptive array. Most analyses on the performance of adaptive arrays assume the uniform reception of the incoming plane waves by each element. Several papers, however, reported the effect of the mutual coupling between the array elements of the various adaptive arrays such as the least mean square (LMS), Howells-Applebaum and power inversion

principles[80]-[82]. Some other papers[83]-[85] dealt with the random errors of the amplitudes or phases of the received signals at the elements. These papers reported significant effects on the performance of the adaptive arrays. If the DCMP adaptive array has such effects, there arises some discrepancy between the desired signals actually received by the elements and those assumed in setting the constraint. Consequently, the desired signal may be regarded as the unwanted one and becomes a target of suppression, which is similar to the cancellation problem of the above (b). Therefore, it reminds us to adopt the tamed adaptive array of the present interest to protect the desired signal in cases of the mutual coupling and random input errors. We shall see the improvement over the conventional DCMP adaptive array.

In the next section, we describe system and input models for the analysis. In Section 5.3, we analyze the performance of the DCMP adaptive array in adverse radio environments such as the problems (a) and (b) mentioned above, and afterwards we introduce the tamed adaptive array as the improved DCMP system in Section 5.4. Section 5.5 is devoted to evaluating the broadband performance of the tamed adaptive array which we deal with as the problem (c). Sections 5.6 and 5.7 are concerned with the performance under the effect of mutual coupling between array elements and under the effect of random input errors, respectively, and the results of the conventional DCMP system and the tamed system are compared. Section 5.8 states the conclusions.

5.2 Description of Models for Analysis

Let us consider a K-element, L-tap adaptive array shown by Fig.3.1 and assume that the elements are isotropic and spaced equally by a half

wavelength. There are three kinds of external wave fields arriving at the system; (1) the desired signal, (2) the c-interference, and (3) the i-interference. Their angles of arrival and average powers are denoted by θ_s, θ_c, θ_i, P_s, P_c and P_i, respectively. Another input, the internal (thermal) noise appears at each tap with the equal average power of P_n. Therefore, various input parameters defined in Chapter 3 such as SNR, SIR and CSR(or r) are given by

$$\text{Input SNR} = \frac{P_s}{L\,P_n} \tag{5.1}$$

$$\text{Input SIR} = \frac{P_s}{P_i} \tag{5.2}$$

$$\text{Input CSR} = r = \frac{P_c}{P_s} \tag{5.3}$$

Throughout this chapter, we assume that r is equal or less than 0 dB.

As the guiding principle, we adopt DCMP approach with the single constraint where the constraint matrix C_d and the constrained response vector **H** are given by eq's.(3.21) and (3.22).

5.3 Protection of the Desired Signal in Adverse Environments

5.3.1 The Effect of the Coherent Interference[73],[86]

We take an example of 4-element, 2-tap system, and calculate eq.(3.31) to obtain the optimum weight. Table 5.1 shows the parameters of the input model and constraint we use. Fig.5.1 shows the results of the relation between the input SNR and the output SINR while changing the c-interference power expressed in terms of the input CSR, r. It is clearly seen that the output SINR deteriorates as r increases. Moreover, it is interesting that there is an optimum value of the internal noise that

Table 5.1 Input model and constraints under the effect of coherent interference.

desired signal (S)	angle of arrival : $\theta_s = 0°$
	power : $P_s = 1$
coherent (C)	angle of arrival : $\theta_c = 60°$
interference	power : $P_c = 1$
incoherent (I)	angle of arrival : $\theta_i = -50°$
interference	power : $P_i = 100$
thermal noise	power : $P_n = 0.01$
constrained angle	: $\theta_d = \theta_s$
constrained frequency	: $f_d = f_o(=1)$

Note: All external waves are narrowbanded.

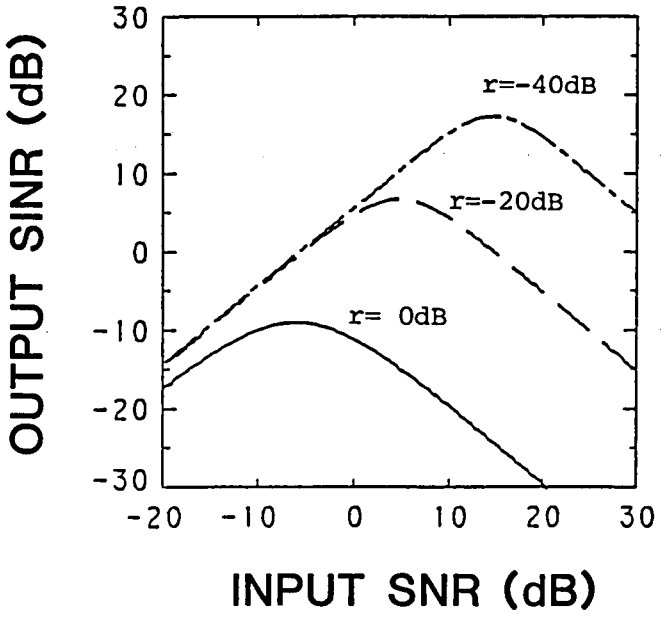

Fig.5.1 The relation between the input SNR and the output SINR under the effect of coherent interference. (see Table 5.1)

maximizes the output SINR, and that this optimum input SNR depends on the power of the c-interference. Next, we examined its dependence on the i-interference input, and found out that neither the power nor the angle of arrival of the i-interference have remarkable effect except for the vicinity of $\theta_c=\theta_i(=60°)$. This means that we can determine the optimum internal noise without the knowledge on the i-interference.

Now, we will denote the above optimum internal noise by P_{no}, and obtain its formula analytically by assuming that no i-interference arrives. For a narrowband input signals, L=2 is sufficient, and hence we can adopt the complex expression defined in Section 3.5 here again. By using notations defined by

$$\mathbf{Z}_s = \mathbf{C}_d = (1/\sqrt{2})[\exp\{j\Psi_1(\theta_s)\},.., \exp\{j\Psi_K(\theta_s)\}]^T \tag{5.4}$$

$$\mathbf{Z}_c = (1/\sqrt{2})[\exp\{j\Psi_1(\theta_c)\},.., \exp\{j\Psi_K(\theta_c)\}]^T \tag{5.5}$$

where

$$\Psi_k(\theta_x) = \pi\{k - (K + 1)/2\} \sin \theta_x, \ (x=s \text{ or } c;\ k=1,.., K) \tag{5.6}$$

we can express the complex correlation matrix as follows:

$$R_{xx} = P_n U + \mathbf{X}_d \mathbf{X}_d^{\dagger} \tag{5.7}$$

$$\mathbf{X}_d = \sqrt{P_s}\mathbf{Z}_s + \sqrt{P_c}\exp(-j\phi_{sc})\mathbf{Z}_c \tag{5.8}$$

where ϕ_{sc} denotes the phase difference of the desired and c-interference measured at the reference point(the center of the array). Since we can obtain R_{xx}^{-1} by applying the matrix inversion formula[63] to eq.(5.7), the complex optimum weight vector given by eq.(3.80) can be derived for this case as follows:

$$\mathbf{W}_{opt} = \zeta[\{2P_n + K(P_s + P_c + 2A_{dc}\sqrt{P_s P_c} \cos \phi_{sc})\}\mathbf{F} - 2H^*(P_s + A_{dc}\sqrt{P_c} \exp(j\phi_{sc})\mathbf{X}_d] \tag{5.9}$$

where

$$\zeta = \{2P_n + KP_c(1 - A_{dc}^2)\}^{-1} \tag{5.10}$$

$$A_{dc} = \frac{2}{K} Z_c{}^T Z_s{}^* = \frac{Z_c{}^T F^*}{H} = \frac{\sin\{K\pi(\sin\theta_s - \sin\theta_c)/2\}}{K\sin\{\pi(\sin\theta_s - \sin\theta_c)/2\}} \tag{5.11}$$

Therefore, the output SNR (denoted by SNR_{out}) can be expressed as follows:

$$SNR_{out} = P^d{}_{out}/P^n{}_{out} \tag{5.12}$$

$$P^d{}_{out} = \mathbf{W}_{opt}{}^\dagger \mathbf{X}_d \mathbf{X}_d{}^\dagger \mathbf{W}_{opt}$$

$$= (P_s + A_{dc}{}^2 P_c + 2A_{dc}\sqrt{P_s P_c}\cos\phi_{sc})(2P_n\zeta|H|)^2 \tag{5.13}$$

$$P^n{}_{out} = P_n \mathbf{W}_{opt}{}^\dagger \mathbf{W}_{opt}$$

$$= (2/K)P_n|H|^2$$

$$+ 2KP_nP_c(1 - A_{dc}{}^2)\zeta|H|^2(P_s + A_{dc}{}^2P_c + 2A_{dc}\sqrt{P_sP_c}\cos\phi_{sc}) \tag{5.14}$$

Thus, equating the derivative of SNR_{out} by P_n to be zero, we have

$$P_{no} = (K/2)\sqrt{P_c(P_s + P_c + 2A_{dc}P_sP_c\cos\phi_{sc})(1 - A_{dc}{}^2)} \tag{5.15}$$

Unless the angle of arrival of the c-interference is close to that of the desired signal, we can approximate

$$A_{dc}{}^2 \ll 1 \tag{5.16}$$

and eq.(5.15) becomes

$$P_{no} \simeq (K/2)\sqrt{P_c(P_s + P_c + 2A_{dc}P_sP_c\cos\phi_{sc})} \tag{5.17}$$

With further approximation, we have

$$P_{no} \simeq (K/2)\sqrt{P_c(P_s + P_c)} \tag{5.18}$$

For K=4, and P_s=P_c=1, we obtain from eq.(5.18)

$$P_{no} \simeq 3 \tag{5.19}$$

Review of the curve for r=0dB in Fig.5.1 showing the optimum input SNR of about -7.8dB (i.e., P_n amounts to 3.01) confirms that eq.(5.19) is a good estimate.

Table 5.2 Input model and constraints in the presence of pointing error.

desired signal (S)	angle of arrival	: θ_s (var.)
	power	: $P_s = 1$
incoherent (I) interference	angle of arrival	: $\theta_i = -50°$
	power	: $P_i = 100$
thermal noise	power	: $P_n = 0.01$
constrained angle		: $\theta_d = 0°$
constrained frequency		: $f_d = f_o(=1)$
pointing error		: $\delta = \theta_s - \theta_d$

Note: All external waves are narrowbanded.

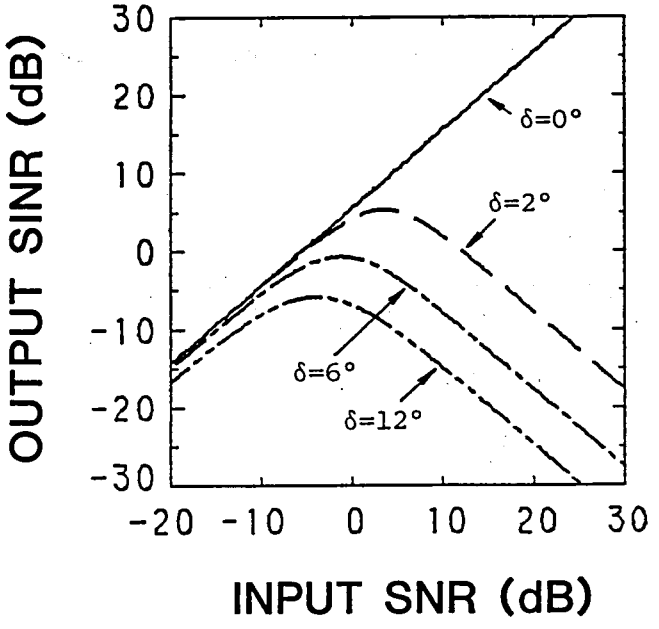

Fig.5.2 The relation between the input SNR and the output SINR under the effect of pointing error. (see Table 5.2)

5.3.2 The Error in Pointing the Angle of Arrival of the Desired Signal[87]

Using the same 4-element, 2-tap system, we calculate the effect of pointing error of the constraint direction. The parameters of the input model and constraint are shown in Table 5.2. Fig.5.2 shows the relation between the input SNR and the output SINR while varying the pointing error δ. With a high input SNR, i.e., weak internal noise, the output SINR is sensitively affected by the error of the constraint direction. With stronger internal noise, however, the decrease of the output SINR is more gradual although the best possible output SINR obtained at the error-free condition is somewhat low compared with the case of weak internal noise.

5.4 The Improved System Using the Pseudo Noise (Tamed Adaptive Antenna)

As we discussed in the previous section, we can improve the output SINR by intentionally adding some amount of internal noise when the c-interference is strong or when the setting of the constraint direction is not accurate enough. This method, however, brings about a problem that the internal noise component in the output increases. Here, we can take advantage of the DCMP algorithm that the feedback signal is generated by the matrix manipulation in a feedback route as will be discussed later. In short, we do not inject any real internal noise in the signal-flow route, but add some pseudo noise in the feedback route to affect the calculation of the optimum weight. Thus, we can escape from increasing the noise component in the signal-flow route output.

5.4.1 The Method of Injecting the Pseudo Noise

We denote the pseudo noise power by α (≥ 0), and modify the input

correlation matrix R_{xx}, i.e., we use R'_{xx} in place of R_{xx} when we calculate the optimum weight. R'_{xx} is given by

$$R'_{xx} = R_{xx} + \alpha U \tag{5.20}$$

The optimum weight vector W'_{opt} is now given by

$$W'_{opt} = R'^{-1}_{xx} C_d (C_d^T R'^{-1}_{xx} C_d)^{-1} H \tag{5.21}$$

Let us consider two extreme cases. With $\alpha=0$, the above W'_{opt} corresponds to W_{opt} of eq.(3.31) and we have an ordinary DCMP array. With α tending to infinity,

$$W'_{opt} = C_d (C_d^T C_d)^{-1} H = F \tag{5.22}$$

and we have the pattern of a uniformly excited array with its mainbeam pointed to the constrained direction. In order to get a mathematical interpretation, let us recall the cost function to be minimized in the conventional system, Q(W) of eq.(3.26), which is rewritten here as follows:

$$Q(W) = \frac{1}{2} W^T R_{xx} W + \Lambda^T (C_d^T W - H) \tag{5.23}$$

For the improved system, we have

$$\begin{aligned} Q'(W) &= \frac{1}{2} W^T R'_{xx} W + \Lambda^T (C_d^T W - H) \\ &= \frac{1}{2} W^T R_{xx} W + \Lambda^T (C_d^T W - H) + \frac{1}{2} \alpha W^T W \end{aligned} \tag{5.24}$$

Thus, we have effectively introduced an additional constraint on the norm of W so that it may not become excessively large.

5.4.2 New Gradient Algorithm

The description of the new algorithm for the improved system using the pseudo noise is now given on the basis of the conventional DCMP algorithm. The new algorithm is first given by

$$W(m+1) = W(m) - \mu \nabla_W Q'[W(m)] \tag{5.25}$$

Therefore, tracing the same process as the conventional one shown in Chapter 3, we obtain the following equation from eq.(5.25):

$$\mathbf{W}(m+1) = P[\mathbf{W}(m) - \mu R'_{xx}\mathbf{W}(m)] + \mathbf{F} \tag{5.26}$$

which is equal to the form of eq.(3.45) where R_{xx} is merely replaced by R'_{xx}. Substituting eq.(5.20) into eq.(5.26) gives

$$\begin{aligned}\mathbf{W}(m+1) &= P[\mathbf{W}(m) - \mu(R_{xx} + \alpha U)\mathbf{W}(m)] + \mathbf{F} \\ &= P[(1 - \mu\alpha)\mathbf{W}(m) - \mu R_{xx}\mathbf{W}(m)] + \mathbf{F}\end{aligned} \tag{5.27}$$

Thus, approximating R_{xx} in eq.(5.27) by $\mathbf{X}(m)\mathbf{X}^T(m)$, we obtain the practical algorithm for the improved system which is written as follows:

$$\mathbf{W}(m+1) = P[(1 - \mu\alpha)\mathbf{W}(m) - \mu\mathbf{X}(m)y(m)] + \mathbf{F} \tag{5.28}$$

Eq.(5.28) shows that the system tries to decrease the norm of the weight by compression factor, $(1 - \mu\alpha)$, at every iteration. The geometrical interpretation of this new algorithm is shown in Fig.5.3, which is compared with the conventional one shown in Fig.3.5.

The convergence condition of this algorithm can be obtained in the same manner as the conventional one given by eq.(3.56), i.e.,

$$0 < \mu < \frac{1}{\lambda'_{max}} \tag{5.29}$$

where λ'_{max} represents the maximum eigenvalue of $PR'_{xx}P$ and, similar to the conventional case, it is related to the maximum eigenvalue of R'_{xx}, σ'_{max} by

$$0 < \lambda'_{max} \leq \sigma'_{max} \tag{5.30}$$

Also, it is clear from eq.(5.20) that the relation $\sigma'_{max} = \sigma_{max} + \alpha$ holds where σ_{max} is the maximum eigenvalue of R_{xx}. Therefore, the sufficient condition of eq.(5.29) is expressed as

$$0 < \mu < \frac{1}{\sigma'_{max}} = \frac{1}{\sigma_{max} + \alpha} \tag{5.31}$$

After all, making reference to eq.(3.58), we can obtain the practical

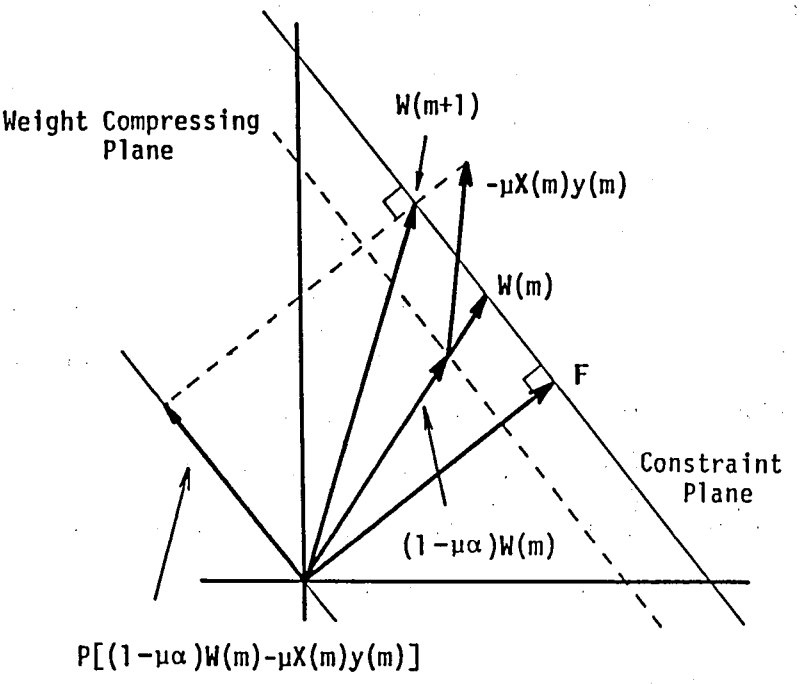

Fig.5.3 Geometrical interpretation of the algorithm of tamed adaptive array.

convergence condition for the new algorithm which is written as

$$0 < \mu < \frac{2}{3\{\mathrm{trace}(R_{xx}) + \alpha\}} \tag{5.32}$$

5.4.3 Numerical results

Optimum weights are calculated by eq.(5.21) for the system of 4-element, 2-tap array. Various characteristics of the array are then derived from them.

Case A the presence of the coherent interference

We use the values of the parameters of input and constraint shown in Table 5.1. Fig.5.4 shows the adapted pattern for three different values of α, the pseudo noise, with r being 0dB. The output components and SINR corresponding to these patterns are summarized in Table 5.3. For the case (a) which is actually the conventional system, the suppression of the i-interference is best while the desired signal is also cancelled by the c-interference. Comparing the output components of the i-interference and internal noise, we notice that the former is unnecessarily low. As we increase α, as in case(b), the suppression capability is somewhat moderated, and the signal is saved from cancellation. If we increase α too much, however, as in case(c), the system does not make a null in the direction of the i-interference and loses its function as an adaptive antenna. This suggests that there is an optimum value for the pseudo noise. Fig's.5.5 and 5.6 show the investigation of how the optimum internal noise is affected by CSR and P_i, respectively. In Fig.5.5, the meaning of the abscissa is twofold. For the solid curves, it is the sum of real and pseudo noise, i.e., $P_n+\alpha$ with an assumed value of $P_n=0.01$. For the dashed curves, the abscissa means true value of P_n. They differ because the pseudo noise does not contaminate the signal-flow route. The

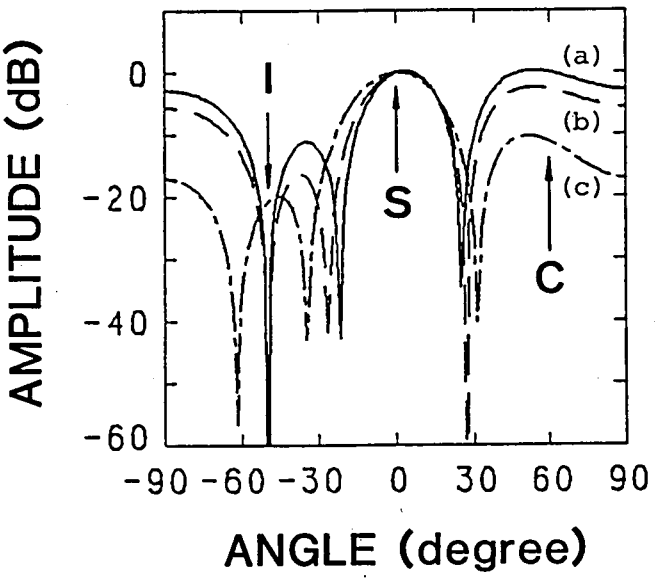

Fig.5.4 The directional patterns for various levels of pseudo noise power(α) where I, S and C in the figure show the angles of arrival of the incoherent interference, desired signal and coherent interference, respectively: (a) α=0, (b) α=1, (c) α=100. (see Table 5.1)

Table 5.3 Output components and SINR corresponding to the patterns in Fig.5.4.

	(a) α=0	(b) α=1	(c) α=100
desired signal	0.187×10^{-4}	0.728×10^{-1}	0.525
i-interference	0.141×10^{-8}	0.102×10^{-4}	0.834
thermal noise	0.838×10^{-2}	0.653×10^{-2}	0.517×10^{-2}
SINR (dB)	-26.51	10.47	-2.04

Note: The desired signal component includes coherent interference.

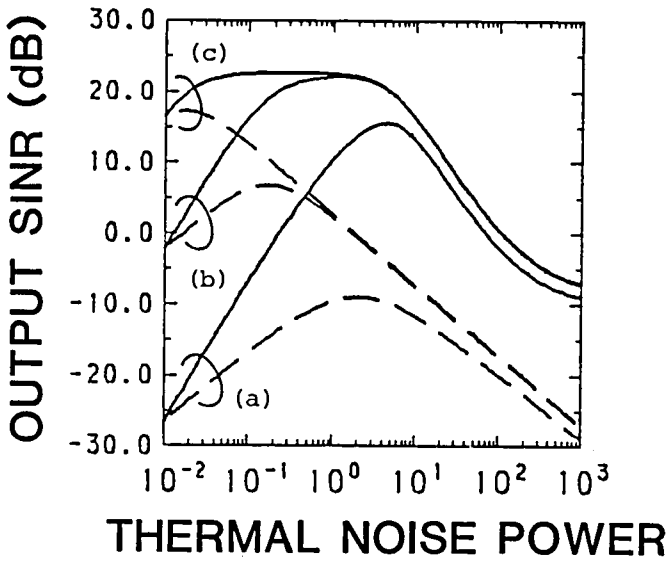

Fig.5.5 Solid curves show the relation between the pseudo noise power(α) and the output SINR while dashed curves show that between the real internal noise and the output SINR. The input coherence-to-signal ratio(r) is varied: (a) r=0dB, (b) r=-20dB, (c) r=-40dB. (see Table 5.1)

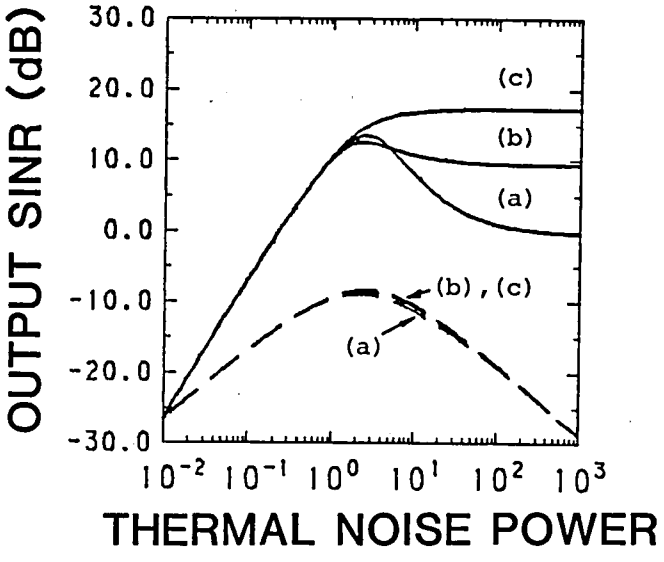

Fig.5.6 Solid curves show the relation between the pseudo noise power(α) and the output SINR while dashed curves show that between the real internal noise and the output SINR. The interference power P_i is varied: (a) P_i=10, (b) P_i=1, (c) P_i=0.1. (see Table 5.1)

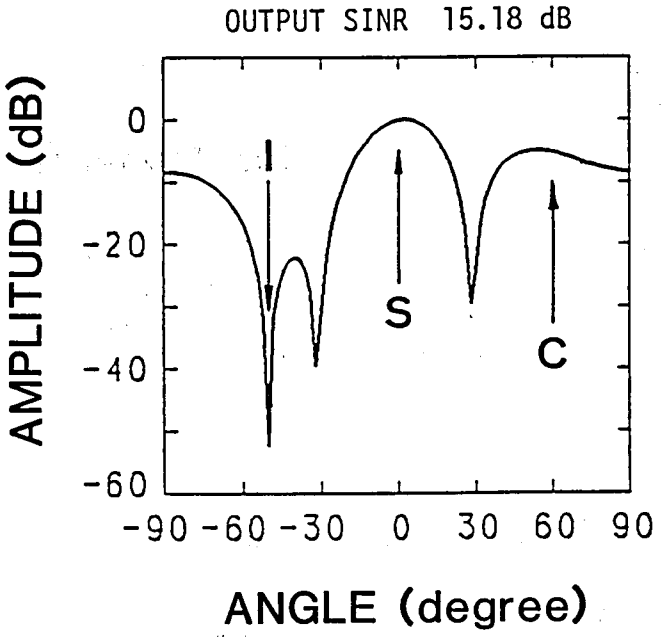

Fig.5.7 The directional pattern obtained by using the optimum pseudo noise power of α=3. I, S and C in the figure show the angles of arrival of the incoherent interference, desired signal and coherent interference, respectively. (see Table 5.1)

solid curve in (c), the case of weak c-interference, shows a plateau of the output SINR which means a wide region of the pseudo noise can produce a good SINR. Therefore, the setting of α for the worst case, i.e., r=0dB, will guarantee good performance for other cases of r<0dB. Now, we fix r=0dB, and vary the power of the i-interference, P_i. Fig.5.6 shows the results. The abscissa has the same twofold meanings as in Fig.5.5. This figure designates that the optimum pseudo noise is almost constant for different P_i's. Also, the optimum values of P_n corresponding to the peak of the dashed curves give high SINR's of the solid curves in all cases of (a) through (c). Although eq.(5.15) is for the real internal noise, the above results suggest that we can utilize it to determine the optimum pseudo noise, α as well. Thus, α may be calculated by the approximation of eq.(5.18) for $P_c=P_s$(or r=0dB):

$$\alpha_{opt} = KP_s/\sqrt{2} \tag{5.33}$$

α_{opt} is proportional to the number of elements, K and the input power of the desired signal, P_s. We only need a rough estimate of P_s since the range of the pseudo noise for good SINR is quite wide as demonstrated above. For the case of 4-element system, and P_s=1, we use eq.(5.33) and approximately decide

$$\alpha_{opt} = 3 \tag{5.34}$$

Fig.5.7 shows the adapted pattern where the parameters are the same as in Fig.5.4 except that α is chosen to be 3. By the obtained optimum weight, the output SINR is calculated to be 15.18dB, in contrast to -26.51dB for the conventional system (α=0).

We carried out numerous calculations with various combinations of the c- and i-interferences. The results conclude that the performance of the improved system is satisfactory unless the angle of arrival of these

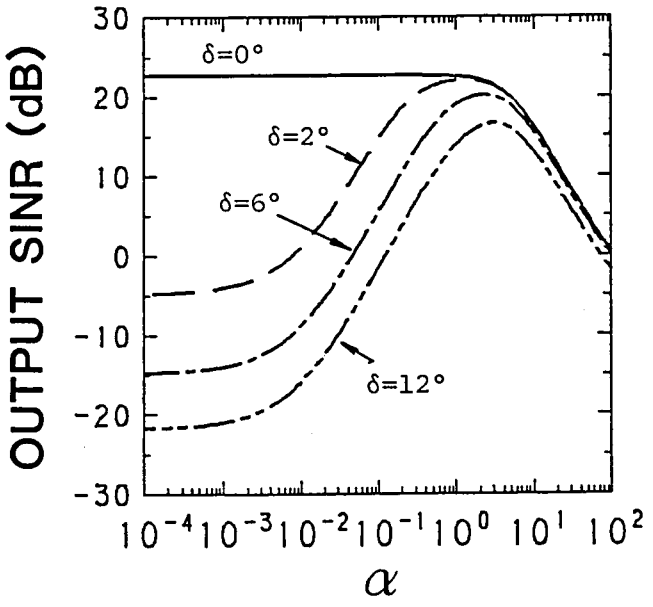

Fig.5.8 The relation between the pseudo noise power(α) and the output SINR in the presence of the pointing error. (see Table 5.2)

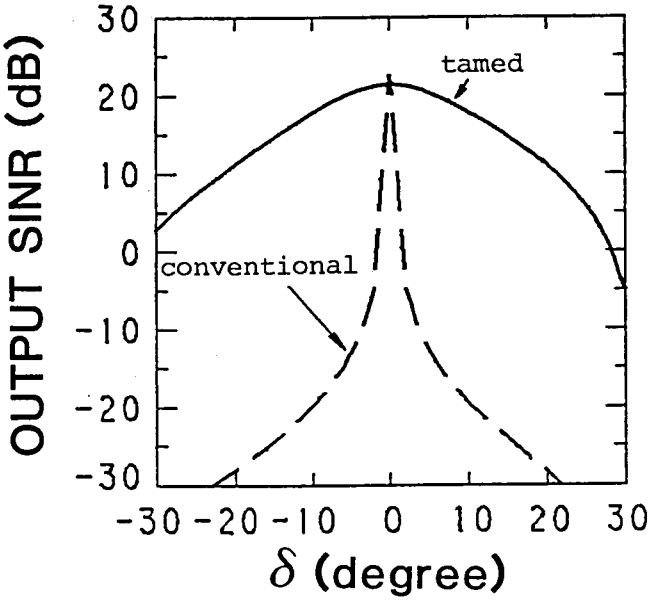

Fig.5.9 The relation between the pointing error(δ) and the output SINR. The solid curve is by the tamed system, while the dashed one, the conventional system. (see Table 5.2)

interferences falls into the vicinity of the desired signal.

Case B Pointing error of the constrained direction

We used the parameters shown in Table 5.2 for the same 4-element, 2-tap system. Fig.5.8 shows the relation between the pseudo noise power and the output SINR for different values of the pointing error, δ. It is seen that the pseudo noise of the same order of the desired signal again gives high SINR throughout. We adopt the same value of α=3 as in the previous case, and calculate the relation between the pointing error and the output SINR. The solid curve in Fig.5.9 show the result. The dashed curve in the same figure is the result by the conventional system and shown here for comparison. It is demonstrated that the tamed system allows us wide margin for the pointing error.

5.5 Broadband Performance of the Tamed Adaptive Antenna

The next topic is the frequency characteristics of an adaptive array in terms of the desired signal[88]. In most DCMP adaptive arrays, the sideband component of the desired signal is taken for the unwanted interference and becomes a target of suppression. This results in the uneven passband characteristics of the system transfer function, hence, distortion of the desired signal. By analogy of space to frequency, the favorable effect shown in the previous section in terms of the pointing error is expected to solve this problem. Our numerical results did prove that this is true. We use a 4-element, 4-tap system[89] and the desired signal is assumed to have a flat spectrum over its specified band as shown by Fig.5.10. We denote the center frequency and bandwidth by f_o and δf, respectively. In the following calculation, the fractional bandwidth is taken to be 40%. Other parameters used in the calculation are shown in

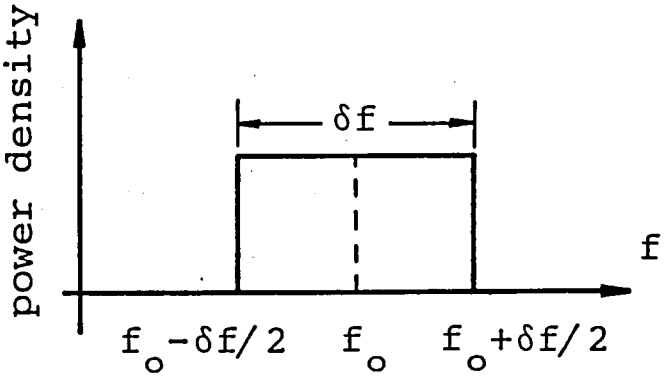

Fig.5.10 Frequency spectrum of broadband signal.

Table 5.4 Input model and constraints for the case of the broadband desired signal.

desired signal (S)	angle of arrival	: $\theta_s = 30°$
	power	: $P_s = 1$
	bandwidth	: $\delta f = 0.4 f_o$
incoherent (I) interference	angle of arrival	: $\theta_i = -50°$
	power	: $P_i = 100$
thermal noise	power	: $P_n = 0.01$
constrained angle		: $\theta_d = \theta_s$
constrained frequency		: $f_d = f_o(=1)$

Note: The incoherent interference is narrowbanded.

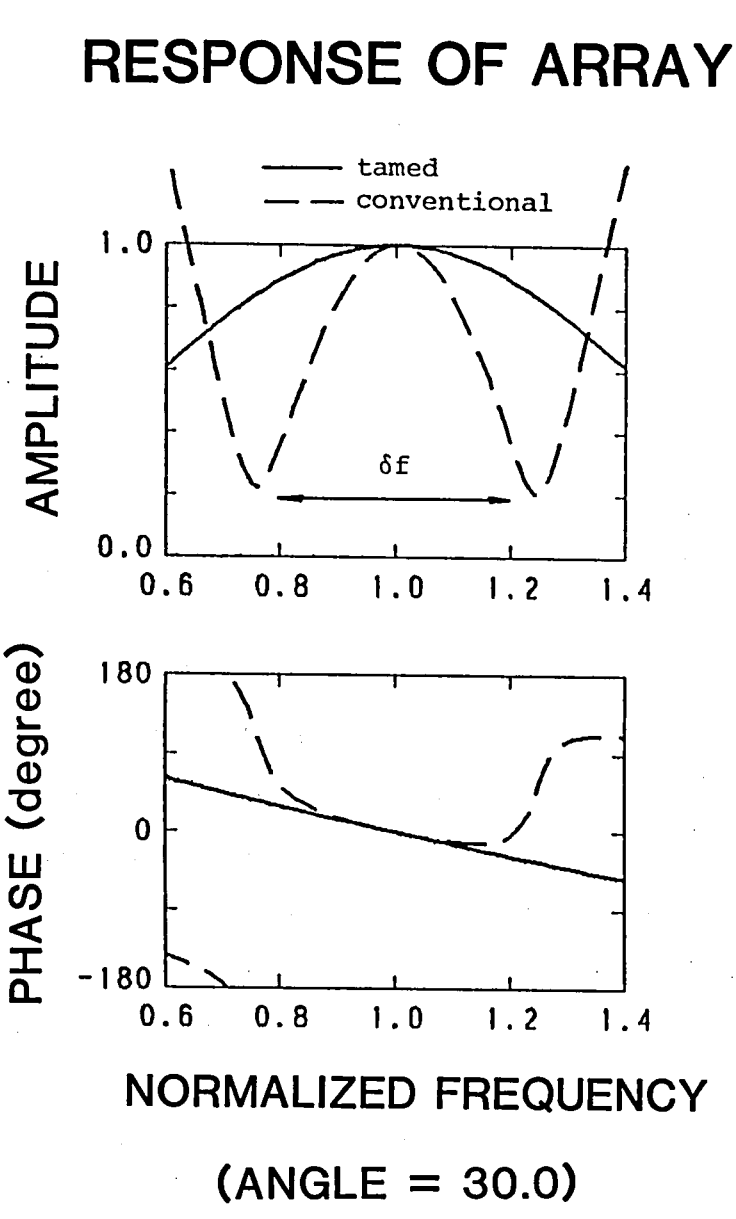

Fig.5.11 The frequency characteristics for the broadbanded desired signal. The solid curves are the results by the tamed system, while the dashed ones are by the conventional system. The former gives 20.99dB in SINR, and the latter, 7.46dB. (see Table 5.4)

Table 5.4. The i-interference is assumed to be narrowbanded. Fig.5.11 compares the frequency responses to the signal from the constrained direction. The amplitude and phase curves of the tamed system are flatter and straighter, respectively, than those of the conventional system. We also obtain higher output SINR of 20.99dB by the tamed system, in contrast to 7.46dB by the conventional system.

5.6 Performance under the Effect of Mutual Coupling

5.6.1 Description of Input Models

Since we treat only the narrowband signals hereafter, we will express them in complex notation. Then, the complex optimum weight vector of the tamed adaptive array is given by

$$\mathbf{W}_{opt} = (R_{xx} + \alpha U)^{-1}\mathbf{C}_d \, [\mathbf{C}_d^{\dagger}(R_{xx} + \alpha U)^{-1}\mathbf{C}_d]^{-1}H^* \tag{5.35}$$

where the pseudo noise α is given by eq.(5.33). The expression for the element output voltages under the effect of the mutual coupling between array elements must be derived. After Ref.[81], the required expression can be obtained by considering the K-element array as a K+1 terminal linear, bilateral network responding to an outside source as shown by Fig.5.12. In Fig.5.12, each port of the K-element array is shown to be terminated in a known load impedance z_L. The array has as its driving source a generator with open circuit voltage v_g and internal impedance z_g. Using standard notation, we can write the Kirchoff relation for the K+1 terminal network as

$$\begin{aligned} v_1 &= z_{11}i_1 + \cdots + z_{1k}i_k + \cdots + z_{1K}i_K + z_{1s}i_s \\ &\vdots \\ v_k &= z_{k1}i_1 + \cdots + z_{kk}i_k + \cdots + z_{kK}i_K + z_{ks}i_s \\ &\vdots \end{aligned} \tag{5.36}$$

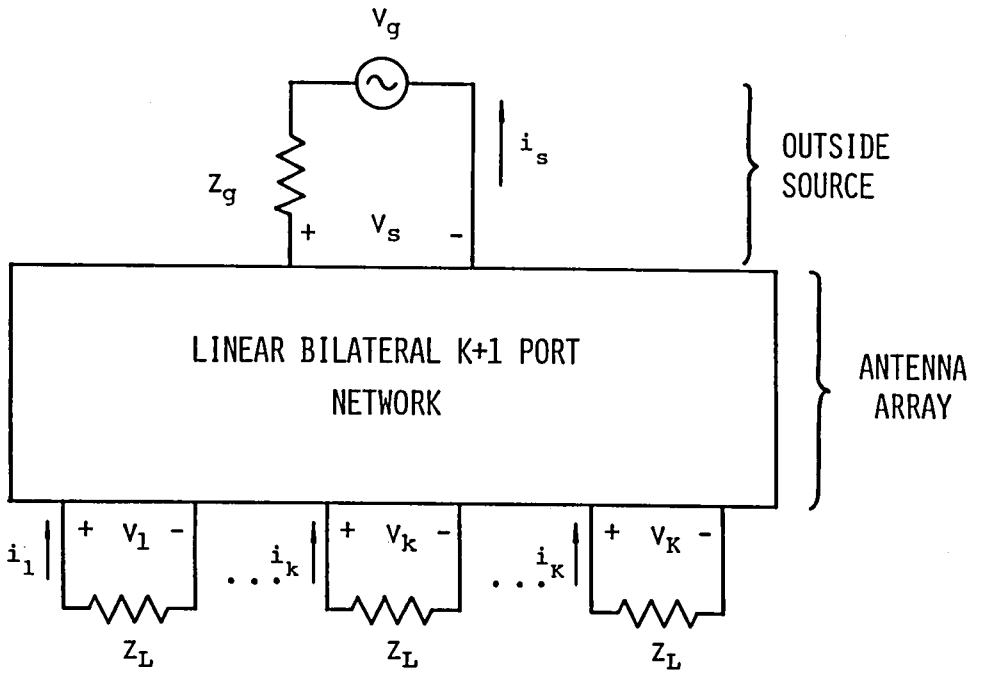

Fig.5.12 Antenna array as a K+1 terminal network.

$$\vdots \quad \vdots \quad \vdots \quad \vdots \quad \vdots$$

$$v_K = z_{K1}i_1 + \cdots + z_{Kk}i_k + \cdots + z_{KK}i_K + z_{Ks}i_s$$

where z_{ik} represents the mutual impedance between the i-th and the k-th ports (in the special case of i=k, it is the self-impedance). Further, making use of the relationship between terminal current and load impedance gives

$$i_k = -\frac{v_k}{z_L} \qquad (k=1, 2,.., K) \tag{5.37}$$

If all the elements in the array are in an open circuit condition, then

$$i_k = 0 \qquad (k=1, 2,.., K) \tag{5.38}$$

and thus from eq.(5.36)

$$v_k = z_{ks}i_s \triangleq v_{ok} \qquad (k=1, 2,.., K) \tag{5.39}$$

Substituting eq's.(5.37) and (5.39) into eq.(5.36), we obtain the following matrix equation:

$$Z_o\mathbf{V} = \mathbf{V}_o \tag{5.40}$$

where

$$Z_o = \begin{bmatrix} 1+z_{11}/z_L & z_{12}/z_L & \cdots & z_{1K}/z_L \\ z_{21}/z_L & 1+z_{22}/z_L & \cdots & z_{2K}/z_L \\ \vdots & \vdots & \vdots & \vdots \\ z_{K1}/z_L & z_{K2}/z_L & \cdots & 1+z_{KK}/z_L \end{bmatrix} \tag{5.41}$$

$$\mathbf{V} = [v_1, v_2,.., v_K]^T \tag{5.42}$$

$$\mathbf{V}_o = [v_{o1}, v_{o2},.., v_{oK}]^T \tag{5.43}$$

Z_o is the impedance matrix normalized by the load impedance z_L, and $\mathbf{V}$ and $\mathbf{V}_o$ are the vectorial expressions of the element output voltages and the open circuit voltages at antenna terminals, respectively. Since the matrix Z_o is nonsingular, eq.(5.40) is reformed as follows:

$$\mathbf{V} = Z_o^{-1}\mathbf{V}_o \tag{5.44}$$

If we ignore the mutual coupling between array elements, then the matrix Z_o becomes the identity matrix multiplied by a scaling factor since the self-impedance z_{kk}'s(k=1,...,K) are identical. Therefore, let $\mathbf{V}'$ represent the element output voltage vector in the absence of the mutual coupling, which can be expressed as

$$\mathbf{V}' = \beta^{-1}\,\mathbf{V}_o \tag{5.45}$$

where $\beta=1+z_{kk}/z_L$ and is a complex constant. Eliminating $\mathbf{V}_o$ with eq's.(5.44) and (5.45), we obtain the following equation:

$$\mathbf{V} = \beta\, Z_o^{-1}\,\mathbf{V}' \tag{5.46}$$

We can use βZ_o^{-1} in eq.(5.46) as a transformation matrix which transforms the element output voltage vector without the effect of mutual coupling into the expression under that effect. By using the above transformation matrix, we can express the input signal vector to the array processor, $\mathbf{X}$, as follows:

$$\mathbf{X} = \beta\, Z_o^{-1}\,\mathbf{V}' + \mathbf{N} \tag{5.47}$$

where $\mathbf{N}$ is the vectorial expression of the thermal noise input. Consequently, the complex correlation matrix is expressed as follows:

$$\begin{aligned} R_{xx} &= E[\mathbf{X}\mathbf{X}^{\dagger}] \\ &= |\beta|^2\, Z_o^{-1}E[\mathbf{V}'\mathbf{V}'^{\dagger}](Z_o^{-1})^{\dagger} + P_n\mathbf{U} \end{aligned} \tag{5.48}$$

$E[\mathbf{V}'\mathbf{V}'^{\dagger}]$ in eq.(5.48) corresponds to the correlation matrix of the input signals in the absence of mutual coupling. If we suppose that the desired signal and only one i-interference are incident on the array, it can be expressed in the following manner after eq.(3.91):

$$E[\mathbf{V}'\mathbf{V}'^{\dagger}] = P_s\mathbf{C}_d\mathbf{C}_d^{\dagger} + P_i\mathbf{Z}_i\mathbf{Z}_i^{\dagger} \tag{5.49}$$

5.6.2 Numerical Examples

Numerical calculation is carried out on a linear, equi-spaced adaptive

array consisting of four, half-wavelength, center-fed dipoles with the adjacent spacing of a half wavelength. The configuration of the array is shown in Fig.5.13. The system adopts side-by-side arrangement of the vertical dipoles. The desired signal and interferences are assumed to be vertically polarized and incident in the horizontal plane. The self- and mutual impedances between the dipoles are computed by the induced electromotive force (EMF) method[90]. The load impedance is equal to the complex conjugate of the self impedance of the single dipole, i.e., $z_L=z_{kk}^*$. The parameters for radio environment are shown in Table 5.5.

We obtain the optimum weight by eq's.(5.35), (5.48) and (5.49), and calculate the directional pattern in the horizontal plane of the array by using

$$D(\theta) = |\{\beta Z_o^{-1}S(\theta)\}^T W_{opt}^*|^2 \tag{5.50}$$

where $S(\theta)$ is a scanning vector which is expressed as follows:

$$S(\theta) = (1/\sqrt{2})[\exp\{j\Psi_1(\theta)\},\ldots,\exp\{j\Psi_K(\theta)\}]^T \tag{5.51}$$

Also, the output SINR can be given by

$$SINR = \frac{P^s_{out}}{P^i_{out} + P^n_{out}} \tag{5.52}$$

where

$$P^s_{out} = P_s|(\beta Z_o^{-1}C_d)^T W_{opt}^*|^2 \tag{5.53}$$

$$P^i_{out} = P_i|(\beta Z_o^{-1}Z_i)^T W_{opt}^*|^2 \tag{5.54}$$

$$P^n_{out} = P_n|W_{opt}|^2 \tag{5.55}$$

We show the directional patterns in the horizontal plane of the conventional DCMP adaptive array (α=0) in Fig.5.14, and those of the tamed adaptive array (α=3) in Fig.5.15, where (a) and (b) in each figure correspond to the patterns in the absence and presence of mutual coupling, respectively. Fig.5.14(b) shows the serious decrease of the response in

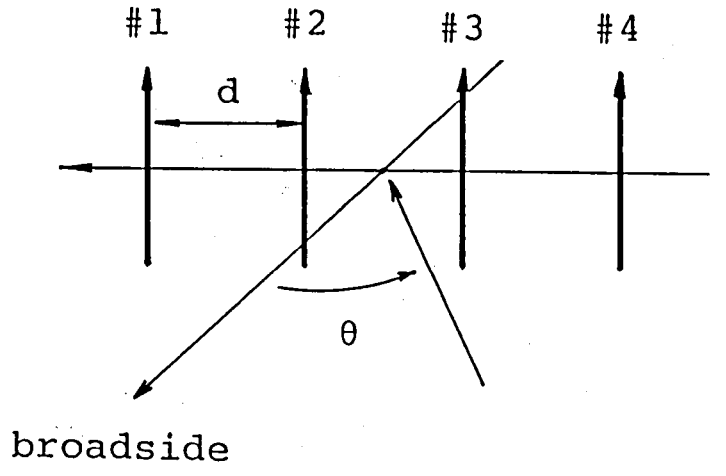

Fig.5.13 An array of four, center-fed, half-wavelength dipoles in side-by-side arrangement.

Table 5.5 Input model and constraints in the presence of mutual coupling or random input errors.

desired signal (S)	angle of arrival	: $\theta_s = 0°$
	power	: $P_s = 1$
incoherent (I) interference	angle of arrival	: $\theta_i = -50°$
	power	: $P_i = 100$
thermal noise	power	: $P_n = 0.01$
constrained angle		: $\theta_d = 0°$
constrained frequency		: $f_d = f_o(=1)$

Note: All external waves are narrowbanded.

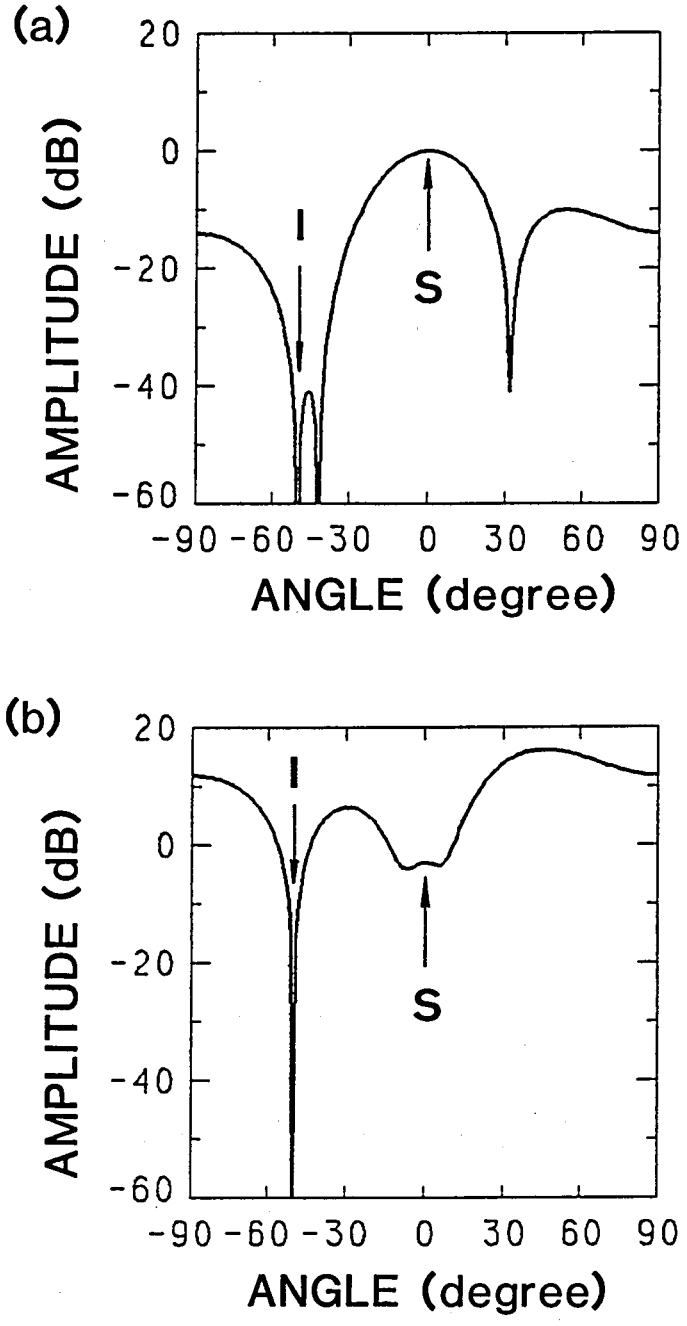

Fig.5.14 The directional patterns of conventional DCMP adaptive array, where I and S in the figures show the angles of arrival of the interference and desired signal, respectively: (a) pattern in the absence of mutual coupling (SINR=22.69dB), (b) pattern in the presence of mutual coupling (SINR=2.53dB). (see Table 5.5)

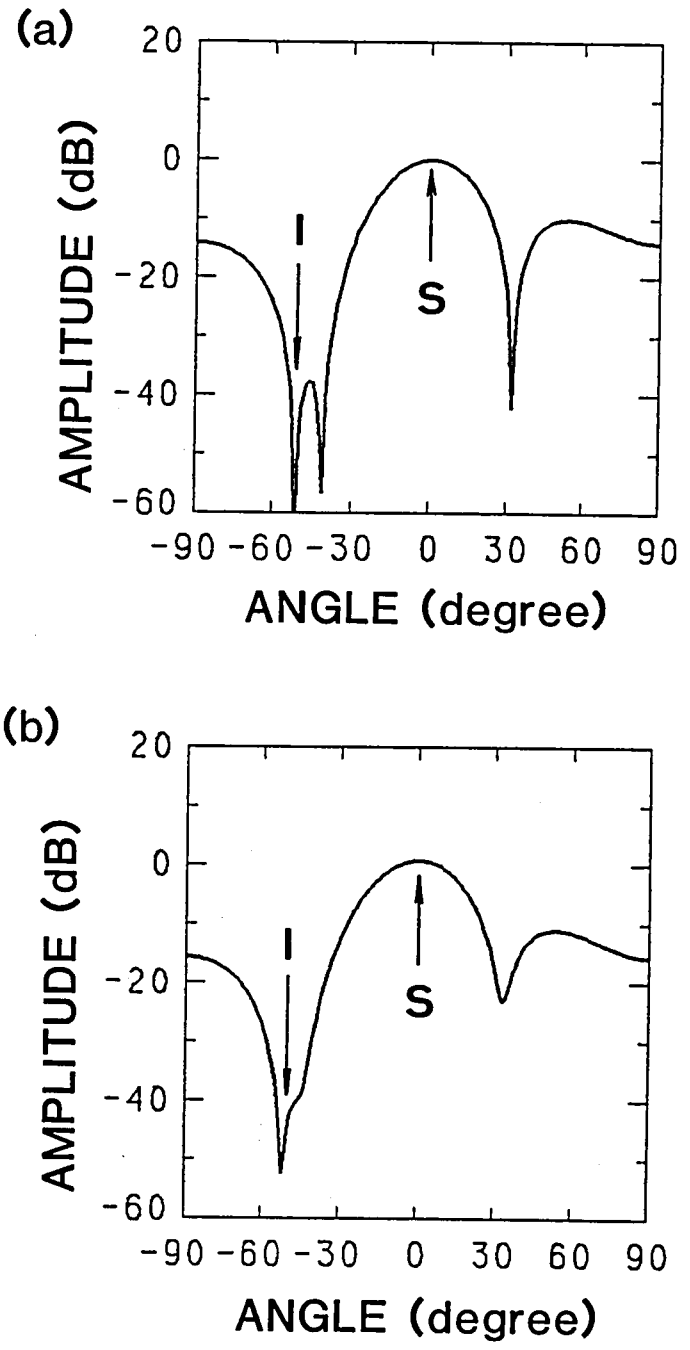

Fig.5.15 The directional patterns of tamed adaptive array (α=3), where I and S in the figures show the angles of arrival of the interference and desired signal, respectively: (a) pattern in the absence of mutual coupling (SINR=21.56dB), (b) pattern in the presence of mutual coupling (SINR=21.41dB). (see Table 5.5)

the direction of the desired signal due to the effect of the mutual coupling. As the result, the output SINR of this conventional DCMP system degrades from 22.69dB for Fig.5.14(a) down to 2.53dB for Fig.5.14(b). On the other hand, the tamed system is little affected by the mutual coupling as shown in Fig.5.15(a) and (b). Good output SINR of 21.41dB is kept even in the presence of mutual coupling.

5.7 Performance under the Effect of Random Input Errors

The mutual coupling is one of the causes of errors in the constraint. Wavefront distortion or array geometry errors are other possible causes. In this section, we will extend our discussion to the effect of general random input errors.

5.7.1 Description of Input Models

For simplicity, we consider here two external waves, the desired signal and i-interference. Let V'_{sk} represent an output voltage of the desired signal at the k-th array element in the absence of random errors, and V_{sk} the output voltage in the presence of those errors. Then, V_{sk} shall be expressed as follows:

$$V_{sk} = (1 + \varepsilon_{sak})V'_{sk}\exp(j2\pi\varepsilon_{spk}), \quad k=1, \ldots, K \tag{5.56}$$

where ε_{sak} and ε_{spk} represent the error components in the amplitude and phase of the desired signal of the k-th array element, respectively. In the vectorial notation, eq.(5.56) is written as follows:

$$\mathbf{V}_s = D_s\mathbf{V}'_s \tag{5.57}$$

where

$$\mathbf{V}_s = [V_{s1}, V_{s2}, .., V_{sK}]^T \tag{5.58}$$

$$\mathbf{V}'_s = [V'_{s1}, V'_{s2}, .., V'_{sK}]^T \tag{5.59}$$

$$D_s = \mathrm{diag}\{(1+\varepsilon_{sa1})\exp(j2\pi\varepsilon_{sp1}),.., (1+\varepsilon_{saK})\exp(j2\pi\varepsilon_{spK})\} \quad (5.60)$$

where diag{ } denotes the matrix having specified elements in the diagonal. Likewise, we assume that the element output voltages of the i-interference, $V_{ik}(k=1,..,K)$, include similar random error components, which is expressed in the vectorial notation as follows:

$$\mathbf{V}_i = D_i \mathbf{V}'_i \quad (5.61)$$

where

$$\mathbf{V}_i = [V_{i1}, V_{i2},.., V_{iK}]^T \quad (5.62)$$

$$\mathbf{V}'_i = [V'_{i1}, V'_{i2},.., V'_{iK}]^T \quad (5.63)$$

$$D_i = \mathrm{diag}\{(1+\varepsilon_{ia1})\exp(j2\pi\varepsilon_{ip1}),.., (1+\varepsilon_{iaK})\exp(j2\pi\varepsilon_{ipK})\} \quad (5.64)$$

where V'_{ik} represent an output voltage of the i-interference at the k-th array element in the absence of random errors, and ε_{iak} and ε_{ipk} are the error components in the amplitude and phase of the i-interference of the k-th array element, respectively. $\mathbf{V}'_s$ and $\mathbf{V}'_i$ are equal to the desired signal and the i-interference input vectors $\mathbf{S}(t)$ and $\mathbf{I}(t)$ given by eq's.(3.89) and (3.90), respectively. In this discussion, we assume that all those error components are statistically independent random variables with zero mean and common variances of σ_a^2 in amplitudes and of σ_p^2 in phases, respectively, namely,

$$E[\varepsilon_{sak}] = E[\varepsilon_{iak}] = 0 \qquad (k=1, 2,.., K) \quad (5.65)$$

$$E[\varepsilon_{spk}] = E[\varepsilon_{ipk}] = 0 \qquad (k=1, 2,.., K) \quad (5.66)$$

$$E[\varepsilon_{sak}^2] = E[\varepsilon_{iak}^2] = \sigma_a^2 \qquad (k=1, 2,.., K) \quad (5.67)$$

$$E[\varepsilon_{spk}^2] = E[\varepsilon_{ipk}^2] = \sigma_p^2 \qquad (k=1, 2,.., K) \quad (5.68)$$

Now, in this situation, the input vector $\mathbf{X}$ is given by

$$\mathbf{X} = \mathbf{V}_s + \mathbf{V}_i + \mathbf{N} \quad (5.69)$$

where $\mathbf{N}$ is the thermal noise input vector. Therefore, the complex correlation matrix R_{xx} is expressed as follows by using eq's.(5.57) and (5.61):

$$R_{xx} = E[\mathbf{X}\mathbf{X}^{\dagger}]$$
$$= E[\mathbf{V}_s\mathbf{V}_s^{\dagger}] + E[\mathbf{V}_i\mathbf{V}_i^{\dagger}] + P_n\mathbf{U}$$
$$= \mathbf{D}_s E[\mathbf{V'}_s\mathbf{V'}_s^{\dagger}]\mathbf{D}_s^{*} + \mathbf{D}_i E[\mathbf{V'}_i\mathbf{V'}_i^{\dagger}]\mathbf{D}_i^{*} + P_n\mathbf{U} \quad (5.70)$$

Considering $E[\mathbf{V'}_s\mathbf{V'}_s^{\dagger}] = P_s\mathbf{C}_d\mathbf{C}_d^{\dagger}$ and $E[\mathbf{V'}_i\mathbf{V'}_i^{\dagger}] = P_i\mathbf{Z}_i\mathbf{Z}_i^{\dagger}$, we obtain further from eq.(5.70)

$$R_{xx} = P_s\mathbf{D}_s\mathbf{C}_d\mathbf{C}_d^{\dagger}\mathbf{D}_s^{*} + P_i\mathbf{D}_i\mathbf{Z}_i\mathbf{Z}_i^{\dagger}\mathbf{D}_i^{*} + P_n\mathbf{U} \quad (5.71)$$

For the case where more than one interferences arrives, we can apply the same input modeling as the above to them.

5.7.2 Numerical Results

We will show the numerical results of the output SINR in the presence of random errors described above. The calculation are carried out on a four-element, linear, equi-spaced adaptive array of the isotropic elements with the element spacing of a half wavelength. The parameters for radio environment in Table 5.5 are used here again. In this situation, after the optimum weight is obtained by using eq.(5.71) in eq.(5.35), P^{s}_{out}, P^{i}_{out} and P^{n}_{out} are respectively given by

$$P^{s}_{out} = E[|\mathbf{V}_s^{T}\mathbf{W}_{opt}^{*}|^2] = P_s|(\mathbf{D}_s\mathbf{C}_d)^{T}\mathbf{W}_{opt}^{*}|^2 \quad (5.72)$$

$$P^{i}_{out} = E[|\mathbf{V}_i^{T}\mathbf{W}_{opt}^{*}|^2] = P_i|(\mathbf{D}_i\mathbf{Z}_i)^{T}\mathbf{W}_{opt}^{*}|^2 \quad (5.73)$$

$$P^{n}_{out} = P_n|\mathbf{W}_{opt}|^2 \quad (5.74)$$

The output SINR is computed by eq's.(5.52) and (5.72)-(5.74).

Fig.5.16 illustrates output SINR of the conventional system as functions of variances, σ_a^2 and σ_p^2. Twenty independent trials of the random errors were used to obtain the average output SINR at each point in Fig.5.16. It is seen from Fig.5.16 that the conventional system suffers from severe deterioration by the random input errors, especially sensitive to phase errors. For example, the SINR degradation from its optimum value at $\sigma_p^2=\sigma_a^2=0$ is 34.88dB where $\sigma_p^2=0.005$ and $\sigma_a^2=0$, and 18.59dB where

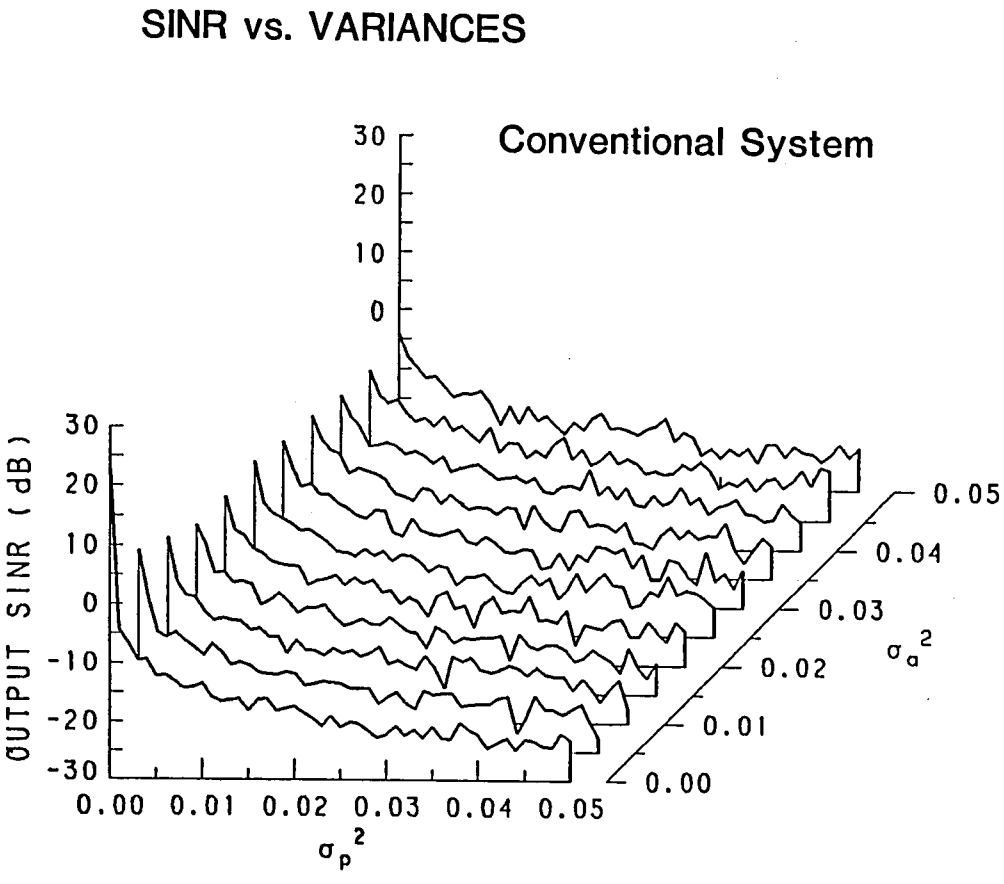

Fig.5.16 Output SINR of conventional DCMP adaptive array as functions of both amplitude variance, σ_a^2, and phase variance, σ_p^2 in the presence of random input errors. Output SINR at each point is an averaged value using twenty independent trials of the random errors. (see Table 5.5)

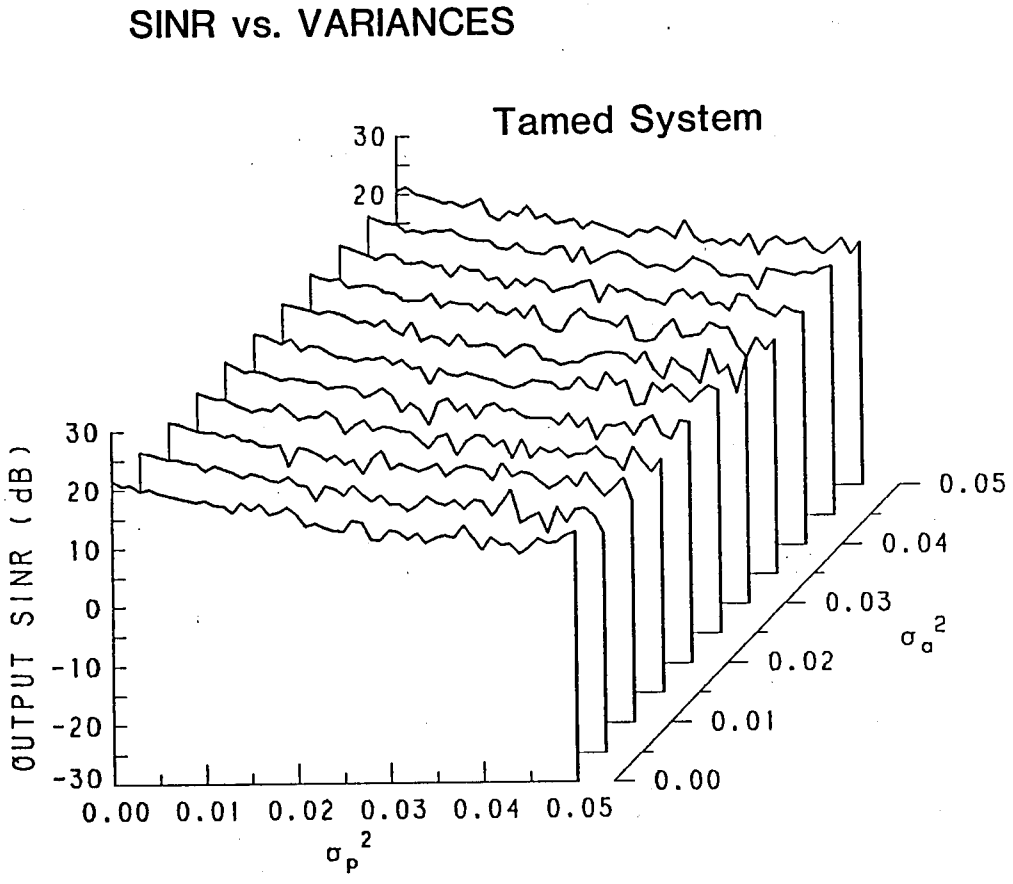

Fig.5.17 Output SINR of tamed adaptive array (α=3) as functions of both amplitude variance, σ_a^2, and phase variance, σ_p^2 in the presence of random input errors. Output SINR at each point is an averaged value using twenty independent trials of the random errors. (see Table 5.5)

σ_a^2=0.005 and σ_p^2=0. Fig.5.17 shows the results of the averaged output SINR of the tamed system that are obtained by the same method as Fig.5.16. The deterioration of SINR due to those errors is very small. Comparing Fig.5.17 with Fig.5.16, we can see that the tamed system is much more robust against the random input errors.

5.8 Concluding Remarks

In this chapter, we discussed the steady-state performance of the adaptive array under the DCMP algorithm suffering from cancellation or distortion of the desired signal in such cases as;

(a) the presence of a coherent interference,

(b) the pointing error of constrained direction, and

(c) the broadband desired signal.

As the results of numerical calculation and theoretical analysis, we found out that we can improve the output SINR by intentionally adding some amount of internal noise when the c-interference is strong or when the setting of the constrained direction is not accurate enough. This method, however, brings about a problem that the internal noise component in the output increases. Then, we took advantage of the DCMP algorithm that the feedback signal is generated by the matrix manipulation in a feedback route. In short, we do not add any real internal noise in the signal-flow route, but inject some "pseudo noise" in the feedback route to affect the calculation of the optimum weight. Thus, we have succeeded in escaping from increasing the noise component in the signal-flow route output. The optimum amount of pseudo noise to be injected was also discussed and its formula is given by eq.(5.33). We named this improved DCMP system "Tamed Adaptive Antenna Array." The tamed adaptive array has been proved

effective to protect the desired signal from the adverse cases of (a) through (c).

All examples concerning the above are for the case of a 4-element array. Though not shown here, other cases were also studied. To summarize the results in short, the array becomes more sensitive to the pointing error and bandwidth of the desired signal as the number of its elements increases(as the natural results of larger aperture). The need of "taming" will be more urgent in such cases. Also, the tamed system is more effective against the coherent interference in a larger array.

As the extension of the above problem (b), we studied the effects of mutual coupling and general random input errors on the steady-state performances of the conventional and tamed DCMP adaptive arrays. Concerning the mutual coupling, we examined the performance by using the four-dipole linear array system and EMF (the induced electromotive force) method for the self- and mutual impedances. As to the random input errors, Gaussian random variables are employed in computation. The results of numerical examples show that such effects cause serious deterioration of the performance of the conventional system due to the suppression of the desired signal. On the other hand, the tamed system is shown to be robust against such effects by providing a good protection of the desired signal.

A similar problem resulting from the effect of mutual coupling is treated in Ref.[81] and a countermeasure is proposed which can be adopted in the Howells-Applebaum adaptive array. This scheme requires precise modification of the steering vector based on the exact knowledge about the mutual impedances. It is evident by the results presented in this chapter that our tamed system is much simpler and suited for wider variety of circumstances.

As stated above, only simple operation of injecting some pseudo noise in the feedback route brings about various remarkable improvements over the performance of the DCMP adaptive array. It is one of noteworthy virtues of the DCMP system which adopts the digital computer as the adaptive signal processor.

CHAPTER 6

ADAPTIVE ARRAY USING SPATIAL AVERAGING TECHNIQUE

6.1 Introduction

An adaptive array working under the guiding principle of directionally constrained minimization of power (DCMP) usually assumes that the interference is not coherent with the desired signal[27],[30]. If, on the other hand, the interference is coherent with the desired signal, which is usually the case in multipath environments, the system tends to utilize this interference to cancel the desired signal under the DCMP algorithm[72],[73],[78],[79],[91]. The tamed adaptive array we proposed in Chapter 5 is an improved system against the coherent interference, but its objective is to protect the desired signal from such cancellation, not to suppress the coherent interference. That is why in this chapter, we investigate further improvement of the system for the purpose of suppressing the coherent interference. Examining carefully the characteristics of the correlation matrix of the complex inputs at identical sensor elements, we have found out the following. In the case of incoherent interference, the correlation matrix is Toeplitz, as well as positive definite and Hermitian, because there is no cross correlation between the desired signal and the incoherent interference. In the case of coherent interference, on the other hand, the correlation matrix is not Toeplitz since each element of the matrix is affected by the cross correlation term between the coherent waves arriving through different

propagation paths. Therefore, it is expected that if by some means the correlation matrix is made Toeplitz, then this modified matrix can be used to determine the weights of the array elements to suppress the coherent interferences as well as the incoherent ones.

Recently, the techniques of spatially averaging the correlation matrices have been reported in the fields of adaptive nulling[72],[53], [54],[92],[93] and direction finding[56],[94]. They divide the array into sub-arrays and average the input correlation matrices of these sub-arrays to get a resultant matrix whose size is the same as that of one sub-array. Thus, the size of the full array is sacrificed in order to "decorrelate" the incoming coherent waves. The published results claim that this technique can suppress the cross correlation term and obtain a well-behaved correlation matrix. Particularly in the case of direction finding of coherent sources, this method brings about satisfactory performance in conjunction with eigenstructure techniques of the correlation matrix[33]-[41],[56],[57]. However, as shown in this chapter, the interference suppression obtained using this techniques is not perfect. The reason for this is that the resultant matrix is not close to Toeplitz by the simple averaging over the finite array aperture.

In this chapter, we will introduce a toeplitzization algorithm for the adaptive array which adopts a new spatial averaging technique and produces a pattern with deep nulls in the direction of each coherent, as well as incoherent, interference[95],[96]. It is named an adaptive spatial averaging since it adapts the variable weights to average the correlation matrices according to the radio environment.

In Section 6.2, we introduce the spatial averaging technique for multipath environments. In Section 6.3, we propose a new algorithm, and demonstrate its successful performance by theoretical and numerical

analysis. Section 6.4 is concerned with the application of the new algorithm to the sampled matrix inversion DCMP adaptive array. Section 6.5 states conclusions.

6.2 A Method and Effect of Spatial Averaging

In the present discussion, we assume that the input signals are narrowband and can be treated by complex expression. As for the array system, we consider a linear, equally spaced array with the isotropic sensor elements. For controlling the element weights, we will adopt the DCMP method in this chapter.

We use a direct method of estimating R_{xx} and determining $\mathbf{W}_{opt}$ by eq.(3.82) which is written as follows here again:

$$\mathbf{W}_{opt} = R_{xx}^{-1}\mathbf{C}_d(\mathbf{C}_d^{\dagger}R_{xx}^{-1}\mathbf{C}_d)^{-1}H^* \tag{6.1}$$

The correlation matrix, R_{xx}, is normally obtained by simple temporal average. Then, the cross correlation between the desired signal and the c-interference is non-zero since their phase relation stays constant. Therefore, the system regards the sum of them as one wave and tries to minimize the output, resulting in the cancellation of the desired signal. That is already demonstrated in Chapter 5.

The phase relation between the desired signal and c-interference can be randomized by spatially moving the receiving point[51],[52]. If one moves the receiving array as a whole in estimating R_{xx}, the phases of those waves at a particular element change differently according to their respective directions of arrival. Thus their phase relation fluctuates. If we measure their cross correlation at several points, it will tend to be nullified by averaging. This is the concept of suppressing the

correlation by spatial averaging. In the following, we will explain it in detail.

Instead of actually moving the whole M-element array, the array can be divided into partially overlapping K-element sub-arrays(K<M) as shown by Fig.6.1. In this case, the cross correlation between the desired signal and c-interference can be suppressed by averaging over the sub-arrays. Let N denote the total number of sub-arrays, and it is expressed as follows:

$$N = M - K + 1 \tag{6.2}$$

We put the common phase center for all sub-arrays at the center of the full array. Then the full M-element input vector is given by

$$\mathbf{X} = [x_1, x_2, \ldots, x_M]^T, \tag{6.3}$$

and the K-element input vector for the n-th sub-array, which shall be denoted by $\mathbf{X}_n$, is expressed as follows:

$$\mathbf{X}_n = [x_n, x_{n+1}, \ldots, x_{n+K-1}]^T \quad (n=1,\ldots,N) \tag{6.4}$$

Accordingly, the correlation matrix of the n-th sub-array, $R_{xx\cdot n}$, is expressed as follows:

$$R_{xx\cdot n} = E[\mathbf{X}_n \mathbf{X}_n^{\dagger}] \quad (n=1,\ldots,N) \tag{6.5}$$

Fig.6.2 shows the relation between $R_{xx\cdot n}$ and R_{xx}, the latter being the correlation matrix of the full array. The spatially averaged correlation matrix, R'_{xx}, is given by

$$R'_{xx} = \sum_{n=1}^{N} v_n R_{xx\cdot n} \tag{6.6}$$

where v_n's(n=1,...,N) are averaging weights for the correlation matrices of the sub-arrays. They are real and subject to the following equation:

$$\sum_{n=1}^{N} v_n = 1 \tag{6.7}$$

Next, we assume that only two waves, the desired signal and a c-

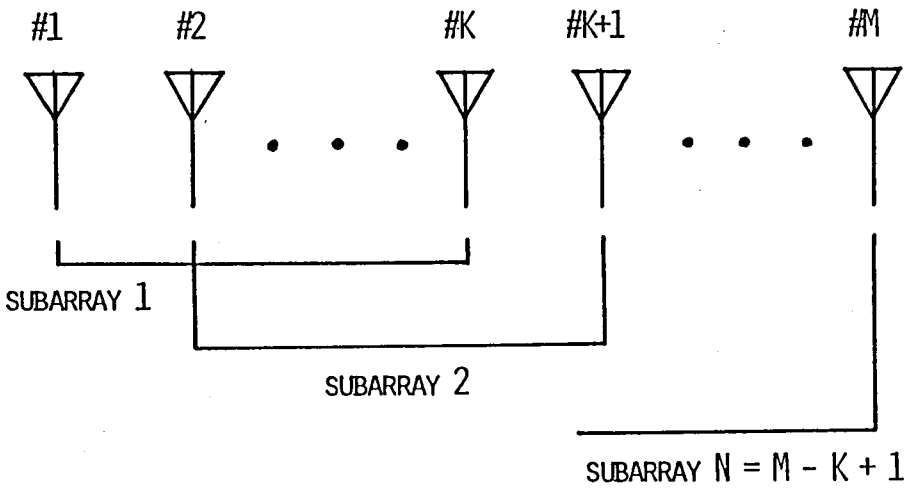

Fig.6.1 M-element full array consisting of overlapping K-element sub-arrays.

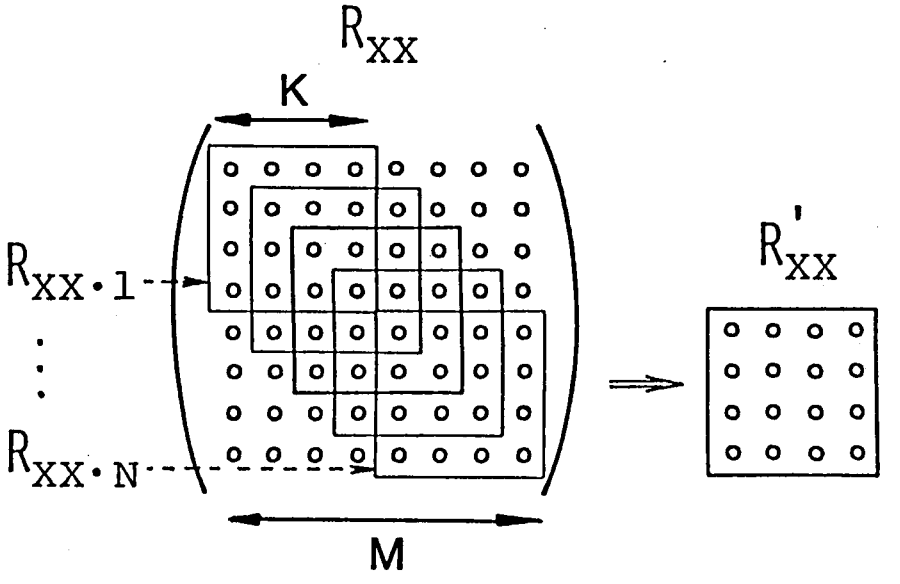

Fig.6.2 The relation between the correlation matrices of the full array and each sub-array.

interference, are incident on the array and we will examine the effect of spatial averaging. The thermal noise shall be neglected here. In this case, x_m, the input signal at the m-th element of the full array can be expressed as follows:

$$x_m = \sqrt{P_s/2}\ \exp[j\{\Psi_m(\theta_s)+\phi_s\}] + \sqrt{P_c/2}\ \exp[j\{\Psi_m(\theta_c)+\phi_c\}] \qquad (6.8)$$

$$(m=1,\ldots,M)$$

$$\Psi_m(\theta_x) = (2\pi d/\lambda)\{m - (M+1)/2\}\ \sin\theta_x \quad (x=s \text{ or } c;\ m=1,\ldots,M) \qquad (6.9)$$

where P_s and P_c are the input powers of the desired signal and the c-interference, θ_s and θ_c are their angles of arrival, and ϕ_s and ϕ_c are their phases at the phase center, respectively. d and λ are the element spacing and the wavelength of the desired signal, respectively. Then, we obtain the (p,q) element of $R_{xx\cdot n}$, $r_{p,q\cdot n}$, by using eq's.(6.4), (6.5) and (6.8):

$$\begin{aligned} r_{p,q\cdot n} &= E[x_{p+n-1}\cdot x^*_{q+n-1}] \\ &= (P_s/2)\ \exp[j(2\pi d/\lambda)(p-q)\sin\theta_s] \\ &\quad + (P_c/2)\ \exp[j(2\pi d/\lambda)(p-q)\sin\theta_c] \\ &\quad + (\sqrt{P_sP_c}/2)(Z_{sc} + Z_{cs}) \qquad (p,\ q=1,\ldots,K) \end{aligned} \qquad (6.10)$$

$$Z_{sc} = \exp[j\{\phi_s-\phi_c+(2\pi d/\lambda)\{(p+n-1)\sin\theta_s - (q+n-1)\sin\theta_c - (M+1)(\sin\theta_s - \sin\theta_c)/2\}\}] \qquad (6.11)$$

$$Z_{cs} = \exp[j\{\phi_c-\phi_s+(2\pi d/\lambda)\{(p+n-1)\sin\theta_c - (q+n-1)\sin\theta_s - (M+1)(\sin\theta_c - \sin\theta_s)/2\}\}] \qquad (6.12)$$

$$(n=1,\ldots,N)$$

The third term of eq.(6.10) is the cross correlation of the present interest. Now, the (p,q) element of R'_{xx}, $r'_{p,q}$, can be derived from eq's.(6.6), (6.7) and (6.10) as follows:

$$r'_{p,q} = \sum_{n=1}^{N} v_n\ r_{p,q\cdot n}$$

$$= (P_s/2)\exp[j(2\pi d/\lambda)(p-q)\sin\theta_s] + (P_c/2)\exp[j(2\pi d/\lambda)(p-q)\sin\theta_c] + (\sqrt{P_s P_c}/2)(\rho\, Z'_{sc} + \rho^* Z'_{cs}) \qquad (p, q=1,\ldots,K) \qquad (6.13)$$

$$Z'_{sc} = \exp[j\{\phi_s-\phi_c+(2\pi d/\lambda)\{p\sin\theta_s - q\sin\theta_c - (K+1)(\sin\theta_s - \sin\theta_c)/2\}\}] \qquad (6.14)$$

$$Z'_{cs} = \exp[j\{\phi_c-\phi_s+(2\pi d/\lambda)\{p\sin\theta_c - q\sin\theta_s - (K+1)(\sin\theta_c - \sin\theta_s)/2\}\}] \qquad (6.15)$$

$$\rho = \sum_{n=1}^{N} v_n \exp[j\{(2\pi d/\lambda)\{n-(N+1)/2\}(\sin\theta_s - \sin\theta_c)\}] \qquad (6.16)$$

Comparing eq.(6.10) with eq.(6.13), we see that the cross correlation terms are modified by the factor ρ. Therefore, we shall call ρ the suppressed correlation factor hereafter. The smaller value of ρ makes the c-interference the more like i-interference and performs the better characteristics. Thus, ρ should be minimized by a proper choice of the v_n's. Conventional averaging techniques adopt fixed values of v_n's. For example, in uniform weighting[53],[54],[72],[92], we have

$$v_n = \frac{1}{N} \qquad (n=1,\ldots,N). \qquad (6.17)$$

In Ref's.[53] and [54], Shan and Kailath claimed that if they use the sub-arrays which are at least as many as signal sources for the above uniform spatial averaging, then they can recover the rank of the correlation matrix that is reduced by the coherency of those signals. It is true that this is sufficient for direction finding of coherent sources with the aid of eigenstructure techniques[33]-[41], but not adequate for adaptive nulling. The reason is as follows.

We first calculate the adapted response in the direction of the c-interference of one sub-array after the spatial averaging in the situation given by eq.(6.8). Taking the thermal noise input into

consideration, the averaged correlation matrix R'_{xx} can be expressed as follows by using eq.(6.13):

$$R'_{xx} = P_n U + P_s C_d C_d^{\dagger} + P_c Z_c Z_c^{\dagger} + \rho \exp\{j(\phi_s-\phi_c)\}\sqrt{P_s P_c} C_d Z_c^{\dagger} + \rho^* \exp\{-j(\phi_s-\phi_c)\}\sqrt{P_s P_c} Z_c C_d^{\dagger} \quad (6.18)$$

where

$$C_d = (1/\sqrt{2})[\exp\{j\Psi_{K\cdot 1}(\theta_s)\}, \ldots, \exp\{j\Psi_{K\cdot K}(\theta_s)\}]^T \quad (6.19)$$

$$Z_c = (1/\sqrt{2})[\exp\{j\Psi_{K\cdot 1}(\theta_c)\}, \ldots, \exp\{j\Psi_{K\cdot K}(\theta_c)\}]^T \quad (6.20)$$

$$\Psi_{K\cdot k}(\theta_x) = (2\pi d/\lambda)\{k - (K+1)/2\} \sin\theta_x \quad (x=s \text{ or } c;\ k=1,..,K) \quad (6.21)$$

Letting

$$X_d = \rho'\sqrt{P_s} C_d + \sqrt{P_c} Z_c \quad (6.22)$$

$$\rho' = \rho \exp\{j(\phi_s - \phi_c)\} \quad (6.23)$$

$$\nu = 1 - |\rho'|^2 = 1 - |\rho|^2, \quad (6.24)$$

we can rewrite eq.(6.18) as follows:

$$R'_{xx} = P_n U + \nu P_s C_d C_d^{\dagger} + X_d X_d^{\dagger} \quad (6.25)$$

The above eq.(6.25) has a form similar to eq.(3.91) in Chapter 3. Therefore, we can obtain the optimum weight W_{opt} for the sub-array in the same manner as the previous derivation. After operating some manipulations, it is expressed as follows:

$$W_{opt} = \zeta(2/K)H^*[\{2P_n + K(P_c + \rho'^* A_{sc}\sqrt{P_s P_c})\} C_d - K(\rho'^*\sqrt{P_s P_c} + A_{sc} P_c) Z_c] \quad (6.26)$$

where

$$\zeta = \{2P_n + KP_c(1 - A_{sc}^2)\}^{-1} \quad (6.27)$$

$$A_{sc} = \frac{\sin\{(K\pi d/\lambda)(\sin\theta_s - \sin\theta_c)\}}{K\sin\{(\pi d/\lambda)(\sin\theta_s - \sin\theta_c)\}} \quad (6.28)$$

Thus, the power responses to the desired signal and the c-interference, which shall be denoted by G_s and G_c, are expressed as

$$G_s = |H|^2 \quad (6.29)$$

$$G_c = |Z_c^T W_{opt}^*|^2$$
$$= \zeta^2 |H\{2P_n A_{sc} - K\rho'\sqrt{P_s P_c}(1 - A_{sc}^2)\}|^2 \quad (6.30)$$

Under the assumption that the input power of the thermal noise is much smaller than those of external waves and that θ_c lies in the sidelobes of the sub-array, we have from eq.(6.30)

$$G_c \simeq (P_s/P_c)|\rho|^2|H|^2 \quad (6.31)$$

Here, for convenience, we define the output CSR (c-interference to signal ratio) as

$$CSR = \frac{P_c G_c}{P_s G_s} \quad (6.32)$$

and, in this situation, the output CSR can be given by

$$CSR \simeq |\rho|^2 \quad (6.33)$$

We see that eq.(6.33) directly relates the suppression of the cross correlation term to the nulling of the c-interference.

In the meanwhile, eq.(6.16) shows that with v_n's given by eq.(6.17), ρ becomes an array factor for the uniformly excited N-element linear array with the mainbeam directed to the desired signal. The directional pattern in general has sidelobes with finite levels and we cannot totally suppress the cross correlation unless the direction of c-interference happens to be at a null of this pattern. Therefore, from eq.(6.33), it follows that the uniform spatial averaging is insufficient for nulling of the c-interference. Frost also stated this fact in a different expression in Ref.[94] that for perfect rejection of the c-interference, a number of sub-arrays are necessary so that the total amount of phaseshifts of the c-interference in the whole array may be evenly distributed over integer multiple cycles of the c-interference's carrier frequency to ensure that the sub-arrays cancel each other when their outputs are summed.

In temporal domain, we could calculate the average over a sufficiently

long interval and expect the cross correlation to vanish when the phase relation was random. In spatial domain, however, the aperture is not large enough for this effect to arise. Even if we could have such a large aperture, we could not achieve the SCR higher than 13.2dB in the case of the c-interference arriving at the peaks of the first sidelobes of the sub-array, which is a well-known fact in the field of linear antenna array. Therefore, we must find some smart method. In fact, eq.(6.16) clearly shows that this problem is the pattern synthesis of the array by controlling the magnitudes of the weights of each element in order to place a null of ρ for the given combination of θ_s and θ_c.

6.3 Adaptive Spatial Averaging Technique

6.3.1 Principle of Toeplitzization

As for the weighted spatial averaging techniques other than the uniform weighting, the Dolph-Chebyshev or Hamming-window type weighting [93] was suggested so that the sidelobes of the array factor of eq.(6.16) could be reduced to some extent, but they have a certain limit as mentioned in the above section. For complete suppression, we will introduce an adaptive averaging technique[95],[96]. As we discussed previously, if the third term in eq.(6.13) is forced to vanish, the correlation matrix R'_{xx} becomes Toeplitz which has equal valued elements along each diagonal. Therefore, we will opt to control the averaging weights, v_n's so as to equalize the elements in the diagonal of the resultant matrix, R'_{xx}. The details of this technique are given below.

Let us define a quantity to be minimized, ε, which is a measure of deviation of the correlation matrix from a Toeplitz form. It is expressed by the sum of the covariances over all the elements of R'_{xx} where the

covariance is defined in terms of each along-diagonal mean. Thus, ε is given by

$$\varepsilon = \sum_{i=0}^{K-2} \sum_{k=1}^{K-i} | r'_{k+i,k} - r'(i) |^2 \tag{6.34}$$

where

$$r'(i) = \frac{1}{K-i} \sum_{k=1}^{K-i} r'_{k+i,k} = \frac{1}{K-i} \sum_{k=1}^{K-i} \left(\sum_{n=1}^{N} v_n \, r_{k+i,k\cdot n} \right) \tag{6.35}$$

$$(i=0,\ldots,K-2)$$

$r'(i)$ is a mean value of $r'_{k+i,k}$'s$(k=1,\ldots,K-i)$, the elements in the i-th sub-diagonal of R'_{xx}. Since the correlation matrices are Hermitian, only the elements of the main- and sub-diagonals (except super-diagonals) in R'_{xx} are taken into consideration in eq's.(6.34) and (6.35). Eq.(6.34) can be also rewritten in a vector form as follows:

$$\varepsilon = \mathbf{V}^T R_{ee} \mathbf{V} \tag{6.36}$$

where

$$\mathbf{V} = [v_1, v_2, \ldots, v_N]^T \tag{6.37}$$

$$R_{ee} = \sum_{i=0}^{K-2} \sum_{k=1}^{K-i} \mathrm{Re}\{\mathbf{e}_{k+i,k} \cdot \mathbf{e}^{\dagger}_{k+i,k}\} \tag{6.38}$$

$$\mathbf{e}_{k+i,k} = [e_{k+i,k\cdot 1}, \ldots, e_{k+i,k\cdot N}]^T \tag{6.39}$$

$$e_{k+i,k\cdot n} = r_{k+i,k\cdot n} - \frac{1}{K-i} \sum_{k=1}^{K-i} r_{k+i,k\cdot n} \tag{6.40}$$

$$(i=0,\ldots,K-2;\ k=1,\ldots,K-i;\ n=1,\ldots,N)$$

where Re{ } denotes the real part and $e_{k+i,k\cdot n}$ is a deviation of the (k+i,k) element of $R_{xx\cdot n}$ from the mean value along its i-th sub-diagonal. Therefore, this problem is considered linearly constrained minimization, and its formulation can be expressed as follows:

$$\min_{\mathbf{V}} (\varepsilon = \mathbf{V}^T R_{ee} \mathbf{V}) \tag{6.41}$$

$$\text{subject to } \mathbf{V}^T \mathbf{I} = 1 \tag{6.42}$$

where eq.(6.42) is a vectorial representation of eq.(6.17) and I denotes a N-dimensional vector in which all the elements are unity. Since R_{ee} is a semi-positive-definite matrix, its inverse matrix does not always exist. Thus, we make R_{ee} invertible by augmenting each element along its main diagonal by a small positive quantity η. Let R'_{ee} represent the reformed matrix, then it is expressed as follows:

$$R'_{ee} = R_{ee} + \eta U \tag{6.43}$$

Now, replacing R_{ee} in eq.(6.41) with R'_{ee} of eq.(6.43) and solving the problem given by eq's.(6.41) and (6.42), we obtain the optimum value of V, i.e., V_{opt}, as follows:

$$V_{opt} = R'^{-1}_{ee} I (I^T R'^{-1}_{ee} I)^{-1} \tag{6.44}$$

Averaging the correlation matrices of sub-arrays by using V_{opt}, we can make the correlation matrix R'_{xx} very close to a Toeplitz form, which in effect corresponds to nullifying of the suppressed cross correlation factor, ρ.

By using this resultant matrix R'_{xx} in eq.(6.1), we can obtain W_{opt}, the optimum weight for the K-element array. Now, either one of sub-arrays may be used as a conventional adaptive array to have this weight applied to, then both i- and c-interferences are suppressed. Here, it should be noticed that the application of this technique is universal since it is an algorithm for modifying the correlation matrix to be used in the adaptive systems in general: It can be used not only in the DCMP adaptive array but also in other systems such as the Widrow[9] or Howells-Applebaum arrays[15].

6.3.2 Theoretical Analysis of Coherency Suppression

In this section, we analyze theoretically the decorrelation by the adaptive spatial averaging technique, and investigate the necessary

degrees of freedom of the system, i.e., the number of sensor elements required for suppressing the c-interferences[97].

Suppose the desired signal and J c-interferences are incident on the array. Then, the input signal at the m-th element of the full array can be expressed as follows:

$$x_m = \sum_{h=0}^{J} \sqrt{P_h/2}\, \exp[j\{\Psi_m(\theta_h)+\phi_h\}] \qquad (m=1,\ldots,M) \tag{6.45}$$

where P_h's, θ_h's, and ϕ_h's(h=0,...,J) are the input powers, the angles of arrival, and the phases at the phase center of the incoming waves, respectively. Among them, let P_o, θ_o, and ϕ_o represent the parameters of the desired signal. The thermal noise is neglected again. Then, in the same manner as the derivation of eq.(6.13), we can obtain the (k+i,k) element of R'_{xx}, i.e., $r'_{k+i,k}$ as follows:

$$\begin{aligned} r'_{k+i,k} &= \sum_{n=1}^{N} v_n\, r_{k+i,k\cdot n} = \sum_{n=1}^{N} v_n\, E[x_{k+i+n-1}\cdot x^*_{k+n-1}] \\ &= \sum_{h=0}^{J} (P_h/2)\, \exp[j\{(2\pi d/\lambda)i \sin\theta_h\}] \\ &\quad + \sum_{h=0}^{J} \sum_{\substack{h'=0 \\ (h\neq h')}}^{J} (\sqrt{P_h P_{h'}}/2)\, \rho_{hh'}\, Z_{hh'}(i,k) \end{aligned} \tag{6.46}$$

$$(i=0,..,K-1,\ k=1,..,K-i)$$

where

$$Z_{hh'}(i,k) = \exp[j\{\phi_h-\phi_{h'}+(2\pi d/\lambda)\{(k+i)\sin\theta_h - k\sin\theta_{h'} - (K+1)(\sin\theta_h - \sin\theta_{h'})/2\}\}] \tag{6.47}$$

$$\rho_{hh'} = \sum_{n=1}^{N} v_n \exp[j\{(2\pi d/\lambda)\{n-(N+1)/2\}(\sin\theta_h - \sin\theta_{h'})\}] \tag{6.48}$$

$$\rho_{hh'} = \rho_{h'h}^* \tag{6.49}$$

$$(h,h'=0,..,\ J,\ h\neq h')$$

Therefore, $\{r'_{k+i,k}-r'(i)\}$'s which appear in the summation of eq.(6.34) are expressed as

$$r'_{k+i,k} - r'(i) = \sum_{\substack{h=0 \\ (h\neq h')}}^{J} \sum_{h'=0}^{J} (\sqrt{P_h P_{h'}}/2)\, \rho_{hh'} \cdot \{Z_{hh'}(i,k) - \frac{1}{K-i} \sum_{k'=1}^{K-i} Z_{hh'}(i,k')\} \qquad (6.50)$$

$$(i=0,..,K-2,\ k=1,..,K-i)$$

The total number of the terms given by eq.(6.50) amounts to $(K-1)(K+2)/2$ by directly calculating $\{K+(K-1)+\cdots+2\}$, but all of them are not independent of each other. This fact can be cleared in the following. Eq.(6.50) can be rewritten as follows in vector and matrix forms:

$$\begin{bmatrix} r'_{1+i,1} - r'(i) \\ r'_{2+i,2} - r'(i) \\ \vdots \\ r'_{K,K-i} - r'(i) \end{bmatrix} = \begin{bmatrix} K-i-1 & -1 & -1 & \cdots & -1 \\ -1 & K-i-1 & -1 & \cdots & \cdots \\ -1 & -1 & \cdots & \cdots & \cdots \\ \cdots & \cdots & \cdots & \cdots & -1 \\ -1 & \cdots & \cdots & -1 & K-i-1 \end{bmatrix} \begin{bmatrix} b(i,1) \\ b(i,2) \\ \vdots \\ \vdots \\ b(i,K-i) \end{bmatrix} \qquad (6.51)$$

$$(i=0,\ldots,K-2)$$

where

$$b(i,k) = \frac{1}{K-i} \sum_{\substack{h=0 \\ (h\neq h')}}^{J} \sum_{h'=0}^{J} (\sqrt{P_h P_{h'}}/2)\, \rho_{hh'}\, Z_{hh'}(i,k) \qquad (6.52)$$

$$(i=0,\ldots,K-2;\ k=1,..,K-i)$$

Let

$$T = \begin{bmatrix} K-i-1 & -1 & -1 & \cdots & -1 \\ -1 & K-i-1 & -1 & \cdots & \cdots \\ -1 & -1 & \cdots & \cdots & \cdots \\ \cdots & \cdots & \cdots & \cdots & -1 \\ -1 & \cdots & \cdots & -1 & K-i-1 \end{bmatrix} \qquad (6.53)$$

T is a [(K-i)×(K-i)] matrix and its rank is proved to be K-i-1 by direct calculation. Therefore, arbitrary (K-i-1) terms of all $\{r'_{k+i,k}-r'(i)\}$'s (k=1,..,K-i) for a certain i-th diagonal in eq.(6.35) are independent of each other, and the remaining term can be represented as a linear combination of those (K-i-1) independent terms. It means that we can set the following equivalent equation in place of eq.(6.34):

$$\varepsilon = \sum_{i=0}^{K-2} \sum_{k=1}^{K-i-1} | r'_{k+i,k} - r'(i) |^2 \tag{6.54}$$

Accordingly, R_{ee} given by eq.(6.38) comes to

$$R_{ee} = \sum_{i=0}^{K-2} \sum_{k=1}^{K-i-1} R(i,k) \tag{6.55}$$

where

$$R(i,k) = Re\{e_{k+i,k} \cdot e^{\dagger}_{k+i,k}\} \quad (i=1,..,K-2;\ k=1,..,K-i-1) \tag{6.56}$$

which are defined for convenience of the following analysis. In this situation, $e_{k+i,k}$ is expressed as follows:

$$e_{k+i,k} = \sum_{\substack{h=0 \\ (h\neq h')}}^{J} \sum_{h'=0}^{J} a_{hh'}(i,k)\, E_{hh'} \quad (i=0,\ldots,K-2;\ k=1,..,K-i-1) \tag{6.57}$$

where

$$a_{hh'}(i,k) = (\sqrt{P_h P_{h'}}/2)\{Z_{hh'}(i,k) - \frac{1}{K-i} \sum_{k'=1}^{K-i} Z_{hh'}(i,k')\} \tag{6.58}$$

$$E_{hh'} = [\exp\{j\Psi_1(h,h')\},\ldots,\ \exp\{j\Psi_N(h,h')\}]^T \tag{6.59}$$

$$\Psi_n(h,h') = (2\pi d/\lambda)\{n - (N+1)/2\}(\sin\theta_h - \sin\theta_{h'}) \tag{6.60}$$

$$(i=0,\ldots,K-2;\ k=1,..,K-i-1;\ h,h'=0,\ldots,J,\ h\neq h';\ n=1,\ldots,N)$$

Using eq's.(6.37) and (6.59) gives the following vectorial expression for $\rho_{hh'}$ of eq.(6.48):

$$\rho_{hh'} = E_{hh'}{}^T V = V^T E_{hh'} \qquad (h,h'=0,\ldots,J,\ h\neq h') \tag{6.61}$$

Now, from eq's.(6.57)-(6.60), R(i,k) of eq.(6.56) can be written as

$$R(i,k) = EA(i,k)E^T \tag{6.62}$$

where

$$A(i,k) = a_1(i,k)a_1^T(i,k) + a_2(i,k)a_2^T(i,k) \tag{6.63}$$

$$E = [E_{01r}\ E_{01j}\ \cdots\ E_{hh'r}\ E_{hh'j}\ \cdots\ E_{(J-1)Jr}\ E_{(J-1)Jj}] \tag{6.64}$$

$$E_{hh'r} = \mathrm{Re}\{E_{hh'}\} \quad (E_{hh'r}=E_{h'hr}) \tag{6.65}$$

$$E_{hh'j} = \mathrm{Im}\{E_{hh'}\} \quad (E_{hh'j}=-E_{h'hj}) \tag{6.66}$$

$$(h,h'=0,\ldots,J,\ h<h')$$

$$a_1(i,k) = \begin{bmatrix} a_{01r}(i,k) + a_{10r}(i,k) \\ a_{10j}(i,k) - a_{01j}(i,k) \\ \vdots \\ a_{hh'r}(i,k) + a_{h'hr}(i,k) \\ a_{h'hj}(i,k) - a_{hh'j}(i,k) \\ \vdots \\ a_{(J-1)Jr}(i,k) + a_{J(J-1)r}(i,k) \\ a_{J(J-1)j}(i,k) - a_{(J-1)Jj}(i,k) \end{bmatrix} \tag{6.67}$$

$$a_2(i,k) = \begin{bmatrix} a_{01j}(i,k) + a_{10j}(i,k) \\ a_{01r}(i,k) - a_{10r}(i,k) \\ \vdots \\ a_{hh'j}(i,k) + a_{h'hj}(i,k) \\ a_{hh'r}(i,k) - a_{h'hr}(i,k) \\ \vdots \\ a_{(J-1)Jj}(i,k) + a_{J(J-1)j}(i,k) \\ a_{(J-1)Jr}(i,k) - a_{J(J-1)r}(i,k) \end{bmatrix} \tag{6.68}$$

$$a_{hh'r}(i,k) = \mathrm{Re}\{a_{hh'}(i,k)\} \tag{6.69}$$

$$a_{hh'j}(i,k) = \mathrm{Im}\{a_{hh'}(i,k)\} \tag{6.70}$$

$$(i=0,\ldots,K-2;\ k=1,..,K-i-1;\ h,h'=0,\ldots,J,\ h\neq h')$$

where Im{ } denotes the imaginary part. The columns of the matrix E are composed of J(J+1) real direction vectors $E_{hh'r}$ and $E_{hh'j}$, so we call it a direction matrix in [N×J(J+1)] dimension. From eq.(6.63), it follows that the rank of A(i,k) which are J(J+1)-dimensional square matrices is two at

most. Thus, considering that direct calculation shows $\mathbf{a}_2(0,k)=\mathbf{0}$ (k=1,..,K-1), the matrix R_{ee} is expressed as follows by substituting eq.(6.62) into eq.(6.55):

$$R_{ee} = EA'E^T \tag{6.71}$$

where

$$A' = \sum_{i=0}^{K-2}\sum_{k=1}^{K-i-1} \mathbf{a}_1(i,k)\mathbf{a}_1^T(i,k) + \sum_{i=1}^{K-2}\sum_{k=1}^{K-i-1} \mathbf{a}_2(i,k)\mathbf{a}_2^T(i,k)$$

$$= DD^T \tag{6.72}$$

$$D = [\mathbf{a}_1(0,1)\cdots\ \mathbf{a}_1(0,K-1)\cdots\ \mathbf{a}_1(i,1)\cdots\ \mathbf{a}_1(i,K-i-1)\cdots\ \mathbf{a}_1(K-2,1)$$
$$\mathbf{a}_2(1,1)\cdots\ \mathbf{a}_2(1,K-2)\cdots\ \mathbf{a}_2(i,1)\cdots\ \mathbf{a}_2(i,K-i-1)\cdots\ \mathbf{a}_2(K-2,1)] \tag{6.73}$$

The above D is a matrix whose columns are composed of $\mathbf{a}_1(i,k)$'s (k=1,.., K-i-1;i=0,..,K-2) and $\mathbf{a}_2(i,k)$'s (k=1,..,K-i-1;i=1,..,K-2). Let n' denote the number of summation in eq.(6.72). Then, n' is

$$n' = (K-1)+2\{(K-2)+(K-3)+\cdots+1\} = (K-1)^2 \tag{6.74}$$

and the D is a [J(J+1)×n'] matrix. By summing up $\mathbf{a}_1(i,k)\mathbf{a}_1^T(i,k)$ and $\mathbf{a}_2(i,k)\mathbf{a}_2^T(i,k)$ for every i and k in eq.(6.72), we have to attain the matrix A' having full rank so that the matrix R_{ee} may have rank of J(J+1) equal to the number of the real direction vectors. This thought is analogous to that of the direction finding with the spatial averaging[56]. Clearly, the rank of A' is equal to the rank of D. Furthermore, from our experiences, we guess that the matrix D is of full rank, whose proof is not shown here because of its difficulty. Therefore, assuming here that the matrix D has been proved to be of full rank, we obtain

$$\text{rank}(A') = \text{rank}(D) = \min\{n',\ J(J+1)\} \tag{6.75}$$

Thus, if and only if the following inequality holds

$$n' = (K-1)^2 \geqq J(J+1), \tag{6.76}$$

the matrix A' has full rank of J(J+1). Solving the above inequality under

the condition that K and J are positive integers, we obtain the simple inequality as follows:

$$K \geq J + 2 \tag{6.77}$$

On the other hand, concerning the direction matrix E, it turns out that the following equation holds as the result of matrix manipulation:

$$\text{rank}(E) = \min\{N, J(J+1)\} \tag{6.78}$$

Therefore, if and only if $N \geq J(J+1)$, the matrix E has full rank of $J(J+1)$. Under the above conditions, the matrix R_{ee} also has rank of $J(J+1)$. The following analysis proceeds under these conditions.

Now, we introduce the modal representation of R_{ee} as follows:

$$R_{ee} = \sum_{i=1}^{N'} \gamma_i \mathbf{u}_i \mathbf{u}_i^T \tag{6.79}$$

where

$$N' = J(J+1) \tag{6.80}$$

and γ_i's and $\mathbf{u}_i$'s are the nonzero eigenvalues and the corresponding eigenvectors of the matrix R_{ee}. Since R_{ee} is a symmetric matrix, we have

$$\mathbf{u}_i^T \mathbf{u}_j = \delta_{ij} \quad (i,j=1,\ldots,N) \tag{6.81}$$

where δ_{ij} is Kronecker's symbol. By analogy of the direction finding[56], it is necessary that the matrix R_{ee} should have the dimension of at least N'+1 to recognize the N' directions, namely,

$$N \geq N'+1 = J(J+1) + 1. \tag{6.82}$$

Since R_{ee} is singular in this case, we must employ R'_{ee} in place of R_{ee} to get the $\mathbf{V}_{opt}$. Using eq.(6.79) under the condition of eq.(6.82), we obtain the modal representation of R'_{ee} as follows:

$$R'_{ee} = \sum_{i=1}^{N'} (\gamma_i+\eta)\, \mathbf{u}_i \mathbf{u}_i^T + \eta \sum_{i=N'+1}^{N} \mathbf{u}_i \mathbf{u}_i^T \tag{6.83}$$

Thus, R'^{-1}_{ee} is expressed as

$$R'^{-1}_{ee} = \sum_{i=1}^{N'} \frac{1}{\gamma_i+\eta}\, \mathbf{u}_i \mathbf{u}_i^T + \frac{1}{\eta} \sum_{i=N'+1}^{N} \mathbf{u}_i \mathbf{u}_i^T \tag{6.84}$$

When we choose the value of η such that

$$\gamma_i >> \eta \qquad (i=1,\ldots,N'), \tag{6.85}$$

we can write the $\mathbf{V}_{opt}$ as follows:

$$\begin{aligned}\mathbf{V}_{opt} &= R'_{ee}{}^{-1}\mathbf{I}(\mathbf{I}^T R'_{ee}{}^{-1}\mathbf{I})^{-1} \\ &= \zeta\{\sum_{i=1}^{N'} \frac{1}{\gamma_i+\eta}(\mathbf{u}_i{}^T\mathbf{I})\mathbf{u}_i + \frac{1}{\eta}\sum_{i=N'+1}^{N}(\mathbf{u}_i{}^T\mathbf{I})\mathbf{u}_i\} \\ &\simeq \frac{\zeta}{\eta}\sum_{i=N'+1}^{N}(\mathbf{u}_i{}^T\mathbf{I})\mathbf{u}_i \end{aligned} \tag{6.86}$$

where

$$\zeta = (\mathbf{I}^T R'_{ee}{}^{-1}\mathbf{I})^{-1} \tag{6.87}$$

Now, by construction, the real direction vectors $\{\mathbf{E}_{hh'r}, \mathbf{E}_{hh'j} | h,h'= 0,..,J, h<h'\}$, which are the columns of the matrix E, lie in the span of the first N' eigenvectors $\{\mathbf{u}_1,..,\mathbf{u}_{N'}\}$ and are therefore orthogonal to the remaining eigenvectors $\{\mathbf{u}_{N'+1},..,\mathbf{u}_N\}$. Thus, we shall have

$$\mathbf{E}_{hh'r}{}^T\mathbf{V}_{opt} \simeq \frac{\zeta}{\eta}\sum_{i=N'+1}^{N}(\mathbf{u}_i{}^T\mathbf{I})(\mathbf{E}_{hh'r}{}^T\mathbf{u}_i) = 0 \tag{6.88}$$

and

$$\mathbf{E}_{hh'j}{}^T\mathbf{V}_{opt} \simeq \frac{\zeta}{\eta}\sum_{i=N'+1}^{N}(\mathbf{u}_i{}^T\mathbf{I})(\mathbf{E}_{hh'j}{}^T\mathbf{u}_i) = 0 \tag{6.89}$$

$$(h,h'=0,\ldots,J,\ h<h')$$

Hence the suppressed correlation factors $\rho_{hh'}$ $(=\rho_{h'h}{}^*)$ with the $\mathbf{V}_{opt}$ are expressed as follows by using eq's.(6.61), (6.88) and (6.89):

$$\rho_{hh'} = \mathbf{E}_{hh'}{}^T\mathbf{V}_{opt} = \mathbf{E}_{hh'r}{}^T\mathbf{V}_{opt} + j\mathbf{E}_{hh'j}{}^T\mathbf{V}_{opt} \simeq 0 \tag{6.90}$$

$$(h,h'=0,\ldots,J,\ h<h')$$

As stated above, the cross correlation terms between coherent waves can be nullified by adopting the adaptive spatial averaging technique. It should be noticed here that the conditions given by eq's.(6.77) and (6.82) determine K and N, i.e., the size and number of the sub-arrays necessary for suppressing the cross correlation terms. Table 6.1 shows them

numerically together with M, the size of the full array.

Table 6.1 Examples of degrees of freedom required by the adaptive spatial averaging technique.

J	K	N	M
1	3	3	5
2	4	7	10
3	5	13	17
4	6	21	26
5	7	31	37
6	8	43	50

J : the number of the c-interferences
K : the size of the sub-array
N : the number of the sub-arrays
M : the size of the full array

6.3.3 Numerical Results

Numerical examples will be shown for a linear array with the element spacing of a half wavelength. First, an eight-element array that does not utilize the spatial averaging is considered as the reference for comparison. Next, we divide the eight-element (M=8) full array into four-element (K=4) sub-arrays for the spatial averaging technique. Therefore, the number of the sub-arrays becomes five (N=5). Table 6.2 shows the parameters we use as the input model. The desired signal and the c-interference are assumed to be in-phase at the phase center. In later examples, only those parameters that are changed will be stated. Fig.6.3 shows the directional pattern adapted by the conventional DCMP

Table 6.2 Parameters of input models for the case of one coherent interference.

desired signal (S)	angle of arrival : $\theta_s = 0°$
	power : $P_s = 1$
coherent (C)	angle of arrival : $\theta_c = 60°$
interference	power : $P_c = 1$
incoherent (I)	angle of arrival : $\theta_i = -50°$
interference	power : $P_i = 100$
thermal noise	power : $P_n = 0.01$

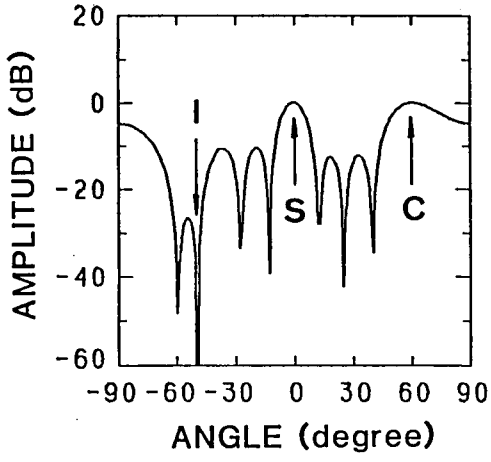

Fig.6.3 The directional pattern by the conventional DCMP adaptive array (M=8) where no spatial averaging is adopted. I, S and C in the figure show the angles of arrival of the incoherent interference, desired signal and coherent interference, respectively. (see Table 6.2)

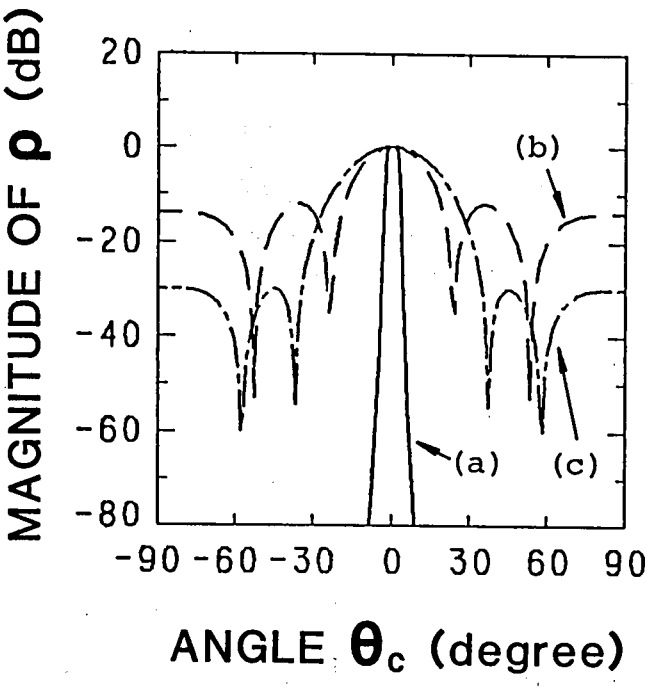

Fig.6.4 The relations between the magnitude of the suppressed correlation factor(ρ) and the angle of arrival of the coherent interference(θ_c) by three methods of the spatial averaging of the correlation matrices (N=5): (a) adaptive spatial averaging (η=10^{-6}), (b) uniform spatial averaging, (c) -30dB Dolph-Chebyshev spatial averaging.
(see Table 6.2)

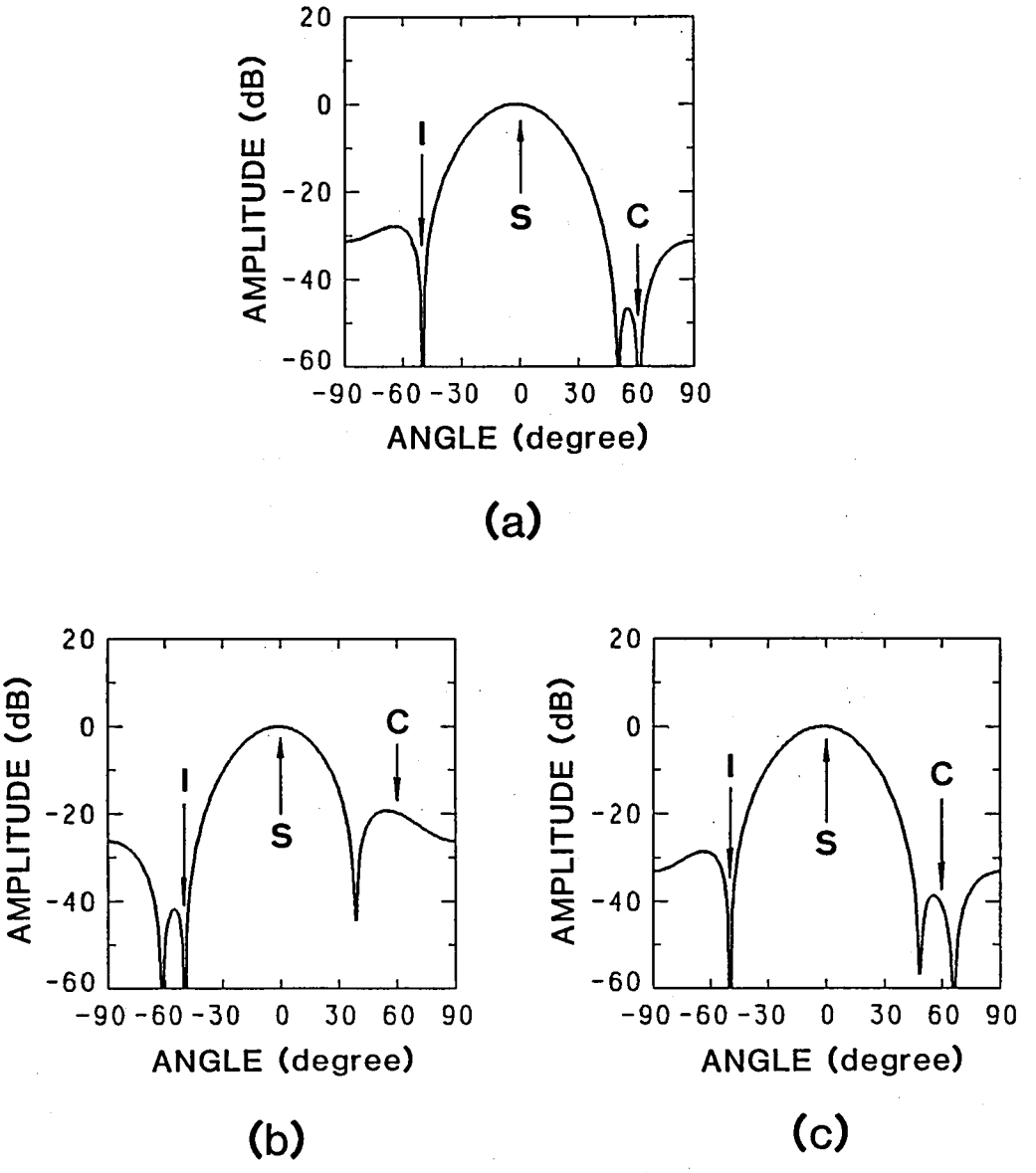

Fig.6.5 The directional patterns by the DCMP adaptive array using the spatial averaging of the correlation matrices (M=8, K=4, θ_c=60°), where I, S and C in the figures show the angles of arrival of the incoherent interference, desired signal and coherent interference, respectively: (a) adaptive spatial averaging (η=10^{-6}), (b) uniform spatial averaging, (c) -30dB Dolph-Chebyshev spatial averaging. (see Table 6.2)

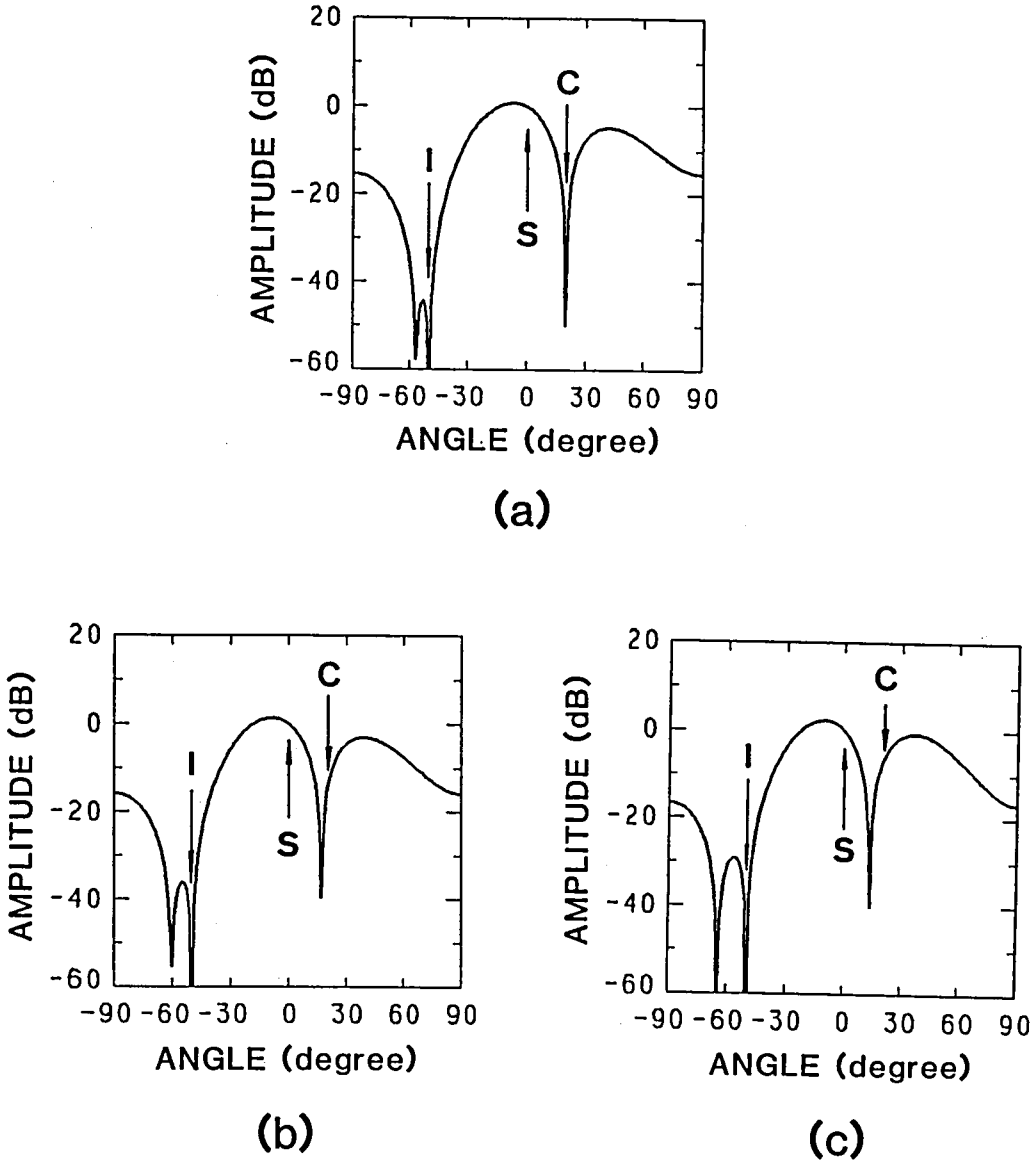

Fig.6.6 The directional patterns by the DCMP adaptive array using the spatial averaging of the correlation matrices (M=8, K=4, θ_C=20°), where I, S and C in the figures show the angles of arrival of the incoherent interference, desired signal and coherent interference, respectively: (a) adaptive spatial averaging (η=10^{-6}), (b) uniform spatial averaging, (c) -30dB Dolph-Chebyshev spatial averaging. (see Table 6.2)

array as the "reference for comparison" defined above. In this figure, we see that the response to the c-interference is such that the desired signal is canceled as the result of power minimization.

Next, we show the effects of the spatial averaging techniques with three different settings of v_n's. The plots in Fig.6.4 are the examples of calculation of eq.(6.16). They show the magnitude of the suppressed correlation factor ρ as the function of θ_c, the angle of arrival of the c-interference. The curve(a) represents the results by our adaptive spatial averaging using eq.(6.44) with η chosen to be 10^{-6}, the curve(b), by the uniform spatial averaging using eq.(6.17), and the curve(c), by the Dolph-Chebyshev spatial averaging with the sidelobe level of -30dB. The curves(b) and (c) are identical to the directional patterns of 5-element uniformly excited linear array and Dolph-Chebyshev array with the sidelobe level of -30dB, respectively. The curve(a) by our technique shows that the excellent suppression of the cross correlation is attained for a wide range of the angle, whereas the curve(b) by the uniform weighting and the curve(c) by the -30dB Dolph-Chebyshev weighting contain some finite sidelobes. Fig's.6.5 and 6.6 show the directional patterns of the adaptive array after these sub-array processing. The former gives the results where θ_c=60°, and the latter, the results where θ_c=20°. (a), (b), and (c) in each figure correspond to the patterns by the adaptive spatial averaging, uniform spatial averaging, and -30dB Dolph-Chebyshev averaging, respectively. While all patterns in Fig's.6.5 and 6.6 show equally good rejection against the i-interference, the responses to the direction of the c-interference are different. In Fig.6.5(a)-(c), the responses are -54.55dB, -19.78dB, and -41.21dB, respectively. In Fig.6.6(a)-(c), on the other hand, they are -49.91dB, -15.52dB, and -7.33dB, respectively. Our technique, i.e., (a) yields the best suppression of the c-interference in

Table 6.3 The elements of the [4 × 4] averaged correlation matrices corresponding to Fig.6.5.

(a) adaptive spatial averaging ($\eta=10^{-6}$)

	1	2	3	4
1	51.010	*	*	*
2	-37.048-j33.325	51.010	*	*
3	5.865+j49.373	-37.048-j33.325	51.010	*
4	29.974-j39.801	5.865+j49.373	-37.048-j33.325	51.010

(b) uniform spatial averaging

	1	2	3	4
1	50.950	*	*	*
2	-37.067-j33.415	51.031	*	*
3	5.846+j49.382	-37.027-j33.226	51.031	*
4	29.915-j39.883	5.846+j49.382	-37.067-j33.415	50.950

(c) -30dB Dolph-Chebyshev spatial averaging

	1	2	3	4
1	51.006	*	*	*
2	-37.049-j33.331	51.011	*	*
3	5.864+j49.374	-37.047-j33.318	51.011	*
4	29.970-j39.807	5.864+j49.374	-37.049-j33.331	51.006

Note: Since the correlation matrices are Hermitian, only the elements in their main- and sub-diagonals are shown. "*" means abbreviation of the elements in the super-diagonals.

Table 6.4 The elements of the [4 × 4] averaged correlation matrices corresponding to Fig.6.6.

(a) adaptive spatial averaging ($\eta=10^{-6}$)

	1	2	3	4
1	51.010	*	*	*
2	-36.354-j33.089	51.010	*	*
3	5.259+j50.165	-36.354-j33.089	51.010	*
4	29.628-j40.319	5.259+j50.165	-36.354-j33.089	51.010

(b) uniform spatial averaging

	1	2	3	4
1	51.003	*	*	*
2	-36.283-j33.048	51.158	*	*
3	5.329+j50.295	-36.206-j33.002	51.158	*
4	29.621-j40.147	5.329+j50.295	-36.283-j33.048	51.003

(c) -30dB Dolph-Chebyshev spatial averaging

	1	2	3	4
1	50.992	*	*	*
2	-36.175-j32.983	51.385	*	*
3	5.437+j50.494	-35.980-j32.866	51.385	*
4	29.610-j39.883	5.437+j50.494	-36.175-j32.983	50.992

Note: Since the correlation matrices are Hermitian, only the elements in their main- and sub-diagonals are shown. "*" means abbreviation of the elements in the super-diagonals.

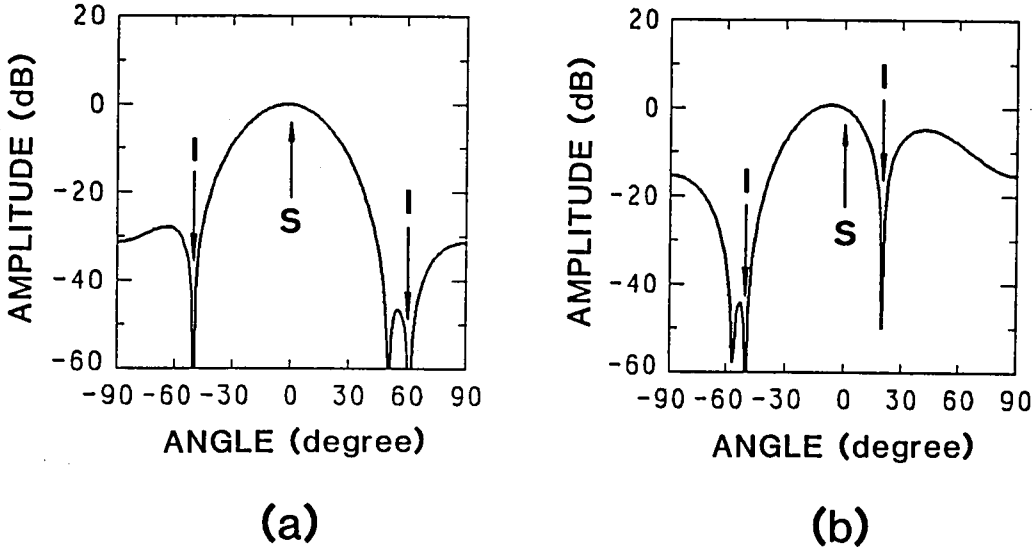

Fig.6.7 The directional patterns by the conventional DCMP adaptive array: (a) the case where the coherent interference of Fig.6.5 is replaced by an incoherent interference with the same power, (b) the case where the coherent interference of Fig.6.6 is replaced by an incoherent interference with the same power. (see Table 6.2)

both cases. The comparatively good result of the -30dB Dolph-Chebyshev averaging is also obtained in the case of θ_c=60° in Fig.6.5(c). It is because the direction of the c-interference happens to lie near a null point of the curve(c) in Fig.6.4. Whereas, in the case of θ_c=20° in Fig.6.6(c), the suppression of the c-interference is worse, since the magnitude of ρ becomes large as shown by Fig.6.4. The resultant averaged correlation matrices are shown in Table's 6.3 and 6.4, which correspond to Fig's.6.5 and 6.6, respectively. It is seen that our adaptive spatial averaging has successfully achieved toeplitzization, whereas the averaged matrices of the other two techniques still have non-uniform diagonals. To further examine how similarly the system using our technique treats the c-interference and the i-interference, we show in Fig.6.7 the conventional DCMP array patterns where the c-interferences of Fig's.6.5 and 6.6 are replaced by i-interferences. There, (a) and (b) correspond to the cases where θ_c=60° and where θ_c=20°, respectively. In Fig.6.7(a) and (b), as naturally expected, nulls are formed in the directions of the newly placed i-interferences, i.e., at 60° in (a) and at 20° in (b), and hence only the desired signal survives in any case. Comparing Fig.6.5(a) with Fig.6.7(a) and Fig.6.6(a) with Fig.6.7(b), respectively, we see that the patterns are almost identical, showing that our adaptive sub-array processing has succeeded in conducting the system to treat the c-interference as if it were an i-interference.

We show another example where the two c-interferences with the same powers as the desired signal are incident on the 10-element full array (M=10) which is divided into the seven sets of 4-element sub-array (N=7 and K=4). These numbers are chosen in compliance with eq's.(6.77) and (6.82). Table 6.5 shows the input data used in this example. The two c-interferences are in-phase with the desired signal at the phase center.

There is no i-interference in this case. Fig.6.8 shows the directional patterns obtained by the processing similar to Fig.6.5 or Fig.6.6. (a), (b), and (c) in Fig.6.8 correspond, respectively, to the same averaging techniques as those in Fig.6.5 or Fig.6.6. The responses to the directions of the two c-interferences are (a) -49.92dB, (b) -16.06dB, and (c) -16.41dB, at -20°; (a) -52.60dB, (b) -18.29dB, and (c) -29.49dB, at 50°. We can see the remarkable difference in suppression of c-interferences between our technique and the others. Table 6.6 shows the resultant averaged correlation matrices corresponding to Fig.6.8. We see that the correlation matrix by our technique has a Toeplitz form, but that the others do not. Moreover, in order to designate the equality of treatment of the c-interferences and the i-interferences by the system using our technique, we show in Fig.6.9 the conventional DCMP array pattern where the both c-interferences of Fig.6.8 are replaced by i-interferences. Coincidence of Fig.6.8(a) with Fig.6.9 demonstrates again that our system virtually treats the c-interferences as i-interferences.

Table 6.5 Parameters of input models for the case of two coherent interference.

desired signal (S)	angle of arrival : $\theta_s = 0°$
	power : $P_s = 1$
coherent (C_1)	angle of arrival : $\theta_{c1} = -20°$
interference 1	power : $P_{c1} = 1$
coherent (C_2)	angle of arrival : $\theta_{c2} = 50°$
interference 2	power : $P_{c2} = 1$
thermal noise	power : $P_n = 0.01$

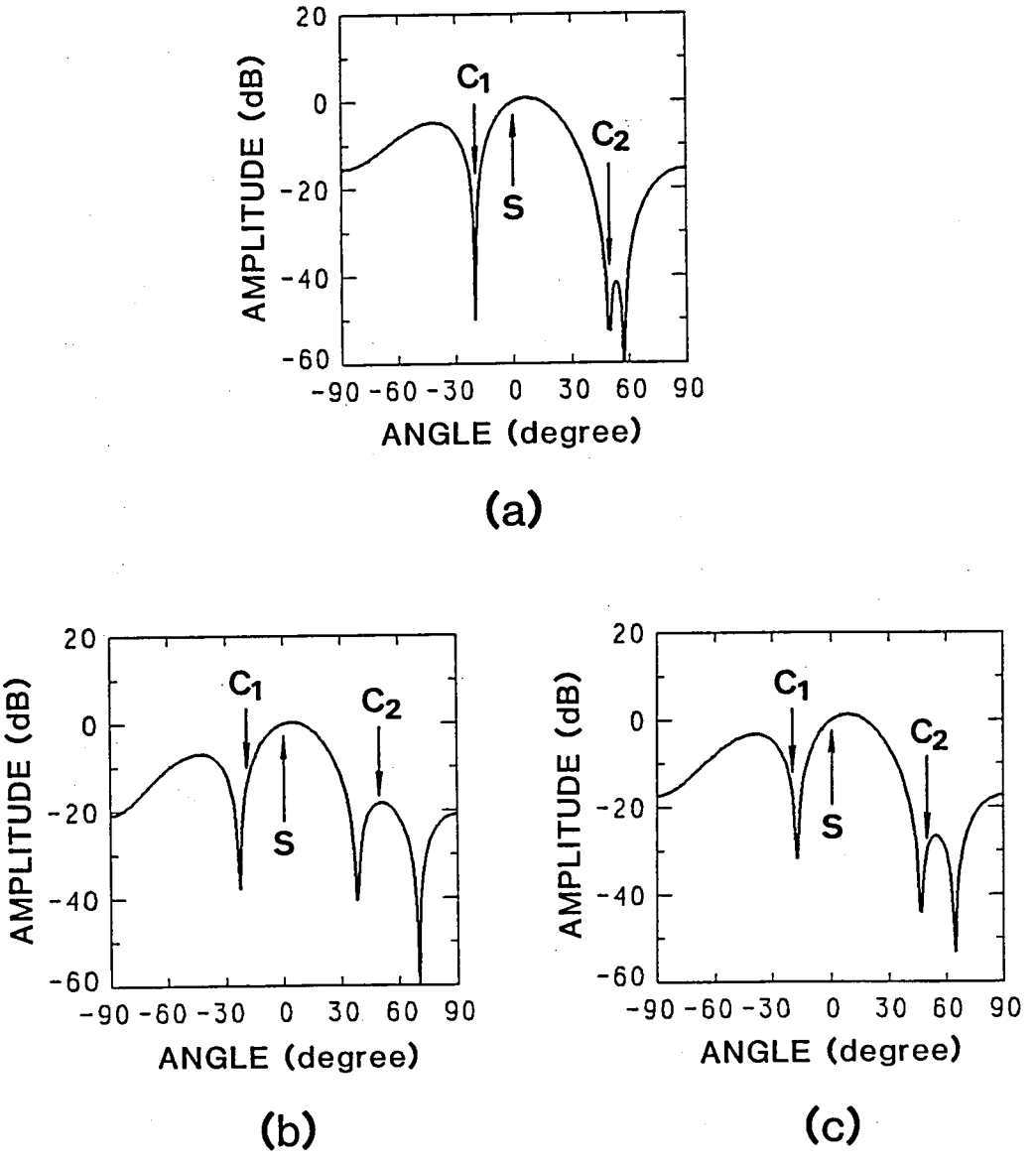

Fig.6.8 The directional patterns by the DCMP adaptive array using the spatial averaging of the correlation matrices (M=10, K=4) where two coherent interferences with the same powers as the desired signal (C_1 and C_2 in the figures) are incident: (a) adaptive spatial averaging ($\eta=10^{-6}$), (b) uniform spatial averaging, (c) -30dB Dolph-Chebyshev spatial averaging. (see Table 6.5)

Table 6.6 The elements of the [4 × 4] averaged correlation matrices corresponding to Fig.6.8.

(a) adaptive spatial averaging ($\eta=10^{-6}$)

	1	2	3	4
1	1.5100	*	*	*
2	0.3672-j0.1044	1.5100	*	*
3	0.2771-j0.9162	0.3672-j0.1044	1.5100	*
4	0.2979+j0.4437	0.2771-j0.9162	0.3672-j0.1044	1.5100

(b) uniform spatial averaging

	1	2	3	4
1	1.3752	*	*	*
2	0.3066-j0.1227	1.4263	*	*
3	0.1786-j0.7539	0.2318+j0.0654	1.4263	*
4	0.2119+j0.4981	0.1786-j0.7539	0.3066-j0.1227	1.3752

(c) -30dB Dolph-Chebyshev spatial averaging

	1	2	3	4
1	1.4727	*	*	*
2	0.4295-j0.1574	1.6555	*	*
3	0.3330-j1.0247	0.5038-j0.1617	1.6555	*
4	0.2689+j0.2669	0.3330-j1.0247	0.4295-j0.1574	1.4727

Note: Since the correlation matrices are Hermitian, only the elements in their main- and sub-diagonals are shown. "*" means abbreviation of the elements in the super-diagonals.

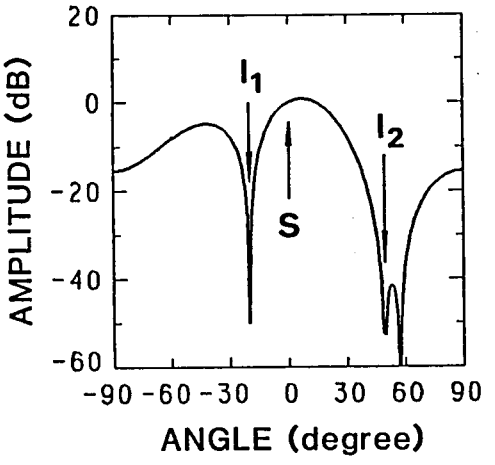

Fig.6.9 The directional pattern by the conventional DCMP adaptive array where the two coherent interferences of Fig.6.8 are replaced by the two incoherent interferences with the same powers (I_1 and I_2 in the figure), respectively.
(see Table 6.5)

Table 6.7 Parameters of input models for different sub-divisions of the array in Fig.6.10.

desired signal (S)	angle of arrival : $\theta_s = 0°$
	power : $P_s = 1$
coherent (C) interference	angle of arrival : $\theta_c = 60°$
	power : $P_c = 1$
thermal noise	power : $P_n = 0.01$

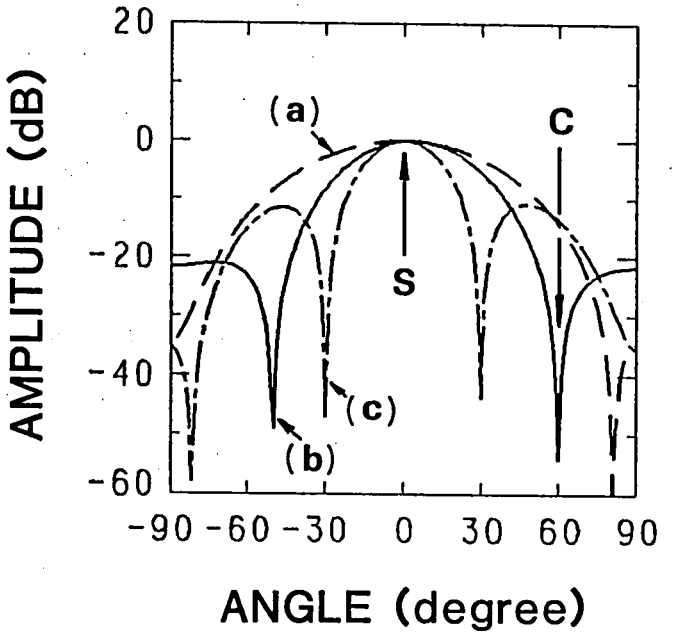

Fig.6.10 The directional patterns by the DCMP adaptive array using the adaptive spatial averaging technique (M=5, $\eta=10^{-6}$), where S and C in the figure show the angles of arrival of the desired signal and coherent interference, respectively: (a) K=2, N=4, (b) K=3, N=3, (c) K=4, N=2.

Finally, we demonstrate numerically that both conditions on K and N, i.e., eq's.(6.77) and (6.82), are indispensable for our adaptive spatial averaging technique. We show examples where one c-interference is incident on the 5-element full array (M=5). The inputs are shown in Table 6.7. The desired signal and the c-interference are assumed to be in-phase at the phase center. The three ways of sub-array division are examined: (a) K=2 and N=4, (b) K=3 and N=3, (c) K=4 and N=2. The cases (a) and (c) satisfy only the condition on N and only the condition on K, respectively. On the other hand, the case (b) satisfies both conditions. Fig.6.10 shows the adapted directional patterns of sub-array after the adaptive sub-array processing. It is seen that the responses in the direction of the coherent interference (60°) are (a) -14.39dB, (b) -54.11dB and (c) -13.61dB. The case (b) in compliance with both conditions shows the remarkable suppression of the c-interference, whereas the suppressions of the cases (a) and (c) are unsuccessful since they do not satisfy both conditions.

After extensive calculation for a variety of parameters whose results are not shown here, we have come to conclude that our technique has an excellent capability to suppress the c-interferences.

6.4 Improved Convergence Characteristics by Adaptive Spatial Averaging

In this section, we will show another merit of our adaptive spatial averaging technique. It is the improved transient behavior for the i-interference as well as the c-interference[98]. Since this technique gives the particular processing to the input correlation matrix, the sampled matrix inversion (SMI) algorithm is adequate for practice. We adopt the algorithm given by eq.(3.87), which is written as follows

again:

$$\begin{cases} R_{xx}(1) = \mathbf{X}(1)\mathbf{X}^{\dagger}(1) \\ R_{xx}(m) = (1 - \beta)R_{xx}(m-1) + \beta\ \mathbf{X}(m)\mathbf{X}^{\dagger}(m) \qquad (m=2,\ 3,..) \end{cases} \tag{6.91}$$

As for β, we let

$$\beta = 1/m \tag{6.92}$$

and use simple SMI. As pointed out by Ref.[99], it is possible that the SMI algorithm has a correlation matrix which is close to singular or ill-conditioned for the situation where signals from some directions less than the number of array elements are present along with a small amount of thermal noise. In such a case, we cannot obtain the inverse matrix accurately, resulting in the misadjusted weight. Therefore, as the countermeasure, we inject the pseudo noise larger than the real thermal noise to the main diagonal of the correlation matrix. This thought stems from the tamed system in Chapter 5. Thus, the weight vector for one of the sub-arrays at the m-th iteration is written as follows:

$$\mathbf{W}(m) = \{R'_{xx}(m) + \alpha U\}^{-1}\mathbf{C}_d[\mathbf{C}_d^{\dagger}\{R'_{xx}(m) + \alpha U\}^{-1}\mathbf{C}_d]^{-1}\mathbf{H}^* \tag{6.93}$$

where $R'_{xx}(m)$ is the correlation matrix after the sub-array processing at the m-th iteration and α is the pseudo noise. Concerning the value of α to be injected in this case, we do not use any longer the value that was given as the optimum in Chapter 5 because the c-interferences can be suppressed by the alternative method, i.e., the adaptive spatial averaging.

Here, we derive another formula of the optimum pseudo noise for this case. It is a well-known fact that the suppression of the interferences become imperfect with too large value of α. That is why we choose as the upper limit of α the value whose injection yields the output powers of the interference and thermal noise of the same order. For convenience of analysis, we assume that we have obtained the exact correlation matrix

R'_{xx} for a radio environment where there are one i-interference and thermal noise. Under this condition, the R'_{xx} can be expressed as follows:

$$R'_{xx} = P_n U + P_i Z_i Z_i^{\dagger} \tag{6.94}$$

where Z_i is given by eq.(3.90). Using the matrix inversion formula[63] in eq.(6.94) and substituting the resultant R'^{-1}_{xx} into eq.(6.93), we obtain the optimum weight as follows:

$$W_{opt} = \zeta[\{2(P_n + \alpha) + KP_i\}F - (2P_i A_{di} H^*)Z_i] \tag{6.95}$$

where

$$\zeta = \{2(P_n + \alpha) + KP_i(1 - A_{di}^2)\}^{-1} \tag{6.96}$$

and A_{di} is given by eq.(3.107). Thus, the output powers of the i-interference and thermal noise are written as

$$P^i_{out} = P_i A_{di}^2 |H|^2 \{2\zeta(P_n + \alpha)\}^2 \tag{6.97}$$

$$P^n_{out} = (2/K)P_n |H|^2 + 2\zeta^2 K P_n P_i^2 A_{di}^2 (1 - A_{di}^2)|H|^2 \tag{6.98}$$

Solving the equation $P^i_{out} = P^n_{out}$ with respect to α under the condition that the i-interference arrives at sidelobes of the sub-array and that $P_i >> P_n$, we obtain

$$\alpha = (1/|A_{di}|)\sqrt{KP_nP_i/2} > \sqrt{KP_nP_i/2} = \alpha_{max} \tag{6.99}$$

We use the above α_{max} as a standard of the value of α.

Next, we show the results of computer simulation for a 8-element (M=8) linear array with the element spacing of a half wavelength. The whole array is divided into 4-element (K=4) sub-arrays for the spatial averaging. Therefore, the number of the sub-arrays is 5 (N=5). For comparison, we also discuss other two systems, i.e., the conventional DCMP system which uses the whole array without employing any spatial averaging techniques and the DCMP system to which we apply the uniform spatial averaging. We consider two external waves, i.e., the desired signal and

one i-interference, and thermal noise exist as the input. Table 6.8 shows the parameters of the input models. In SMI algorithm, in order to smooth the behavior of the system, the inverse correlation matrix necessary for obtaining the weight vector is calculated at every ten samplings, which we will call one iteration hereafter. As the measure of performance, we use the output SINR and it is calculated at the m-th iteration by

$$SINR(m) = \frac{P^{s}_{out}(m)}{P^{i}_{out}(m) + P^{n}_{out}(m)} \tag{6.100}$$

where

$$P^{s}_{out}(m) = P_s \mathbf{W}^{\dagger}(m)\mathbf{C}_d\mathbf{C}_d^{\dagger}\mathbf{W}(m) \tag{6.101}$$

$$P^{i}_{out}(m) = P_i \mathbf{W}^{\dagger}(m)\mathbf{Z}_i\mathbf{Z}_i^{\dagger}\mathbf{W}(m) \tag{6.102}$$

$$P^{n}_{out}(m) = P_n \mathbf{W}^{\dagger}(m)\mathbf{W}(m) \tag{6.103}$$

Fig's.6.11 and 6.12 show the variations of SINR with the SMI algorithm. They represent the cases where $P_n=10^{-2}$ and $P_n=10^{-4}$, respectively. In these figures, (a) and (b) correspond to the results of one 4-element sub-array after the adaptive and the uniform spatial averaging processings, respectively. On the other hand, (c) corresponds

Table 6.8 Parameters of input models used in computer simulation for SMI algorithm.

desired signal (S)	angle of arrival : $\theta_s = 0°$
	power : $P_s = 1$
incoherent (I) interference	angle of arrival : $\theta_i = -45°$
	power : $P_i = 100$
thermal noise	power : P_n (var.)

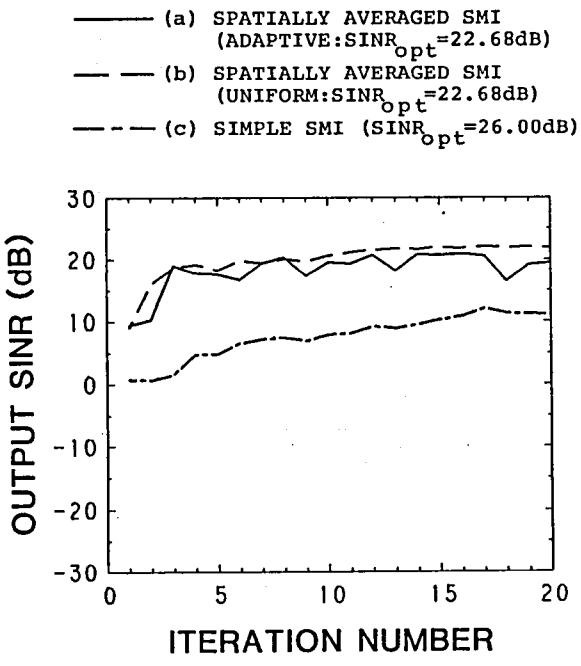

Fig.6.11 The variations of SINR by SMI algorithm ($P_n=10^{-2}$): (a) adaptive spatial averaging ($\eta=10^{-6}$), (b) uniform spatial averaging, (c) no spatial averaging. (see Table 6.8)

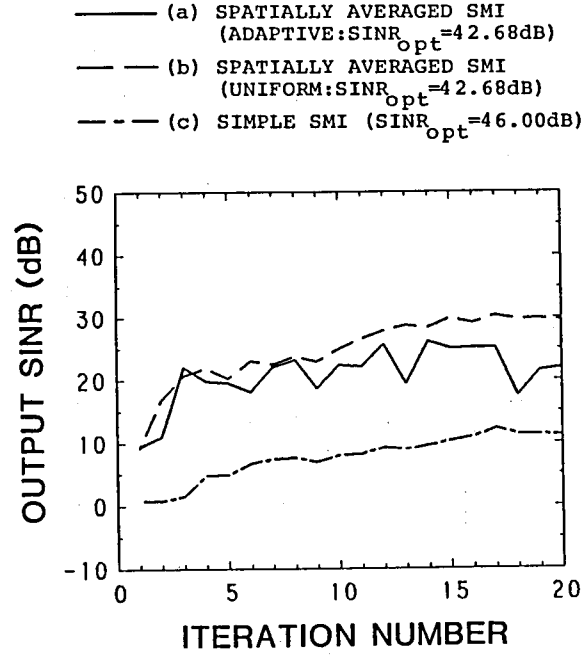

Fig.6.12 The variations of SINR by SMI algorithm ($P_n=10^{-4}$): (a) adaptive spatial averaging ($\eta=10^{-6}$), (b) uniform spatial averaging, (c) no spatial averaging. (see Table 6.8)

to the result of the conventional 8-element adaptive array. The curves reach their own optimum SINR's when each system obtains the exact correlation matrix by a sufficiently long observation. The optimum SINR's are 22.68dB in Fig.6.11(a) and (b), 26.00dB in Fig.6.11(c), 42.68dB in Fig.6.12(a) and (b), and 46.00dB in Fig.6.12(c). We see that the systems using the spatial averaging techniques, as shown by (a) and (b) in both figures, reach the higher SINR rapidly. The reason for this is that the spatial averaging techniques give the more accurate correlation matrix by incorporating the effect of the spatial averaging into that of the temporal averaging. Comparing the (a) with (b), the adaptive spatial averaging yields slight fluctuation. It is due to the random thermal noise. Particularly, in the case of smaller thermal noise power as shown by Fig.6.12, this trend is remarkable. It designates that the adaptive spatial averaging technique is more liable to be affected by the random thermal noise. Therefore, in Fig.6.12, the high SINR is not attained even at the 20-th iteration by our system (a) compared with its optimum SINR of 42.68dB.

In order to improve the above performance, we inject the pseudo noise. The value of the pseudo noise must be larger than the real thermal noise and be smaller than that of α_{max} given by eq.(6.99), so we choose it as follows here:

$$\alpha = \alpha_{max}/20 \tag{6.104}$$

which is selected after our experience. The variations of SINR obtained in the cases of $P_n=10^{-2}$ and $P_n=10^{-4}$ are shown in Fig's.6.13 and 6.14, respectively. (a), (b), and (c) in these figures correspond to the same systems as in Fig's.6.11 and 6.12. The values of the pseudo noise by eq.(6.104) are 0.07 in Fig.6.13(a) and (b), 0.1 in Fig.6.13(c), 0.007 in Fig.6.14(a) and (b), and 0.01 in Fig.6.14(c). In Fig.6.13, it is seen

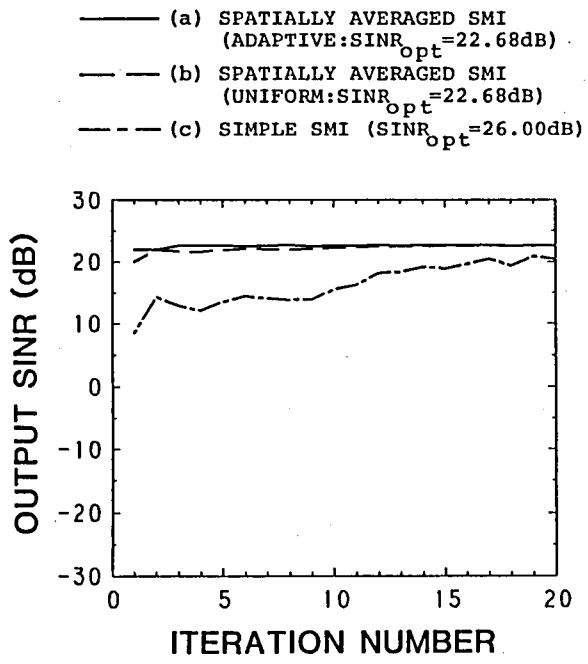

Fig.6.13 The variations of SINR by SMI algorithm when the pseudo noise is injected ($P_n=10^{-2}$): (a) adaptive spatial averaging ($\eta=10^{-6}$), (b) uniform spatial averaging, (c) no spatial averaging. (see Table 6.8)

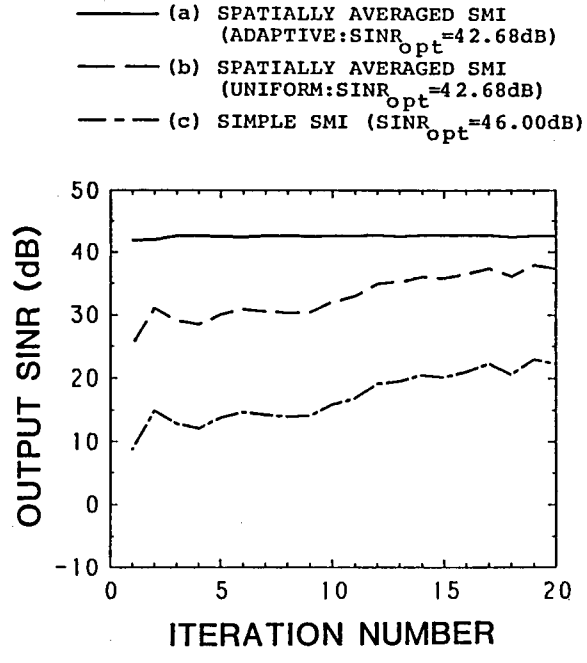

Fig.6.14 The variations of SINR by SMI algorithm when the pseudo noise is injected ($P_n=10^{-4}$): (a) adaptive spatial averaging ($\eta=10^{-6}$), (b) uniform spatial averaging, (c) no spatial averaging. (see Table 6.8)

that all systems are improved by injecting the pseudo noise. Therefore, especially the systems using the spatial averaging techniques attain the SINR very close to its optimum one with few sampling data, compared with Fig.6.11. This improvement is observed remarkably in comparison of Fig.6.14 with Fig.6.12 for the case of smaller thermal noise of $P_n=10^{-4}$. Although all systems are improved also in Fig.6.14, the system using the adaptive spatial averaging has the most noteworthy improvement. Thus, it is emphasized that we can obtain more effectively the exacter correlation matrix by applying the adaptive spatial averaging technique to the imperfect matrix by temporal average alone and furthermore by suppressing the effect of the random thermal noise with the pseudo noise.

For setting the pseudo noise by eq's.(6.99) and (6.104), we need information on the input power of the i-interference. However, it is almost impossible for the unknown radio environments. Therefore, we try to use the input power of the desired signal in place of that of i-interference for the standard of pseudo noise. Let α_o denote the formula in place of α_{max} based on the above. Then, it is written as

$$\alpha_o = \sqrt{KP_nP_s/2} \tag{6.105}$$

In the situations of Fig's.6.11-6.14, the pseudo noise given by eq.(6.104) can be expressed as follows:

$$\alpha = \alpha_o/2 \tag{6.106}$$

With the various values of input power of i-interference, we carried out computer simulation similar to Fig's.6.11-6.14 for the adaptive spatial averaging technique using eq.(6.106). As the results, it has been shown that the setting of the pseudo noise by eq.(6.106) yields satisfactory suppression of the i-interference regardless of its input power. Moreover, by other examples, we confirmed that the value of pseudo noise

given by eq.(6.106) is almost optimum.

Thus, the adaptive spatial averaging technique brings about rapid and steady transient performance in the SMI algorithm for suppression of the i-interference with the aid of the pseudo noise. The effect of the rapid convergence is also confirmed for the suppression of the c-interference by other examples which are not shown here.

6.5 Concluding Remarks

In this chapter, we proposed a technique by which we can cancel the coherent interferences as well as the incoherent ones. The technique is based on the spatial averaging of the correlation matrices obtained by the sub-arrays that are extracted from the full array and partially overlapped with each other. The performance of conventional averaging techniques with fixed weights depends on the incident angle of the interference and suffers from degradation in certain situations. On the other hand, our new averaging technique is to adapt the averaging weights in accordance with the radio environment so that the averaged matrix may have a Toeplitz form. We named it adaptive spatial averaging technique. The theoretical analysis was performed on this adaptive spatial averaging, and the number of antenna elements necessary for suppressing the coherent interferences has been obtained as the results. Although this technique can be applied to any adaptive arrays, the demonstration was made in the directionally constrained minimization of power (DCMP) adaptive array. The results of numerical calculation show that the new adaptive array is effective to suppress the coherent interferences as well as incoherent ones. It should be emphasized that our adaptive array creates deep nulls in all directions of the coherent interferences instead of depending on their cancellation

with each other, whose merits are suggested by Luthra[61].

Next, we applied the adaptive spatial averaging technique to the sampled matrix inversion (SMI) adaptive array in practice, and we examined the transient performance in suppressing the interference. We carried out computer simulation especially for the case where the incoherent interference arrives. The results show that our system rapidly converges to the high SINR with the aid of the pseudo noise, compared with the system using the uniform spatial averaging and the conventional full array system. Besides, we analyzed the pseudo noise and gave its optimum value. Thus, it has been cleared that the adaptive spatial averaging also brings about efficient transient performance for suppression of the incoherent interferences in the SMI algorithm.

CHAPTER 7

ALTERNATIVE PRINCIPLE OF POWER MINIMIZATION UNDER A CORRELATION CONSTRAINT

7.1 Introduction

In the preceding chapters, various applications of the adaptive array with the directional constraints has been discussed.

We introduce an alternative guiding principle of power minimization in this chapter. The new principle sets the constraint condition on the cross correlation between the desired signals at the input and output of the array by making use of information about the characteristics of the desired signal such as its angle of arrival, its frequency spectrum, and so on. Obviously, it is different from the conventional DCMP method constraining the voltage transfer function of the system to the desired direction. It has already been reported that this new principle achieves good constraining of the broadband desired signal[48],[77]. By analogy, it is expected that this new principle can work well under the broadband constraint in angular domain. This suggests that it may be applied to improve the performance of the conventional DCMP under the effect of the beam pointing error.

In Section 7.2, we first explain the principle of power minimization under a correlation constraint. Sections 7.3 and 7.4 are concerned with the performance of the adaptive array with this new principle to the broadband desired signal and to the pointing error, respectively. In Section 7.5, we deal with the above problems simultaneously, i.e., the

performance to the broadband desired signal in the presence of pointing error. Finally, Section 7.6 states conclusions.

7.2 The Concept of Power-Minimizing Method under a Correlation Constraint

We introduce the new guiding principle called the correlation-constrained minimization of power (CCMP) method. The CCMP method is different from the conventional DCMP method only in terms of the constraint condition. The constraint condition in the conventional DCMP method is for specifying the voltage response of the system in the direction from which the desired signal arrives. On the other hand, the new CCMP method sets the constraint condition for specifying the cross correlation between the input desired signal at the reference point and the output desired signal. In the following, we give the detailed explanation.

We use the linear array as shown by Fig's.3.1 and 3.2. First, for setting the constraint condition, we introduce the model of the desired signal which is incident from the specified direction of θ_d with the unit power level. Let $d_o(t)$ denote this signal at the reference point (the center of the array). The input vector by this model desired signal, which shall be denoted by $\mathbf{D}(t)$, is expressed as follows:

$$\mathbf{D}(t) = [d_1(t),\ d_2(t),\ldots,\ d_{KL}(t)]^T \tag{7.1}$$

where

$$d_p(t) = d_o(t-T_p) \tag{7.2}$$

$$T_p = (d_k/c)\ \sin\theta_d + (q-1)\tau \tag{7.3}$$

$$p = k + K(q-1) \qquad (p=1,..,KL;\ k=1,..,K;\ q=1,..,L) \tag{7.4}$$

c: light velocity, τ: time delay between adjacent taps

T_p stands for the time delay of the modeled desired signal at the p-th tap

point with reference to the array center. The array output of this modeled desired signal, $y_d(t)$, is given by

$$y_d(t) = \mathbf{D}^T(t)\mathbf{W} = \mathbf{W}^T\mathbf{D}(t) \tag{7.5}$$

Thus, the constraint condition for the CCMP method is written as

$$E[d_o(t) \cdot y_d(t)] = P_o \tag{7.6}$$

where P_o is a scalar constant specifying the cross correlation between the modeled desired signals at the input and the output. Substituting eq.(7.5) into eq.(7.6), we have

$$\mathbf{r}_d^T\mathbf{W} = P_o \tag{7.7}$$

where $\mathbf{r}_d$ represents the auto-correlation vector of the modeled desired signal which is defined by

$$\mathbf{r}_d = E[d_o(t)\mathbf{D}(t)] \tag{7.8}$$

Eq.(7.7) is a linear equation with respect to $\mathbf{W}$ and it is adopted as the constraint condition of the CCMP method. This principle is formulated as follows:

$$\min_{\mathbf{W}} (P_{out} = \mathbf{W}^T\mathbf{R}_{xx}\mathbf{W})$$
$$\text{subject to } \mathbf{r}_d^T\mathbf{W} = P_o \tag{7.9}$$

and the optimum weight vector is obtained by solving the following cost function in the same manner as the DCMP in Chapter 3:

$$Q(\mathbf{W}) = \frac{1}{2}\mathbf{W}^T\mathbf{R}_{xx}\mathbf{W} + \Lambda(\mathbf{r}_d^T\mathbf{W} - P_o) \tag{7.10}$$

where Λ is an undetermined Lagrange multiplier. The optimum weight vector is thus written as:

$$\mathbf{W}_{opt} = \mathbf{R}_{xx}^{-1}\mathbf{r}_d(\mathbf{r}_d^T\mathbf{R}_{xx}^{-1}\mathbf{r}_d)^{-1}P_o \tag{7.11}$$

Likewise, we can also obtain readily the optimization algorithms of this CCMP method which have the forms with $\mathbf{r}_d$ and P_o in place of C_d and $\mathbf{H}$, respectively, in the DCMP algorithms. As for the value of P_o, we choose hereafter

$$P_o = 1 \tag{7.12}$$

Next, we analyze the characteristics of the CCMP method. We express the correlation matrix R_{xx} as the sum of the desired signal component R_{ss} and the noise (including interferences) component R_{nn}. Namely,

$$R_{xx} = R_{ss} + R_{nn} \tag{7.13}$$

If characteristics of the modeled desired signal are completely equal to those of the actual desired signal, then R_{ss} can be expressed further as

$$R_{ss} = P_s R_{DD} \tag{7.14}$$

where R_{DD} is a correlation matrix of the input vector by the modeled desired signal and it is defined by

$$R_{DD} = E[\mathbf{D}\mathbf{D}^T] \tag{7.15}$$

Substituting eq's.(7.13), (7.14), and (7.15) into $P_{out}=\mathbf{W}^T R_{xx}\mathbf{W}$, we have the output power written as follows:

$$P_{out} = \mathbf{W}^T R_{nn}\mathbf{W} + P_s \mathbf{W}^T R_{DD}\mathbf{W} \tag{7.16}$$

We can modify the above equation as follows by using eq.(7.6) and the assumption $E[d_o^2]=P_o=1$:

$$\begin{aligned} P_{out} &= \mathbf{W}^T R_{nn}\mathbf{W} + P_s E[y_d^2] \\ &= \mathbf{W}^T R_{nn}\mathbf{W} + P_s E[(y_d - d_o)^2] + P_s \end{aligned} \tag{7.17}$$

From eq.(7.17), minimization of the total output power P_{out} under the constraint condition of eq.(7.7) is interpreted as twofold performances, i.e., minimization of the output noise power and minimization of the difference between the waveforms of the output desired signal and the modeled desired signal at the reference point. That is how the CCMP method suppresses the unwanted interferences and/or thermal noise while preserving the desired signal at the array output.

Besides, as easily seen from eq.(7.17), there exists a trade-off between minimization of the noise power and preservation of the desired signal, which depends on the input power ratio of the desired signal and

the unwanted signal. Therefore, in order to enhance the ability to preserve the desired signal, we modify the actual input correlation matrix R_{xx} by adding intentionally the correlation matrix of the modeled desired signal R_{DD} and increase seemingly the power of the desired signal in calculating the optimum weight in the signal processor. Thus, the optimum weight vector is calculated using the following R'_{xx} in place of R_{xx}:

$$R'_{xx} = R_{xx} + \alpha_s R_{DD} \tag{7.18}$$

where α_s is a non-negative scalar. In this case, the equation corresponding to eq.(7.17), which shall be denoted by P'_{out}, is written as

$$P'_{out} = \mathbf{W}^T R_{nn} \mathbf{W} + (P_s + \alpha_s) E[(y_d - d_o)^2] + P_s + \alpha_s \tag{7.19}$$

From eq.(7.19), it follows that preservation of the desired signal can be enhanced by α_s. Accordingly, the optimum weight vector using eq.(7.18) is expressed as

$$\mathbf{W}_{opt} = R'^{-1}_{xx} \mathbf{r}_d (\mathbf{r}_d^T R'^{-1}_{xx} \mathbf{r}_d)^{-1} P_o \tag{7.20}$$

This principle is named "improved CCMP method"[48],[77], and we analyze this improved method hereafter.

In the following analysis, the performance of the DCMP method with the multiple constraints is mentioned for comparison. The multiple constraint conditions for frequencies or angles can be derived in the same straightforward manner as the single constraint in Chapter 3.

7.3 Performance to Broadband Desired Signal

7.3.1 Formulation of Models

As stated in Chapter 5, when the broadband desired signal is incident on the conventional DCMP adaptive array, the sideband component of the desired signal is taken for the unwanted interference and becomes a target

of suppression. In Chapter 5, we proposed the tamed adaptive array by which we attained the satisfactory broadband characteristics. However, this is a system for protecting the sideband component of the desired signal from fierce suppression by adaptation and not for actively constraining the response to the sideband component to have the specified value. Especially, the more number of antenna elements or taps does the system consist of, the more urgently it needs the constraint for the sideband. Therefore, for the purpose of constraining it, we must use another method. In this section, we show that the improved CCMP method is adequate for this problem.

The evaluation of the constraining performance is supposed to depend on the modulation method, but as the general measure for it, we consider the deviation of the transfer function to the desired signal from the ideal non-distorted one, as well as the output SINR. Let σ represent the above measure of distortion. Then, it is expressed as

$$\sigma = \frac{1}{A} \sqrt{\frac{1}{\delta f_s} \int_{f_o-\delta f_s}^{f_o+\delta f_s} |y(f) - y_h(f)|^2 \, df} \qquad (7.21)$$

where f_o and δf_s are the center frequency and the bandwidth of the desired signal, respectively, "A" is the amplitude of the specified response to the desired signal (where A=1), $y(f)$ is the actual transfer function to the desired signal, and $y_h(f)$ is the non-distorted transfer function which is the closest to $y(f)$. $y_h(f)$ is obtained by calculating the average of the amplitude of $y(f)$ and linear approximation of the phase of $y(f)$ over the specified bandwidth. In the following discussion, after Ref.[48], we will judge the system good if $\sigma \leqq 0.05$.

Next, we describe the input signals and the modeled desired signal for the constraint. We assume that the incoming broadband signals and the

modeled desired signal have flat spectra over their respectively specified bands where their spectra are symmetric as to their center frequencies, respectively, as shown by Fig.5.10. Let f_d and δf_d denote the center frequency and the bandwidth of the modeled desired signal, respectively. Then, the normalized correlation function of this signal, $R_f(\Delta t)$ (where Δt is a time lag), is related to the power spectrum by the following equation resulting from the well-known Wiener-Khintchine theorem[100]:

$$R_f(\Delta t) = \mathrm{Re}\{R_{fc}(\Delta t)\} \tag{7.22}$$

with

$$R_{fc}(\Delta t) = \frac{1}{\delta f_d} \int_{f_d-\delta f_d/2}^{f_d+\delta f_d/2} \exp(j2\pi f \Delta t)\, df \tag{7.23}$$

The $R_f(\Delta t)$ after executing the integration of eq.(7.23) is written as

$$R_f(\Delta t) = \cos(2\pi f_d \Delta t) \cdot \mathrm{sinc}(\pi \delta f_d \Delta t) \tag{7.24}$$

where sinc( ) is a function defined by

$$\mathrm{sinc}(X) = \frac{\sin X}{X} \tag{7.25}$$

Considering that the power is divided into L taps at each channel, the p-th entry of $\mathbf{r}_d$, r_{dp}, and the (p,p') entry of R_{DD}, $r_{p,p'}$, are expressed as follows, respectively by using eq's.(7.3) and (7.21)[48],[77]:

$$\begin{aligned} r_{dp} &= (1/\sqrt{L})\, R_f(T_p) \\ &= (1/\sqrt{L})\, \cos(2\pi f_d T_p) \cdot \mathrm{sinc}(\pi \delta f_d T_p) \quad (p=1,..,KL) \end{aligned} \tag{7.26}$$

$$\begin{aligned} r_{p,p'} &= (1/L)\, R_f(T_p - T_{p'}) \\ &= (1/L)\, \cos\{2\pi f_d (T_p - T_{p'})\} \cdot \mathrm{sinc}\{\pi \delta f_d (T_p - T_{p'})\} \\ &\qquad (p,p'=1,..,KL) \end{aligned} \tag{7.27}$$

In practice, f_d and δf_d are determined from the a priori knowledge on the frequency characteristics of the desired signal.

In such ways as shown above, the constraint condition for the broadband desired signal is settled.

7.3.2 Numerical Results

The numerical examples are shown on the 4-element, 4-tap broadband adaptive array with isotropic elements and the equal spacing of a half wavelength corresponding to the center frequency of the desired signal. For comparison, we also discuss the performance of the DCMP method with the double-frequency constraints which sets the constraint conditions on the two close frequencies $f_1=f_d-0.285\delta f_d$ and $f_2=f_d+0.285\delta f_d$[48]. Table 7.1 shows the parameters of the input and constraint used as the standard. The interference in Table 7.1 means the incoherent interference, which will be kept the same in the following tables.

First, we investigate the optimum value of α_s for the improved CCMP method. Fig.7.1 shows the variations of the output SINR and distortion σ in terms of α_s for the five values of the interference power ranging from 0 to 100. (a), (b), and (c) in Fig.7.1 correspond to the results where

Table 7.1 Parameters of input models and constraints for the broadband desired signal.

desired signal (S)	angle of arrival	: $\theta_s = 90°$
	power	: $P_s = 1$
	bandwidth	: $\delta f_s = 0.4 f_o$
interference (I)	angle of arrival	: $\theta_i = -50°$
	power	: $P_i = 100$
	bandwidth	: $\delta f_i = 0$
thermal noise	power	: P_n (var.)
constrained angle		: $\theta_d = \theta_s$
constrained center frequency		: $f_d = f_o(=1)$
constrained bandwidth		: $\delta f_d = \delta f_s$

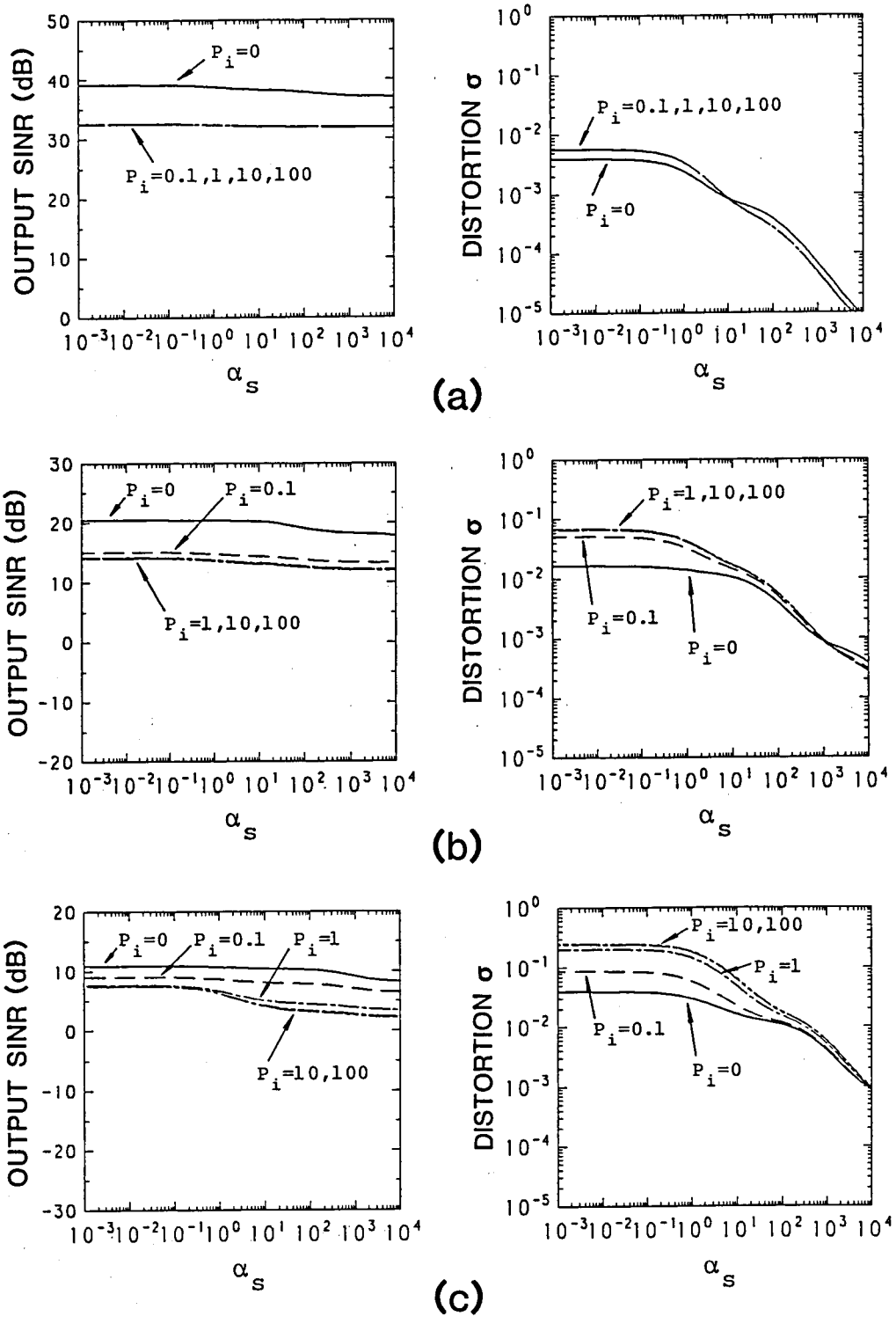

Fig.7.1 Variations of the output SINR and distortion σ in terms of α_s for the improved CCMP system where $\delta f=\delta f_d=0.4$: (a) $P_n=10^{-4}$, (b) $P_n=10^{-2}$, (c) $P_n=10^{-1}$. (see Table 7.1)

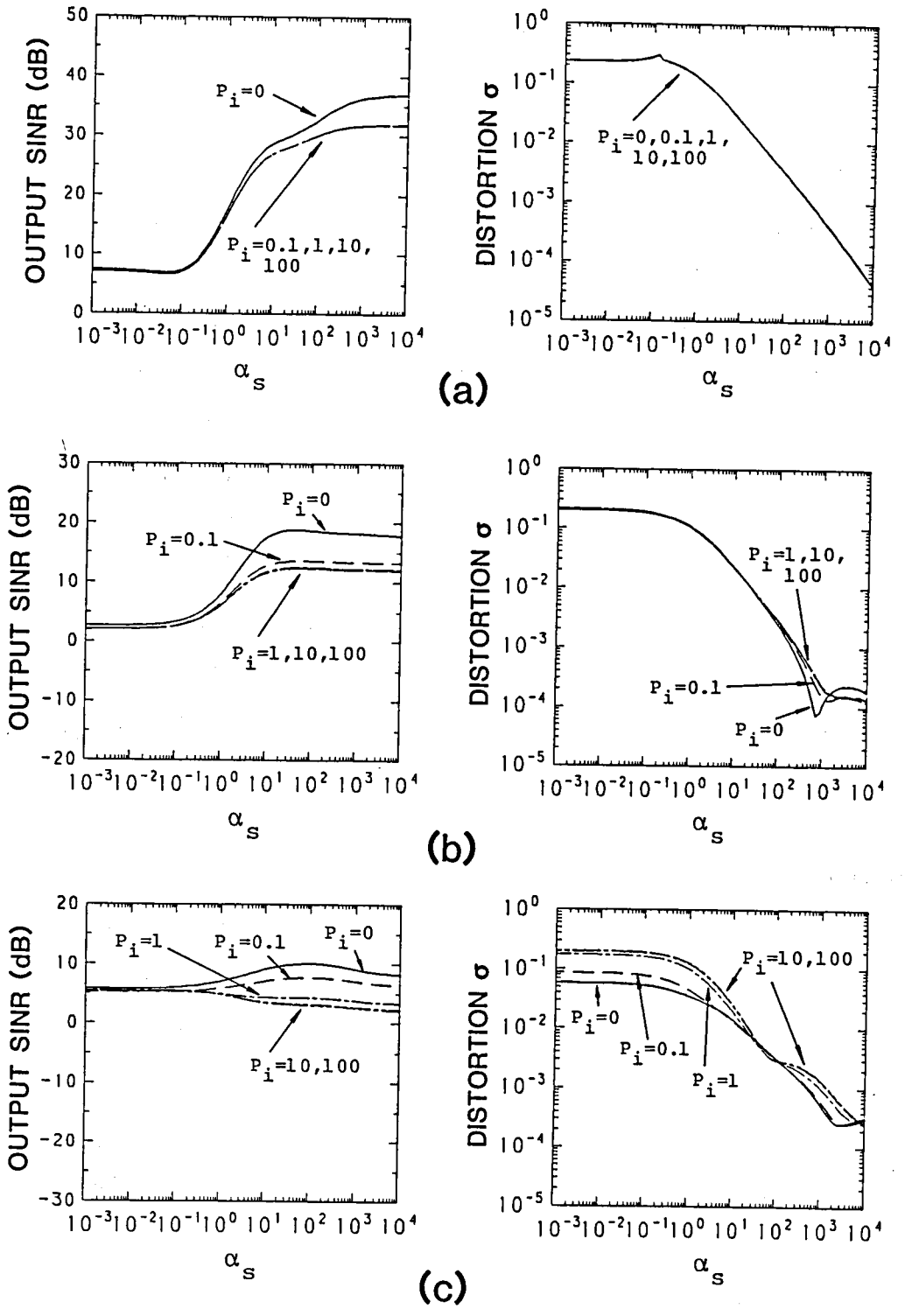

Fig.7.2 Variations of the output SINR and distortion σ in terms of α_s for the improved CCMP system where $\delta f=0.2$ and $\delta f_d=0.4$: (a) $P_n=10^{-4}$, (b) $P_n=10^{-2}$, (c) $P_n=10^{-1}$. (see Table 7.1)

$P_n=10^{-4}$, $P_n=10^{-2}$, and $P_n=10^{-1}$, respectively. From these figures, we can see that the larger α_s and the smaller thermal noise yields the lower distortion of the output broadband desired signal, which is also pointed out by Ref.[49]. In addition, it should be noticed that for the larger value of α_s, distortion σ is little affected by the interference power. On the other hand, the output SINR's do not vary so seriously with α_s as the distortion. This suggests that we may determine the value of α_s based upon the distortion. We see that when we have α_s larger than about $10^4 P_n$, distortion σ can be reduced to less than 0.01 regardless of the interference power. If, however, the constrained bandwidth is discrepant from the real bandwidth of the desired signal (i.e., $\delta f_s \neq \delta f_d$), the situation differs from the above. Fig.7.2 shows the results similar to Fig.7.1 where $\delta f_s=0.2$ and $\delta f_d=0.4$. In this case, both SINR and distortion σ vary remarkably with α_s, and α_s larger than about 100 times P_s gives high SINR and low distortion. Thus, we obtain the following relation as the standard for the lower bound of the value of α_s:

$$\alpha_s \geq \max\{10^4 P_n,\ 10^2 P_s\} \tag{7.28}$$

By other examples, we verified the choice of α_s by the above relation is successful. Since the SINR of the system is not seriously degraded by too large α_s as shown in Fig's.7.1 and 7.2, a little larger approximate estimates of P_n and P_s are preferable for α_s of eq.(7.28). As for the upper bound of α_s, we do not refer to it particularly for the same reason.

Next, we assume the interference is incident from the broadside (0°) and has the same bandwidth as the desired signal. For simplicity, we express the common bandwidth of the incoming waves as δf. Fig's.7.3-7.5 show the relations between the output SINR and the bandwidth δf and between the distortion σ and δf for three different bandwidth

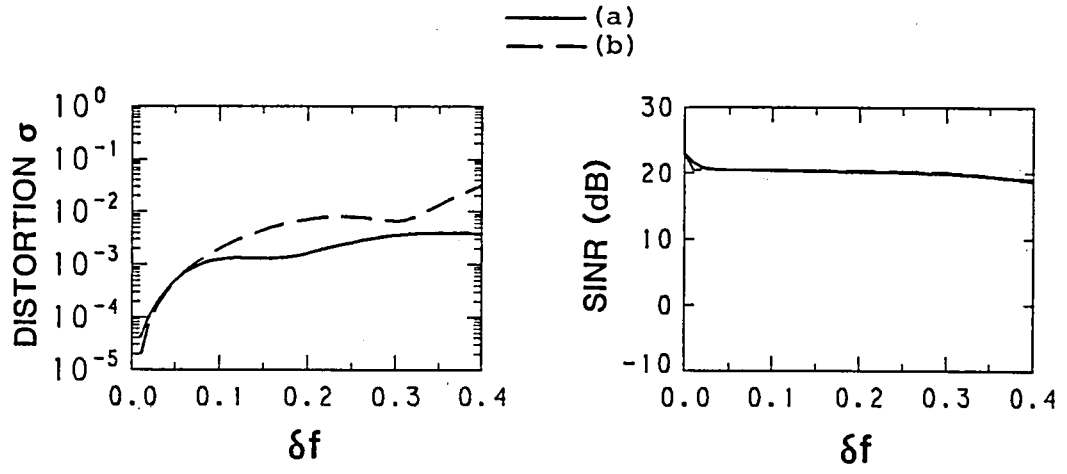

Fig.7.3 Relations of the output SINR and the distortion σ with the bandwidth of incoming waves δf where $\delta f_d=\delta f$: (a) the improved CCMP, (b) the double-frequency constraints DCMP. (see Table 7.1)

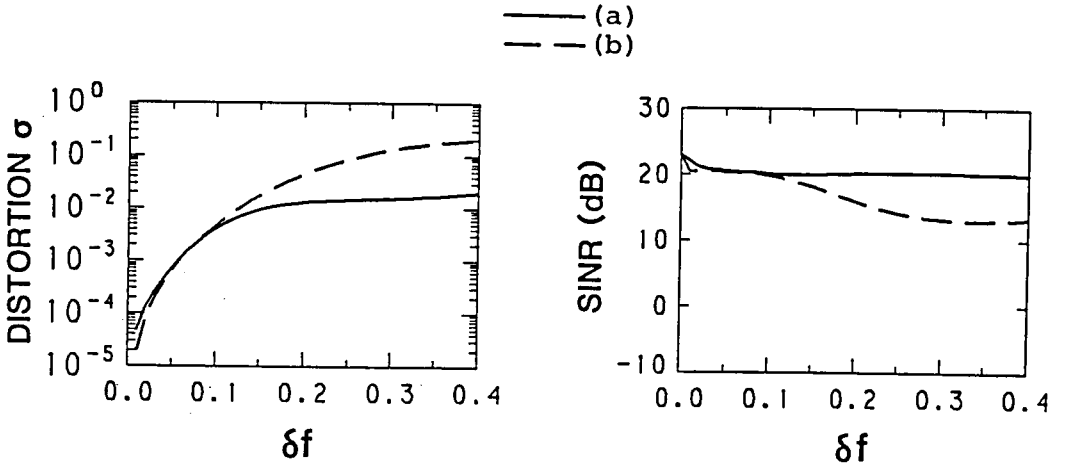

Fig.7.4 Relations of the output SINR and the distortion σ with the bandwidth of incoming waves δf where $\delta f_d=0.75\delta f$: (a) the improved CCMP, (b) the double-frequency constraints DCMP. (see Table 7.1)

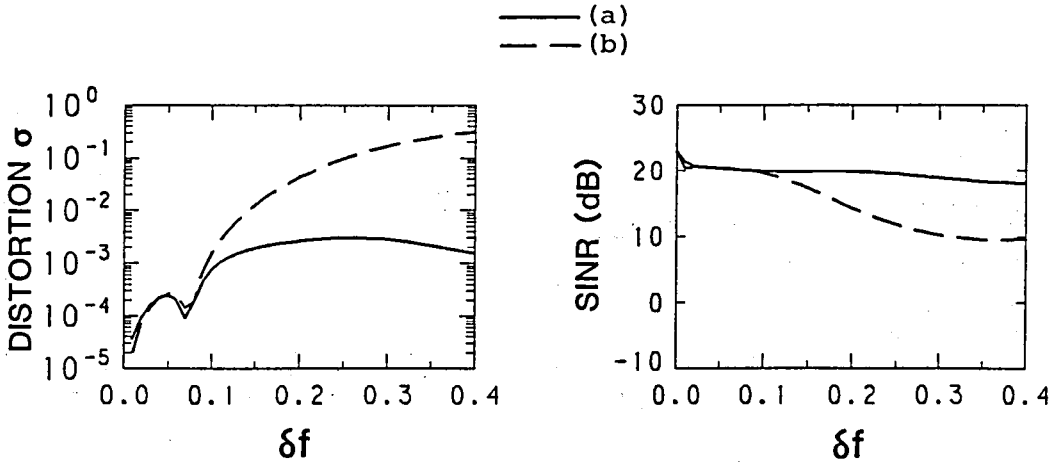

Fig.7.5 Relations of the output SINR and the distortion σ with the bandwidth of incoming waves δf where $\delta f_d = 1.25\delta f$: (a) the improved CCMP, (b) the double-frequency constraints DCMP. (see Table 7.1)

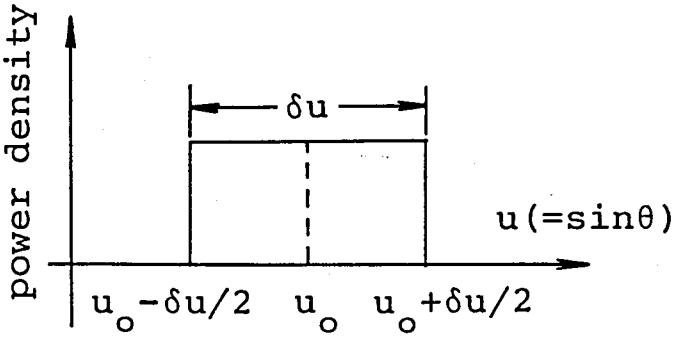

Fig.7.6 Angular spectrum of the modeled desired signal for the wide-angle constraint of the improved CCMP.

constraining. In Fig's.7.3-7.5, the results are represented where $\delta f_d=\delta f$, $\delta f_d=0.75\delta f$, and $\delta f_d=1.25\delta f$, respectively, and curves(a) and (b) in each figure correspond to the improved CCMP method with α_s being 100 in compliance with eq.(7.28) and the DCMP method with the double-frequency constraints, respectively. These figures describe that the improved CCMP method gives better constraining performance than the DCMP with the double-frequency constraints on the whole. Particularly, when the constrained bandwidth includes some error, the difference between both methods becomes remarkable and the improved CCMP method still has good constraining characteristics. Thus, the improved CCMP is also shown to be robust against the setting error of the constrained bandwidth and hence enlarges the margin for determining the constrained bandwidth.

7.4 Performance to Pointing Error

7.4.1 Formulation of Models

In this section, we deal with the countermeasure against the beam pointing error in the conventional DCMP method other than the tamed adaptive array in Chapter 5. As stated in Chapter 5, if there exists the pointing error, the desired signal becomes a target of suppression, resulting in deterioration of SINR. In Section 7.3, we have realized the way of constraining the broadband desired signal with the improved CCMP method. By analogy, we can expect that it is possible for the improved CCMP method to be applied to the broadband constraint in angular domain. Therefore, this section is devoted to such an application of the improved CCMP method.

First, we must define the modeled desired signal for the constraint condition. To settle some wider margin for the directional constraint, we

consider the modeled desired signal with its power spectrum spread over a certain angular region as shown in Fig.7.6. This angular spectrum has a flat power density at the region from $u_o-\delta u/2$ to $u_o+\delta u/2$ and zero elsewhere, where $u=\sin\theta$ is the reduced angular variable. Each angular component contained in this flat spectrum is assumed to be uncorrelated with the others. It is entirely on the analogy of the frequency spectrum of Fig.5.10. Let us consider the normalized correlation function between the p-th and p'-th inputs of the modeled desired signal which are at the q-th tap of the k-th element and the q'-th tap of the k'-th element of the array, respectively. Then, the normalized correlation function R_u is given by

$$R_u(\zeta_{pp'},\tau_{pp'}) = \mathrm{Re}\{R_{uc}(\zeta_{pp'},\tau_{pp'})\} \tag{7.29}$$

with

$$R_{uc}(\zeta_{pp'},\tau_{pp'}) = \frac{1}{\delta u}\int_{u_o-\delta u/2}^{u_o+\delta u/2} \exp\{j(2\pi\zeta_{pp'}/\lambda)u+2\pi f_d\tau_{pp'}\}du \tag{7.30}$$

$$(p,p'=1,..,KL)$$

where

$$\zeta_{pp'} = d_k - d_{k'} \qquad (k,k'=1,..,K) \tag{7.31}$$

$$\tau_{pp'} = \tau_q - \tau_{q'} \qquad (q,q'=1,..,L) \tag{7.32}$$

$$\lambda = c/f_d$$

where d_k is the position of the k-th antenna element with reference to the array center (see Fig.3.2), τ_q is the time delay at the q-th tap with reference to the first tap in the channel, and c is the light velocity. The subscript p is related to subscripts k and q by eq.(7.4) and p' is related to k' and q' by

$$p' = k' + K(q' - 1) \quad (p'=1,..,KL;\ k'=1,..,K;\ q'=1,..,L) \tag{7.33}$$

Thus, we have the following analytic form of R_u:

$$R_u(\zeta_{pp'},\tau_{pp'}) = \cos\{(2\pi\zeta_{pp'}/\lambda)u_o+2\pi f_d\tau_{pp'}\}\cdot\mathrm{sinc}(\pi\delta u\zeta_{pp'}/\lambda) \tag{7.34}$$

Considering that the power is divided into L taps at each channel, we obtain the formulas of the p-th entry of r_d, r_{dp}, and the (p,p') entry of R_{DD}, $r_{p,p'}$, which are written as follows:

$$r_{dp} = (1/\sqrt{L})\ R_u(d_k,\tau_q) \tag{7.35}$$

$$r_{p,p'} = (1/L)\ R_u(\zeta_{pp'},\tau_{pp'}) \tag{7.36}$$

The values of δu and u_o are chosen beforehand from the apriori information on the desired direction and upon prospect of the pointing error.

As shown above, the constraint condition for the narrowband desired signal in the presence of the pointing error is established, which resembles the broadband constraint condition in the frequency domain discussed in Section 7.3.

7.4.2 Numerical Results

The numerical calculation is carried out on the 4-element, 2-tap

Table 7.2 Parameters of input models and constraints for the wide-angle constraint.

desired signal (S)	angle of arrival	: θ_s (var.)
	power	: $P_s = 1$
interference (I)	angle of arrival	: $\theta_i = -50°$
	power	: $P_i = 100$
thermal noise	power	: P_n (var.)
constrained angular region		: $u_o = 0(\theta_d=0°)$
		δu (var.)
constrained frequency		: $f_d = f_o(=1)$

Note: All external waves are narrowbanded.

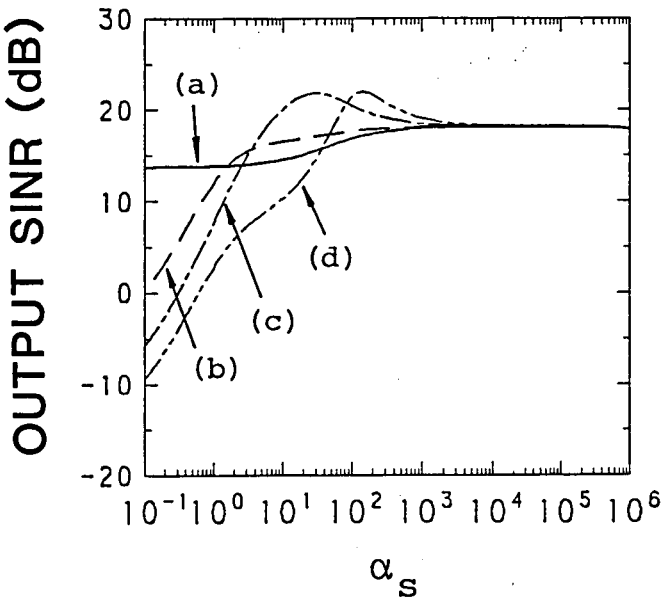

Fig.7.7 Relations between the output SINR and α_s for the wide-angle constraint of the improved CCMP where $P_n=10^{-2}$: (a) $\theta_s=0°$, (b) $\theta_s=2°$, (c) $\theta_s=4°$, (d) $\theta_s=6°$. (see Table 7.2)

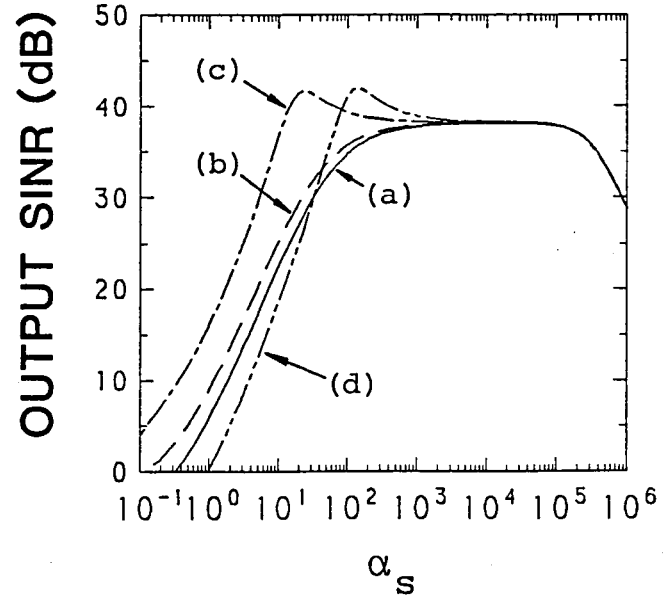

Fig.7.8 Relations between the output SINR and α_s for the wide-angle constraint of the improved CCMP where $P_n=10^{-4}$: (a) $\theta_s=0°$, (b) $\theta_s=2°$, (c) $\theta_s=4°$, (d) $\theta_s=6°$. (see Table 7.3)

narrowband adaptive array. As the representative of the DCMP with the multiple constraints, the double-directional constraints system is discussed for comparison, which sets the constraint conditions at the two close directions θ_1 and θ_2(specified later)[30]. Table 7.2 shows the parameters of the input and constraint under the effect of the pointing error.

Fig's.7.7 and 7.8 show the relations between the output SINR and α_s. Fig.7.7 represents the results where $P_n=10^{-2}$ and Fig.7.8 those where $P_n=10^{-4}$. The curves (a), (b), (c), and (d) in Fig's.7.7 and 7.8 correspond to the cases where $\theta_s=0°$, $\theta_s=2°$, $\theta_s=4°$, and $\theta_s=6°$, respectively. From these figures, we can see that high SINR is obtained in the wide region of the value of α_s ranging from about 10^2P_s to 10^5P_s. In the following examples, $\alpha_s=100$ for $P_s=1$ is adopted, which is in the same order as the case of broadband constraint discussed in Section 7.3.

Fig's.7.9 and 7.10 show the variations of the array response in the direction of the desired signal for various parameters of constraints. Fig.7.9 represents the case where $P_n=10^{-2}$ and Fig.7.10 the case where $P_n=10^{-4}$. In both figures, no interference arrives, which is the rather adverse circumstances to the constraint of the desired signal in the presence of the pointing error. The curves (a), (b), (c), and (d) in Fig's.7.9 and 7.10 correspond to the results where $\delta u=0(\pm 0°)$, $\delta u=0.07(\pm 2°)$, $\delta u=0.14(\pm 4°)$, and $\delta u=0.21(\pm 6°)$, respectively. The curve (a) of $\delta u=0$ in each figure is equivalent to the conventional DCMP with the single constraint and is shown sensitive to the pointing error. In contrast, the curves (b)-(d) of larger δu's show robustness of the improved CCMP system against the pointing error: the deterioration of the array response is less than 0.7dB for $P_n=10^{-2}$ and less than 0.9dB for $P_n=10^{-4}$, as long as the desired signal arrives within the constrained

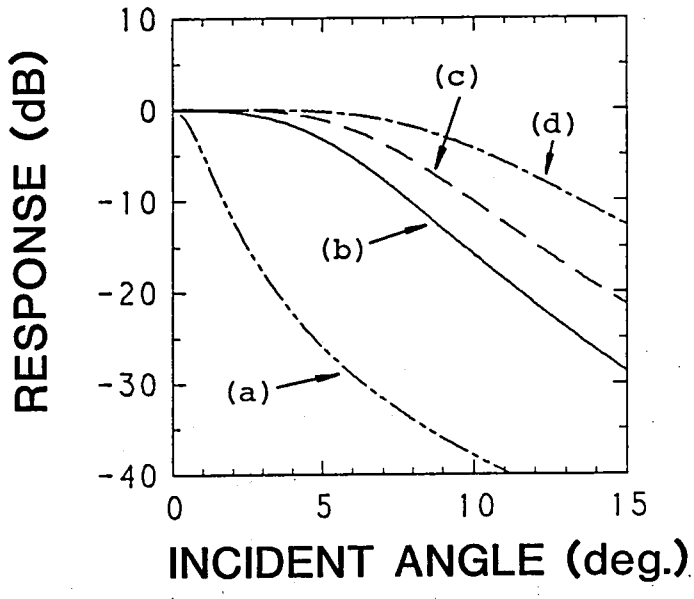

Fig.7.9 Variations of the array response in the direction of the desired signal for the wide-angle constraint of the improved CCMP where $P_n=10^{-2}$ and no interference arrives: (a) $\delta u=0(\pm 0°)$, (b) $\delta u=0.07(\pm 2°)$, (c) $\delta u=0.14(\pm 4°)$, (d) $\delta u=0.21(\pm 6°)$. (see Table 7.2)

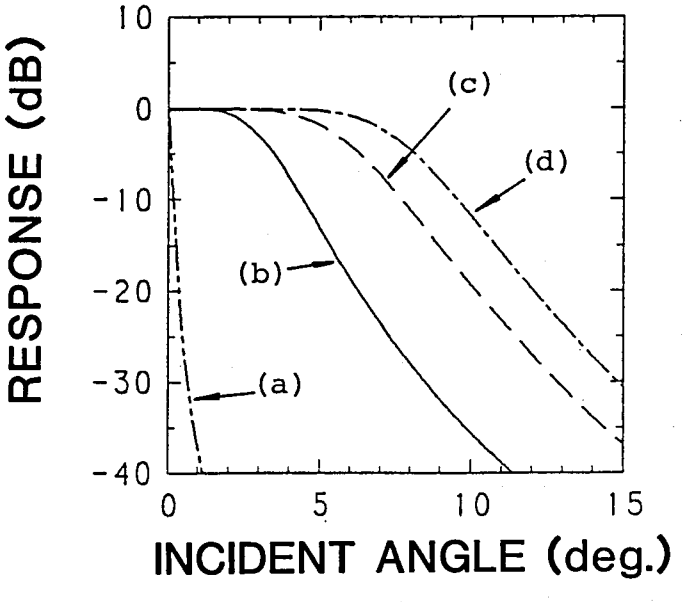

Fig.7.10 Variations of the array response in the direction of the desired signal for the wide-angle constraint of the improved CCMP where $P_n=10^{-4}$ and no interference arrives: (a) $\delta u=0(\pm 0°)$, (b) $\delta u=0.07(\pm 2°)$, (c) $\delta u=0.14(\pm 4°)$, (d) $\delta u=0.21(\pm 6°)$. (see Table 7.2)

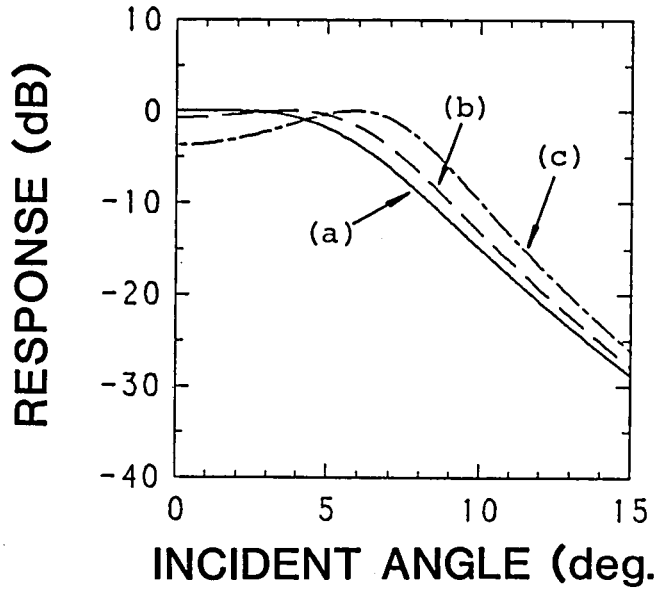

Fig.7.11 Variations of the array response in the direction of the desired signal for the DCMP double-directional constraints at (θ_1,θ_2) where $P_n=10^{-2}$ and no interference arrives: (a) $(\theta_1,\theta_2)=(-2°,2°)$, (b) $(\theta_1,\theta_2)=(-4°,4°)$, (c) $(\theta_1,\theta_2)=(-6°,6°)$. (see Table 7.2)

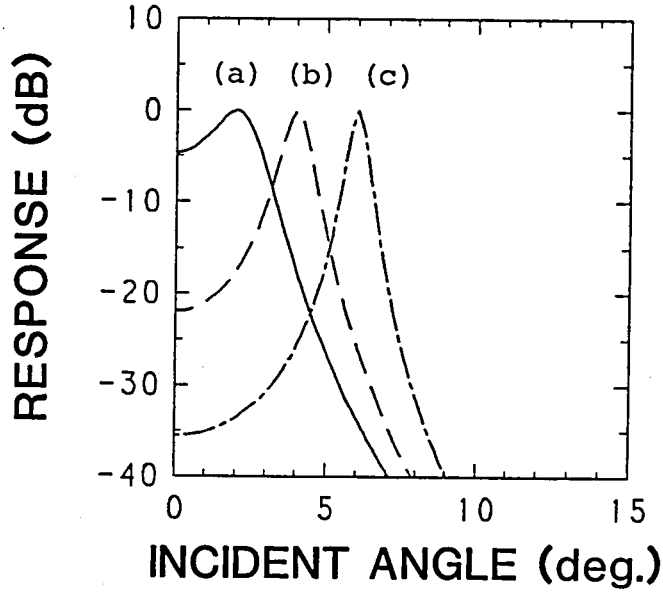

Fig.7.12 Variations of the array response in the direction of the desired signal for the DCMP double-directional constraints at (θ_1,θ_2) where $P_n=10^{-4}$ and no interference arrives: (a) $(\theta_1,\theta_2)=(-2°,2°)$, (b) $(\theta_1,\theta_2)=(-4°,4°)$, (c) $(\theta_1,\theta_2)=(-6°,6°)$. (see Table 7.2)

angular region δu. On the other hand, for the double-directional constraints, the same relations as Fig's.7.9 and 7.10 are shown in Fig's.7.11 and 7.12, respectively. The curves (a), (b), and (c) in Fig's.7.11 and 7.12 correspond to the cases where $(\theta_1,\theta_2)=(-2°,2°)$, $(\theta_1,\theta_2)=(-4°,4°)$, and $(\theta_1,\theta_2)=(-6°,6°)$, respectively. Other parameters are the same as those of Fig's.7.9 and 7.10. Since the double constraints system prescribes the responses in only two directions, the array responses are seen to be seriously degraded in the middle of the two constrained directions, which is remarkable in the case of smaller thermal noise of Fig.7.12. Therefore, the system with the double-directional constraints requires a larger number of constrained angles, i.e., degrees of freedom, for the wider-angle constraint. Thus, it is demonstrated that the improved CCMP method is superior to the double constraints DCMP.

However, one problem arises in the improved CCMP method for the wide-angle constraint. It is increment of the output thermal noise due to the wider beamwidth, which results in a little degradation of the output SINR. For the countermeasure against this problem, injection of a certain amount of the pseudo noise is considered again. Fig.7.13 shows the example of support by the pseudo noise α_n where $P_n=10^{-4}$, $\delta u=0.21(\pm 6°)$, and $\alpha_s=100$. The abscissa in Fig.7.13 means the pseudo noise α_n, and it is related to the output SINR of the ordinate with parameters of the angle of arrival of the desired signal. The curves (a), (b), (c), and (d) in Fig.7.13 correspond to the cases where $\theta_s=0°$, $\theta_s=2°$, $\theta_s=4°$, and $\theta_s=6°$, respectively. It is seen that the pseudo noise of about 0.1 gives good support in any curve. Other examples confirmed us that the optimum pseudo noise for the wide-angle constraint by the improved CCMP method with $\alpha_s=100P_s$ is about $10^{-3}(P_s+\alpha)$.

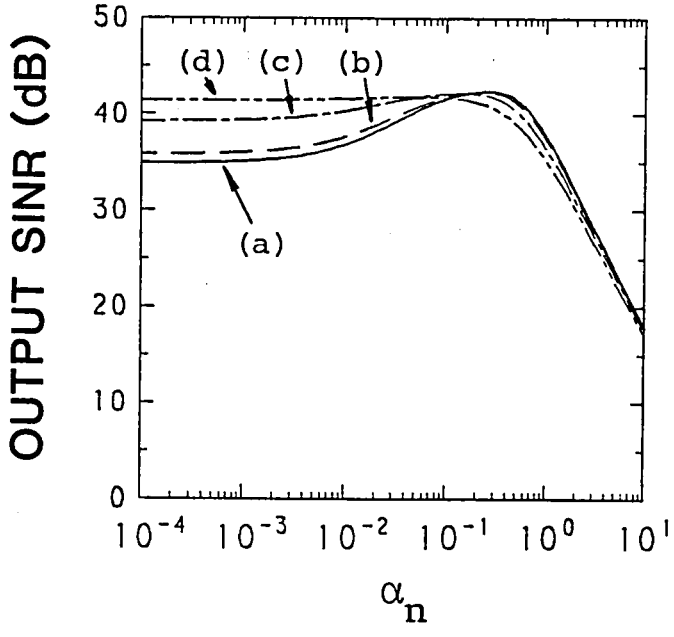

Fig.7.13 Relations between the output SINR and the pseudo noise α_n for the improved CCMP where $P_n=10^{-4}$: (a) $\theta_s=0°$, (b) $\theta_s=2°$, (c) $\theta_s=4°$, (d) $\theta_s=6°$. (see Table 7.2)

7.5 Performance to Broadband Desired Signal in the Presence of Pointing Error

7.5.1 Formulation of Models

This section discusses both problems of Sections 7.3 and 7.4 simultaneously and extends the improved CCMP method to the constraint of the broadband desired signal in the presence of the pointing error.

Similar to the previous sections, we first define the modeled desired signal for the constraint condition of the present interest. In order to constrain the desired signal widely in the angular and frequency domains, we consider the modeled desired signal with the two-dimensional power spectrum spread over certain angle and frequency regions as shown in Fig.7.14. This power spectrum has a flat power density at the region from $u_o-\delta u/2$ to $u_o+\delta u/2$ and from $f_d-\delta f_d/2$ to $f_d+\delta f_d/2$, and zero elsewhere. All the components involved by this flat spectrum are assumed to be uncorrelated with each other. It is interpreted as fusion of the previous respective spectra. Let R_{fu} represent the normalized correlation function between the p-th and p'-th inputs of this type of modeled desired signal. Then, R_{fu} is derived from the following equations:

$$R_{fu}(\zeta_{pp'},\tau_{pp'}) = \mathrm{Re}\{R_{fuc}(\zeta_{pp'},\tau_{pp'})\} \tag{7.37}$$

with

$$R_{fuc}(\zeta_{pp'},\tau_{pp'}) = \frac{1}{\delta u \delta f_d} \int_{f_d-\delta f_d/2}^{f_d+\delta f_d/2} \int_{u_o-\delta u/2}^{u_o+\delta u/2} \cdot \exp\{j(2\pi\zeta_{pp'}/\lambda)u+2\pi f\tau_{pp'}\}\,du\,df \tag{7.38}$$

$$\lambda = c/f$$

Thus, we have the following form of R_{fu}:

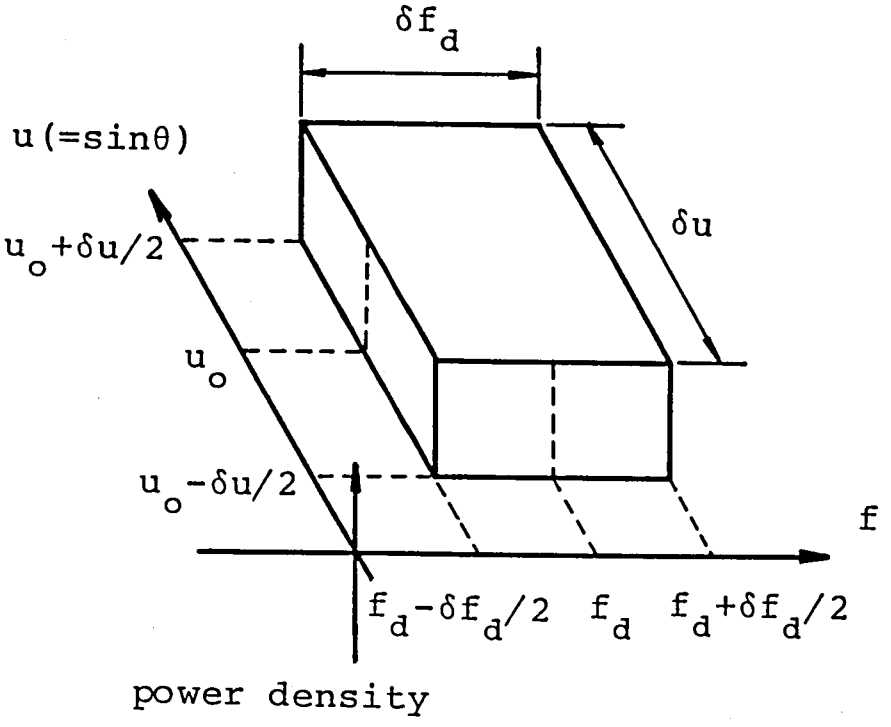

Fig.7.14 Two-dimensional power spectrum of the modeled desired signal for the broadband constraint in the angular and frequency domains by the improved CCMP.

$$R_{fu}(\zeta_{pp'},\tau_{pp'}) = \begin{cases} \dfrac{c}{2\pi\zeta_{pp'}\delta f_d \delta u}[S_i(A_1) - S_i(A_2) - S_i(A_3) + S_i(A_4)] & (\zeta_{pp'}\neq 0) \\ \cos(2\pi f_d \tau_{pp'})\cdot \mathrm{sinc}(\pi \delta f_d \tau_{pp'}) & (\zeta_{pp'}=0) \end{cases} \quad (7.39)$$

where $S_i(x)$ is the sine integral which is given by

$$S_i(x) = \int_0^x \frac{\sin v}{v}\, dv \quad (7.40)$$

and

$$A_1 = 2\pi(f_d + \delta f_d/2)\{(\zeta_{pp'}/c)(u_o + \delta u/2) + \tau_{pp'}\} \quad (7.41)$$

$$A_2 = 2\pi(f_d - \delta f_d/2)\{(\zeta_{pp'}/c)(u_o + \delta u/2) + \tau_{pp'}\} \quad (7.42)$$

$$A_3 = 2\pi(f_d + \delta f_d/2)\{(\zeta_{pp'}/c)(u_o - \delta u/2) + \tau_{pp'}\} \quad (7.43)$$

$$A_4 = 2\pi(f_d - \delta f_d/2)\{(\zeta_{pp'}/c)(u_o - \delta u/2) + \tau_{pp'}\} \quad (7.44)$$

Using eq's.(7.39)-(7.44), we obtain the formulas of the p-th entry of $\mathbf{r}_d$ and the (p,p') entry of R_{DD}, which are given by

$$r_{dp} = (1/\sqrt{L})\, R_{fu}(d_k,\tau_q) \quad (7.45)$$

$$r_{p,p'} = (1/L)\, R_{fu}(d_k - d_{k'},\tau_q - \tau_{q'}) \quad (7.46)$$

$$(p,p'=1,..,KL;\ k,k'=1,..,K;\ q,q'=1,..,L)$$

The values of δf_d, f_d, δu, and u_o are determined beforehand from the a priori knowledge on the characteristics of the desired signal and upon prospect of the pointing error.

As shown above, the constraint condition for the broadband desired signal in the presence of the pointing error is established as extension of Sections 7.3 and 7.4.

7.5.2 Numerical Results

We show the numerical examples carried out on the 4-element, 4-tap broadband adaptive array used in Section 7.3. For comparison, the performance of the DCMP system with the double-directional and double-frequency constraints is also shown here. It is assumed that the desired

Table 7.3 Parameters of input models for the broadband constraint in the angular and frequency domains.

desired signal (S)	angle of arrival	: θ_s (var.)
	power	: $P_s = 1$
	bandwidth	: $\delta f_s = \delta f$
interference (I)	angle of arrival	: $\theta_i = -50°$
	power	: $P_i = 100$
	bandwidth	: $\delta f_i = \delta f$
thermal noise	power	: P_n (var.)

Table 7.4 Parameters of constraints adopted by the improved CCMP and the DCMP with multiple constraints for the broadband constraint in the angular and frequency domains.

(a) improved CCMP

constrained angular region	: $u_o-\delta u/2 = 24°$	$(30°\pm6°)$
	$u_o+\delta u/2 = 36°$	
constrained frequency band	: $\delta f_d = \delta f$	
	$f_d = f_o(=1)$	
$\alpha_s = 100$, $\alpha_n = 0$		

(b) DCMP with multiple constraints (four constraints)

constrained angles and frequencies :

$(26.58°, f_d-0.285\delta f_d)$, $(33.42°, f_d-0.285\delta f_d)$,

$(26.58°, f_d+0.285\delta f_d)$, $(33.42°, f_d+0.285\delta f_d)$.

where $\delta f_d = \delta f$,

$f_d = f_o(=1)$.

signal and interference have the same form of frequency spectrum shown by Fig.5.10 and their bandwidths are equal (denoted by δf). Table 7.3 shows the parameters of the inputs, and Table 7.4 shows the parameters of the constraint for the improved CCMP and the DCMP with the multiple constraints. As the measure of the performance, the distortion σ defined in Section 7.3 and output SINR are employed.

Fig.7.15 shows the relations between the output SINR and bandwidth δf and between the distortion σ and δf for the improved CCMP method. The curves (a)-(c) in Fig.7.15 represent the results where $\theta_S=24°$, $\theta_S=30°$, and $\theta_S=36°$, respectively. It is seen that as long as the desired signal' with its bandwidth δf of less than 0.4 arrives within the specified angular region, the constraint is successful with $\sigma \leqq 0.039$ and SINR $\geqq$ 14.2dB. The same relations for the DCMP with the multiple constraints are shown in Fig.7.16. The parameters of constraints in Table 7.4 are chosen as the best ones from Ref's.[30], [48] and [101] and also from our experiences. The curves (a)-(c) in Fig.7.16 correspond to those in Fig.7.15, respectively. In this figure, the multiple constraints system has characteristics of constraining with $\sigma \leqq 0.053$ and SINR $\geqq$ 9.94dB for $\delta f \leqq 0.4$, which is slightly inferior to the improved CCMP system.

Moreover, the noteworthy difference between both methods is observed for the case of smaller thermal noise. Fig's.7.17 and 7.18 show such examples where $P_n=10^{-4}$. The former represents the results by the improved CCMP, and the latter the results by the DCMP with the multiple constraints. The curves (a)-(c) in each figure have the same meanings as those of Fig.7.15 or 7.16. In this case, the DCMP system yields large distortion over 0.05 for the bandwidth δf of more than 0.1. Also, as for the output SINR of it, low SINR of less than 12.2dB are seen for δf ranging from 0.0 to 0.4. It is because the desired signal component with

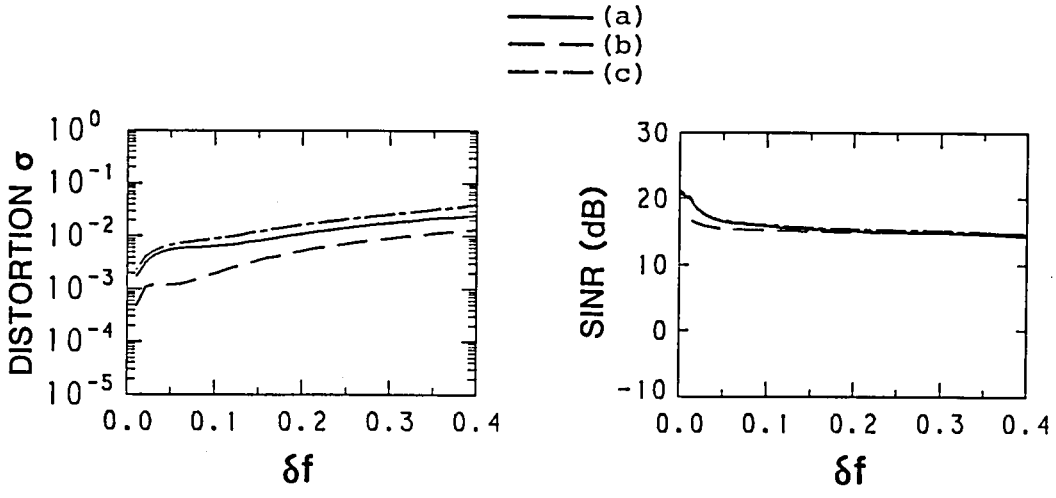

Fig.7.15 Relations of the output SINR and the distortion σ with the bandwidth of incoming waves δf for the improved CCMP with the broadband constraint in the angular and frequency domains where $P_n=10^{-2}$: (a) $\theta_s=24°$, (b) $\theta_s=30°$, (c) $\theta_s=36°$. (see Tables 7.3 and 7.4)

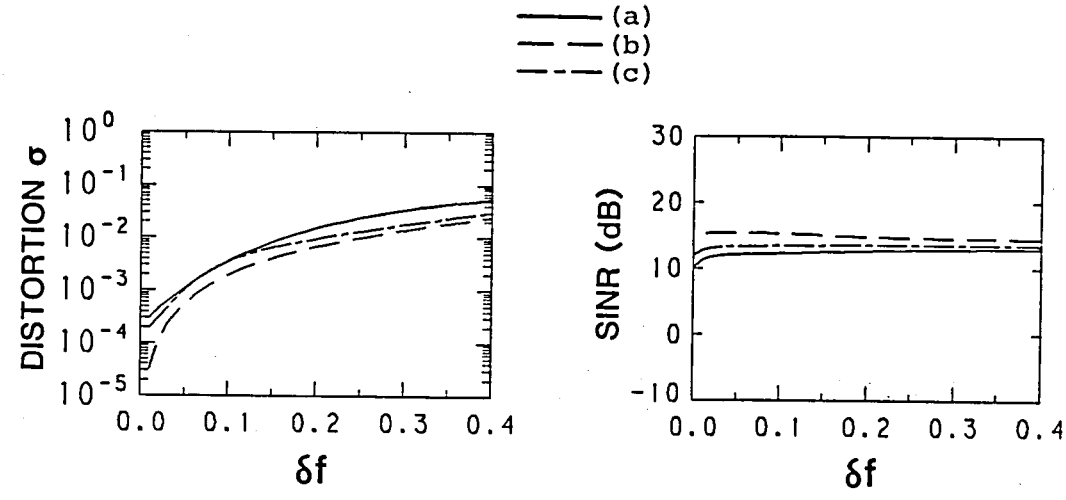

Fig.7.16 Relations of the output SINR and the distortion σ with the bandwidth of incoming waves δf for the DCMP with multiple constraints where $P_n=10^{-2}$: (a) $\theta_s=24°$, (b) $\theta_s=30°$, (c) $\theta_s=36°$. (see Tables 7.3 and 7.4)

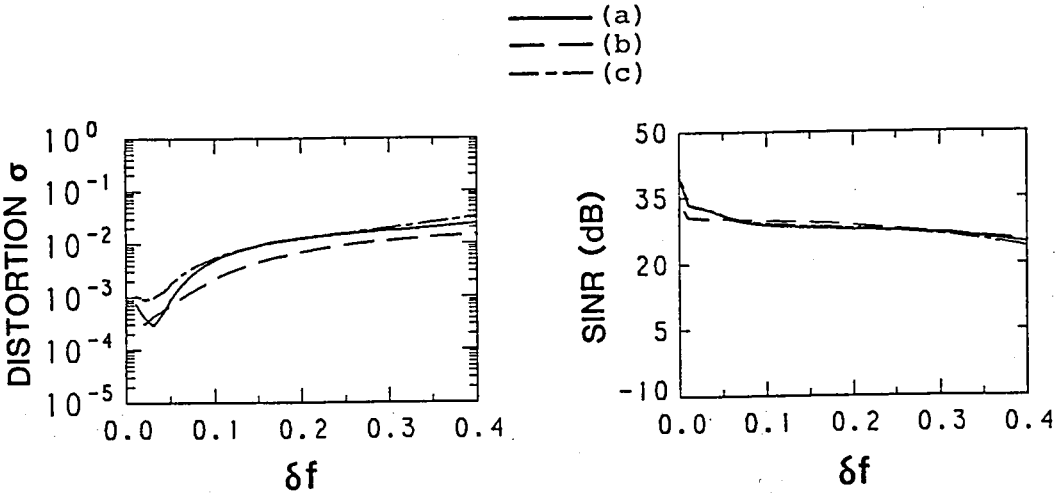

Fig.7.17 Relations of the output SINR and the distortion σ with the bandwidth of incoming waves δf for the improved CCMP with the broadband constraint in the angular and frequency domains where $P_n=10^{-4}$: (a) $\theta_s=24°$, (b) $\theta_s=30°$, (c) $\theta_s=36°$. (see Tables 7.3 and 7.4)

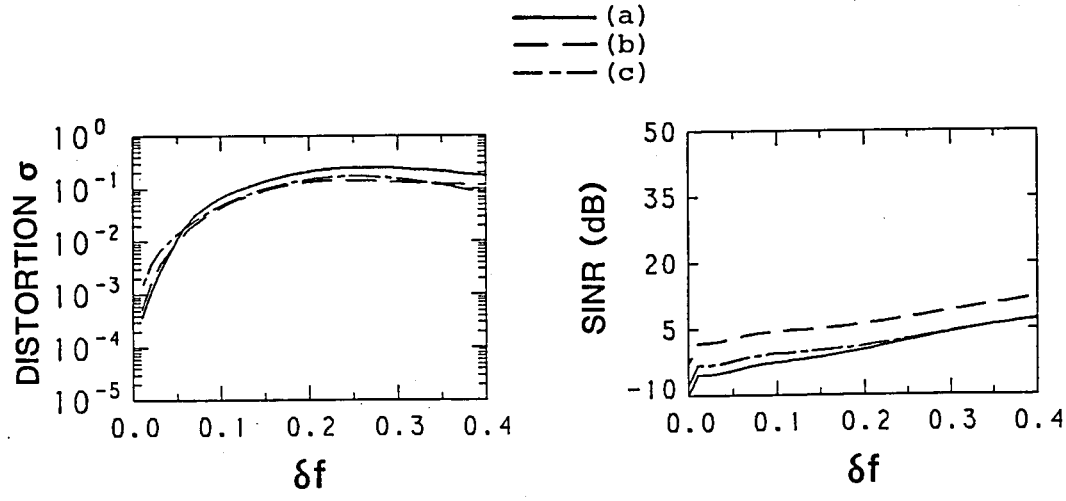

Fig.7.18 Relations of the output SINR and the distortion σ with the bandwidth of incoming waves δf for the DCMP with multiple constraints where $P_n=10^{-4}$: (a) $\theta_s=24°$, (b) $\theta_s=30°$, (c) $\theta_s=36°$. (see Tables 7.3 and 7.4)

the unconstrained angles or frequencies other than the four constrained ones becomes a target of fierce suppression. On the other hand, the improved CCMP, which constrains the angles and frequencies averaged over the region, has better constraining performance with $\sigma \leq 0.032$ and SINR $\geq$ 23.7dB for $\delta f \leq 0.4$.

Although the results are not shown here, we examined the performance of both systems for the case where the constrained bandwidth δf_d has a certain amount of discrepancy from δf, and we have attained the similar conclusion.

7.6 Concluding Remarks

In this chapter, we have introduced an alternative guiding principle of power minimization. The new principle prescribes the cross correlation between the desired signals at the input and the output of the array by the available a priori knowledge on the characteristics of the desired signal in terms of its angle of arrival or frequency spectrum. This new principle is called the correlation-constrained minimization of power (CCMP) method. The conventional DCMP method constrains the voltage transfer function of the system to the direction from which the desired signal arrives. In contrast with this, the constraint condition of the CCMP method is interpreted as the one obtained by averaging the conventional DCMP constraint over the specified frequency and/or angular region. Furthermore, the characteristics of the CCMP method can be improved by intentionally increasing the component of the desired signal in the input correlation matrix, which we call "the improved CCMP method". We analyzed the improved CCMP method in this chapter.

Although it has already been reported by Ref's.[48] and [77] that this

improved CCMP method brings about good constraining of the broadband desired signal, we gave reinvestigation to such performance at first. Next, by analogy between the frequency domain and the angular domain, this improved CCMP method has been applied to the problem of the error in the beam pointing toward the desired signal. Numerical examples have verified that the improved CCMP method can give another remedy for the degradation of performance due to the beam pointing error which is a serious problem in the conventional DCMP. Finally, we extended the improved CCMP method to the constraint of the broadband desired signal in the presence of the pointing error, and we examined the performance by numerical calculation. As the results, we have seen that the broadband desired signal can be constrained successfully as long as it arrives within the angular region prescribed by the improved CCMP method.

Through the numerical calculation, the performance of the DCMP method with the multiple constraints was also shown for comparison. After all, such comparison has confirmed us that the improved CCMP method is superior to the DCMP method with the multiple constraints on the whole.

CHAPTER 8

EFFECTS OF INITIAL VALUES ON THE TRANSIENT PERFORMANCE IN VARIOUS ADAPTIVE ALGORITHMS

8.1 Introduction

The common objective of various adaptive arrays is to suppress the interferences while maintaining the desired signal. Most adaptive arrays adopt the feedback approach based on the gradient method to attain such an optimum performance. It has been discussed by many authors that the transient performance of the adaptive array in a realistic environment is affected by the divergence of eigenvalues of the input correlation matrix due to particular angular distribution and power variations of the interferences. However, we shall add a different viewpoint on another aspect that affects the transient performance.

In control problems, the selection of the initial values is often a matter of great importance since it very likely affects the transient behavior of the system. Strangely, this problem has not attracted much interest in the field of adaptive antennas. Concerning the least mean square (LMS) adaptive array, some papers set identical weight values on all the elements of the array[8],[9],[63],[102], some set zeros on all but one weight[31],[103], some set the uniform magnitude on the weights whose phases are such that they produce the mainbeam pointing to the desired signal[20], and so on.

This chapter considers the directionally constrained minimization of power (DCMP) adaptive array[27],[29],[30], the LMS adaptive array and the

maximum signal-to-noise ratio (MSN) adaptive array[15]. We will demonstrate how dramatically the transient behavior of the systems is affected by the initial weight values, and we emphasize the importance of their choice[104].

In the next section, we first describe the system and input models for the analysis and computer simulation carried out throughout this chapter. Sections 8.3 to 8.5 are devoted to analyze and examine the transient performances of adaptive arrays under the principles of DCMP, LMS, and MSN, respectively. We discuss the results in Section 8.6, and finally state conclusions in Section 8.7.

8.2 General Description

The adaptive processors that control the weights are classified according to the guiding principles. Before we proceed to discuss them in detail, the features that are common to all systems are described first.

In the present discussion, we assume that the input signals are narrowbanded and can be treated by complex expressions. The K-element adaptive array system with isotropic elements is adopted. As for the input, we consider that two plane waves, the desired signal and i-interference, are incident on the array. Another input, thermal noise of equal power is assumed to exist at each weight. For simplicity, we call the i-interference merely the interference hereafter.

In order to verify the theoretical analysis, computer simulation is carried out on a 4-element (K=4) linear array with equal spacing of a half wavelength. Table 8.1 shows the parameters we use as the model input in the computer simulation. In later examples, only those parameters that are changed will be stated, while other parameters left unmentioned are

kept the same as shown in Table 8.1. The sampling feedback control is carried out where a sufficient number of sampled data are averaged to smooth the behavior of the system.

Table 8.1 Input data used in computer simulation.

desired signal (S)	angle of arrival : $\theta_s = 0°$
	power : $P_s = 1$
interference (I)	angle of arrival : $\theta_i = -50°$
	power : $P_i = 100$
thermal noise	power : $P_n = 0.01$

8.3 Directionally Constrained Minimization of Power (DCMP) Adaptive Array

8.3.1 Principle and Analysis

The principle of the DCMP adaptive array is already described in detail in Chapter 3. The optimum weight vector at the stationary state is written as follows again:

$$\mathbf{W}_{opt} = R_{xx}^{-1}\mathbf{C}_d(\mathbf{C}_d^{\dagger}R_{xx}^{-1}\mathbf{C}_d)^{-1}H^* \tag{8.1}$$

where the constraint vector $\mathbf{C}_d$ and the constrained response H are also given by eq's.(3.68) and (3.69), respectively. In the present situation, the correlation matrix R_{xx} can be expressed in the same form as eq.(3.91), which is rewritten as

$$R_{xx} = P_n U + P_s \mathbf{C}_d \mathbf{C}_d^{\dagger} + P_i \mathbf{Z}_i \mathbf{Z}_i^{\dagger} \tag{8.2}$$

where U is the identity matrix and $\mathbf{Z}_i$ is the direction vector of the interference given by eq.(3.90).

By feedback, the optimum weight vector, $\mathbf{W}_{opt}$ is asymptotically reached by the steepest gradient algorithm, which are rewritten as follows here:

$$\mathbf{W}(m+1) = P[\mathbf{W}(m) - \mu \mathbf{X}(m) y^*(m)] + \mathbf{F} \tag{8.3}$$

$$P = U - \mathbf{C}_d(\mathbf{C}_d{}^{\dagger}\mathbf{C}_d)^{-1}\mathbf{C}_d{}^{\dagger} = U - (2/K)\mathbf{C}_d\mathbf{C}_d{}^{\dagger} \tag{8.4}$$

$$\mathbf{F} = \mathbf{C}_d(\mathbf{C}_d{}^{\dagger}\mathbf{C}_d)^{-1}H^* = (2/K)\mathbf{C}_d \tag{8.5}$$

For analysis, we must reformulate the above adaptive algorithm to a form of vector differential equation. First, taking the expectation of eq.(8.3) with the aid of the complex expression of eq.(3.48), i.e., $\mathbf{W}(m)=P\mathbf{W}(m)+\mathbf{F}$, we have

$$E[\mathbf{W}(m+1)] = E[\mathbf{W}(m)] - \mu\, PR_{xx}P\, E[\mathbf{W}(m)] - \mu\, PR_{xx}\mathbf{F} \tag{8.6}$$

With T_s as the notation for the sampling interval, eq.(8.6) can be rewritten as follows:

$$\frac{E[\mathbf{W}(m+1)] - E[\mathbf{W}(m)]}{T_s} + \frac{\mu}{T_s} PR_{xx}P\, E[\mathbf{W}(m)] = -\frac{\mu}{T_s} PR_{xx}\mathbf{F} \tag{8.7}$$

We return here from the discrete quantity to the continuous one and obtain a differential equation by tending T_s to zero in eq.(8.7). Rewriting $E[\mathbf{W}(m)]$ as $\mathbf{W}(t)$ for simplicity of the expression, we thus obtain

$$\frac{d\mathbf{W}(t)}{dt} + qPR_{xx}P\,\mathbf{W}(t) = -qPR_{xx}\mathbf{F} \tag{8.8}$$

where q is the equivalent step size per unit time and is related to μ and T_s by the following equation:

$$q = \mu/T_s \tag{8.9}$$

We call it a feedback gain hereafter. By using $\mathbf{C}_d$ and H of eq's.(3.68) and (3.69) and considering $\theta_d=\theta_s$, we can rewrite $\mathbf{F}$ as

$$\mathbf{F} = (2/K)\mathbf{C}_d$$

$$= (\sqrt{2}/K)[\exp\{j\Psi_1(\theta_s)\},\ \ldots,\ \exp\{j\Psi_K(\theta_s)\}]^T \tag{8.10}$$

where

$$\Psi_k(\theta_s) = -(2\pi d_k/\lambda)\sin\theta_s \qquad (k=1,..,K) \tag{8.11}$$

As stated in Chapter 3, this **F** is the uniform excitation with progressive phasing so as to point the mainbeam to the desired direction, θ_s.

Eq.(8.8) can be solved as follows[30]:

$$\mathbf{W}(t) = \mathbf{W}_{opt} + \{\frac{\mathbf{G}_2^{\dagger}\mathbf{W}(0)}{\mathbf{G}_2^{\dagger}\mathbf{G}_2} + \frac{\mathbf{G}_2^{\dagger}\mathbf{P}\mathbf{R}_{xx}\mathbf{F}}{\lambda_2\mathbf{G}_2^{\dagger}\mathbf{G}_2}\}\,\mathbf{G}_2\exp(-q\lambda_2 t)$$

$$+\sum_{k=3}^{K}\frac{\mathbf{G}_k^{\dagger}\mathbf{W}(0)}{\mathbf{G}_k^{\dagger}\mathbf{G}_k}\,\mathbf{G}_k\exp(-q\lambda_k t) \tag{8.12}$$

where the λ_k's and $\mathbf{G}_k$'s (k=1,..., K) are the eigenvalues and eigenvectors of $\mathbf{P}\mathbf{R}_{xx}\mathbf{P}$, respectively. Since $\mathbf{P}\mathbf{R}_{xx}\mathbf{P}$ is Hermitian, K eigenvectors $\mathbf{G}_k$'s are orthogonal to each other, and λ_k's are expressed as follows[30]:

$$\begin{cases} \lambda_1 = 0 & (8.13)\\ \lambda_2 = (K/2)P_i(1-A_{si}^2) + P_n & (8.14)\\ \lambda_k = P_n \quad \text{for } k = 3,..., K & (8.15) \end{cases}$$

where A_{si} represents the normalized array factor, $\mathbf{Z}_i^T\mathbf{F}^*/H$. For a linear, equispaced array with the element spacing of a half wavelength, A_{si} is given by

$$A_{si} = \frac{\sin\{K\pi(\sin\theta_s - \sin\theta_i)/2\}}{K\sin\{\pi(\sin\theta_s - \sin\theta_i)/2\}} \tag{8.16}$$

When the angular separation between θ_s and θ_i is larger than the beamwidth of the array factor A_{si} so that $A_{si}^2 \ll 1$ and also P_i is much larger than P_n, the λ_k's in eq's.(8.14) and (8.15) can be approximated by

$$\begin{cases} \lambda_2 = (K/2)P_i \\ \lambda_k = P_n \quad \text{for } k = 3,..., K \end{cases} \tag{8.17}$$

In this case, the time constants in the third term of eq.(8.12) are much larger than the other in the second term, as is easily seen by eq.(8.17).

It is this third term that causes slow convergence of the weight vector to the optimum state. If, however, a proper selection of the initial weight vector is made, so that it may be orthogonal to G_k's (k=3,..,K), the third term vanishes. An example of such weight vectors is **F** given by eq.(8.5). Since $G_1=C_d$ as given by Ref.[30], **F** can be shown to be $(2/K)G_1$ by eq.(8.10). Thus, **F** is orthogonal to G_k's, where k=2,..,K. With **W**(0) chosen to be **F**, eq.(8.12) becomes

$$W(t) = W_{opt} + \frac{G_2^{\dagger}PR_{xx}F}{\lambda_2 G_2^{\dagger}G_2} G_2 \exp(-q\lambda_2 t) \tag{8.18}$$

8.3.2 Computer Simulation

The simulation is based on the sampling feedback system with the algorithm given by eq's.(8.3)-(8.5). Taking into consideration that $0 < \mu < 2/\{3\text{trace}(R_{xx})\}$ is required for stability as shown in Chapter 3, our choice is

$$\mu = \frac{1}{5\ \text{trace}(R_{xx})} \tag{8.19}$$

We consider the following three cases of the initial weight vector setting:

(a) **W**(0)=**F**, the uniform excitation vector with the mainbeam directed to the desired signal as shown by eq.(8.10).

(b) **W**(0)=M_1, the vector with zero weights for all elements except the first one, i.e.,

$$M_1 = [\sqrt{2},\ 0,\ 0,\ldots,\ 0]^T. \tag{8.20}$$

(c) **W**(0)=M_2, the vector with zero weights for all elements except the second one, i.e.,

$$M_2 = [0,\ \sqrt{2},\ 0,\ \ldots,\ 0]^T. \tag{8.21}$$

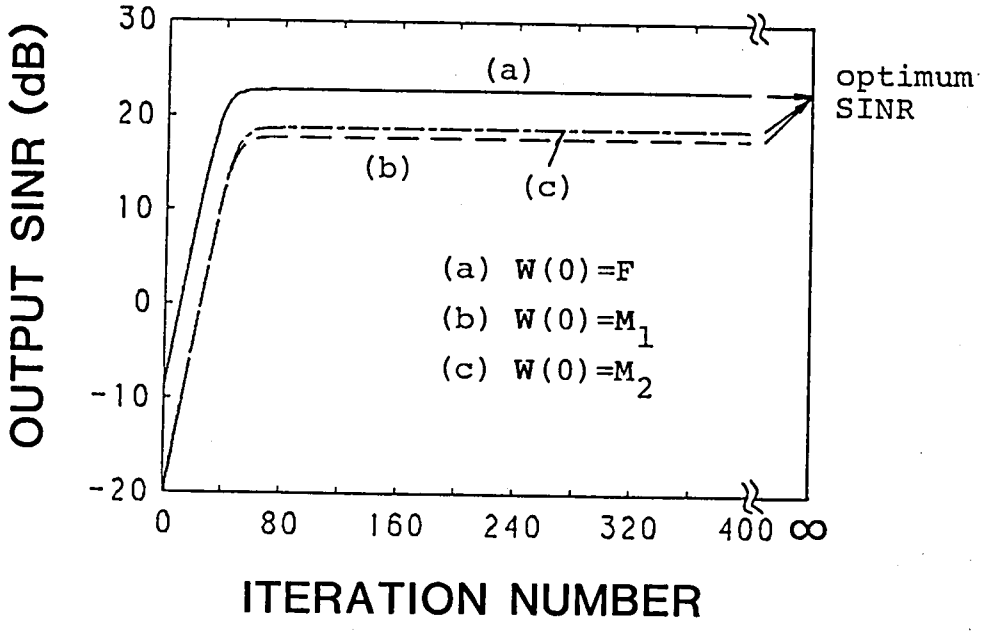

Fig.8.1 The learning curves of the output SINR for three different settings of the initial value, $\mathbf{F}$, $\mathbf{M}_1$ and $\mathbf{M}_2$ in the DCMP adaptive array.

The magnitudes of above weight vectors are chosen so that the desired response may be obtained in the absence of interference. Fig.8.1 shows the results by the simulation. The learning curves of the output SINR for the above three cases are shown. By theory, all curves must finally reach the same value of SINR, but the curves (b) and (c) are converging so slowly as if they were aiming at certain lower SINR's than that for (a). In these situations, the system must suffer from low SINR for a long time before the adaptation is completed. As mentioned previously, this is caused by the third term of eq.(8.12) which contains large time constants. In contrast, as is seen in eq.(8.18), the trouble-making third term vanishes in the case (a) for $\mathbf{W}(0)=\mathbf{F}$, which results in fast convergence.

8.4 Least Mean Square (LMS) Adaptive Array

8.4.1 Principle and Analysis

The guideline of the LMS adaptive array dictates minimization of the error between the actual array output signal and the reference signal. The reference signal is a so-called replica of the desired signal. The optimum weight vector is obtained by minimizing the following cost function[8],[9]:

$$\varepsilon(\mathbf{W}) = E[|d_r - y|^2] \tag{8.22}$$

where d_r denotes the reference signal. $\varepsilon(\mathbf{W})$ of eq.(8.22) can be rewritten as follows by using $y=\mathbf{X}^T\mathbf{W}^*$:

$$\varepsilon(\mathbf{W}) = \mathbf{W}^\dagger R_{xx}\mathbf{W} - \mathbf{W}^\dagger \mathbf{r}_{xd} - \mathbf{W}^T \mathbf{r}_{xd}^* + E[|d_r|^2] \tag{8.23}$$

where $\mathbf{r}_{xd}$ is the correlation vector between the input and the reference signal and defined by

$$\mathbf{r}_{xd} = E[\mathbf{X}d_r^*] \tag{8.24}$$

Differentiating eq.(8.23) with respect to $\mathbf{W}^*$ yields the gradient $\nabla\{\varepsilon(\mathbf{W})\}$

as

$$\nabla\{\varepsilon(\mathbf{W})\} = R_{xx}\mathbf{W} - \mathbf{r}_{xd} \tag{8.25}$$

where the differentiation by complex number is compliance with Ref.[65]. By equating eq.(8.25) to be zero, we have the optimum weight vector which is written as

$$\mathbf{W}_{opt} = R_{xx}^{-1}\mathbf{r}_{xd} \tag{8.26}$$

The steepest gradient algorithm for the LMS system can be expressed as the following iterative relation:

$$\mathbf{W}(m+1) = \mathbf{W}(m) - \mu\, \nabla[\varepsilon\{\mathbf{W}(m)\}] \tag{8.27}$$

Substituting the gradient of eq.(8.25) into eq.(8.27), we obtain

$$\mathbf{W}(m+1) = \mathbf{W}(m) + \mu\, [\mathbf{r}_{xd} - R_{xx}\mathbf{W}(m)] \tag{8.28}$$

Similar to the DCMP algorithm, R_{xx} and $\mathbf{r}_{xd}$ in eq.(8.28) are replaced by their instantaneous values $\mathbf{X}(m)\mathbf{X}^{\dagger}(m)$ and $\mathbf{X}(m)d_r^{*}(m)$, respectively, in practice. Thus, the LMS gradient algorithm is expressed as follows[105]:

$$\mathbf{W}(m+1) = \mathbf{W}(m) + \mu\, e^{*}(m)\mathbf{X}(m) \tag{8.29}$$

$$e(m) = d_r(m) - y(m) \tag{8.30}$$

where "e" is the error, i.e., difference between the reference signal and the array output. The optimum weight vector of eq.(8.26) is asymptotically reached by the above algorithm. However, for analysis in the following, we make use of the algorithm of eq.(8.28) rather than that of eq's.(8.29) and (8.30) since the former corresponds to the expected expression of the latter.

We can reformulate the algorithm given by eq.(8.28) to the following continuous equation in the same method as the DCMP algorithm:

$$\frac{d\mathbf{W}(t)}{dt} + qR_{xx}\mathbf{W}(t) = q\mathbf{r}_{xd} \tag{8.31}$$

where q is the feedback gain and is connected with μ and the sampling

interval T_s by eq.(8.9).

Now, eq.(8.31) can be solved by a method similar to the DCMP adaptive array:

$$W(t) = W_{opt} + \{ \frac{Q_1^{\dagger}W(0)}{Q_1^{\dagger}Q_1} - \frac{Q_1^{\dagger}r_{xd}}{\sigma_1 Q_1^{\dagger}Q_1} \} Q_1 \exp(-q\sigma_1 t)$$

$$+ \{ \frac{Q_2^{\dagger}W(0)}{Q_2^{\dagger}Q_2} - \frac{Q_2^{\dagger}r_{xd}}{\sigma_2 Q_2^{\dagger}Q_2} \} Q_2 \exp(-q\sigma_2 t)$$

$$+ \sum_{k=3}^{K} \frac{Q_k^{\dagger}W(0)}{Q_k^{\dagger}Q_k} Q_k \exp(-q\sigma_k t) \qquad (8.32)$$

where the σ_k's and Q_k's (k=1,..., K) represent the eigenvalues and eigenvectors of R_{xx}, respectively, with K eigenvectors Q_k's being orthogonal to each other. The σ_k's are derived from R_{xx} of eq.(8.2) as follows after Ref.[31]:

$$\begin{cases} \sigma_1 = (K/4)\{P_s + P_i + \sqrt{(P_s - P_i)^2 + 4P_sP_iA_{si}^2}\} + P_n \\ \sigma_2 = (K/4)\{P_s + P_i - \sqrt{(P_s - P_i)^2 + 4P_sP_iA_{si}^2}\} + P_n \\ \sigma_k = P_n \quad \text{for } k = 3,..., K \end{cases} \qquad (8.33)$$

For the case where $A_{si}^2 \ll 1$, $P_n \ll P_s$, and $P_n \ll P_i$ as assumed in the DCMP system, σ_k's can be approximated as follows:

If $P_i \geq P_s$,

$$\begin{cases} \sigma_1 = (K/2)P_i \\ \sigma_2 = (K/2)P_s \\ \sigma_k = P_n \quad \text{for } k = 3,..., K \end{cases} \qquad (8.34)$$

If $P_i < P_s$,

$$\begin{cases} \sigma_1 = (K/2)P_s \\ \sigma_2 = (K/2)P_i \\ \sigma_k = P_n \quad \text{for } k = 3,..., K \end{cases} \qquad (8.35)$$

Eq's.(8.34) and (8.35) assure that σ_1 is not smaller than σ_2, which means that the time constant in the second term of eq.(8.32) is not larger than that in the third term. The time constants in the fourth term of eq.(8.32) are much larger than the other two in the second and third terms. It is this fourth term that causes slow convergence of the weight vector to the optimum state. A proper selection of the initial weight vector such as $\mathbf{W}(0)=\mathbf{F}$ solves this problem, similar to the previous DCMP system, since $\mathbf{F}$ is shown to be a linear combination of $\mathbf{Q}_1$ and $\mathbf{Q}_2$, and orthogonal to $\mathbf{Q}_k$'s(k=3,.., K)[31]. In this case, eq.(8.32) can be expressed as follows:

$$\mathbf{W}(t) = \mathbf{W}_{opt} + \{\frac{\mathbf{Q}_1^{\dagger}\mathbf{W}(0)}{\mathbf{Q}_1^{\dagger}\mathbf{Q}_1} - \frac{\mathbf{Q}_1^{\dagger}\mathbf{r}_{xd}}{\sigma_1\mathbf{Q}_1^{\dagger}\mathbf{Q}_1}\}\,\mathbf{Q}_1\exp(-q\sigma_1 t)$$

$$+ \{\frac{\mathbf{Q}_2^{\dagger}\mathbf{W}(0)}{\mathbf{Q}_2^{\dagger}\mathbf{Q}_2} - \frac{\mathbf{Q}_2^{\dagger}\mathbf{r}_{xd}}{\sigma_2\mathbf{Q}_2^{\dagger}\mathbf{Q}_2}\}\,\mathbf{Q}_2\exp(-q\sigma_2 t) \qquad (8.36)$$

Since the magnitude of $\mathbf{F}$ is arbitrary in practice, we set

$$\mathbf{W}(0) = V\mathbf{F} \qquad (8.37)$$

where V is a variable scalar. Furthermore, assuming that the exact reference signal is established in the system, we have

$$\mathbf{r}_{xd} = P_s\mathbf{C}_d = (KP_s/2)\mathbf{F} \qquad (8.38)$$

Since the third term in eq.(8.36) has a larger time constant than the second one, the best performance is achieved when the coefficient of the third term is equal to zero. By putting eq's.(8.37) and (8.38) into eq.(8.36) and equating the coefficient of the third term to be zero, we obtain the optimum values of V as follows:

$$V = KP_s/(2\sigma_2) \qquad (8.39)$$

Eq.(8.39) can be rewritten from eq's.(8.34) and (8.35) as follows:

$$\begin{cases} V = 1 & (\text{if } P_i \geq P_s) \quad (8.40) \\ V = P_s/P_i & (\text{if } P_i < P_s) \quad (8.41) \end{cases}$$

By the above equations, V must be estimated.

8.4.2 Computer Simulation

For the computer simulation based on the sampling feedback system, the algorithm of eq's.(8.29) and (8.30) is employed. As for the value of the step size, the choice of eq.(8.19) is adopted which is the same as the previous DCMP case.

For simplicity, we assume that the exact reference signal is established in the system by some means. Similar to the DCMP adaptive array, we first consider the three cases of initial weight vector, $\mathbf{F}$, $\mathbf{M}_1$ and $\mathbf{M}_2$ as shown previously in Section 8.3. Fig.8.2 shows the SINR learning curves. Although eq.(8.32) dictates that all curves should asymptotically reach the same value of SINR, the rates of convergence of (b) and (c) are much slower than that in (a) as previously shown by the DCMP adaptive array. The trouble-making fourth term of eq.(8.32) which contains large time constants causes the slow convergence in (b) and (c). On the other hand, the case (a) for $\mathbf{W}(0)=\mathbf{F}$ results in the fast convergence because of the extinction of the fourth term.

Next, the cases are compared where the magnitudes of the initial weights are inaccurately given for the case of $\mathbf{W}(0)=\mathbf{F}$. We use six different values of V ranging from 0 to 100. The results of the learning curves of SINR are shown in Fig.8.3, where (a), (b), (c) and (d) correspond to P_i=100, P_i=10, P_i=1 and P_i=0.1, respectively. The difference of the behavior with respect to the values of V and P_i is mainly caused by the magnitude of the coefficient of the third term in eq.(8.36) that has the largest time constant. These figures show that the

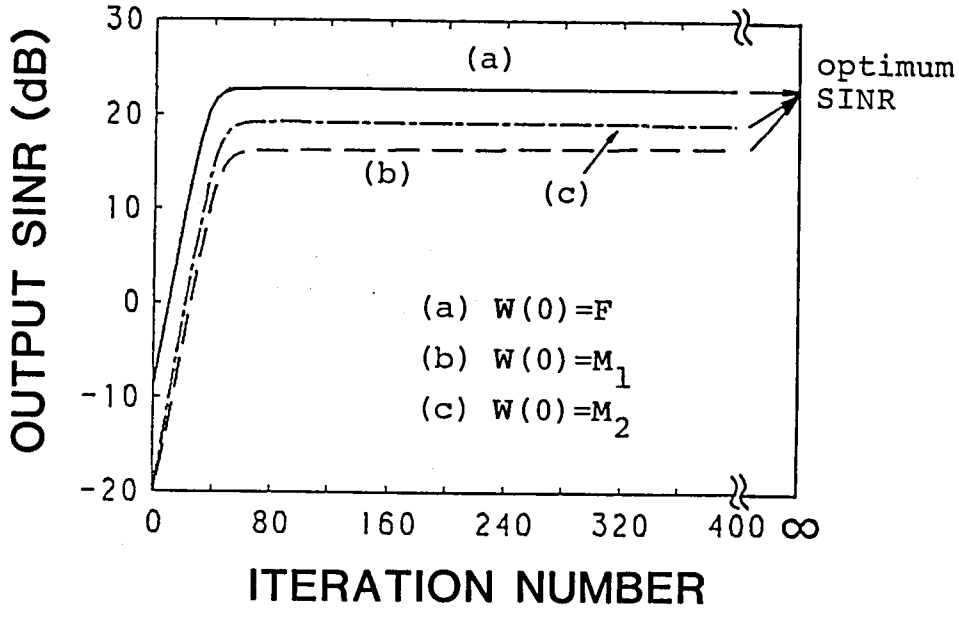

Fig.8.2 The learning curves of the output SINR for three different settings of the initial value, F, M_1 and M_2 in the LMS adaptive array.

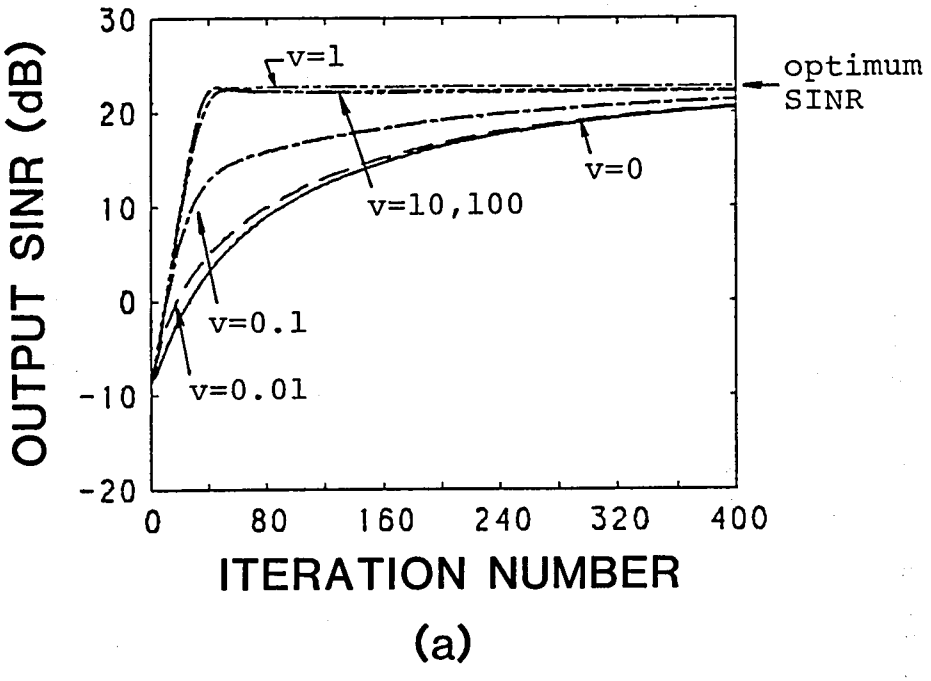

Fig.8.3 The learning curves of the output SINR for six different settings of the initial value, VF with V=0, 0.01, 0.1, 1, 10 and 100 in the LMS adaptive array for the various levels of the interference powers: (a) P_i=100, (b) P_i=10, (c) P_i=1, (d) P_i=0.1.

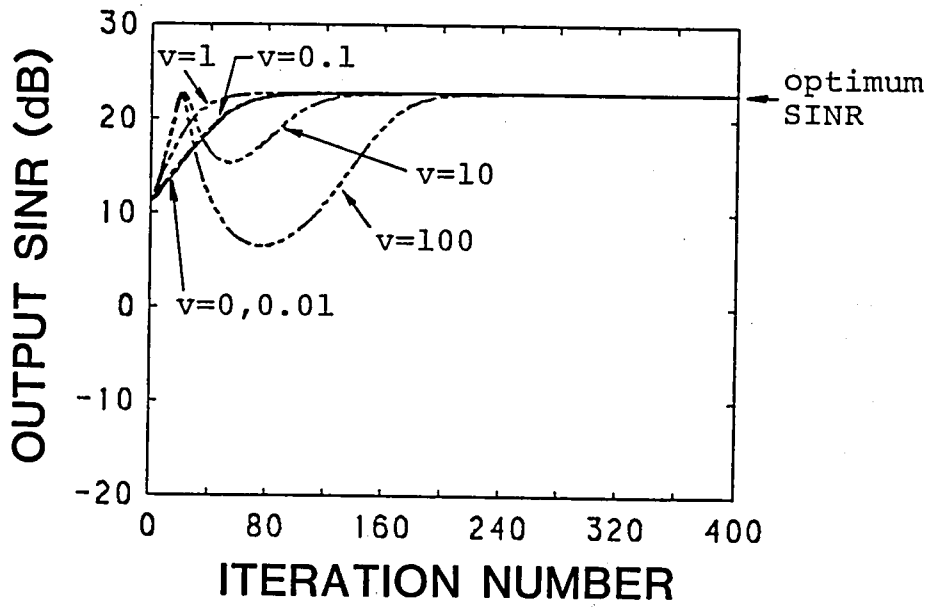

(c)

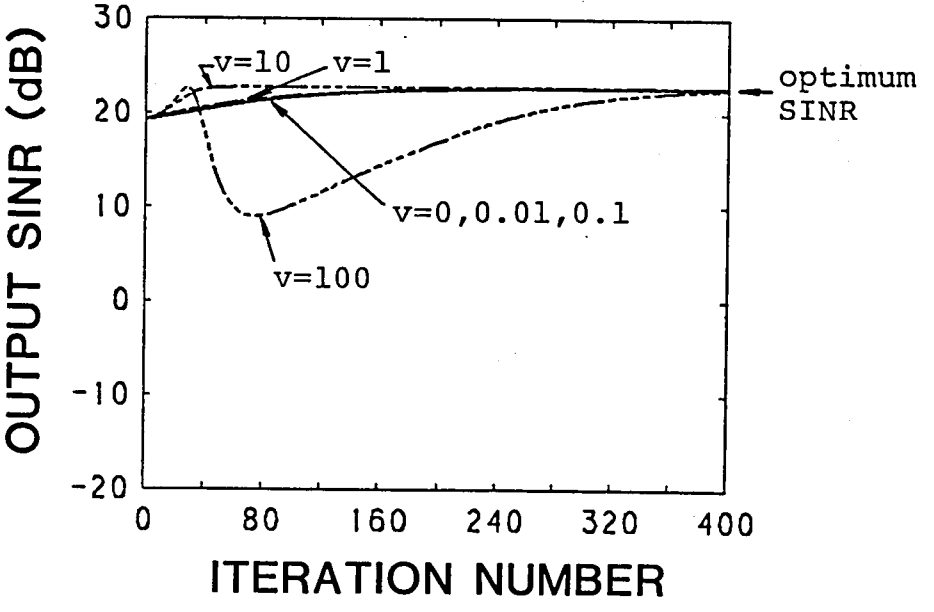

(d)

Fig.8.3 (continued)

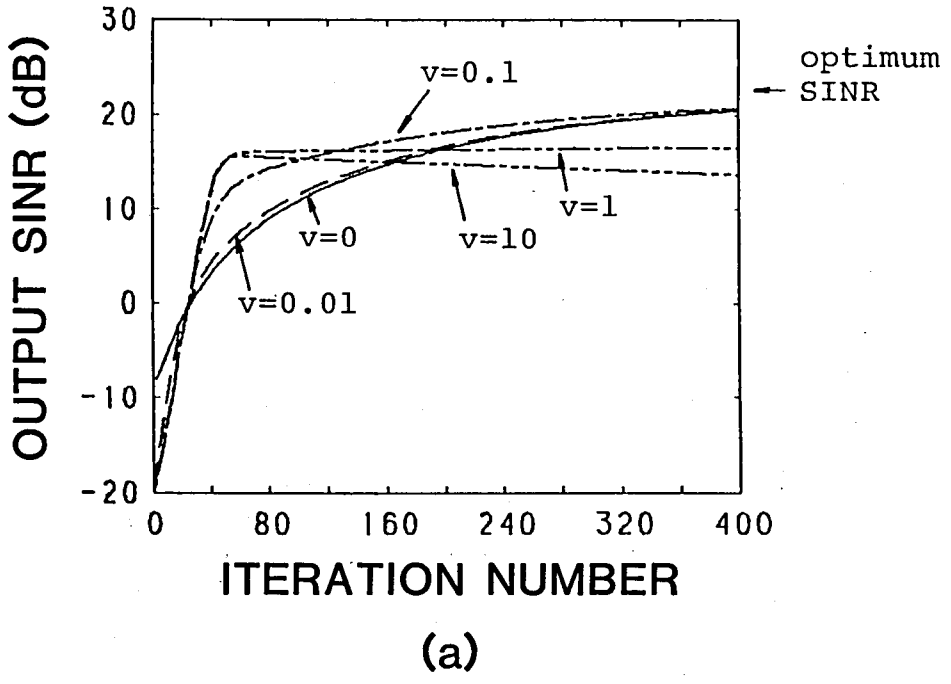

Fig.8.4 The learning curves of the output SINR for five different settings of the initial value, VM_1 with V=0, 0.01, 0.1, 1 and 10 in the LMS adaptive array for the various levels of the interference powers: (a) P_i=100, (b) P_i=10, (c) P_i=1, (d) P_i=0.1.

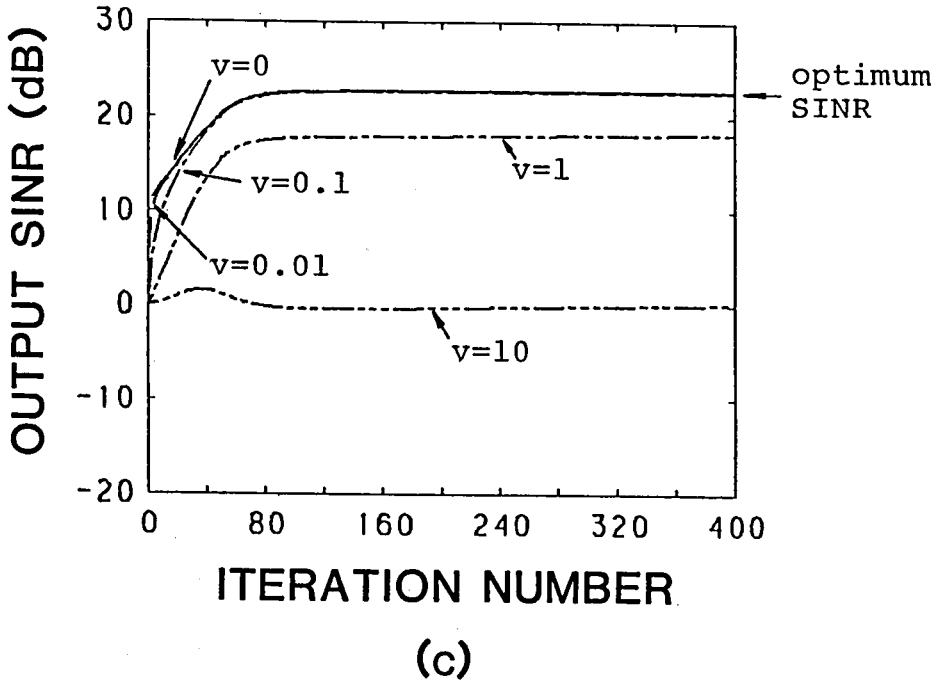

(c)

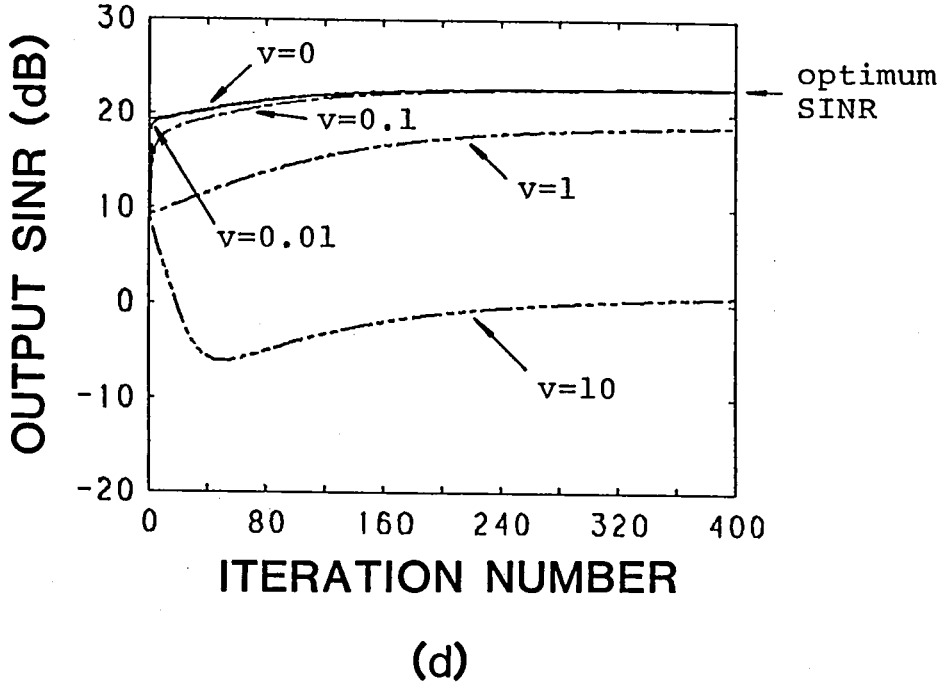

(d)

Fig.8.4 (continued)

best transient performance is obtained when V=1, for cases (a), (b) and (c); and when V=10, for case (d). These results confirm the above theory. The figure for case (d) shows that good transient performance is not greatly affected by V if V is smaller than the optimum value of 10. This means that V=1 is the safe choice when no information about the magnitude of the interference is available beforehand. After all, it is concluded that the best transient performance is achieved when $\mathbf{W}(0)=\mathbf{F}$ which is derived from eq's.(8.37) and (8.40).

More dramatic performance is seen when the magnitudes of the initial weights are inaccurately given for the case where $\mathbf{W}(0)=\mathbf{M}_1$ or $\mathbf{M}_2$. Fig.8.4 shows the results of the learning curves of SINR when $\mathbf{M}_1$ is multiplied by a factor V. The figures, 8.4(a), (b), (c), and (d) correspond to P_i=100, P_i=10, P_i=1 and P_i=0.1, respectively. Although all curves must reach the same value of SINR by theory, a variety of transient performances are observed. The case of V=10 especially shows an extremely poor performance, which may be attributed to both the large coefficients and the large time constants of the fourth term in eq.(8.32). It is interesting that when V is low, better results are achieved than when V=1. This can be understood by recalling that the zero vector (V=0) is a special case of orthogonal vectors to $\mathbf{Q}_k$'s(k=3,.., K).

8.5 Maximum Signal-to-Noise Ratio (MSN) Adaptive Array

The MSN adaptive array operates to maximize the output signal-to-noise ratio, and it most frequently adopts an analogue implementation which is also called the Howells-Applebaum system[15],[64],[106]. Fig.8.5 shows the analogue implementation of the MSN algorithm. The feedback loop in Fig.8.5 is mainly composed of mixers, a low-pass filter which has time

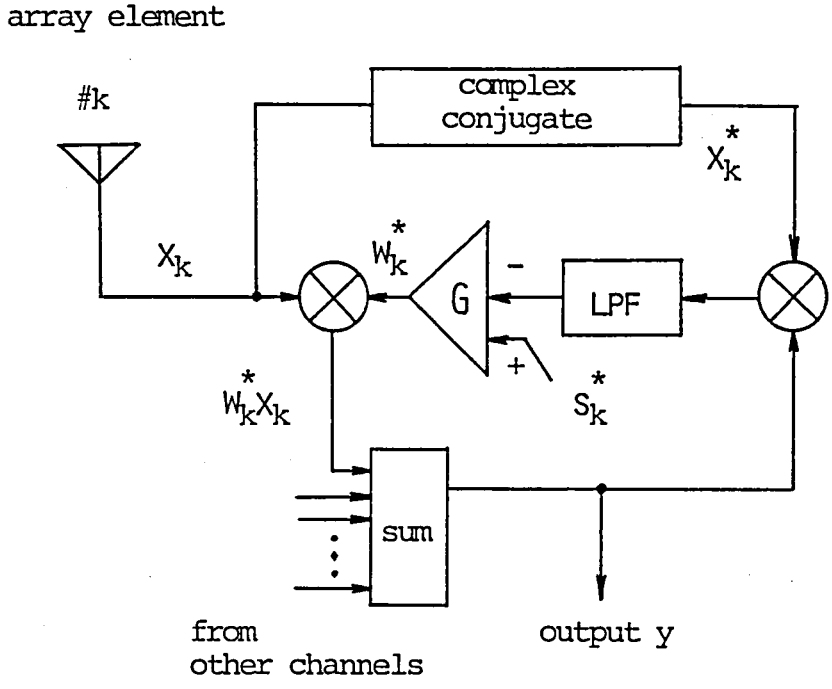

Fig.8.5 Analogue implementation of the MSN algorithm.

constant τ_o, and an amplifier with the high gain G. In this figure, s_k's are the steering signals by which the mainbeam of the array is directed to the desired signal. In this situation, they are expressed as

$$s_k = (\alpha/\sqrt{2})\ \exp\{j\Psi_k(\theta_s)\} \qquad (k=1,..,\ K) \tag{8.42}$$

where α is an arbitrary scalar constant which determines the magnitude of the steering signals. Similar to **X** and **W**, we represent s_k's as the vectorial form **S** which is called the steering vector. This steering vector **S** is connected with **F** in eq.(8.10) by

$$\mathbf{S} = (K\alpha/2)\mathbf{F} \tag{8.43}$$

The differential vector equation describing the dynamic behavior of the feedback loops can be shown to be[15],[64]

$$\tau_o \frac{d\mathbf{W}(t)}{dt} + (G\mathbf{R}_{xx} + U)\mathbf{W}(t) = G\mathbf{S} \tag{8.44}$$

The optimum weight vector at the stationary state is given by

$$\mathbf{W}_{opt} = (\mathbf{R}_{xx} + U/G)^{-1}\mathbf{S} \tag{8.45}$$

Eq.(8.44) can be solved readily as follows in the same manner as the LMS governing equation of eq.(8.31)[64]:

$$\begin{aligned}\mathbf{W}(t) = \mathbf{W}_{opt} &+ \{\frac{\mathbf{Q}_1^{\dagger}\mathbf{W}(0)}{\mathbf{Q}_1^{\dagger}\mathbf{Q}_1} - \frac{G}{G\sigma_1+1}\frac{\mathbf{Q}_1^{\dagger}\mathbf{S}}{\mathbf{Q}_1^{\dagger}\mathbf{Q}_1}\}\ \mathbf{Q}_1\ \exp(-\frac{G\sigma_1+1}{\tau_o}t) \\ &+ \{\frac{\mathbf{Q}_2^{\dagger}\mathbf{W}(0)}{\mathbf{Q}_2^{\dagger}\mathbf{Q}_2} - \frac{G}{G\sigma_2+1}\frac{\mathbf{Q}_2^{\dagger}\mathbf{S}}{\mathbf{Q}_2^{\dagger}\mathbf{Q}_2}\}\ \mathbf{Q}_2\ \exp(-\frac{G\sigma_2+1}{\tau_o}t) \\ &+ \sum_{k=3}^{K}\frac{\mathbf{Q}_k^{\dagger}\mathbf{W}(0)}{\mathbf{Q}_k^{\dagger}\mathbf{Q}_k}\mathbf{Q}_k\ \exp(-\frac{G\sigma_k+1}{\tau_o}t)\end{aligned} \tag{8.46}$$

Assuming that the gain G is sufficiently high, as is usually the case with the MSN algorithm, we can approximate eq.(8.46) to the following

equation:

$$W(t) = W_{opt} + \{\frac{Q_1^{\dagger}W(0)}{Q_1^{\dagger}Q_1} - \frac{Q_1^{\dagger}S}{\sigma_1 Q_1^{\dagger}Q_1}\} Q_1 \exp(-q\sigma_1 t)$$

$$+ \{\frac{Q_2^{\dagger}W(0)}{Q_2^{\dagger}Q_2} - \frac{Q_2^{\dagger}S}{\sigma_2 Q_2^{\dagger}Q_2}\} Q_2 \exp(-q\sigma_2 t)$$

$$+ \sum_{k=3}^{K} \frac{Q_k^{\dagger}W(0)}{Q_k^{\dagger}Q_k} Q_k \exp(-q\sigma_k t) \qquad (8.47)$$

where

$$q = G/\tau_o \qquad (8.48)$$

Since the steering vector S in eq.(8.42) is generally equivalent to the correlation vector r_{xd} in eq.(8.24), eq.(8.45) is equivalent to eq.(8.32). Therefore, the previous analysis on the LMS adaptive array may be extended to the MSN adaptive array if r_{xd} is exchanged for S. When this steering vector S is used as initial weights, the fourth term of eq.(8.47) vanishes since S can be shown orthogonal to Q_k's(k=3,..., K). Thus, eq.(8.47) leads to

$$W(t) = W_{opt} + \{\frac{Q_1^{\dagger}W(0)}{Q_1^{\dagger}Q_1} - \frac{Q_1^{\dagger}S}{\sigma_1 Q_1^{\dagger}Q_1}\} Q_1 \exp(-q\sigma_1 t)$$

$$+ \{\frac{Q_2^{\dagger}W(0)}{Q_2^{\dagger}Q_2} - \frac{Q_2^{\dagger}S}{\sigma_2 Q_2^{\dagger}Q_2}\} Q_2 \exp(-q\sigma_2 t) \qquad (8.49)$$

In practice, the frequency and angle of arrival of the desired signal are known, but its magnitude is not. Therefore, we set

$$W(0) = (2/K)VS = \alpha VF \qquad (8.50)$$

where V is a variable scalar. Since the third term in eq.(8.49) has a larger time constant than the second one, the best performance is achieved when the coefficient of the third term is equal to zero. Substituting

eq.(8.50) into eq.(8.49) and equating the coefficient of the third term to be zero yield the optimum values of V as follows:

$$V = K/(2\sigma_2) \tag{8.51}$$

Furthermore, eq.(8.51) can be rewritten from eq's.(8.34) and (8.35) as follows:

$$\begin{cases} V = 1/P_s & (\text{if } P_i \geq P_s) \quad (8.52) \\ V = 1/P_i & (\text{if } P_i < P_s) \quad (8.53) \end{cases}$$

By the above equations, V must be estimated in the MSN algorithm.

Next, we carried out the computer simulation for the case of the sampling feedback system. Replacing $\mathbf{r}_{xd}$ with $\mathbf{S}$ and R_{xx} with $\mathbf{X}(m)\mathbf{X}^{\dagger}(m)$, respectively, in the LMS algorithm of eq.(8.28), then we can obtain the following discrete MSN algorithm corresponding to the continuous one with the sufficiently high gain G:

$$\mathbf{W}(m+1) = \mathbf{W}(m) + \mu\,[\mathbf{S} - \mathbf{X}(m)y^{*}(m)] \tag{8.54}$$

where μ is related to $q(=G/\tau_o)$ by $\mu=qT_s$(T_s: sampling interval). In the simulation, the same choice of eq.(8.19) was adopted for the value of μ.

The results obtained using the algorithm of eq.(8.54) are the same as Fig's.8.3 and 8.4 in the LMS algorithm, where $\alpha=P_s$ in the MSN. Therefore, it is concluded that the best transient performance of the MSN algorithm is achieved when $V=1=1/P_s$, namely, $\mathbf{W}(0)=\{2/(KP_s)\}\mathbf{S}=(\alpha/P_s)\mathbf{F}$ which is derived from eq.(8.50).

8.6 Discussion

Several computer simulations have been carried out for other values of parameters, and we observed similar results so long as θ_i lies outside of the mainbeam.

Theoretically, the necessary condition for the initial weight vector

to force the noise-related terms in eq's.(8.12), (8.32), and (8.47) to vanish is that it has a form of linear combination of eigenvectors G_1 and G_2, or Q_1 and Q_2. These eigenvectors are also expressed as linear combinations of the direction vectors of the desired signal and interference, and hence the hyper-space spanned by those G_1 and G_2, or Q_1 and Q_2 is called a signal subspace. On the other hand, the complementary space for the signal subspace is called a noise subspace and is spanned by the remaining $G_3,..,G_K$, or $Q_3,..,Q_K$. Both subspaces are orthogonal to each other. It is easily proved that the optimum weight vector lies in the signal subspace and also is almost orthogonal to the direction vector of interference. Therefore, the results obtained in previous sections describe geometrically that it is desirable to perform the adaptation only within the signal subspace in order to converge rapidly the system to the optimum state.

It should be noted here that the analysis in the preceding sections is valid only when the degrees of freedom of the system, i.e., the number of weights, are enough to accommodate more than two signal-related eigenvalues of R_{xx} or $PR_{xx}P$. If not, the trouble-making terms do not exist either in eq.(8.12), (8.32), or (8.47), eliminating the present problem of convergence due to the noise-related time constants. This fact may account for the ignorance on the problem of the initial weights in the field of adaptive arrays, since most papers deal with the number of degrees of freedom that is necessary and sufficient for suppressing the incoming interferences. In the real world, however, it is difficult to know the number of interferences beforehand.

8.7 Concluding Remarks

This chapter considered the effect of the initial values on the transient performance of adaptive arrays based on the steepest gradient method. We studied on the three kinds of guiding principles, i.e., the directionally constrained minimization of power (DCMP), the least mean square (LMS), and the maximum signal-to-noise ratio (MSN). In each principle, the transient behavior was first investigated theoretically and the significance of the initial value was pointed out, and afterward the computer simulation demonstrated the theoretical results. In the following, we remark the conclusions on the three adaptive arrays, respectively.

The DCMP array has no serious effect since its already usable information as to the frequency and angle of arrival of the desired signal is sufficient for setting the optimum initial weight.

The LMS array is frequently preferred since it does not require the information on the angle of arrival of the desired signal. To our surprise, however, a good estimate on both the direction and magnitude of the desired signal is found to be indispensable to achieve a good transient performance. Without any a priori information, all-zero setting is recommended.

The MSN, or Howells-Applebaum array, is supposed to work with the same information as the DCMP array, i.e., the frequency and angle of arrival of the desired signal, but it is shown that a good estimate on the magnitude of the desired signal is also necessary in order to guarantee good transient performance.

In summary, the best choice of the initial weight is the uniform excitation with such phaseshift as to point its mainbeam to the desired signal. In addition, good prediction of the magnitude of the incoming signal is also required, as to the LMS and MSN adaptive arrays.

CHAPTER 9

SUMMARY AND CONCLUSIONS

In this thesis, we have made theoretical and computation studies on adaptive arrays, particularly the adaptive array with the directional constraints, toward wider applications of them.

Since the detailed results of the investigations of Chapters 4, 5, 6, 7 and 8 are discussed in the last sections of those chapters, we will present the compact résumé on their most noteworthy aspects here.

In Chapter 3, we pay attention to the adaptive array which operates under the principle of the directionally constrained minimization of power (DCMP). This DCMP method was developed in the laboratory where the author studies presently and has been the main topic in this thesis. The guiding principle is formulated as

$$\min_{\mathbf{W}} (P_{out} = \mathbf{W}^T R_{xx} \mathbf{W}) \qquad \text{eq.(3.24)}$$

$$\text{subject to } C_d{}^T \mathbf{W} = \mathbf{H} \qquad \text{eq.(3.25)}$$

the optimum weights given by

$$\mathbf{W}_{opt} = R_{xx}{}^{-1} C_d (C_d{}^T R_{xx}{}^{-1} C_d)^{-1} \mathbf{H} \qquad \text{eq.(3.31)}$$

and the optimization algorithm expressed as

$$\mathbf{W}(m+1) = P[\mathbf{W}(m) - \mu X(m) y(m)] + \mathbf{F} \qquad \text{eq.(3.49)}$$

In Chapter 4, an adaptive antenna array system under the principle of DCMP with phase-only control is proposed. A new penalty function

$$Q(\Phi) = P_{out} + 2\beta P_s \sum_{k=1}^{K} \{1 - \cos(\phi_k - \phi_{ko})\} \qquad \text{eq.(4.12)}$$

is introduced where $\beta=K$ is chosen as the optimum value. Good results were obtained by the computer simulation. However, the suppression of the

interference is not sufficient when the phase-shifters are quantized.

In Chapter 5, we have proposed a robust adaptive array system named "Tamed Adaptive Antenna". "Pseudo noise" is injected into the control loop of the DCMP adaptive array. The correlation matrix is modified as $R_{xx}+\alpha U$ in place of R_{xx}, and the optimum value of α is

$$\alpha_{opt} = KP_s/\sqrt{2} \qquad \text{eq.(5.33)}$$

It is confirmed that the tamed system preserves the desired signal in the adverse circumstances such as; (a) coherent interference, (b) beam pointing error, (c) broadband desired signal, and (d) mutual coupling between array elements or general random input errors.

In Chapter 6, the technique is demonstrated which suppresses the interferences that are coherent with the desired signal. The full array is divided into partially overlapped sub-arrays and the Toeplitz correlation matrix is obtained by the adaptive spatial averaging. The averaged matrix R'_{xx} is given by

$$R'_{xx} = \sum_{n=1}^{N} v_n R_{xx \cdot n} \qquad \text{eq.(6.6)}$$

where the cross correlation between the coherent waves is decorrelated by determining v_n adaptively to the radio environment. For suppression of the J coherent interferences, K and N, i.e., the necessary size and number of the sub-arrays must be such that

$$\begin{cases} K \geq J + 2 & \text{eq.(6.77)} \\ N \geq J(J+1) + 1 & \text{eq.(6.82)} \end{cases}$$

The results of simulation confirmed the excellent suppression of coherent interferences. Furthermore, this technique results in the rapid convergence to the optimum state against both coherent and incoherent interferences.

In Chapter 7, a new constraint for the adaptive antenna based on the power minimization is introduced. The cross correlation between the desired signals at the input and the array output is constrained by

$$\mathbf{r}_d^T\mathbf{W} = P_o \qquad \text{eq.(7.7)}$$

This principle is named the correlation-constrained minimization of power (CCMP) method. It protects the desired signal successfully in the cases of the broadband desired signal and the pointing error. The CCMP method is effective even when these difficult settings are too severe for the tamed adaptive array to handle.

In Chapter 8, it is revealed that the excess degrees of freedom of the adaptive array system have a reverse effect of very slow convergence. The DCMP system can avoid it by the proper choice of the initial weight which points the mainbeam to the desired signal with uniform excitation. The LMS (Least Mean Square) and MSN (Maximum Signal-to-Noise Ratio) adaptive arrays, on the contrary, have a fatal defect that they also require the a priori information on the magnitude of the desired signal to prevent the slow convergence.

In conclusion, we have studied the various performances of the adaptive arrays under newly introduced principles for several applications and obtained valuable understanding on them. Especially, we recommend the tamed DCMP adaptive array. It is simple and robust against a variety of adverse circumstances, although it requires the approximate estimate of the input power of the desired signal, P_s. When the desired signal has broader bandwidth and the pointing error is larger, the CCMP system shall be used. Where the coherent interferences exist, the preprocessing by the adaptive spatial averaging technique should be incorporated into the main adaptive processings such as the DCMP or the CCMP.

REFERENCES

[1] C.L.Dolph, "A Current Distribution for Broadside Arrays Which Optimizes the Relationship between Beam Width and Side-Lobe Level," Proc. IRE, vol.34, pp.335-348, June 1946.

[2] T.T.Taylor, "Design of Line-Source Antennas for Narrow Beamwidth and Low Sidelobes," IRE Trans. Antennas and Propagation, vol.AP-3, pp.16-28, Jan. 1955.

[3] "IEEE Standard Definitions of Terms for Antenna," IEEE Trans. Antennas and Propagation, vol.AP-17, pp.264-269, May 1969.

[4] IEEE Trans. Antennas and Propagation (Special Issue on Active and Adaptive Antennas), vol.AP-12, Mar. 1964.

[5] D.L.Margerum, "Self-Phased Arrays," in Microwave Scanning Antennas, vol.3, Chapter 5, edit. by R.C.Hansen, New York: Academic Press, 1966.

[6] P.W.Howells, "Intermediate Frequency Side-Lobe Canceller," U.S. Patent 3202990, Aug. 24, 1965.

[7] B.Widrow, "Adaptive Filters I: Fundamentals," Stanford Univ. Electronics Labs., Syst. Theory Lab., Center for Syst. Res., Rep. SU-SEL-66-126, Tech. Rep. 6764-6, Dec. 1966.

[8] B.Widrow, "Adaptive Filters," in Aspects of Network and System Theory, edit. by Kalman, R.E., and De Claris, Holt, Rinehart and Winston, New York, pp.563-587, 1970.

[9] B.Widrow et al., "Adaptive Antenna System," Proc. IEEE, vol.55, pp.2143-2159, Dec. 1967.

[10] F.Bryn, "Optimum Signal Processing of Three-Dimensional arrays Operating on Gaussian Signals and Noise," J. Acoust. Soc. Am.,

vol.34, pp.289-297, Mar. 1962.

[11] S.W.W.Shor, "Adaptive Technique to Discriminate against Coherent Noise in a Narrow-Band System," J. Acoust. Soc. Am., vol.39, pp.74-78, Jan. 1966.

[12] P.E.Green, Jr., R.A.Frosch and C.F.Romney, "Principles of an Experimental Large Aperture Seismic Array (LASA)," Proc. IEEE, vol.53, pp.1821-1833, Dec. 1965.

[13] R.T.Lacoss, "Adaptive Combining of Wideband Array Data for Optimal Reception," IEEE Trans., vol.GE-6, pp.78-86, May 1968.

[14] B.D.Steinberg, "Principles of Aperture and Array System Design," A Wiley-Interscience Publication, John Wiley & Sons, 1975.

[15] S.P.Applebaum, "Adaptive Arrays," Special Project Laboratory Report, SPL-TR66-1, Syracuse Univ. Research Corp., Aug. 1966.

[16] L.E.Brennan and I.S.Reed, "Theory of Adaptive Radar," IEEE Trans. Aerospace Electronic Syst., vol.AES-9, pp.237-252, Mar. 1973.

[17] L.E.Brennan, E.L.Pugh and I.S.Reed, "Control Loop Noise in Adaptive Array Antennas," IEEE Trans. Aerospace Electronic Syst., vol.AES-7, pp.254-262, Mar. 1971.

[18] L.E.Brennan and I.S.Reed, "Effect of Envelope Limiting in Adaptive Array Control Loops," IEEE Trans. Aerospace Electronic Syst., vol.AES-7, pp.698-700, July 1971.

[19] K.Takao, M.Fujita and T.Nishi, "Responses of a Signal-Processing Array to Modulated Inputs," Paper of Tech. Group on Antennas and Propagation, IECE Japan, No.AP74-33, 1974.

[20] L.J.Griffiths, "A Simple Adaptive Algorithm for Real Time Processing in Antenna Arrays," Proc. IEEE, vol.57, pp.1696-1704, Oct. 1969

[21] J.H.Chang and F.B.Tuteur, "A New Class of Adaptive Array Processor," J. Acoust. Soc. Am., vol.49, pp.639-649, Mar. 1971.

[22] C.L.Zahm, "Effects of Errors in the Direction of Incidence on the Performance of an Adaptive Array," Proc. IEEE, vol.60, pp.1008-1009, Aug. 1972.

[23] J.Capon, R.J.Greenfield and R.J.Kolker, "Multidimensional Maximum-Likelihood Processing of a Large Aperture Seismic Array," Proc. IEEE, vol.55, No.2, pp.192-211, Feb. 1967.

[24] L.J.Griffiths, "Signal Extraction Using Real-Time Adaptation of a Linear Multichannel Filter," SEL-68-017, Tech, Rep. No.6788-1, System Theory Lab., Stanford Univ., Feb. 1968.

[25] S.P.Applebaum and D.J.Chapman, "Adaptive Arrays with Main Beam Constraint," IEEE Trans. Antennas and Propagation, vol.AP-24, pp.650-661, Sept. 1976.

[26] A.Booker and C.Y.Ong, "Multiple-Constraint Adaptive Filtering," Geophysics, vol.36, pp.498-509, June 1971.

[27] O.L.Frost, III, "Adaptive Least Squares Optimization Subject to Linear Equality Constraints," SEL-70-055, Technical Report, No.6796-2, Information System Lab., Stanford Univ., Aug. 1970.

[28] M.J.Levin, "Maximum-Likelihood Array Processing," Lincoln Laboratories, MIT, Lexington, Mass., Semiannual Tech. Summary Rep. on Seismic Discrimination, Dec. 1964.

[29] O.L.Frost, III, "An Algorithm for Linearly Constrained Adaptive Array Processing," Proc. IEEE, vol.60, pp.926-935, Aug., 1972.

[30] K.Takao, M.Fujita and T.Nishi, "An Adaptive Antenna Array under Directional Constraint," IEEE Trans. Antennas and Propagation, vol.AP-24, pp.662-669, Sept. 1976.

[31] C.L.Zahm, "Application of Adaptive Arrays to Suppress Strong Jammers in the Presence of Weak Signals," IEEE Trans. Aerospace Electronic Syst., vol.AES-9, pp.260-271, Mar. 1973.

[32] I.S.Reed, J.D.Mallett and L.E.Brennan, "Rapid Convergence Rate in Adaptive Arrays," IEEE Trans. Aerospace Electronic Syst., vol.AES-101, pp.853-863, Nov. 1974.

[33] V.F.Pisarenko, "The Retrieval of Harmonics from a Covariance Function," Geopys. J. Roy. Astron. Soc., vol.33, pp.247-266, 1973.

[34] W.S.Ligett, "Passive Sonar: Fitting Models to Multiple Time Series," in Signal Processing, edit. by J.W.Griffiths et al., New York: Academic Press, pp.327-345, 1973.

[35] N.L.Owsley, "Spectral Signal Set Extraction," in Aspects of Signal Processing, Part II, edit. by G.Tacconi, Dordecht, The Netherlands: Reidel, pp.469-475, 1977.

[36] R.O.Schmidt, "Multiple Emitter Location and Signal Parameter Estimation," IEEE Trans. Antennas and Propagation, vol.AP-34, pp.276-280, Mar. 1986.

[37] R.O.Schmidt and R.F.Franks, "Multiple Source DF Signal Processing: An Experimental System," IEEE Trans. Antennas and Propagation, vol.AP-34, pp.281-290, Mar. 1986.

[38] S.S.Reddi, "Multiple Source Location-A Digital Approach," IEEE Trans. Aerospace Electronic Syst., vol.AES-15, pp.95-105, Jan. 1979.

[39] G.Bienvenu and L.Kopp, "Adaptivity to Background Noise Spatial Coherence for High Resolution Passive Methods, " Proc. IEEE Conf. Acoust., Speech, Signal Processing (ICASSP 80), Denver, CO, vol.1, pp.307-310, Apr. 1980.

[40] D.H.Johnson and S.R.Degraff, "Improving the Resolution of Bearing in Passive Sonar Arrays by Eigenvalue Analysis," IEEE Trans. Acoust., Speech, Signal Processing, vol.ASSP-30, pp.638-647, Aug. 1982.

[41] M.Wax, T.J.Shan and T.Kailath, "Spatio-Temporal Spectral Analysis by Eigenstructure Methods," IEEE Trans. Acoust., Speech, Signal Processing, vol.ASSP-32, pp.817-827, Aug. 1984.

[42] W.F.Gabriel, "Using Spectral Estimation Techniques in Adaptive Processing Antenna Systems," IEEE Trans. Antennas and Propagation, vol.AP-34, pp.291-300, Mar. 1986.

[43] F.Haber and M.Zoltowski, "Spatial Spectrum Estimation in a Coherent Signal Environment Using an Array in Motion," IEEE Trans. Antennas and Propagation, vol.AP-34, pp.301-310, Mar. 1986.

[44] M.H.Er and A.Cantoni, "Derivative Constraints for Broad-Band Element Space Antenna Array Processors," IEEE Trans. Acoust., Speech, Signal Processing, vol.ASSP-31, pp.1378-1393, Dec. 1983.

[45] K.M.Buckley and L.J.Griffiths, "An Adaptive Generalized Sidelobe Canceller with Derivative Constraints," IEEE Trans. Antennas and Propagation, vol.AP-34, pp.311-319, Mar. 1986.

[46] L.J.Griffiths and C.W.Jim, "An Alternative Approach to Linearly Constrained Adaptive Beamforming," IEEE Trans. Antennas and Propagation, vol.AP-30, pp.27-34, Jan. 1982.

[47] K.M.Buckley and L.J.Griffiths, "Spatial Filtering with Broadband Minimum Variance Beamformers," Proc. IEEE AP-S Int. Symp., USA, pp.575-578, June 1986.

[48] K.Takao and T.Ishizaki, "Constraints of the Output-Power-Minimization Adaptive Array for a Broadbanded Desired Signal," Trans. IECE Japan, vol.J68-B, pp.411-418, Mar. 1985.

[49] T.Ishizaki and K.Takao, "Characteristics of Adaptive Arrays Constraining the Broadband Desired Signal," Nat. Conv. Rec., IECE Japan, No.S6-4, 1983.

[50] M.H.Er and A.Cantoni, "A New Set of Linear Constraints for

Broad-Band Time Domain Element Space Processors," IEEE Trans. Antennas and Propagation, vol.AP-34, pp.320-329, Mar. 1986.

[51] W.F.Gabriel, "Spectral Analysis and Adaptive Array Superresolution Techniques," Proc. IEEE, vol.68, pp.654-666, June 1980.

[52] B.Widrow et al., "Signal Cancellation Phenomena in Adaptive Antennas: Causes and Cures," IEEE Trans. Antennas and Propagation, vol.AP-30, pp.469-478, May 1982.

[53] T.J.Shan and T.Kailath, "A New Adaptive Antenna System for Coherent signals and Interference," Proc. 17th Asilomar Conf., pp.401-405, 1983.

[54] T.J.Shan and T.Kailath, "Adaptive Beamforming for Coherent signals and Interference," IEEE Trans. Acoust., Speech, Signal Processing, vol.ASSP-33, pp.527-536, June 1985.

[55] J.E.Evans, J.R.Johnson and D.F.Sun, "Application of Advanced Signal Processing Techniques to Angle of Arrival Estimation in ATC Navigation and Surveillance Systems," MIT Lincoln Laboratory Tech. Report 582, (FAA-RD-82-42), 1982.

[56] T.J.Shan, M.Wax and T.Kailath, "Spatial Smoothing Approach for Location Estimate of Coherent Sources," Proc. 17th Asilomar Conf., pp.367-371, 1983.

[57] T.J.Shan, M.Wax and T.Kailath, "On Spatial Smoothing for Direction-of-Arrival Estimate of Coherent Signals," IEEE Trans. Acoust., Speech, Signal Processing, vol.ASSP-33, pp.806-811, Aug. 1985.

[58] Y.L.Su, T.J.Shan and B.Widrow, "Parallel Spatial Processing: A Cure for Signal Cancellation in Adaptive Arrays," IEEE Trans. Antennas and Propagation, vol.AP-34, pp.347-355, Mar. 1986.

[59] K.Komiyama and K.Takao, "Adaptive Array of Paired Elements," Paper of Tech. Group on Antennas and Propagation, IECE Japan, No.AP77-

100, 1978.

[60] T.K.Citron and T.Kailath, "Eigenvector Methods and Beamforming: A First Approach," Proc. 17th Asilomar Conf., pp.271-275, 1983.

[61] A.K.Luthra, "A Solution to the Adaptive Nulling Problem with a Look-Direction Constraint in the Presence of Coherent Jammers," IEEE Trans. Antennas and Propagation, vol.AP-34, pp.702-710, May 1986.

[62] K.Komiyama and K.Takao, "Stationary Characteristics of the Directionally Constrained Adaptive Array," Trans. IECE Japan, vol.J63-B, pp.634-641, June 1980.

[63] J.E.Hudson, Adaptive Array Principles, New York, London: Peter Peregrinus Ltd., 253P., 1981.

[64] D.E.N.Davies et al, "Array Signal Processing," in The Handbook of Antenna Design, vol.2, Chapter 13, pp.330-456, edit. by A.W.Rudge, K.Milne, A.D.Oliver and P.Knight, London: Peter Peregrinus Ltd., 1983.

[65] D.H.Brandwood, "A Complex Gradient Operator and its Application in Adaptive Array Theory," IEE Proc., vol.130, Pts. F and H, No.1, Feb. 1983.

[66] C.A.Baird and G.G.Rassweiler, "Adaptive Sidelobe Nulling Using Digitally Controlled Phase-Shifters," IEEE Trans. Antennas and Propagation, vol.AP-24, pp.638-649, Sept. 1976.

[67] M.K.Leavitt, "A Phase Adaptation Algorithm," IEEE Trans. Antennas and Propagation, vol.AP-24, pp.754-756, Sept. 1976.

[68] P.A.Thompson, "Adaptation by Direct Phase-Shift Adjustment in Narrow-Band Adaptive Antenna Systems," IEEE Trans. Antennas and Propagation, vol.AP-24, pp.756-760, Sept. 1976.

[69] J.J.Lee, M.Mikasa and H.E.Foster, "An Adaptive Pillbox Array Antenna," Proc. IEEE AP-S Int. Symp., pp.375-382, 1980.

[70] R.A.Shore, "The Use of Nonlinear Programming Techniques for Phase-Only Null Synthesis," AP-S Int.Symp., pp.207-210, 1983.

[71] N.Kikuma and K.Takao, "A Directionally Constrained Adaptive Array with Phase-Only Control," Trans. IECE Japan, vol.E68, pp.325-330, May 1985.

[72] K.Komiyama, Y.Yoneda and K.Takao, "An Adaptive Array for a Coherent Interference," Nat. Conv. Rec. on Opt. and Radio Wave Electron., IECE Japan, No.80, 1976.

[73] N.Kikuma and K.Takao, "The Behavior of the Adaptive Array under Directionally Constrained Minimization of Power When a Coherent Interference is Incident," Nat. Conv. Rec., IECE Japan, No.S6-3, 1983.

[74] W.D.White, "Angular Spectra in Radar Applications," IEEE Trans. Aerospace Electronic Syst., vol.AES-15, pp.895-899, 1979.

[75] A.Cantoni and L.Godara, "Resolving the Directions of Sources in a Correlated Field Incident on an Array," J. Acoust. Soc. Am. vol.64, pp.1247-1255, 1980.

[76] T.Ishizaki and K.Takao, "Constraints of an Adaptive Array for the Wideband Desired Signal," Paper of Tech. Group on Antennas and Propagation, IECE Japan, No.AP82-87, 1982.

[77] T.Ishizaki and K.Takao, "An Adaptive Array by Correlation Constraint," Paper of Tech. Group on Antennas and Propagation, No.AP82-123, 1983.

[78] N.Kikuma and K.Takao, "Tamed Adaptive Antenna," Nat. Conv. Rec., IECE Japan, No.787, 1984.

[79] K.Takao and N.Kikuma, "Tamed Adaptive Antenna Array," IEEE Trans. Antennas and Propagation, vol.AP-34, pp.388-394, Mar. 1986.

[80] S.T.Alexander and J.F.Kauffman, "Effects of Mutual Coupling upon the

LMS Adaptive Antenna Array Algorithm," Milcom 82, vol.2, pp.36.1.1-36.1.5, 1982.

[81] I.J.Gupta and A.A.Ksienski, "Effect of Mutual Coupling on the Performance of Adaptive Arrays," IEEE Trans. Antennas and Propagation, vol.AP-31, pp.785-791, Sept. 1983.

[82] Z.Yimin, K.Hirasawa and K.Fujimoto, "Performance of Power Inversion Adaptive Array with the Effect of Mutual Coupling," Proc. ISAP, Japan, vol.3, pp.803-806, Aug. 1985.

[83] R.J.Evans and K.M.Ahmed, "Robust Adaptive Array Antennas," J. Acoust. Soc. Am. 71(2), Feb. 1982.

[84] R.T.Compton,Jr., "The Effect of Random Steering Vector Errors in the Applebaum Adaptive Array," IEEE Trans. Aerospace Electronic Syst., vol.AES-18, pp.392-400, Sept. 1982.

[85] M.H.Er and A.Cantoni, "A New Approach to the Design of Robust Narrow-Band Array Processors," Proc. IEEE Conf. Acoust., Speech, Signal Processing (ICASSP 86), Japan, vol.4, pp.2527-2530, Apr. 1986.

[86] N.Kikuma and K.Takao, "The Behavior of the Adaptive Array Against a Coherent Interference," Paper of Tech. Group on Antennas and Propagation, IECE Japan, No.AP83-20, 1983.

[87] N.Kikuma and K.Takao, "The Effect of the Pointing Error of the Desired Signal Direction on the Tamed Adaptive Antenna," Paper of Tech. Group on Antennas and Propagation, IECE Japan, No.AP84-32, 1984.

[88] N.Kikuma and K.Takao, "The Behavior of the Tamed Adaptive Array to the Wideband Desired Signal," Paper of Tech. Group on Antennas and Propagation, IECE Japan, No.AP84-73, 1984.

[89] T.Ishizaki and K.Takao, "Suppression of a Broadband Interference

with a Multi-Tap Adaptive Array," Paper of Tech. Group on Antennas and Propagation, IECE Japan, No.AP81-140, 1982.

[90] P.S.Carter, "Circuit Relations in Radiating Systems and Applications to Antenna Problems," Proc. IRE, vol.20, pp.1004-1041, June 1932.

[91] N.Kikuma and K.Takao, "The Behavior of the Adaptive Array against a Coherent Interference," Paper of Tech. Group on Antennas and Propagation, IECE Japan, No.AP83-20, 1983.

[92] H.Watanabe and S.Nishimoto, "Characteristics of Correlated Interference Rejection Using an Adaptive Antenna with Spatial Learning," Paper of Tech. Group on Space Aerial Navigat. Electron., IECE Japan, No.SANE83-54, 1984.

[93] H.Watanabe, R.Azuma and A.Noguchi, "Interference Rejection Characteristics of Spatially Averaged Learning Adaptive Antenna," Paper of Tech. Group on Antennas and Propagation, IECE Japan, No.AP84-94, 1984.

[94] O.L.Frost, "Adaptive Interference and Multipath Rejection in Linear Direction-Finding Arrays," Proc. IEEE Conf. Acoust., Speech, Signal Processing (ICASSP 86), Japan, vol.4, pp.2499-2502, Apr. 1986.

[95] K.Takao, N.Kikuma and T.Yano, "An Adaptive Antenna to Suppress Coherent Interference," Paper of Tech. Group on Antennas and Propagation, IECE Japan, No.AP85-28, 1985.

[96] K.Takao, N.Kikuma and T.Yano, "Toeplitzization of Correlation Matrix in Multipath Environment," Proc. IEEE Conf. Acoust., Speech, Signal Processing (ICASSP 86), Japan, vol.3, pp.1873-1876, Apr. 1986.

[97] N.Kikuma snd K.Takao, "Consideration on Degrees of Freedom Required by the Adaptive Spatial Averaging Technique for Adaptive Arrays,"

Paper of Tech. Group on Antennas and Propagation, IECE Japan, No.AP86-121, 1987.

[98] N.Kikuma snd K.Takao, "Application of the Adaptive Spatial Averaging Technique to SMI Adaptive Arrays," Paper of Tech. Group on Antennas and Propagation, IECE Japan, No.AP86-52, 1986.

[99] R.W.Jenkins, "Implementing a Matrix-Inversion Algorithm in a Limited-Precision Adaptive Array Processor," Proc. IEEE AP-S Int. Symp., Canada, vol.I, pp.289-292, June 1985.

[100] S.M.Kay and S.L.Marple,Jr., "Spectrum Analysis-A Modern Perspective," Proc. IEEE, vol.69, No.11, pp.1380-1419, Nov. 1981.

[101] M.Ohmiya, Y.Ogawa and K.Itoh, "A Comparison of Adaptive Antennas on Desired Signal Arrival Angle Errors," Trans. IECE Japan, vol.J67-B, pp.1438-1445, Dec. 1984.

[102] B.Widrow et al., "A Comparison of Adaptive Algorithms based on the Methods of Steepest Descent and Random Search," IEEE Trans. Antennas and Propagation, vol.AP-24, pp.615-637, Sept. 1976.

[103] R.A.Monzingo and T.W.Miller, Introduction to Adaptive Arrays, New York: Wiley, 543P., 1980.

[104] N.Kikuma and K.Takao, "Effect of Initial Values of Adaptive Arrays," IEEE Trans. Aerospace Electronic Syst., vol.AES-22, pp.688-694, Nov. 1986.

[105] B.Widrow et al., "The Complex LMS Algorithm," Proc. IEEE, vol.63, pp.719-720, Apr. 1975.

[106] N.Kikuma and K.Takao, "Significance of Initial Weights in the Howells-Applebaum Adaptive Array," Paper of Tech. Group on Antennas and Propagation, IECE Japan, No.AP85-11, 1985.